

**Satellite and Fluorescence Remote Sensing**  
**for Rice Nitrogen Status Diagnosis**  
**in Northeast China**

Inaugural-Dissertation  
zur  
Erlangung des Doktorgrades  
der Mathematisch-Naturwissenschaftlichen Fakultät  
der Universität zu Köln

vorgelegt von  
**Shanyu Huang**  
aus Fujian, China

Köln, 2019



Berichterstatter: Prof. Dr. Georg Bareth

Prof. Dr. Karl Schneider

Tag der mündlichen Prüfung: 13.02.2019



## Abstract

Nitrogen (N), as the most important element of crop growth and development, plays a decisive role in ensuring yield. However, the problems of over-application of N fertilizers have been repeatedly reported in China, which resulted in low N use efficiency and high risk of environmental pollution. The requirements of developing technologies for real-time and site-specific diagnosis of crop N status are the foundation to realize the precision N management, and also benefit to the improvement of the N use efficiency. Remote sensing technology provides a promising non-intrusive solution to monitor rice N status and to realize the precision N management over large areas. This research focuses on proposing N nutrition diagnosis methods and developing N fertilizer management strategies for paddy rice of cold regions in Northeast China. The main contents and results are presented as follows:

This study developed a new critical N ( $N_c$ ) dilution curve for paddy rice of cold regions in Northeast China. The curve could be described by the equation  $N_c = 27.7W^{-0.34}$  if  $W \geq 1$  Mg dry matter (DM) ha<sup>-1</sup> or  $N_c = 27.7$  g kg<sup>-1</sup> DM if  $W < 1$  Mg DM ha<sup>-1</sup>, where  $W$  is the aboveground biomass. Results indicated that the new  $N_c$  dilution curve was suitable for diagnosing short-season Japonica rice N status in Northeast China. The validation result indicated that it worked well to diagnose plant N status of the 11-leaf variety rice.

This study investigated the potential of the satellite remote sensing data for diagnosing rice N status and guiding the topdressing N application at the stem elongation stage in Northeast China. 50 vegetation indices (VIs) were computed based on the FORMOSAT-2 satellite data, and they were correlated with the field-based agronomic variables, i.e., aboveground biomass (AGB), leaf area index (LAI), plant N concentration (PNC), plant N uptake (PNU), chlorophyll meter readings, and N nutrition index (NNI, defined as the ratio of actual PNC and critical PNC according to the new  $N_c$  dilution curves). The results presented that 45% of variation in the NNI was obtained by using a direct estimation method based on the best VI according to the FORMOSAT-2 satellite data, while 52% of the variation in the NNI was yielded by an indirect estimation method, which firstly used the VIs to estimate AGB and PNU, respectively, then estimated NNI according to these two variables. Moreover, based on the critical N uptake curve, a N recommendation algorithm was proposed. The algorithm was based on the difference between the estimated PNU and the critical PNU to adjust the topdressing N application rate. The results demonstrated that FORMOSAT-2 images have the potential to estimate rice N status and guide panicle N fertilizer applications in Northeast China.

This study also evaluated the potential improvements of the newest satellite sensors with

the red edge band for diagnosing rice N status in Northeast China. The canopy-scale hyperspectral data were upscaled to simulate the wavebands of RapidEye, WorldView-2, and FORMOSAT-2, respectively. The VI analysis, stepwise multiple linear regression (SMLR), and partial least squares regression (PLSR) were performed to evaluate the N status indicators. The results indicated that the VIs based on the RE band from RapidEye and WorldView-2 data could explain more variability for N indicators than the VIs from FORMOSAT-2 data having no RE band. Moreover, the SMLR and PLSR results revealed that both the near-infrared and red edge band were important for N status estimation.

The proximal fluorescence sensor Multiplex<sup>®</sup>3 was used to evaluate the potential of fluorescence spectrum for estimating the N status of the cold regional paddy rice at different growth stages. The Multiplex indices and their normalized N sufficient indices (NSI) were used to estimate the five N status indicators, i.e., AGB, leaf N concentration (LNC), PNC, PNU, and NNI. The results indicated that there were strong relationships between the fluorescence indices (i.e., BRR\_FRF, FLAV, NBI\_G, and NBI\_R) and (i.e., LNC, PNC, NNI), with the coefficient of determination ( $R^2$ ) between 0.40 and 0.78. In particular, NNI was well estimated by these fluorescence indices. Moreover, the NSI data improved the accuracy of the N diagnosis.

These results of this study were useful for N nutrition diagnosis and variable fertilization of the cold regional paddy rice, which were significant for the ecological environment protection and the national food security.

## Zusammenfassung

Stickstoff (N), als wichtigstes Element des Pflanzenwachstums und der -entwicklung, spielt eine entscheidende Rolle für die Ertragssicherung. In China wurden jedoch wiederholt Probleme mit der übermäßigen Anwendung von N-Düngemitteln gemeldet, was zu einer geringen N-Nutzungseffizienz und einer hohen Umweltgefährdung führte. Um die Nutzungseffizienz des zugeführten Stickstoffs zu verbessern, werden Strategien entwickelt, welche die Düngung dem Bedarf der Pflanzen sowohl in zeitlicher und räumlicher Dimension anpassen (*Precision Farming*). Dies erfordert die Entwicklung von Technologien zur ortsspezifischen Bestimmung der N-Versorgung in Echtzeit. Die Fernerkundung bietet eine vielversprechende nicht-invasive Methode zur Überwachung des N-Status im Feld, um dann für große Flächen ortsspezifische Düngestrategien abzuleiten. Die in dieser Arbeit vorgestellte Forschung fokussiert darauf, Methoden für die Bestimmung des N-Versorgungszustands von Reispflanzen vorzuschlagen und N-Düngestrategien für Nassreisanbau in kühlen Regionen zu entwickeln. Das Untersuchungsgebiet liegt in Nordostchina. Die wichtigsten Inhalte und Ergebnisse sind wie folgt:

Eine neue kritische N ( $N_c$ )-Verdünnungskurve für Nassreisanbau in kühlen Regionen in Nordostchina wurde entwickelt. Mit dieser Gleichung wird die Verdünnungskurve beschrieben:  $N_c = 27,7W^{-0,34}$  für  $W$  (oberirdische Biomasse)  $\geq 1$  Mg Trockensubstanz (DM)  $\text{ha}^{-1}$  oder  $N_c = 27,7 \text{ g kg}^{-1} \text{ DM}$  für  $W < 1$  Mg DM  $\text{ha}^{-1}$ . Ergebnisse zeigten die Eignung dieser neuen  $N_c$ -Verdünnungskurve für die Bestimmung des N-Status von Japonica-Reis in Nordostchina. Die Validierungsanalyse erzielte gute Ergebnisse für die Bestimmung des N-Status einer 11-blättrigen Reissorte.

Das Potential von FORMOSAT-2 Satellitenbildern für die Bestimmung der N-Versorgung wurde analysiert, um Düngeempfehlungen für das phänologische Stadium des Schossens abzuleiten. Hierzu wurden 50 Vegetationsindizes (VIs) basierend auf FORMOSAT-2-Daten berechnet und die Korrelationen mit im Feld gemessenen agronomischen Parametern (oberirdische Biomasse AGB, Blattflächenindex LAI, N-Konzentration in der Pflanze PNC, N-Aufnahme der Pflanze PNU, Chlorophyllmeter-Daten CM und *Nitrogen Nutrition Index* NNI) analysiert. Der NNI ist definiert als das Verhältnis zwischen der tatsächlichen und der kritischen PNC, gemäß der neu entwickelten  $N_c$ -Verdünnungskurve. Die Ergebnisse zeigten, dass 45% der NNI-Variation mit dem geeignetsten FORMOSAT-2-VI erklärt werden konnten (direkte Methode). Die indirekte Methode, zuerst AGB und PNU mit Hilfe der VIs aus den Fernerkundungsdaten abzuleiten und dann den NNI zu berechnen, erzielte ein besseres Ergebnis ( $R^2 = 0,52$ ). Auf der kritischen N-Aufnahme-Kurve basierend, wurde ein Verfahren zur N-Düngeempfehlung

vorgeschlagen. Dieses nutzt die berechnete Differenz zwischen dem geschätzten und dem kritischen PNU-Wert, um die N-Düngeempfehlungen während der Vegetationsperiode abzuleiten. Die Eignung der FORMOSAT-2-Daten für die Bestimmung des N-Status von Reispflanzen konnte bewiesen werden. Somit lassen sich während der Anbauphase Düngeempfehlungen für Reis in Nordostchina ableiten.

Weiterhin wurde die Eignung von neueren Satellitensensoren mit Spektraldaten im *Red Edge*-Bereich (RE) bewertet, den N-Versorgungszustand von Reis in Nordostchina zu detektieren. Im Feld gemessene hyperspektrale Daten dienten der Simulation der Spektralkanäle von FORMOSAT-2, RapidEye und Worldview-2. Um die Ableitung von N-Status-Parametern zu bewerten, wurden diese Methoden eingesetzt: Analyse von Vegetationsindizes (VI), die stufenweise multiple lineare Regressionsanalyse (SMLR) und die Regressionsanalyse nach der Methode der kleinsten Quadrate (PLSR). Die Ergebnisse zeigten, dass die auf dem RE basierenden VIs aus RapidEye und WorldView-2-Daten mehr Variabilität der N-Indikatoren erklären konnten als die VIs aus den FORMOSAT-2-Daten (ohne Spektralinformation im RE). Außerdem zeigten die Ergebnisse der SMLR und PLSR, dass die Spektralkanäle sowohl im nahen Infrarot als auch im RE wichtig für die Ableitung des N-Status sind.

Der im Feld einsetzbare Fluoreszenz-Sensor Multiplex<sup>®</sup>3 wurde evaluiert, um die Eignung des Fluoreszenz-Spektrums für die Ableitung des N-Status während verschiedener phänologischer Phasen im Nassreisanbau (in kühlen Regionen) zu bewerten. Die Multiplex-Indizes und ihre normalisierten *N sufficient*-Indizes (NSI) wurden verwendet, um fünf N-Status-Indikatoren (AGB, Blatt-N-Konzentration LNC, PNC, PNU und NNI) abzuleiten. Die Ergebnisse weisen darauf hin, dass es starke Beziehungen zwischen den Fluoreszenz-Indizes (z.B. BRR\_FRF FLAV, NBI\_G und NBI\_R) und z.B. LNC, PNC und NNI gibt ( $R^2$ -Werte zwischen 0,48 und 0,78). Insbesondere die NNI-Werte konnten gut aus diesen Fluoreszenz-Indizes abgeleitet werden. Die NSI-Daten verbesserten die Genauigkeit der N-Bestimmung.

Die Ergebnisse dieser Arbeit sind für die Bestimmung der N-Versorgung und damit für die Anpassung der Düngegaben für den Nassreisanbau in kühlen Regionen einsetzbar. So kann ein Beitrag zum Umweltschutz und gleichzeitig zur nationalen Nahrungsmittelsicherheit geleistet werden.

## Acknowledgements

My Ph.D. study at the University of Cologne will soon come to an end and, at the completion of my graduation thesis; I wish to express my sincere appreciation to all those who have offered me help during my doctoral research period.

Firstly, I would like to express my heartfelt gratitude to my supervisor, Ass. Professor Yuxin Miao, from China Agricultural University, and Professor Georg Bareth, from the University of Cologne. I am very grateful to my supervisors for offering the abroad-study opportunity through their project cooperation and create a high-level research platform for me. Without their constant encouragement and guidance, this thesis could not have reached its present form. Ass. Prof. Miao has devoted a lot of time and energy in every step of my research work and thesis, from the selection of research topics, the design, and implementation of the experiments, the writing, and modification of the thesis, and the publication of journal papers. All of these are inseparable from his illuminating instruction. I give my sincere gratitude to Prof. Bareth for his strong support and careful guidance in doctoral research and thesis writing. Ass. Prof. Miao and Prof. Bareth also gave great help and guidance in my life, which warmed and benefited me a lot. I learned not only academics from my supervisors but also their noble spirit. I also owe a special debt of gratitude to Prof. Fei Yuan and Dr. Victoria I.S. Lenz-Wiedemann for their help in articles writing and their valuable suggestions for revision, which has made great progress in my English writing. I want to express my gratitude to Prof. Dr. Karl Schneider for his review of the dissertation and instructive comments. In addition, I would like to thank Prof. Uwe Rascher for his help and support in the study of rice nitrogen stress based on fluorescence remote sensing.

Secondly, I give my hearty thanks to the teachers and colleagues who have worked with me. Thanks to my group colleagues, Qiang Cao, Guangming Zhao, Yinkun Yao, Hongye Wang, Weifeng Yu, Xiaobo Ma, Chuanxiang Tan, Kang Yu, Lei Gao, Jianning Shen, Shanshan Cheng, Shanshan Hu, LinLin Xin, etc. for having a pleasant cooperation with me during my study and work! My thanks would also go to Martin Gnyp, Victoria I.S. Lenz-Wiedemann, Nora Tilly, Juliane Bendig, and others from the University of Cologne. Thanks for their help during my life and study in Germany! Special thanks go to many professors from China Agricultural University and officials from Heilongjiang Land Reclamation, who provided assistance for the smooth progress of this research! And I would also like to thank our cooperating farmers!

Finally, I would like to sincerely thank my family members and my husband Dr. Huichun Ye! It was their support and understanding that gave me courage!

## Table of contents

Abstract .....	i
Zusammenfassung .....	iii
Acknowledgements .....	v
Table of contents .....	vi
List of Figures and Tables .....	ix
Chapter 1: General introduction .....	1
1.1 Preface and introduction .....	1
1.2 Research problems and aims .....	3
1.3 Thesis outline .....	6
Chapter 2: Basics .....	8
2.1 The cold region rice and the study area .....	8
2.1.1 Cold region rice .....	8
2.1.2 Study area .....	9
2.2 Crop critical N dilution curve and application .....	11
2.3 Remote and proximal sensing of crop N status .....	16
2.3.1 Remote Sensing based on reflected electromagnetic radiation .....	16
2.3.2 Fluorescence and their proximal remote sensing .....	24
Chapter 3: A New Critical Nitrogen Dilution Curve for Rice Nitrogen Status Diagnosis in Northeast China .....	26
3.1 Introduction .....	27
3.2 Materials and methods .....	29
3.2.1 Study area .....	29
3.2.2 Field experiments design .....	29
3.2.3 Plant sampling and analysis .....	30
3.2.4 Data analysis .....	32
3.3 Results .....	32
3.3.1 Evaluation of the existing $N_c$ dilution curves .....	32
3.3.2 Development of new $N_c$ dilution curve .....	33
3.4 Discussion .....	36
3.5 Conclusions .....	39
3.6 References .....	40
Chapter 4: Satellite Remote Sensing-Based In-Season Diagnosis of Rice Nitrogen Status in Northeast China .....	43
4.1 Introduction .....	44
4.2 Materials and methods .....	46
4.2.1 Study site .....	46
4.2.2 Field information .....	47
4.2.3 Remote sensing images and preprocessing .....	47
4.2.4 Field data collection and analysis .....	48

4.2.5 Data analysis .....	49
4.2.6 The estimation of NNI .....	51
4.3 Results.....	52
4.3.1 Variability of rice N status indicators .....	52
4.3.2 Vegetation index analysis.....	53
4.3.3 Nitrogen status diagnosis .....	54
4.4 Discussion .....	58
4.4.1 Direct estimation of NNI.....	58
4.4.2 Indirect estimation of NNI .....	58
4.4.3 Applications for rice N status diagnosis and topdressing N recommendation .....	60
4.4.4 Challenges and future research needs .....	61
4.5 Conclusions.....	62
4.6 References.....	63
Chapter 5: Potential of RapidEye and WorldView-2 Satellite Data for Improving Rice Nitrogen Status Monitoring at Different Growth Stages.....	69
5.1 Introduction.....	70
5.2 Materials and methods .....	73
5.2.1 Study area.....	73
5.2.2 Experiment design.....	73
5.2.3 Determining N status indicators with plant sampling and analysis.....	74
5.2.4 Field spectral measurements and re-sampling .....	75
5.2.5 Data analysis .....	77
5.3 Results.....	79
5.3.1 Variability of the N status indicators .....	79
5.3.2 Correlation between N indicators and vegetation indices .....	80
5.3.3 Stepwise multiple linear regression analysis.....	84
5.3.4 Partial least squares regression modeling .....	85
5.3.5 Validation of the estimation models .....	89
5.4 Discussion .....	92
5.4.1 Impacts of growth stages on N status monitoring .....	92
5.4.2 Importance of the red edge and other bands for N status estimation .....	92
5.4.3 Limitations of this study .....	94
5.5 Conclusions and future outlooks.....	94
5.6 References.....	96
Chapter 6: Proximal Fluorescence Sensing for In-Season Diagnosis of Rice Nitrogen Status.....	103
6.1 Introduction.....	104
6.2 Materials and methods .....	106
6.2.1 Experiment design.....	106
6.2.2 Fluorescence measurements.....	107
6.2.3 Plant sampling and measurements .....	108
6.2.4 Statistical analysis .....	109
6.3 Results.....	110
6.3.1 Comparison of the different measurement modes of the Multiplex sensor.....	110
6.3.2 Changes in Multiplex indices (“on-the-go” mode) over growth stages under varied	

---

N supply .....	113
6.3.3 Correlations between Multiplex indices (“on-the-go” mode) and N status indicators ..	115
6.3.4 Validation of the estimation models for N status indicators .....	115
6.3.5 Comparing the Multiplex index-based and the normalized sufficiency index-based N nutrition status diagnosis results.....	119
6.4 Discussion .....	120
6.4.1 Estimation of crop N indicators by fluorescence indices .....	120
6.4.2 Normalized nitrogen sufficiency fluorescence indices.....	122
6.4.3 The application potential and limitations of Multiplex sensor .....	123
6.5 Conclusions .....	124
6.6 References .....	125
Chapter 7: General Discussion.....	131
7.1 N concentration and NNI remote sensing estimation .....	131
7.2 Satellite remote sensing application potential .....	132
7.3 Fluorescence remote sensing application potential .....	134
7.4 Remote sensing-based in-season N management strategies .....	135
7.5 Limitations of the thesis .....	136
Chapter 8: Conclusions and future outlook.....	137
8.1 Conclusions .....	137
8.2 Future outlook .....	138
General References (chapters 1, 2, 7).....	140
Appendix A: Eigenanteil .....	155
Appendix B: Erklärung .....	158
Appendix C: Publication List.....	159

## List of Figures and Tables

Fig. 2-1 The tillering dynamics and corresponding growth stages of a typical 130-day for cold region rice .....	9
Fig. 2-2 The study site is located in Qixing Farm of Sanjiang Plain .....	11
Fig. 2-3 Spectral characteristic of green plants.....	17
Fig. 3-1 Evaluation of the previously established critical N ( $N_c$ ) dilution curves using data from short-season Japonica rice grown under N-limiting and non-N-limiting conditions (Experiments 1-16) in Northeast China .....	33
Fig. 3-2 Critical points used to define the critical N ( $N_c$ ) dilution curve for short-season Japonica rice in Northeast China .....	34
Fig. 3-3 N nutrition index (NNI) of short-season Japonica rice in Northeast China with different N application rates during the growing season in 2013 .....	34
Fig. 3-4 Grain yield of short-season Japonica rice under different N treatments in Experiment 17 conducted in 2013 in Northeast China.....	36
Fig. 3-5 Relationships between relative grain yield (RY) and N nutrition index (NNI) of short-season Japonica rice in the experiments conducted in 2010-2012 in Northeast China at two sites with two cultivars.....	36
Fig. 3-6 Comparison of different critical N dilution ( $N_c$ ) curves for rice.....	37
Fig. 4-1 Selected vegetation indice regression vs. rice aboveground biomass, LAI, plant N uptake, and N nutrition index, Heilongjiang Province, China, 2011-2012.....	56
Fig. 4-2 Relationship between observed and predicted N nutrition index using MCARI-estimated biomass and RVI3-estimated plant N uptake in 2011 and 2012 .....	56
Fig. 4-3 Examples of predicted rice nitrogen nutrition index maps of two fields at pixel-level and plot-level .....	57
Fig. 4-4 Example of a plant N uptake difference map of a farmer's field .....	58
Fig. 5-1 Band response functions for: FORMOSAT-2, RapidEye, and WorldView-2 satellite sensors used in this study .....	76
Fig. 5-2 Relationships between: FORMOSAT-2, RapidEye, WorldView-2-based vegetation indices and aboveground biomass, plant N uptake, N nutrition index, at the panicle initiation, stem elongation, heading, and across all stages.....	81
Fig. 5-3 Comparison of different vegetation indices calculated using FORMOSAT-2, RapidEye and WorldView-2 satellite data for the relationships with aboveground biomass, plant N uptake, and N nutrition index at the panicle initiation and heading stages .....	84
Fig. 5-4 Variable Importance in Projection values as function of wavelengths formatted to FORMOSAT-2, RapidEye, and WorldView-2 spectra for aboveground biomass estimation at the panicle initiation, stem elongation, heading, and across stages.....	88
Fig. 5-5 Variable Importance in Projection values as function of wavelengths formatted to FORMOSAT-2, RapidEye, and WorldView-2 spectra for plant N uptake estimation at the panicle initiation, stem elongation, heading, and across stages .....	89
Fig. 5-6 Variable Importance in Projection values as function of wavelengths formatted to FORMOSAT-2, RapidEye, and WorldView-2 spectra for plant N concentration and N	

nutrition index estimation at the panicle initiation, stem elongation, and heading stages.....	90
Fig. 6-1 Box plots of selected Multiplex indices values for the above canopy, on-the-go, and leaf scale measuring mode at the panicle initiation and the stem elongation stages in 2013 .....	111
Fig. 6-2 Mean value comparisons for each Multiplex index for the three growth stages and each N application rate for variety KY 131 in 2013 .....	114
Fig. 6-3 The relative error values of the validation analysis based on the regression models of the Multiplex indices and the N status indicators at the panicle initiation, stem elongation, and heading stages .....	119
Table 2-1 The critical N dilution curves found in previous literature based on the regression $N_c = aW^{-b}$ ....	15
Table 2-2 Specifications of different satellites .....	22
Table 3-1 Details of the N rate experiments conducted from 2008 to 2013 in the Sanjiang Plain of Heilongjiang Province, Northeast China.....	31
Table 3-2 Critical points selected for establishing the critical N dilution curve for short-season Japonica rice in Northeast China.....	35
Table 4-1 Detailed information about the farmers' fields selected for this study .....	47
Table 4-2 Vegetation indices evaluated in this study for estimating rice N status indicators .....	50
Table 4-3 Descriptive statistics of rice N status indicators for 2011 and 2012 .....	52
Table 4-4 Descriptive statistics of rice N status indicators for different fields .....	53
Table 4-5 The top 10 coefficients of determination ( $R^2$ ) for the relationships between vegetation indices based on the FORMOSAT-2 satellite images and rice N status indicators.....	55
Table 5-1 Details of the nitrogen rate experiments conducted from 2008 to 2011 in Jiansanjiang, Heilongjiang Province, Northeast China.....	74
Table 5-2 The properties of the FORMOSAT-2, RapidEye, and WorldView-2 satellite sensors .....	76
Table 5-3 Vegetation indices evaluated in this study for estimating rice N status indicators.....	78
Table 5-4 Descriptive statistics of the measured aboveground biomass, plant N concentration, plant N uptake, and N nutrition index for the model estimation and validation at the panicle initiation, stem elongation, heading and across stages.....	79
Table 5-5 The top five coefficients of determination ( $R^2$ ) for the relationships between vegetation indices based on the wavebands of FORMOSAT-2, RapidEye, WorldView-2 and aboveground biomass, plant N concentration at the panicle initiation, stem elongation, heading, and across stages.....	82
Table 5-6 The top five coefficients of determination ( $R^2$ ) for the relationships between vegetation indices based FORMOSAT-2, RapidEye, WorldView-2 and plant N uptake, N nutrition index at the panicle initiation, stem elongation, heading, and across stages.....	83
Table 5-7 Stepwise multiple linear regression models based on simulated multi-spectral FORMOSAT-2, RapidEye, WorldView-2 wavebands for estimating aboveground biomass and plant N uptake, N nutrition index, and plant N concentration at the panicle initiation, stem elongation, heading and across stages.....	86
Table 5-8 Aboveground biomass, plant N concentration, plant N uptake, and N nutrition index modeling (calibration subset) by partial least square regression analysis using the wavelengths based on the FORMOSAT-2, RapidEye, WorldView-2 datasets at the panicle initiation, stem elongation, heading and across stages .....	87
Table 5-9 Comparison of the validation results for the best performed vegetation indices, the	

stepwise multiple linear regression models, and the partial least squares regression models for biomass, plant N uptake, N nutrition index, and plant N concentration estimations at the panicle initiation, stem elongation, and heading stages .....	91
Table 6-1 Details of N rates experiments with twice cultivars conducted during 2012-2013.....	107
Table 6-2 Description of the variables and indices recorded by the Multiplex sensor (modified from Table 1 by Zhang <i>et al.</i> , 2012). .....	109
Table 6-3 Significance test (ANOVA) of Multiplex variables measured in three modes: above canopy, “on-the-go”, and leaf scale at the panicle initiation, stem elongation, and heading growth stages for the rice varieties Kongyu 131 and Longjing 21 in 2013. ....	112
Table 6-4 The coefficients of determination ( $R^2$ ) for the linear relationships between standard, and normalized Multiplex indices and N status indicators for two varieties at the panicle initiation, stem elongation, and heading growth stages .....	117
Table 6-5 Equations and coefficients of determination of linear regression models at different growth stages based on the best performing Multiplex index and crop N indicators .....	118
Table 6-6 Agreement and Kappa statistics for different indices and corresponding normalized indices regarding diagnostic results (N Nutrition Index) at different growth stages .....	120



## Chapter 1: General introduction

### 1.1 Preface and introduction

Global agriculture is facing huge challenges in the next decades (Chen *et al.*, 2014). On the one hand, the world population continues to grow in the future, but on the other hand, with the increased living standard, more consumption of animal protein will be demanded (Godfray *et al.*, 2010; Tilman *et al.*, 2011). Therefore, it was forecasted that global demand for the crop would increase by more than 100% by 2050 (Tilman *et al.*, 2011). Rice (*Oryza sativa* L.) is one of the most important crops in the world, and more than two-thirds of China's population relies on rice as the staple food. According to the annual consumption of rice in China, it was estimated that the demand would increase by 30% or more by 2030 (Shen *et al.*, 2013). China is one of the major rice-production countries with an average annual output accounting for 29% of the world (Zhang *et al.*, 2012). One of the major japonica rice producing areas is located in Northeast China. It is called cold regional paddy rice. Due to its sparse population in this area as well as the good taste and good quality, the food commercialization rate of the cold region rice is as high as 75% (Shen *et al.*, 2013). Therefore, it plays an important role in ensuring food security in China. Owing to the expansion of non-arable land, the increase in crop yields has become the only option to ensure global food security.

Nitrogen (N), as the most important element of crop growth and development, is a major component of chlorophyll and plays a decisive role in ensuring yield. Since the Green Revolution (1960s), N fertilizer has made a significant contribution to food security in the past few decades. Owing to the application of N fertilizer, more population are being fed, especially in China. China fed 22% of the population with only 9% of the world's arable land (Zhang *et al.*, 2011). However, this is partly attributed to a 37-fold increase in N fertilizer application, equivalent to 30% of the world's total consumption (Zhang *et al.*, 2012). N fertilizer is also the most important factor for high yield in rice production, next to water (Peng *et al.*, 2002). At the same time, a large amount of N fertilizer was consumed, accounting for 36% of the global rice N fertilizer consumption (Peng *et al.*, 2002; Heffer, 2009). Farmers always tend to apply high rates of N fertilizer in order to obtain a high yield. In addition, the problem of excessive application has become increasingly prominent. The excessive N fertilizer couldn't be absorbed by crops, resulting in the seasonal utilization of N in China being as low as 20%-35%, much lower than that of the world (up to 50%) (Zhu, 1998; Cui *et al.*, 2008; Dobermann, 2007). For example, the agronomic efficiency of N fertilizer for rice is only 11.7 kg kg<sup>-1</sup> in China, much lower than those of developed countries

(20-25 kg kg<sup>-1</sup>) (Zhang *et al.*, 2008; Jin, 2012). The N partial factor productivity (PFP<sub>N</sub>) of rice in China is also as low as 41 kg kg<sup>-1</sup> (Chen *et al.*, 2014). That is lower than other major rice-producing countries in Asia, such as Philippines, Indonesia, and Japan (Cassman *et al.*, 1996, 2002; Peng *et al.*, 2002; Zhang *et al.*, 2012). Excessive N fertilizer can incur many crop growth issues, such as lodging, pests, and diseases, late maturity and mildew problems, etc. It not only results in crop production loss but also affects the product quality. The excessive investment in N fertilizer drives severe ecological and environmental problems, such as eutrophication of surface waters (Le *et al.*, 2010), soil acidification (Guo *et al.*, 2010), greenhouse gas emissions (Zhang *et al.*, 2004), and other forms of air pollution (Liu *et al.*, 2013). Therefore, how to increase yield under limited arable land, while improving N use efficiency and reducing environmental impact is the most critical issue for rice in China.

The low use efficiency of N fertilizer is due to various reasons. The most important one is caused by unreasonable N fertilizer management strategies, which do not match the N supplies well with crop requirements (Fageria & Baligar, 2005). First, a large proportion or excess of N fertilizer is applied at the early stage of crop growth. In Northeast China, farmers usually apply almost all N fertilizers as the base and the first topdressing fertilizer at tillering stage for rice, and rarely topdress them as panicle fertilizers. However, due to the low temperature in early growth stage, rice growth is often inhibited, resulting in the excessive application of N fertilizer that could not be absorbed and increase the risk of environmental pollution (Peng *et al.*, 2015). Peng *et al.* (2015) also demonstrated that by reducing the amount of the base and first topdressing N fertilizer and increasing the panicle or grain fertilizer, the N use efficiency could be greatly improved. Another reason for the low N use efficiency is the overlook of spatial variability in the field and the use of uniform N fertilizer rates. In fact, soil nutrients in the field vary widely (Scharf *et al.*, 2002; Cao *et al.*, 2012), and the variation in optimal N application rates in different fields are large (Cao *et al.*, 2012). Inamura *et al.* (2004) reported that the spatial structural variation and the N absorption accounted for 75.4% and 41.8% of the rice yield variation, respectively. Therefore, matching N fertilizer and crop needs in both space and time, also called precise management, is crucially important. This is the core of precision agriculture. Studies have shown that precision N management strategies can simultaneously achieve dynamic management of N and grantee high yield (Gianquinto *et al.*, 2011), and can improve N use efficiency (Doberman *et al.*, 2002; Miao *et al.* 2009).

In-seasonal N demand can be assessed by its N concentration status at any stage of crop development. This requires the development of real-time and site-specific diagnostic techniques for on-site crop N status to guide the application of N (Cao *et al.*, 2016). The traditional methods for monitoring crop N nutritional status include field investigation, sampling, and biochemical analysis. However, these methods have the disadvantages of time lag, destructiveness, and high cost. Some non-destructive N diagnostic methods, including

the Green Window, leaf color chart, and the chlorophyll meter, have been widely used to assess crop N status and determine N application rate (Thind & Gupta, 2010; Peng *et al.*, 1996). Remote sensing methods have also been developed and implemented to estimate crop N status. Remote sensing refers to a non-contact measurement of electromagnetic radiation that is reflected by the observed object. Remote sensing technology combines mathematical theory with spectral information processing methods and models to obtain real-time monitoring information of soil fertility, crop nutrition, growth status, and other crop parameters, which can provide scientific and precise management foundations for farmland. Satellite remote sensing imagery has great application potential in precision agriculture, due to its ability to obtain the visualization information quickly and accurately over a larger region. Significant progress has been made for satellite remote sensing and a number of satellites can collect imagery with sub-meter resolution, more number of bands, and daily return frequency (Mulla, 2013; Mulla & Miao, 2016). The confusion and uncertainties of the information acquired by the optical remote sensing sensors reduce the sensitivity to the target parameters. Therefore, remote sensing approaches only relevant to target parameters were developed. For example, the Light Detection and Ranging remote sensing can map the shape of an object, and fluorescence remote sensing monitors the chlorophyll conditions. At the same time, the development of combined analysis of different remote sensing technologies is also popular.

To this end, according to the demands of crops, the precision N management strategy by matching N supply in time and space is an important way to reduce the risk of environmental contamination and improve crop productivity and N fertilizer use efficiency. In order to achieve precision N management, N nutrition diagnostic indicators and rapid real-time, high-precision diagnostic methods are necessary.

## 1.2 Research problems and aims

Through the above introduction, we know that in order to improve the use efficiency of N fertilizer and achieve precision management of N fertilizer, it is necessary to develop a real-time management system. The theoretical basis of the system is based on understanding of the demand for crop N nutrition and the realization of in-season crop N nutritional status diagnosis. Plant N concentration (PNC) has long been a commonly used indicator of plant N status (Fageria, 2009). It has been reported that PNC decreased with aboveground biomass during the growing season in dense canopies (Greenwood *et al.*, 1986; Lemaire *et al.*, 2008; Ziadi *et al.*, 2010b), whatever the climatic conditions or the varieties (Lemaire *et al.*, 2005). Generally, the formula 1-1 is used to describe the dilution process of N concentration with increasing shoot biomass during crop growth (Greenwood *et al.*, 1990; Lemaire *et al.*, 2008):

$$N = a W^{-b} \quad (1-1)$$

where,  $W$  stands for aboveground biomass (dry matter, DM) in  $\text{Mg ha}^{-1}$ ,  $N$  stands for plant N concentration in shoots in  $\text{g kg}^{-1}$  DM,  $a$  is the N concentration when  $W$  is  $1 \text{ Mg DM ha}^{-1}$ , and  $b$  is the dilution factor. The minimum PNC that maintains the maximum growth rate of aboveground biomass is called the critical PNC ( $N_c$ ) (Greenwood *et al.*, 1986). During a period of growth, the power function relationship between  $N_c$  and biomass reflects the critical N concentration dilution curve. It has been suggested that species-specific  $N_c$  dilution curves should be developed for more precise diagnosis of plant N status according to each species' histological, morphological and eco-physiological characteristics (Lemaire & Gastal, 1997). The optimal demand for N is the crop N status corresponding to the maximum growth at different growth stages (Ata-Ul-Karim *et al.*, 2017). Therefore,  $N_c$  dilution curves can provide diagnostic criteria. The N nutrition index (NNI) can be derived from the  $N_c$  dilution curve. It is defined as the ratio of the actual measured PNC ( $N_a$ ) over  $N_c$  according to the  $N_c$  dilution curves (Lemaire *et al.*, 2008). NNI can more quantitatively measure the N status of crops, and has become an important indicator of crop N nutrition diagnosis in many studies (Lemaire *et al.*, 2008; Ziadi *et al.*, 2008b; Yue *et al.*, 2012). However, so far, no study has evaluated the existing  $N_c$  dilution curves for rice in Northeast China. Considering the differences in climate and cultivars in Northeast China and other major rice producing areas in China, a new  $N_c$  dilution curve may need to be developed to diagnose rice N status in this region.

NNI has been proved to be a reliable index for diagnosing crop N status than PNC or Plant N uptake (PNU) (Lemaire *et al.*, 2008; Cao *et al.*, 2013; Chen, *et al.*, 2013; Yao *et al.*, 2014; Ly *et al.*, 2017; Ravier *et al.*, 2017; Zhao *et al.*, 2018). However, the calculation of NNI requires destructive sampling and chemical analysis to determine aboveground biomass and PNC, which is costly and time-consuming and, thus, impractical for site-specific N management across large areas. Recently, there is an increasing interest in using proximal and remote sensing technologies to estimate the crop NNI non-destructively (Lemaire *et al.*, 2008; Cao *et al.*, 2013; Yao *et al.*, 2014). Several researchers have successfully used the chlorophyll meter data to estimate the NNI of wheat (Prost & Jeuffroy, 2007; Ravier *et al.*, 2017), and maize (Ziadi *et al.*, 2008b; Zhao *et al.*, 2018), and rice (Yuan *et al.*, 2016; Ata-Ul-Karim, *et al.*, 2016a). Crop canopy sensors, divided into two classes: passive canopy sensors (e.g., Field Spec) and active crop sensors (e.g., GreenSeeker, Crop Circle ACS 470), are more efficient and promising than leaf sensors for estimating crop NNI across large fields (Mistele & Schmidhalter, 2008; Chen *et al.*, 2013; Cao *et al.*, 2016; Xia *et al.*, 2016). However, the data obtained by chlorophyll meter or canopy sensors are point measurements at the leaf or canopy level, which are unsuitable for precision N management across large areas (Miao *et al.*, 2009). Alternatively, aerial and satellite remote sensing offers a promising non-intrusive solution to monitor crop N status and to guide site-specific N recommendations over large areas (Zarco-Tejada *et al.*, 2013; Mulla, 2013; Mulla & Miao,

2016; Maresma *et al.*, 2018). For in-season site-specific N management, a satellite sensor with relatively high spatial resolution is required. In addition, high temporal resolution is also crucially important, as cloudy weather conditions are quite common in most crop planting regions. There is only a narrow time window to collect and process remote sensing images, produce topdressing fertilization prescription, and implement fertilizer applications. The satellite platforms such as FORMOSAT-2, RapidEye, WorldView-2/3/4 offer unprecedented capabilities with more bands and higher spatial and temporal resolutions. So far, little has been reported on rice NNI estimation using satellite remote sensing in Northeast China. Therefore, it is urgent to research and evaluate the potential of using high spatiotemporal resolution satellite data to estimate rice NNI at a key growth stage for guiding panicle N fertilizer application in Northeast China.

Moreover, the optical sensors are influenced by soil and/or water background noises prior to canopy closure. Conversely, saturation in the measured index often occurs under high biomass conditions. The reflectance signals are more related to biomass and leaf area index (LAI) rather than chlorophyll concentration or indirectly PNC, especially before canopy closure, resulting in low diagnosis accuracies (Yu *et al.*, 2013). Fluorescence sensing signals are mainly affected by leaf chlorophyll concentration instead of soil and/or water backgrounds or biomass conditions; hence, they are more related to crop N status (Tremblay *et al.*, 2011; Longchamps & Khosla, 2014). It was therefore hypothesized that fluorescence sensing could be used to estimate N status reliably before canopy closure. In a recent study, Longchamps and Khosla (2014) found that fluorescence sensing could detect N variability as early as the V5 stage of maize, and was not influenced by soil background. In another study, Li *et al.* (2013) found fluorescence sensor parameters were highly related to chlorophyll meter readings in rice. Padilla *et al.* (2016) indicated that the fluorescence indices of chlorophyll and flavonols contents, such as the simple fluorescence (SFR) and the flavonol index (FLAV), and the ratio of the chlorophyll to flavonols contents, defined as the balance index (NBI), could be used as reliable indicators of crop N status in autumn and spring cucumber crops. Therefore, proximal fluorescence-based sensors are also promising tools for monitoring rice N status in Northeast China.

For modern precision agricultural production, it is essential to carry out remote sensing-based early crop N diagnosis and N management strategies. In this dissertation, I focused on the research of N nutrition diagnosis and N management strategy for cold region paddy rice in Northeast China. Through conducting the experiments based on multi-source remote sensing technologies, this study aims to further clarify diagnostic criteria of N nutrition in cold paddy rice, establish N nutrition diagnosis methods based on proximal and satellite remote sensing technologies, and promote precision N management strategies. This is of great significance for achieving the protection of the ecological environment while ensuring national food security.

### 1.3 Thesis outline

This thesis focuses on the topic of N nutrition status diagnosis and precision N management for rice in Northeast China. It consists of eight chapters. The first chapter introduces the research background and scientific issues and summarizes the outline of the thesis. The second chapter mainly presents the theoretical basis of the research content covered in Chapters 3 through 6, which are the main chapters of the thesis and are published as peer-reviewed journals or conference articles. Finally, Chapter 7 provides a general discussion of the results. Chapter 8 summarizes the main conclusions of this study and the outlook for future research. The contents of Chapters 3-8 are briefly summarized as follows:

Chapter 3 evaluates the previously developed  $N_c$  dilution curves for rice in Northeast China and presents a more suitable  $N_c$  dilution curve in this region. As the results indicated that none of the two previously developed  $N_c$  dilution curves was suitable to diagnose N status of the short-season Japonica rice in Northeast China. A new  $N_c$  dilution curve was developed, and it worked well for N status diagnosis according to the validation result.

Chapter 4 investigates the potential of using FORMOSAT-2 satellite images to diagnose rice N status and guide topdressing N application at the stem elongation stage in Northeast China. Based on the FORMOSAT-2 imagery, a total of 50 vegetation indices (VIs) were computed and correlated with field-based agronomic variables. In addition, the study compares the direct and indirect NNI estimation approaches. Finally, based on the critical N uptake curve which was derived from the  $N_c$  dilution curve which established in Chapter 3, a topdressing N recommendation method for rice of Northeast China was developed.

Chapter 5 evaluates the potential improvements of the newest satellite sensors, RapidEye and WorldView-2, for rice N status monitoring. The canopy-scale hyperspectral data were upscaled to simulate the wavebands of RapidEye and WorldView-2. The simulated FORMOSAT-2 wavebands were used as the reference for comparison. VI analysis, stepwise multiple linear regression (SMLR), and partial least squares regression (PLSR) were performed to derive plant N status indicators. The results indicated that the VIs based on the red edge band of RapidEye and WorldView-2 data explained more variability for N indicators than their FORMOSAT-2-based counterparts did. Moreover, the SMLR results revealed that both the near-infrared and red edge band were important for N status estimation. The PLSR analysis confirmed the significance of the NIR band. Overall, both the RapidEye and WorldView-2 data with red edge band improved the results relative to FORMOSAT-2 data.

Chapter 6 explores the potential of using proximal fluorescence sensor (Multiplex<sup>®</sup>3) to estimate N status at different growth stages for rice in the cold region. The most suitable Multiplex measurement mode was identified. The results indicated that different N application rates significantly affected most of the fluorescence indices, especially the

simple fluorescence ratios (SFR\_G, SFR\_R), blue-green to red fluorescence ratio (BRR\_FRF), flavonols (FLAV), and N balance indices (NBI\_G, NBI\_R). There were strong relationships between the fluorescence indices (BRR\_FRF, FLAV, NBI\_G, and NBI\_R) and N indicators, with coefficients of determination ( $R^2$ ) values between 0.40 and 0.78. In particular, NNI was well estimated by these fluorescence indices.

Chapter 7 generally discusses the objectives and results of this thesis, and focuses primarily on (1) N concentration and NNI estimation using remote sensing, (2) satellite and fluorescence remote sensing application potential, (3) fluorescence remote sensing data fusion for crop N monitoring, (4) remote sensing-based in-season N management strategies, and (5) the limitation of the thesis.

Chapter 8 summarizes the dissertation and provides an outlook for future research.

## Chapter 2: Basics

### 2.1 The cold region rice and the study area

#### 2.1.1 Cold region rice

The cold region rice is planted in the area north of latitude 43°N of the permafrost region, which is also one of the most northern paddy areas in the world. In China, it mainly refers to Heilongjiang Province (43°26'-53°33'N) located in the Northeast. The Japonica rice, which is adapted to the cooler climate, is also grown in the same high latitude in other countries, such as Japan and Russia (Leff *et al.*, 2004). Heilongjiang Province is located in the temperate zone and the cold temperate zone. The average annual temperature is less than 1 °C. Temperature is one of the primary considerations in arranging the agricultural planting systems. Heilongjiang Province is divided into six zones based on the accumulated active temperature, i.e., the duration of the daily average temperature higher than 10 °C. Their corresponding accumulated temperature ranges refer to above 2700 °C, 2500-2700 °C, 2300-2500 °C, 2100-2300 °C, 1900-2100 °C, and less than 1900 °C, respectively. Adapted to the local temperature conditions, most of the varieties bred for the cold region rice are 9-14 leaves on the main culm with a 2150-2700 °C accumulated temperature requirement. The growth duration for cold region rice is approximately 120-145 days from emergence to maturity when cultivated in the appropriate area (Data source: China Rice Data Center). In order to increase more accumulated temperature, a two-stages cultivation technique, including greenhouse seedling cultivation and field cultivation, was adopted for the cold region rice. Li *et al.* (2005) showed that the two-stages cultivation technique broke the limitation of the short frost-free period in northern cold areas, which can increase the accumulated temperature by more than 150-200 °C. When three-four leaves emerge on seedlings, good quality seedlings will be transplanted in the field.

From the germination to maturity, the cold region rice has three main growth stages: vegetative, reproductive, and ripening. The vegetative stage covers a period from germination to panicle initiation; the reproductive stage is from panicle initiation to heading; and the ripening period refers to heading to maturity. After transplanting, rice begins to grow tillers. With the increase in the number of primary tillers, more tillers develop explosively, and then reach the maximum number at the stem elongation stage. The effective tillers develop before the panicle initiation stage. That is because the tillers formed after the panicle initiation will gradually die instead of mature eventually, and they are defined as invalid tillers. Therefore, from the stem elongation to the heading growth stage, the number of tillers

gradually declines, and finally reaches a stable level until maturity. The start of the panicle initiation stage marks the beginning of the reproductive growth period. However, at this point, the tillering has not yet completed. Therefore, there is an overlapping period of the vegetative and the reproductive growth stages, which begins from the panicle initiation and ends at the stem elongation growth stage. This is an important period for topdressing N application. Fig. 2-1 summarizes the tillering dynamics and the corresponding growth stages of a typical 130-day for cold region rice (Fig. 2-1). Although there is a large difference among different rice varieties, the days of growth range from 120 to 145 days. It generally takes 30 days from the beginning of panicle initiation to heading and approximately 30-40 days from heading to maturity. The time required for the different cultivars in these two periods is not much different, and the main difference in the growth period is the length of the vegetative stage (Yoshida, 1981).

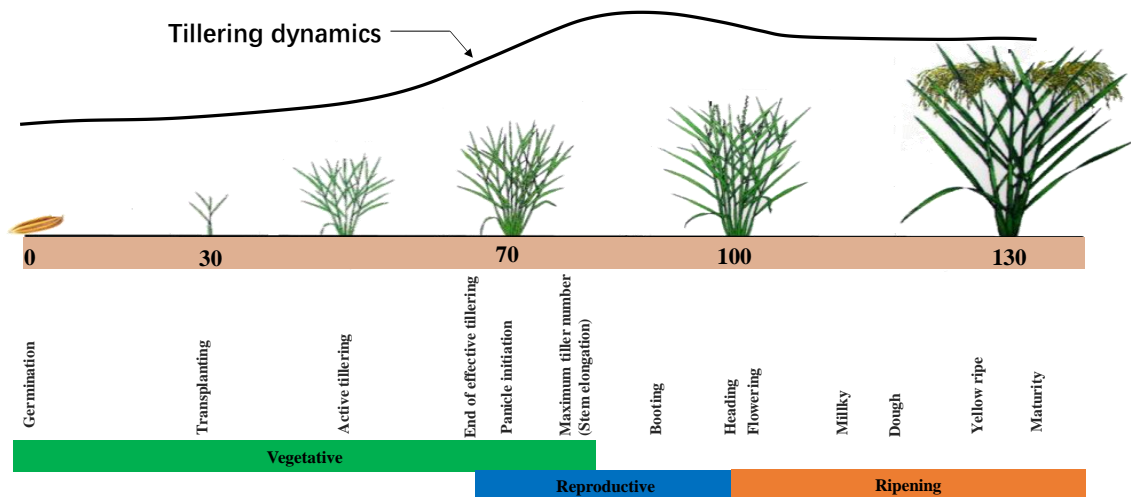


**Fig. 2-1** The tillering dynamics and corresponding growth stages of a typical 130-day for cold region rice

### 2.1.2 Study area

Over the past three decades, China's rice cultivation structure has undergone major adjustments due to the factors of economic efficiency and consumer demand. The production area of paddy rice showed a clear shift from South China to North China: the sown area in various southern provinces has continued to decrease, while the planting area in northern provinces has increased nearly 1.5 times (Wang, 2011). In particular, the cultivation area of rice in Northeast China has increased the fastest, from 0.85 million hectares in 1980 to 4.55 million hectares in 2016. It dominates roughly 15.1% rice planting area of China (National Bureau of Statistics 2017), equating to approximately 1.96% rice cultivation area of the world. Among them, Heilongjiang Province has now become the largest province of

rice cultivation in North China. In 2016, the rice area of Heilongjiang Province reached 3.20 million hectares (National Bureau of Statistics 2017). Due to the sparse population of Heilongjiang Province, its per capita acreage is three times more than the national average, reaching 0.66 hectares. Therefore, it is an important commodity grain base, which provides more than 70% grain commodities (Jiang *et al.*, 2014). Now, Heilongjiang strongly supports China's food security (Yu, 2014).

Heilongjiang Province, as a major area for the production of cold paddy rice, has important advantages in climatic and geographical conditions. The province's sunshine hours are between 2300 and 2800 hours, of which the growing season (from May to September) sunshine hours accounts for 44%-48%. In the growing season, the sunshine duration is generally above 14 hours and the sunshine percentage is above 50%, which is significantly higher than that in the southern rice cropping area. The annual total solar radiation is between  $40 \times 10^8$  and  $50 \times 10^8$  joules per square meter, of which the total solar radiation from May to September accounts for 54%-60%. The diurnal temperature variation of the growing season ranges from 6 to 8 °C, while the annual diurnal temperature difference is above 10-12 °C. The larger temperature difference is beneficial for accumulating photosynthetic products, which is a good foundation for obtaining high yield. The rainy season in Heilongjiang Province dominates the crop growing season. The average annual precipitation in the province is mostly between 400-650 mm, and the growing season accounts for 80%-90% of the total. The frost-free period in the province lasts 100-160 days. The initial frost in most areas of Heilongjiang Province appears in late September, and the final frost ends in late April or early May. Heilongjiang Province has fertile soil, which belongs to one of the three black soil belts in the world. Composed of alluvial soil, the main soil types in the vast plain include black soil, chernozem, meadow soil, and other fertile soils. These soils are rich in humus with organic matter content of 1.24%-3.42%. Heilongjiang Province has rich water resources. There are four major river systems—Heilong River, Songhua River, Ussuri River, and Suifen River, and three major lakes—Xingkai Lake, Jingpo Lake, and Wudalianchi Lake, and other 1918 rivers and streams, as well as 640 lakes. The run-off of the whole province is 65.58 billion cubic meters. The total groundwater volume is 26.23 billion cubic meters. It has the most abundant water resources in the fourteen north provinces. Due to its location of high latitude tundra, the frequency of pests and diseases is low. Therefore, in the production areas of Heilongjiang Province, rice yield maintains at a relatively high level. In addition, it is the high-quality production area for japonica rice with an optimum quality rate higher than 70%. Nowadays, the cold region rice has become a favorite main food for high-level consumers due to its good quality, and it is the major source of high-grade rice for export abroad.

Our study site is located in Qixing Farm, Jiansanjiang Branch Bureau (132°31'26"-134°22'26"E, 46°49'47"-48°12'58"N), which belongs to the fourth accumulated temperature

zone in Sanjiang Plain, Heilongjiang Province (Fig. 2-2). The Sanjiang Plain is formed by the Heilongjiang, Songhua and Ussuri River basins. A hundred years ago, the Sanjiang Plain was mainly composed of native grassland, wetlands, and other ecosystems (Gao *et al.*, 2018). Nearly 80% of the wetlands have been reclaimed as farmland in recent decades at the plain (Gao *et al.*, 2018). Today, there are 15 large and medium-sized state-owned farms in the Jiansanjiang Branch Bureau with a total area of  $1.22 \times 10^4$  km<sup>2</sup>, of which 85% is for agricultural land. It mainly grows rice, corn, soybeans, wheat, and other economic crops, of which rice accounts for about two-thirds of the planting area. The annual average temperature of Jiansanjiang is 1-2 °C, and the annual rainfall is 500-600 mm, of which the rainfall in the crop growing season accounts for 60%-70%. The frost-free period is approximately 110-135 days. The total sunshine hours for a year are 2300-2600 h.

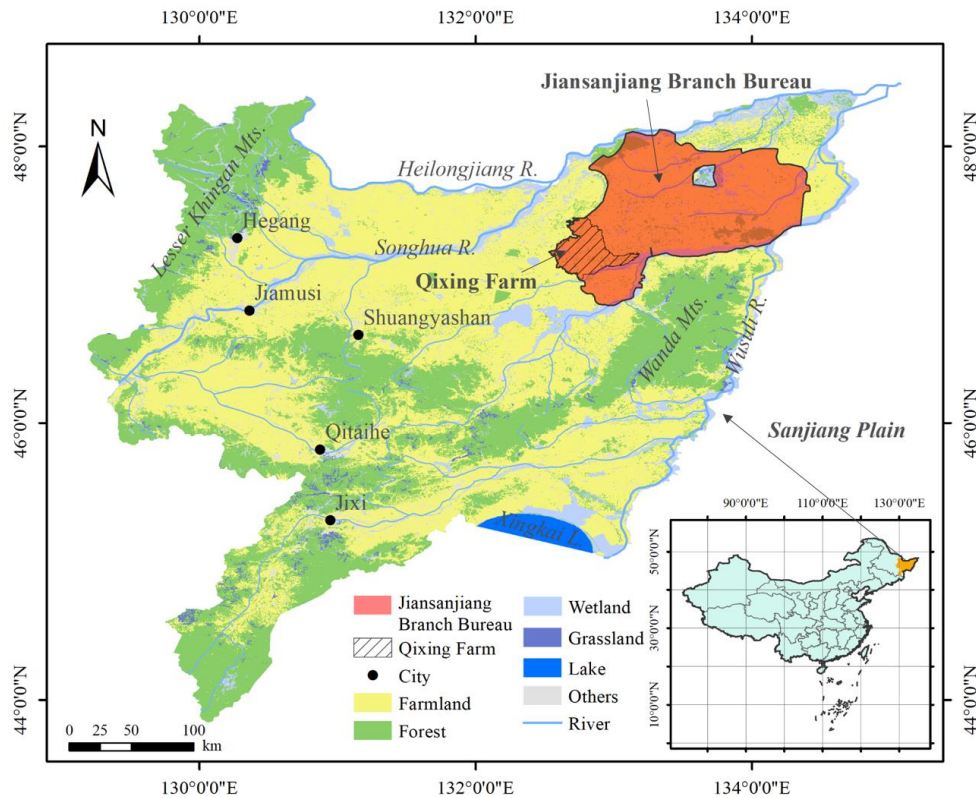


**Fig. 2-2** The study site is located in Qixing Farm of Sanjiang Plain.

## 2.2 Crop critical N dilution curve and application

In dense canopy, the N concentration in plants gradually decreases due to crop growth and light competition. Even when ample N is supplied, it does not change the declining trend of the N concentration. This is due to the non-uniform leaf N concentration in the canopy and the increasing proportion of structures and storage tissues containing lower N concentration (Hirose & Werger, 1987; Pons & Percy, 1994; Plénet & Lemaire, 1999). The

ubiquitous dilution can be expressed as a negative power function, known as a "dilution curve" (Greenwood *et al.*, 1986; Greenwood *et al.*, 1990). The researchers found that, although climate variability can lead to large variation in yield potential, crop uptake of N and mineralization of N in soils at different years, the decreasing rate of N concentrations with increasing biomass for the grasses and Lucerne are very close between years (Lemaire & Salette, 1984a, b; Lemaire *et al.*, 1985). The inter year-stable for N dilution curve indicates that it may be more suitable for precision N management.

The critical N dilution curve is defined in the following function:

$$N_c = a'W^{-b'} \quad (2-1)$$

where,  $N_c$  is the minimum N concentration in plants needed for maximum growth rate of the crop (Ulrich, 1952).  $a'$  and  $b'$  are estimated parameters for the critical N dilution curve. Due to differences in the cumulative rate of crop biomass at different growth stages, the crop's demand for N changes. Therefore, the optimal amount of N required for maintaining the maximize growth rate at each stage of growth is different. The critical N dilution curve consists of a series of critical N concentrations and their corresponding shoot biomass of the entire growth period. According to the concept of the N critical dilution curve, the N status can be identified as sub-optimal or supra-optimal by comparing the N concentration below or above the curve under a given biomass. Therefore, the critical N concentration is the basis of the diagnosis of crop N status.

Nitrogen Nutrition index (NNI), proposed by Lemaire *et al.* (1989), which can be expressed as:

$$NNI = \frac{N_a}{N_c} \quad (2-2)$$

NNI is an ideal indicator for crop N nutrition diagnosis because it can quantify the intensity of crop N deficiency or excess (Lemaire & Gastal, 1997). When  $NNI > 1$ , it indicates that the N fertilizer is excessive; when  $NNI = 1$ , it indicates that the N fertilizer is optimal; when  $NNI < 1$ , it indicates insufficient N nutrition.

In addition, similar to the critical N concentration curve, the minimum N content necessary to achieve the maximum crop growth rate can also be calculated as:

$$CN_{up} = a'W^{1-b'} \quad (2-3)$$

where the  $CN_{up}$  stands for critical N uptake expressed in  $\text{kg ha}^{-1}$ . Formula 2-3 can be named as the critical N uptake curve. Through the critical N uptake curve, the N requirement of crops can be accurately estimated and dynamically analyzed.

Greenwood *et al.* (1990) proposed a procedure for identifying critical data points of N that has been widely used for establishing N critical dilution curve (Yue *et al.*, 2014; Sheehy *et al.*, 1998; Ziadi *et al.*, 2010a). Justes *et al.* (1994) proposed a more accurate procedure for

establishing N critical dilution curve based on multi-year-site N fertilizer experiment, but the method required a larger dataset. Herrmann and Taube (2004) improved the procedure of Justes *et al.* (1994) by determining the critical N concentration point based on the quadratic plus platform regression method. The Herrmann and Taube (2004)'s procedure could avoid the situation that the curve cannot be established when the gradient of N application rate is too small to be discriminated, and when the data set is too small to calculate the regression line. After more than two decades of development, a series of critical N dilution curves for food and cash crops have been established, such as maize (*Zea mays* L.) (Plénet & Lemaire, 1999; Herrmann & Taube, 2004; Yue *et al.*, 2014), rice (*Oryza sativa* L.) (Sheehy *et al.*, 1998; Ata-U-Karim *et al.*, 2013), winter wheat (*Triticum aestivum* L.) (Justes *et al.*, 1994; Yue *et al.*, 2012), spring wheat (*T.aestivum* L.) (Ziadi *et al.*, 2010a), winter barley (*Hordeum vulgare* L.) (Zhao, 2014), potato (*Solanum tuberosum* L.) (Bélanger *et al.*, 2001; Abdallah *et al.*, 2016), oilseed rape (*Brassica napus* L.) (Colnenne *et al.*, 1998), beet (*Beta vulgaris* L. *ssp.* *Vulgaris*) (Chakwizira *et al.*, 2016) and so on (Xue *et al.*, 2007). Table 2-1 summarizes the critical N concentration curves for major food crops and some cash crops.

From Table 2-1, C4 plants (maize) have lower parameter  $a$  values than C3 plants (wheat, rice, barley, potatoes, etc.). This confirms the observation of Greenwood *et al.* (1990), who determined the critical N dilution curves for the C4 and C3 crops using the equations  $N_c = 41.0W^{-0.50}$  and  $N_c = 57.0W^{-0.50}$ , respectively. In general, C4 crops have lower parameter  $a$  values than C3 crops, because of the lower metabolic protein requirements for C4 crops than C3 (Greenwood *et al.*, 1990). The  $b$  values of the critical N concentration curves of potato and beet are relatively high, because the plant N concentration will decrease faster due to the accumulation of stored material such as tuber or root (Bélanger *et al.*, 2001; Abdallah *et al.*, 2016; Chakwizira *et al.*, 2016; Lemaire & Gastal, 1997). For C3 crops, the coefficients of the critical N concentration curves of various species are all different, indicating interspecies differences (Table 2-1). Although there are differences in climatic conditions, the critical N concentration curves for spring maize established in France and Germany are very close (Plénet & Lemaire, 1999; Herrmann & Taube, 2004). Moreover, Ziadi *et al.* (2008a) also confirmed that the critical curve was able to distinguish N-limiting from non-N-limiting group in Canada. However, under different climatic zones, crops may undergo some morphological changes in order to adapt to the climate. Therefore, in some cases, the critical N concentration curve of the same species in a region does not apply to another region (Yue *et al.*, 2012, 2014). In order to diagnose N status more accurately, each species should develop critical N dilution curves based on morphological and ecophysiological characteristics (Lemaire & Gastal, 1997).

NNI is one of the most widely used tools for in-season N nutrition diagnosis and precision N management (Lemaire *et al.*, 2008; Yuan *et al.*, 2016). It is a precise and specific

indicator, which can effectively distinguish deficiency, optimal or luxury of N status during the entire growth period, and can quantitatively describe the degree of excess or deficiency. The NNI can be used for various crops. In addition, this variable is very robust and does not depend on variety or soil and weather conditions (Justes *et al.*, 1994; Lemaire & Gastal, 1997). Significant relationships between NNI and relative yield of wheat, maize, and rice were observed in previous research (Ziadi *et al.*, 2010a; Ziadi *et al.*, 2008b; Ata-Ul-Karim *et al.*, 2016b). NNI can also be used to interpret the response of crops to N nutrition, and continuous observations can trace back the N supply condition during crop growth (Lemaire *et al.*, 2008). Lemaire and Meynard (1997) used NNI as a diagnostic tool for analyzing agronomic data of the trials in order to account for yield differences. Although NNI is the reflection of the instantaneous N status, the calculation of its persistent deficit over a period of time can be used to interpret the N supply status of the crop during the entire growth period, thus explaining the difference in yield. The supply of N to the critical organ formation period can also explain the yield components. Jeuffroy and Bouchard (1999) used the extent and duration of NNI deficiency during anthesis to explain the relative grain number differences in wheat. Justes *et al.* (1997) explained the differences in grain protein content.

**Table 2-1** The critical N dilution curves found in previous literature based on the regression  $N_c = a'W^{-b'}$ , where  $N_c$  is the critical shoot N (g kg<sup>-1</sup>) and  $W$  is the shoot biomass dry weight (t ha<sup>-1</sup>),  $a'$  and  $b'$  are coefficients of the regression.

Species	Location	Critical N Dilution Curve	Plant sampling period	References
Spring maize	Southwest of France	$N_c = 34.0W^{-0.37}$	Emergence to silking stage	Plénet & Lemaire (1999)
Spring maize	Northern Germany	$N_c = 34.1W^{-0.39}$	Early vegetative to silage	Herrmann & Taube (2004)
Summer maize	North China Plain, China	$N_c = 27.2W^{-0.27}$	V6 to milk stage (R3)	Yue <i>et al.</i> (2014)
Rice	Philippines, China, and Australia	$N_c = 52.0W^{-0.52}$	-	Sheehy <i>et al.</i> (1998)
Rice (Japonica)	Jiangsu Province, China	$N_c = 35.3W^{-0.28}$	Tillering to anthesis stage	Ata-Ul-Karim <i>et al.</i> (2013)
Winter wheat	Northern France	$N_c = 53.5W^{-0.44}$	Tillering to anthesis stage	Justes <i>et al.</i> (1994)
Winter wheat	North China Plain, China	$N_c = 41.5W^{-0.38}$	Tillering to anthesis stage	Yue <i>et al.</i> (2012)
Spring wheat	Québec, Canada	$N_c = 38.5W^{-0.57}$	27 to 96 days after seeding	Ziadi <i>et al.</i> (2010a)
Winter barley	Jiangsu and Henan Province, China	$N_c = 47.6W^{-0.39}$	Feekes 3 to Feekes 10.51	Zhao, 2014
Potato	Belgian	$N_c = 53.7W^{-0.45}$	From June to August	Abdallah <i>et al.</i> (2016)
Potato (Cultivar1)	New Brunswick, Canada	$N_c = 45.7W^{-0.42}$	From July to August	Bélangier <i>et al.</i> (2001)
Potato (Cultivar2)	New Brunswick, Canada	$N_c = 50.4W^{-0.42}$	From July to August	Bélangier <i>et al.</i> (2001)
Oilseed rape	France	$N_c = 44.8W^{-0.25}$	Three-leaf to anthesis stage	Colnenne <i>et al.</i> (1998)
Beet	New Zealand	$N_c = 49.0W^{-0.52}$	Emergence to harvest	Chakwizira <i>et al.</i> (2016)
Cotton	Henan Province, China	$N_c = 49.7W^{-0.13}$	Initial flowering to boll-opening stage	Xue <i>et al.</i> 2007
Cotton	Jiangsu Province, China	$N_c = 43.0W^{-0.13}$	Initial flowering to boll-opening stage	Xue <i>et al.</i> 2007

## 2.3 Remote and proximal sensing of crop N status

Remote sensing refers to the technique of non-contact measurement of electromagnetic wave signals (e.g. visible light, infrared, microwave, etc.) of target objects by various sensors. According to the mechanism of electromagnetic waves and surface objects, the characteristics of the objects and their change information can be analyzed. Remote sensing integrates a number of disciplines such as spectroscopy, physics, informatics, geography, earth science, ecology, and so on. Nowadays, remote sensing has a wide range of applications and far-reaching significance in agriculture. Currently, remote sensing measurement platforms include satellites, aircrafts, unmanned aerial vehicles (UAV), and proximal equipment (tractors or hand-held devices). Multi-spectral and hyperspectral remote sensing are commonly used techniques. In addition to reflection, transmission, and absorption, plant leaves can also emit energy through fluorescence or thermal emission (Mulla, 2013). This section will introduce the principle and research basis of remote sensing in crop N information extraction, as well as the progress in remote sensing research at different levels and different research methods.

### 2.3.1 Remote Sensing based on reflected electromagnetic radiation

#### 2.3.1.1 Spectral characteristic of green plants

The differences in the degree of absorption and emission changes of various targets, lead to different spectral reflectivity. The reflectance spectral curve of vegetation has apparent fluctuation, with multiple peaks and valleys in the wavelength range of 350-2500 nm (Fig. 2-3). The influence of leaf structure, pigments, and water within the leaves determine reflected the energy of plants. As shown in Fig. 2-3, in the visible spectrum (400-700 nm), the reflectance and transmittance rates are very low, while the absorptance is high. Due to the strong absorption of plant pigments, especially the chlorophylls, two absorption valleys are formed in the bluish (400-500 nm) and reddish (600-700 nm) wavelength regions. Thus, the vegetation with chlorophyll appears green as a result of its minor reflectance peak at the green spectrum of 500-600 nm. Reflectance increases dramatically near the red edge, around 700 nm wavelength, which is a typical feature of green plants and, unlike other objects, can be used to monitor the status of crop growth. In the near-infrared (NIR) spectrum (700-1100 nm), the reflected energy from healthy plants can be as high as 50% due to the effects of cell structure. The shortwave and mid-infrared spectrum (1100-2500 nm) can also be used to study selected features of plant structure: carotenoids, protein, starch, and cellulose, which absorbs energy at 2104 nm wavelength. Additionally, leaf water content leads to strong absorption characteristics around 1450, 1840 and 2700 nm (Orych *et al.*, 2014). The magnitudes of spectral reflectance of different plants are different. The changes and

differences of spectral reflectance are the basis of monitoring plant growth and other parameters, as well as the basis of vegetation remote sensing (Li, 2008).

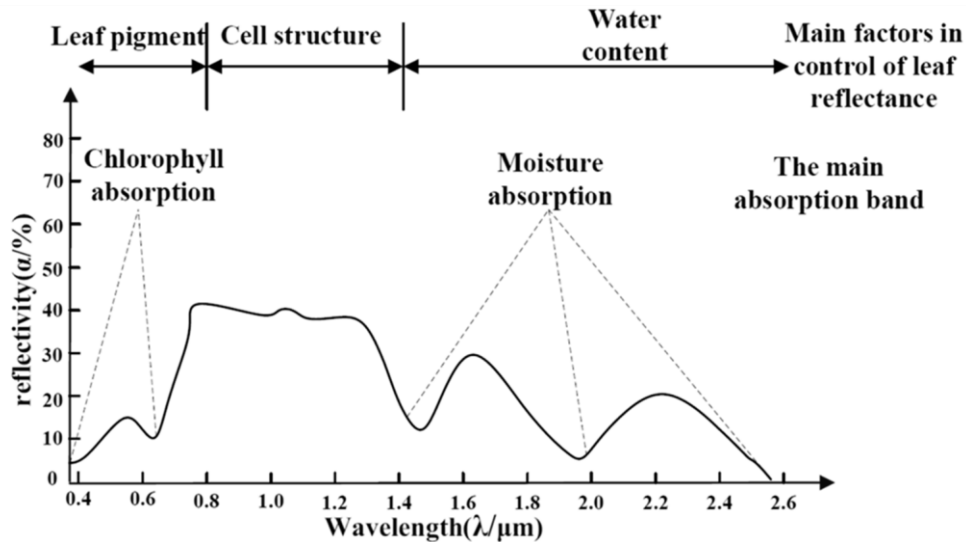


Fig. 2-3 Spectral characteristic of green plants (modified from Li, 2008)

### 2.3.1.2 Remote sensing diagnosis of crop N nutrition: mechanism and approaches

N nutrition not only directly affects the constitution and content of chlorophyll in crops but also has a significant effect on the leaf area index (LAI) of crops. Due to the absorption and reflection characteristics of chlorophyll in the visible region, and the high reflectivity of vegetation leaves in the NIR region, different chlorophyll content and LAI will affect the amount of radiation. Therefore, the N nutrition status of the crop as indicated by chlorophyll content and LAI can be estimated by detecting the spectral response of the crop canopy. Noura *et al.* (2009) found that the spectral characteristics of leaves in rice under N deficiency were significantly different from those in normal nutrition conditions, and the difference of chlorophyll content was the main intrinsic factor leading to differences in spectral characteristics. Numerous studies have also shown that there is a good correlation between N and chlorophyll (Baret *et al.*, 2006; Schlemmer *et al.*, 2013; Peng *et al.*, 2017). Remote sensing applied to crop N nutrition diagnosis is based on the quantitative estimation of agronomic parameters, such as the relationship of remote sensing information and the green LAI, the chlorophyll content, biomass, and N uptake, etc. The improvement of instruments and the development of relationships between reflectance and plant properties have enhanced quantification of agronomic parameters. Remote sensing technology has been widely used in crop N nutrition diagnosis and monitoring in recent years and has made great progress. The quantitative remote sensing methods applied to N nutrition estimation are mainly realized by screening sensitive bands, and using the selected bands in vegetation

indices, statistical methods, and physical models.

### 1) Crop N Nutrition Diagnosis Based on Sensitive Spectrum, Vegetation Index, and Statistics Analysis

Plant remote sensing depends on the measured spectral properties of leaves and canopies. Remote sensing quantification of leaf N nutrition status is generally achieved indirectly through estimation of plant chlorophyll concentration or content. By observing the spectral responses under a range of chlorophyll concentrations, it was found that the leaf reflectance increased with the decrease of leaf greenness or chlorophyll content in the visible spectral region (Hatfield *et al.*, 2008). However, the blue light band (400-500 nm) has no advantage in distinguishing different chlorophyll concentrations due to its strong absorption of chlorophyll (Gitelson & Merzlyak, 1994, 1996). The strong absorption characteristics of the red light band (around 670 nm) makes the reflectance highly correlated with the chlorophyll concentration below 100 mg/m<sup>2</sup>, while when the chlorophyll concentration is higher than 100 mg/m<sup>2</sup>, the red wavelength does not change with the increase of chlorophyll concentration (Gitelson & Merzlyak, 1996; Hatfield *et al.*, 2008). Green (530-590 nm) and red edge (around 690-730 nm) do not saturate under very high chlorophyll concentration and show high sensitivity to chlorophyll changes (Chappelle *et al.*, 1992; Gitelson & Merzlyak, 1994). Many studies have shown that the most important spectral bands for predicting N value are located in visible, NIR and red edge regions (Clevers & Kooistra, 2012; Li *et al.*, 2014b). However, the role of the green and red edge band in estimating N is gradually being appreciated. Horler *et al.* (1983) were among the first to show the importance of the red edge inflection point for detecting plant stress. Since then, the red edge band has often been used to estimate chlorophyll or N content (Clevers *et al.*, 2002; Dash & Curran, 2004; Cho & Skidmore, 2006; Clevers & Kooistra, 2012; Clevers & Gitelson, 2013; Clevers *et al.*, 2017).

Based on the study of sensitive wavelengths, vegetation indices are also widely used for monitoring vegetation conditions. A vegetation index (VI) refers to the mathematical combination of specific bands. The purpose of using VIs is to reduce the impact of environmental backgrounds (such as soil, atmosphere, sun-target-sensor geometry), and to improve the sensitivity of remote sensing data to target parameters (Moulin, 1999; Gitelson, 2013). The earliest constructed VIs, such as the Simple Ratio Index (RVI, Jordan, 1969), is the ratio of NIR and red reflectance, whereas the Normalized Difference Vegetation Index (NDVI, Rouse *et al.*, 1973) is the difference between the NIR and red reflectance values divided by their sum ( $NDVI = \frac{R_{nir} - R_{red}}{R_{nir} + R_{red}}$ ). They are the most commonly used VIs for satellites remote sensing. Over the past four decades, Landsat Thematic Mapper (TM) imagery-derived NDVI and other broadband VIs have been widely used to quantify crop variables such as biomass, LAI, plant height, and grain yield (Tucker, 1979; Wiegand *et al.*, 1992; Thenkabail *et al.*, 1994). The progress in the diagnosis of N nutrition by satellite and

aerial remote sensing technologies will be described in more detail in the next section. By developing new VIs and narrow-band VIs, more theoretical and field work has further improved the relationships between VIs and physiological parameters such as vegetation coverage, biomass, and LAI. At the same time, they can also reflect the N and chlorophyll content (Hansen & Schjoerring 2003; Eitel *et al.*, 2008; Yu *et al.* 2013).

In recent years, the red edge band has gradually received increasing attention in the estimation of N, so has the VIs based on the red edge band. The VIs using red edge band instead of red band can explain more variations in N nutrition indicators (Dong *et al.*, 2015). The red edge region has proven to be highly important in estimating chlorophyll or N content (Clevers *et al.*, 2002; Dash & Curran, 2004). Barnes *et al.* (2000) derived the Canopy Chlorophyll Content Index (CCCI), which combines NDVI and Normalized Difference Red Edge index (NDRE). Rodriguez *et al.* (2006) found CCCI explained up to 69% variation in N content in dryland wheat, regardless of crop moisture status and crop cover. Fitzgerald *et al.* (2010) used the three bands near the red edge to construct a canopy CCCI to predict the N nutrition status of the wheat canopy.

Linear stepwise regression is the most commonly used statistical model for spectral-based vegetation research. It uses spectral data or their transformed forms as independent variables to estimate plant physical and biochemical parameters and thus establish regression empirical models. According to the number of independent variables, they can be divided into a one-dimensional linear regression model and a multiple linear regression model. In reality, a biochemical parameter is usually not only sensitive to one band, but to multiple bands. Therefore, Stepwise Multiple Linear Regression (SMLR) can estimate vegetation parameters more accurately. In addition to being used for modeling, it can also be used to select the most sensitive spectral bands for predicting the dependent variable. Many studies have used this method for spectral data analysis and have proven to be very useful for spectral information extraction (Osborne *et al.*, 2002; Jacquemoud *et al.*, 1995; Gnyp *et al.*, 2014). Thenkabail *et al.* (2000) used SMLR to identify sensitive band combinations to estimate crop biomass and LAI, and found a 4-band model could account for up to 92% of parameter variability. Yu *et al.* (2013) constructed a 6-band model by using SMLR which significantly improve the accuracy of estimating N concentration in rice compared to the optimized narrow-band based NDVI or RVI.

Although the VI approach is widely used in the diagnosis of crop N nutrition status, it only uses a number of relevant bands in a large number of spectral data, resulting in a large amount of information redundancy. Statistical procedures such as Principal Component Analysis, Partial Least Squares Regression (PLSR), and Wavelet Transform reduce the multicollinearity and dimensions by decomposing spectral data into subsets of independent factors. Rather than using key wavebands to calculate spectral indices, these methods incorporate full-spectrum reflectance data into statistical models for crop trait estimation and

developed the algorithms to reduce dimensionality and mine the data for spectral features associated with crop traits (Thorp *et al.*, 2017). PLSR is common when analyzing multivariate data. For example, Ecartot *et al.* (2013) developed a PLSR model to estimate durum wheat leaf N content and leaf mass per unit area from spectral reflectance data measured between 400 and 2500 nm. Hansen and Schjoerring (2003) used hyperspectral reflectance data (438-884 nm) as independent variables to establish a regression model of winter wheat N content using PLSR. Martin *et al.* (2008) established a PLSR N content model with reflectances ranging from 750 to 1250 nm in the NIR region. In addition, there are improved PLS algorithms, such as Powered PLS (PPLS) (Indahl, 2005), which enhance the pre-selection based on the importance of variables (Kusnierek & Korsaeath, 2015).

## 2) Application of Satellite Remote Sensing in Crop N Nutrition Diagnosis

The spatial heterogeneity of soil properties is ubiquitous. Precision N management requires a deeper understanding of the temporal and spatial variability. Aerial and satellite remote sensing is a promising technology in crop growth monitoring and real-time management for large production fields (Mulla, 2013; Zarco-Tejada *et al.*, 2013; Maresma *et al.*, 2018). As early as the 1970s, satellite remote sensing images were used in agricultural applications. Landsat TM and the Moderate Resolution Imaging Spectrometer (MODIS) are the most commonly used remote sensing data for monitoring and assessing the spatial variability of crop growth conditions and yield (Liu *et al.*, 2012; Gitelson *et al.*, 2012). However, limited by their coarse spatial resolution (30 m for Landsat TM, 0.25-1 km for MODIS) and temporal resolution (16 days for Landsat TM), their utility for capturing crop growth parameters at critical growth stages or environmental information were hampered (Magney *et al.*, 2017). In recent years, satellite platforms have provided unprecedented capabilities: spatial resolution has increased from tens of meters to sub-meters, revisit time have increased from tens of days to one day, and some new satellites have been able to record more wavebands. For example, QuickBird, Spot6/7, FORMOSAT-2, RapidEye, WorldView-2/3/4, Sentinel-2, etc. can be used as tools for scientists and farmers to better monitor crop N status, green LAI, and yield (Table 2-2). Among them, the RapidEye satellite is a breakthrough as the first satellite system to provide red edge band with high spatial resolution. WorldView-2 is also a milestone in satellite development. It not only includes bands similar to the RapidEye, but also provides additional coastal (400-450 nm), yellow (585-625 nm), and second NIR (860-1040 nm) wavebands. According to Chan *et al.* (2004), the optimal spatial resolution for biomass or yield estimation is 1-3 m, for variable rate fertilization is 5-10 m with a narrow topdressing time window. Although many commercial satellites with high spatial resolutions can meet the requirements of N diagnostics and precision N management. Due to the time limit for topdressing and the effect of weather conditions, their applications are constrained by their temporal resolution. Among them,

FORMOSAT-2, RapidEye, and WorldView-2 with high revisit capability are the satellites with the best potential for N nutrition diagnosis and precision management. Worldview-4 were not included in the discussion due to its late launch time. And the PlantScope constitutes hundreds of satellites which possible to capture imagery every day. Due to the high cost of satellite images, many studies have used the proximal hyperspectral data to simulate the satellite waveband (Yang *et al.*, 2008; Bsaibes *et al.*, 2009; Bausch & Khosla, 2010). Good progress has also been made through these studies. Chapter 4 of this dissertation has examined the application potential of FORMOSAT-2 satellite images for N nutrition diagnosis and precision N management in cold region rice in Northeast China. Chapter 5 has evaluated the application potential of the FORMOSAT-2, RapidEye, and WorldView-2 through hyperspectral data simulations.

**Table 2-2** Specifications of different satellites

<b>Satellites</b>	<b>Launch time</b>	<b>Revisit time (day)</b>	<b>Resolution of Panchromatic (m)</b>	<b>Resolution of Multispectral (m)</b>	<b>Panchromatic (nm)</b>	<b>Multispectral (nm)</b>
IKONOS	1999	1-3	1	4	450-900	450-520, 510-600, 630-700, 760-850
QuickBird	2001	1-6	0.61-0.72	2.44-2.88	450-900	450-520, 520-600, 630-690, 760-900
Spot6/7	2012/2014	1	1.5	6	450-750	450-520, 530-590, 625-695, 760-890
FORMOSAT-2	2004	1-6	2	8	520-820	450-520, 520-600, 630-690, 760-900
RapidEye	2008	1-6.5		5	-	440-510, 520-590, 630-685, 690-730, 760-850
Worldview-2	2009	1.1	0.5	1.8	450-800	450-510, 510-580, 630-690, 770-895, 585-625, 400-450, 705-745, 860-1040
Worldview-3	2014		0.31	1.24		400-450, 450-510, 510-580, 585-625, 630-690, 705-745, 770-895, 860-1040, 1195-1225, 1550-1590, 1640-1680, 1710-1750, 2145-2185, 2185-2225, 2235-2285, 2295-2365
Worldview-4	2016	1	0.31	1.24	450-800	665-690, 510-580, 450-510, 780-920
Sentinel-2	2015	5	-	10, 20, 60	-	423-463, 425-555, 525-595, 635-695, 690-720, 725-755, 763-803, 727-957, 845-885, 925-965, 1355-1395, 1520-1700, 2010-2370
GF-2	2014	5	1	4	450-900	450-520, 520-590, 630-690, 770-890
PlanetScope	2014	1	-	3	-	455-515, 500-590, 590-670, 780-860

### 3) Advances in Remote Sensing Monitoring of N Nutrition Index

The NNI can be calculated at any time in the crop's life cycle. However, the calculation of NNI requires destructive sampling and chemical analysis to determine biomass and plant N concentration, therefore impractical for in-season site-specific N management across large areas. The accurate estimation of NNI using remote sensing technology also means rapid and real-time N nutrition diagnosis. The future direction of sensors development in N nutrition management is to directly estimate nutrient deficiencies without the use of reference strips (Mulla, 2013). Therefore, there is an increasing interest in using proximal and remote sensing technologies to estimate the crop NNI non-destructively (Lemaire *et al.*, 2008; Houlès *et al.*, 2007; Cao *et al.*, 2013; Yao *et al.*, 2014). Lemaire *et al.* (1997) suggested that the N concentration of the upper leaves of the canopy was more stable and well correlated with the NNI. Several studies also showed that N concentration of the upper leaves of the canopy was a good proxy of crop NNI (Farruggia *et al.*, 2004; Gastal & Lemaire, 2002; Ziadi *et al.*, 2009). These also provide a theoretical basis for the application of remote sensing technology in the rapid estimation of NNI.

Several researchers have successfully used chlorophyll meter data to estimate the NNI of wheat (Prost & Jeuffroy, 2007; Ziadi *et al.*, 2010b), maize (Ziadi *et al.*, 2008b), and rice (Yuan *et al.*, 2016). Crop canopy sensors are more efficient and promising than leaf sensors for monitoring crop N status across large fields (Cao *et al.*, 2016; Yao *et al.*, 2014). Xia *et al.* (2016) used GreenSeeker active optical sensor to estimate NNI. A passive hyperspectral canopy sensor was also applied to estimate maize NNI by Chen *et al.* (2013). However, these data are point measurements at the leaf or canopy level and they are unsuitable for precision N management across large areas (Miao *et al.*, 2009). Aerial and satellite remote sensing is a promising technology to monitor crop N status for large production fields (Mulla, 2013). The FARMSTAR project, introduced by the EADS (European Aeronautic Defense and Space) company, has provided recommendation maps for N or chemicals for farmers since 2002 based on an effective combination of satellite remote sensing images and agronomy expertise (Coquil & Bordes, 2005). They have been used to predict the NNI maps. However, it is difficult to estimate N concentration based on the broadband VIs derived from satellite imagery, which also makes a direct estimation of NNI challenging. González-Piqueras *et al.* (2017) found the red edge VIs-Red Edge Position, MERIS Terrestrial Chlorophyll Index (MTCI), Angular Insensitivity Vegetation Index (AIVI), and CCCI based on narrow wavebands were highly correlated with N content ( $R^2 > 0.93$ ). These VIs also performed well when derived from the broad wavebands of Sentinel-2 ( $R^2 > 0.90$ ). Cilia *et al.* (2014) applied aerial hyperspectral sensing to estimate maize NNI indirectly. They used the ratio of Modified Chlorophyll Absorption Rate Index and Modified Triangular Vegetation Index 2 (MCARI / MTVI2) and MTVI2 to estimate corn PNC ( $R^2 = 0.59$ ) and biomass ( $R^2 = 0.80$ ).

Next, they combined the predicted PNC and biomass maps to generate an NNI map, which agreed well with the NNI obtained by destructive sampling and analysis ( $R^2 = 0.70$ ). Vuolo *et al.* (2017) combined satellite imagery and models to estimate the LAI and biomass, and estimated the N concentration using the VIs recommended by Cilia *et al.* (2014) in order to calculate NNI indirectly. Villodre *et al.* (2017) recommended N fertilizers during crop growth period by estimating the difference of actual N uptake and critical N uptake. However, how to estimate NNI and differential N uptake more accurately needs to be further studied.

### 2.3.2 Fluorescence and their proximal remote sensing

The polyphenolic compound (Phen) is a carbon-rich secondary product of plant metabolism (Meyer *et al.*, 2006). Its main function is to prevent harmful ultraviolet radiation (Caldwell *et al.*, 1983) and defend against pests and pathogens (Hahlbrock & Scheel, 1989; Kiraly, 1964). The synthesis of polyphenols is induced by biotic or abiotic stress (Ksouri *et al.*, 2007). For example, the availability of N affects both protein synthesis and polyphenol synthesis. This is because the common precursor of both proteins and polyphenolic compounds is phenylalanine, which can be used in an alternative approach to synthesize proteins or polyphenols. When N supply is sufficient, phenylalanine is assigned to synthesize protein in a larger amount. Correspondingly, the amount for polyphenol synthetic is less. On the contrary, in the case of insufficient N, phenylalanine produces less synthetic protein than polyphenols (Jones & Hartley, 1999). Phen mainly includes flavonoids, anthocyanins, hydroxycinnamic acids, condensed tannins, and lignin (Meyer *et al.*, 2006). Among them, flavonoids and hydroxycinnamic acid derivatives have the highest amount. Flavonoids are mainly stored in the vacuoles of epidermal cells and also present in the mesophyll cells. Hydroxycinnamic acid normally bind to the cell walls (Knogge & Weissenböck, 1986; Liu *et al.*, 1995; Burchard *et al.*, 2000).

Under excitation light, the leaves emit fluorescence at peaks of 440 nm (blue), 520 nm (green), 690 nm (red), 740 nm (NIR) (Langsdorf *et al.*, 2000). Among them, chlorophyll mainly excites red and NIR fluorescence, while Phen compounds emit blue and green fluorescence. Researchers found that under high and low N treatments, the ratios of blue and red or NIR, red and NIR fluorescence of plant leaves were greatly different (Buschmann & Lichtenthaler, 1998; Langsdorf *et al.*, 2000). The fluorescence spectral ratio  $F_{690}/F_{740}$  was significantly correlated with chlorophyll content (Gitelson *et al.* 1999; Cerovic *et al.* 2009). On the other hand, Phen compounds (mainly flavonoids) have typical ultraviolet (UV) absorption peak bands in UV-A and UV-B (Cerovic *et al.*, 2002). Under UV light source, the absorption peak by a large number of compounds causes the amount of UV light transmitted through the epidermis to be almost zero (Day *et al.*, 1994). At the same time, the red light or NIR light sources have been used as the reference to detect the chlorophyll content under the

epidermis. Using the ratio of these two, the N nutrition status of the plant can be more accurately reflected. Based on this principle, two portable fluorescent sensors named Dualex and Multiplex were produced. It has been reported that there is a good correlation between the Dualex reading and the Phen content extracted from the leaves ( $R^2 = 0.94$ ) (Goulas *et al.*, 2004; Cerovic *et al.*, 2008). Previous studies have shown that the readings of Dualex are inversely correlated with leaf N content, and gradually decrease with the increase of N application rate (Cartelat *et al.*, 2005; Tremblay *et al.*, 2007). Multiplex is an active sensor that contains four emission light sources (UV-A, green, red or blue) to excite fluorescence in plant tissue. This sensor has three filter detectors for fluorescence recording, including blue-green fluorescence, red fluorescence, and NIR fluorescence. Different excitation lights have different ability to penetrate the leaves, with the UV radiation blocked by the epidermis, the green radiation penetrating the maximum and the red penetrating the minimum. Compared to Dualex, Multiplex can further detect the internal structures of leaves.

N nutrition estimation techniques based on chlorophyll fluorescence may have advantages than reflectance spectroscopy. Firstly, studies have shown that when stress occurs, changes in chlorophyll fluorescence can be detected earlier than damage to photosynthetic organs (Lichtenthaler 1996; Lenk *et al.* 2007). Demotes-Mainard *et al.* (2008) found that changes in plant N concentration took place about two weeks earlier than changes in biomass. Furthermore, Phen is a more specialized indicator that is directly related to the nutritional status of N and avoids misjudgments caused by a decrease of chlorophyll content due to sulfur deficiency (Samson *et al.*, 2000). Moreover, the ratio of chlorophyll content to Phen (Chl/Phen) increases the sensitivity to N status. The study showed that the value of Chl/Phen is 86% higher than that of N-deficient plants, while chlorophyll content is only 43% higher (Cartelat *et al.*, 2005). Portable proximal fluorescence instruments such as Dualex and Multiplex have achieved good results in estimating NNI (Padilla *et al.*, 2014; Padilla *et al.*, 2016). It is necessary to study the potential of N status estimation based on fluorescence sensors, which may be used as a supplementary means to the reflectance-based method for N status estimation and precision N management.

## Chapter 3: A New Critical Nitrogen Dilution Curve for Rice Nitrogen Status Diagnosis in Northeast China

SHANYU HUANG<sup>1,2</sup>, YUXIN MIAO<sup>1,3,\*</sup>, QIANG CAO<sup>4</sup>, YINKUN YAO<sup>1</sup>, GUANGMING ZHAO<sup>5</sup>, WEIFENG YU<sup>1</sup>, JIANNING SHEN<sup>1</sup>, KANG YU<sup>1,2</sup>, and GEORG BARETH<sup>2</sup>

Published in: *Pedosphere* 2018, 28(5), 814–822, doi: 10.1016/S1002-0160(17)60392-8

*Formatting and orthography of the manuscript are adapted to the dissertation style.*

- <sup>1</sup> International Center for Agro-Informatics and Sustainable Development, College of Resources and Environmental Sciences, China Agricultural University, Beijing 100193, China
- <sup>2</sup> Institute of Geography, University of Cologne, 50923 Cologne, Germany
- <sup>3</sup> Precision Agriculture Center, Department of Soil, Water and Climate, University of Minnesota, St. Paul 55108, USA
- <sup>4</sup> National Engineering and Technology Center for Information Agriculture, Nanjing Agricultural University, Nanjing 210095, China
- <sup>5</sup> Qixing Farm, Jiansanjiang, Jiamusi 156399, China

\*Corresponding author. E-mail: ymiao@cau.edu.cn, ymiao@umn.edu

### Abstract

In-season diagnosis of crop nitrogen (N) status is crucial for precision N management. Critical N ( $N_c$ ) dilution curve and N nutrition index (NNI) have been proposed as effective methods to diagnose N status of different crops. The  $N_c$  dilution curves have been developed for Indica rice in the tropical and temperate zones and Japonica rice in the subtropical-temperate zone, but they have not been evaluated for short-season Japonica rice in Northeast China. The objectives of this study were to evaluate the previously developed  $N_c$  dilution curves for rice in Northeast China and to develop a more suitable  $N_c$  dilution curve in this region. A total of 17 N rate experiments were conducted in Sanjiang Plain, Heilongjiang Province in Northeast China from 2008 to 2013. The results indicated that none of the two previously developed  $N_c$  dilution curves was suitable to diagnose N status of the short-season Japonica rice in Northeast China. A new  $N_c$  dilution curve was developed and can be described by the equation of  $N_c = 27.7W^{-0.34}$  if  $W \geq 1$  Mg dry matter (DM) ha<sup>-1</sup> or  $N_c = 27.7$  g kg<sup>-1</sup> DM if  $W < 1$  Mg DM ha<sup>-1</sup>, where  $W$  is the aboveground biomass. This new curve was lower than the previous curves. It was validated using a separate dataset, and it could discriminate non-N-limiting and N-limiting nutritional conditions. Additional studies are needed to further evaluate it for diagnosing N status of different rice cultivars in

Northeast China and develop efficient non-destructive methods to estimate NNI for practical applications.

### 3.1 Introduction

China is the world's largest producer of rice (*Oryza sativa* L.) and consumer of nitrogen (N) fertilizer. Over-application of N and improper timing of fertilization have resulted in very low N recovery efficiency (20%-30%) and agronomic N efficiency (5-10 kg kg<sup>-1</sup>) (Peng *et al.*, 2009). Precision N management aims to match N supply and demand in both space and time, making it a promising strategy to improve N use efficiency in crop production (Miao *et al.*, 2009; Yao *et al.*, 2012). This strategy requires the development of efficient plant-based diagnostic tools for evaluating crop N status.

Plant N concentration (PNC) is a commonly used indicator of plant N status, and various threshold values have been established for different crops (Fageria, 2009). It has been reported that PNC decreases with aboveground biomass (AGB) during the growing season in dense canopies (Greenwood *et al.*, 1986; Lemaire *et al.*, 2008; Ziadi *et al.*, 2010a), regardless of the climatic conditions of the year or the species and genotype (Lemaire *et al.*, 2005). This decline of PNC with AGB can be described by a negative power function called N dilution curve:  $N = aW^{-b}$ , where  $N$  is the PNC expressed as g kg<sup>-1</sup> dry matter (DM),  $W$  is the AGB expressed in Mg DM ha<sup>-1</sup>,  $a$  is the PNC (g kg<sup>-1</sup> DM) when crop biomass is 1 Mg DM ha<sup>-1</sup>, and  $b$  is the dilution coefficient (Lemaire *et al.*, 2008). The minimum PNC necessary to achieve maximum AGB production is defined as the concentration of critical N ( $N_c$ ) (Ulrich, 1952). The  $N_c$  dilution curve describes the relationship between the  $N_c$  and the aboveground biomass and can be used to determine the  $N_c$  at a specific plant biomass. The N nutrition index (NNI) can be calculated as the ratio of the actual measured PNC over  $N_c$  to diagnose plant N status (Lemaire *et al.*, 2008). If the NNI value equals to 1, it indicates optimum N status, while a value greater or smaller than 1 indicates excessive or deficient N status, respectively.

Even though general  $N_c$  dilution curves have been established for C3 and C4 crops (Greenwood *et al.*, 1990; Lemaire & Gastal, 1997), it has been suggested that species-specific  $N_c$  dilution curves should be developed for more precise diagnosis of plant N status according to each species' histological, morphological, and ecophysiological characteristics (Lemaire & Gastal, 1997). Justes *et al.* (1994) developed an  $N_c$  dilution curve for winter wheat (*Triticum aestivum* L.) in France, which has been used for winter wheat N status diagnosis worldwide (Stockle & Debaeke, 1997; Jeuffroy & Recous, 1999). However, Yue *et al.* (2012) found that the NNI values calculated with this  $N_c$  dilution curve were less than 1 for all the N treatments conducted in North China Plain (NCP), even for the treatments with excessive N applications. As a result, they developed a new  $N_c$  dilution curve for winter

wheat in NCP, and it was lower than that of Justes *et al.* (1994). This could be due to differences in climatic conditions and wheat cultivars (Yue *et al.*, 2012). For spring maize (*Zea mays* L.), Plénet and Lemaire (1999) developed an  $N_c$  dilution curve in France, which was found to be valid in eastern Canada (Ziadi *et al.*, 2008a). However, when it was tested for spring maize in Northeast China by Li *et al.* (2012), all the data points for AGB greater than 1 Mg DM ha<sup>-1</sup> were under the  $N_c$  dilution curve of Plénet and Lemaire (1999), as observed for winter wheat in NCP. As a result, a new  $N_c$  dilution curve was developed for spring maize in Northeast China. Chen *et al.* (2013) also evaluated the  $N_c$  dilution curve of Plénet and Lemaire (1999) as well as a similar curve developed by Herrmann and Taube (2004) in Germany for summer maize in Shandong Province of China and found that both these curves were suitable for this region. It should be noted that their evaluation was based on one year's N rate experiment using one summer maize cultivar (Zhengdan 958). However, Yue *et al.* (2014) also evaluated the  $N_c$  dilution curve of Plénet and Lemaire (1999) with 16 experiments involving 9 cultivars in NCP and found this curve was inappropriate for summer maize N status diagnosis in NCP. Therefore, a specific  $N_c$  dilution curve was developed (Yue *et al.*, 2014). These results indicated the importance of evaluating the  $N_c$  dilution curves developed in other countries or regions using multi-site-year and cultivar data.

For rice, Sheehy *et al.* (1998) established an  $N_c$  dilution curve ( $N_c = 51.8W^{-0.52}$ ) for high-yielding Indica rice in the tropics (Philippines) and temperate environments (China and Australia). They supported the concept of an  $N_c$  dilution curve independent of the climatic zone. However, this  $N_c$  dilution curve was found to be inappropriate for Japonica rice in the Yangtze River reaches of China, and a new  $N_c$  dilution curve was developed for Japonica rice ( $N_c = 35.3W^{-0.28}$ ) (Ata-Ul-Karim *et al.*, 2013). Will this  $N_c$  dilution curve has developed in the Yangtze River reaches work for Japonica rice in other parts of China, especially in Northeast China?

Northeast China is the coolest region in China with a long and cold winter and short and warm summer (Chen *et al.*, 2012; Yang *et al.*, 2007). During the past three decades, Northeast China has experienced the most obvious warming, with temperature increase mainly in the winter. Due to climate warming, abundant water resources, and higher profits, rice farming in Northeast China has been increasing very fast during the past decades and now it is the major Japonica rice production region in China (Zhao *et al.*, 2013). Development of precision N management strategies that can improve both rice yield and N use efficiency in Northeast China is crucially important for China's food security and sustainable development (Yao *et al.*, 2012; Zhao *et al.*, 2013). There have been some efforts to use NNI to calibrate measurements from remote sensing technologies for non-destructive diagnosis of rice N status in Northeast China (Cao *et al.*, 2013; Yao *et al.*, 2014). However, no study has been reported to evaluate the existing  $N_c$  dilution curves for rice in Northeast China. Considering the differences in climate and cultivars in Northeast China as compared

with the tropics and Yangtze River reaches, a new  $N_c$  dilution curve may need to be developed for diagnosing rice N status in this region. The objectives of this study were to prove the hypothesis that the existing  $N_c$  dilution curves were not suitable for diagnosing Japonica rice N status in Northeast China and to develop a more appropriate  $N_c$  dilution curve for this region.

## 3.2 Materials and methods

### 3.2.1 Study area

The study area (47.2°N, 132.8°E) is located in the Sanjiang Plain of Heilongjiang Province, Northeast China. The Sanjiang Plain was formed by the alluviation from the tributaries of Heilong River, Songhua River, and Wusuli River. It is characterized by a cool-temperate sub-humid continental monsoon climate with very cold winter and warm summer. The mean annual temperature and precipitation are about 2 °C and 550-600 mm, respectively, with about 70% rainfall occurring from July to September (Wang & Yang, 2001). The annual sunshine duration is 2300-2600 h, and the whole year frost-free period is about 120-140 d (Yan *et al.*, 2002). The main soil type in the region is Albic soil, classified as Mollic Planosols in the FAO-UNESCO system and Typical Argialbolls in Soil Taxonomy (Xing *et al.*, 1994).

Two sites were selected for this study. Site 1 (47°15'52"N, 132°39'05"E) has been planted in rice since 1992 and Site 2 (47°13'59"N, 132°38'50"E) started rice planting in 2002.

### 3.2.2 Field experiments design

A total of 17 N rate experiments were conducted from 2008 to 2013 at the study sites involving two Japonica rice cultivars: Kongyu 131 and Longjing 21 (Table 3-1). Kongyu 131 is a commonly planted cultivar in this region, with 11 leaves, four elongation nodes, and time to maturity of about 127 d. Longjing 21 is a 12-leaf cultivar with time to maturity of 133 d. All of the experiments adopted a randomized complete block design with three or four replications. The N fertilizer was applied in three splits for Experiments 1, 2, 5, 6, 11, 12, and 15-17: 40%-45% as the basal application before transplanting, 20%-30% at tillering stage, and 30%-35% at stem elongation stage. For Experiments 3, 4, 7, 8, 13, and 14, N fertilizers were applied in two splits: 60% as basal application and 40% at tillering stage. For Experiments 9 and 10, N fertilizers were applied in four splits: 40% as a basal application, 25% at tillering stage, 20% at stem elongation stage, and 10% at heading stage.

All experiments used urea (N:P:K = 46:0:0) as the N fertilizer, superphosphate (N:P:K = 0:46:0) as the P fertilizer, and KCl (N:P:K = 0:0:60) or K<sub>2</sub>SO<sub>4</sub> (N:P:K = 0:0:33) as the K fertilizer. In each experiment, sufficient P (45-60 kg P<sub>2</sub>O<sub>5</sub> ha<sup>-1</sup>) and K (60-105 kg K<sub>2</sub>O ha<sup>-1</sup>) fertilizers were applied to make sure P and K nutrients would not be limiting. All the P

fertilizers were applied as basal fertilizers before transplanting and the K fertilizers were applied in two splits, with 50% as basal fertilizer and 50% as panicle fertilizer at the stem elongation stage.

### 3.2.3 Plant sampling and analysis

Plant samples were collected at several critical growth stages, including panicle initiation (PI), stem elongation (SE), booting (B), heading (H), flowering (F), and grain filling (GF) stages. The sampling stages and dates differed with experiments and the detailed information is listed in Table 3-1. Three to six hills rice plants were randomly selected and cut at ground surface according to the average number of tillers per hill in each pot. The plant samples were rinsed with water and the roots were removed. Then the samples were separated into leaves, stems, and panicles (for samples collected at and after heading stage). The separated samples were put into the oven at 105 °C for 0.5 h for deactivation of enzymes and then dried for 3-4 d at 70-80 °C until constant weight was attained. The biomass weight of three to six hills of rice plants was converted to the unit of Mg ha<sup>-1</sup> based on the planting density of each plot. After being weighed, the samples were ground to pass through 1-mm sieve. A sub-sample of 0.3-0.4 g from each sample was digested using H<sub>2</sub>SO<sub>4</sub> and H<sub>2</sub>O<sub>2</sub>, and the N concentration was determined using the standard Kjeldahl-N titration method. The whole plant N concentration (PNC) was calculated according to the following formula:

$$PNC = \frac{W_l * N_{cl} + W_s * N_{cs} + W_p * N_{cp}}{W_l + W_s + W_p} \quad (3-1)$$

where  $W_l$ ,  $W_s$ ,  $W_p$  stand for the weight of the leaves, stems and panicles, respectively, and  $N_{cl}$ ,  $N_{cs}$ ,  $N_{cp}$  stand for the N concentration of the leaves, stems and panicles, respectively.

At maturity, three 1 m<sup>2</sup> areas were randomly identified in each plot and cut for grain yield determination. At the same time, the grain water content was tested. The final yield was adjusted to 140 g kg<sup>-1</sup> water content.

**Table 3-1** Details of the N rate experiments conducted from 2008 to 2013 in the Sanjiang Plain of Heilongjiang Province, Northeast China

Experiment	Site	Year	Cultivar	N Rates kg ha <sup>-1</sup>	Transplanting/ Harvesting Date	Sampling Stage <sup>a)</sup>	Sampling Date
1	1	2008	Kongyu 131	0,35,70,105,140	29-May / 21-September	PI, SE, H, F, GF	30-June, 8-July, 24-July, 4-August, 16-August
2	2	2008	Kongyu 131	0,35,70,105, 140	13-May / 22-September	PI, SE, H, GF	27-June, 7-July, 23-July, 17-August
3	1	2008	Kongyu 131	0, 23, 45, 68, 91	29-May / 21-September	H, F, GF	24-July, 4-August, 16-August
4	2	2008	Kongyu 131	0, 23, 45, 68, 91	13-May / 22-September	H, F, GF	23-July, 3-August, 17-August
5	1	2009	Kongyu 131	0, 35, 70, 105, 140	24-May / 27-September	PI, SE, B, H, GF	26-June, 5-July, 18-July, 1-August, 19-August
6	2	2009	Kongyu 131	0, 35, 70, 105, 140	20-May / 27-September	PI, SE, B, H, GF	27-June, 5-July, 18-July, 1-August, 19-August
7	1	2009	Kongyu 131	0, 23, 45, 68, 91	24-May / 27-September	PI, SE, B, H, GF	26-June, 5-July, 18-July, 1-August, 19-August
8	2	2009	Kongyu 131	0, 23, 45, 68, 91	20-May / 27-September	PI, SE B, H, GF	27-June, 5-July, 18-July, 1-August, 19-August
9	2	2010	Kongyu 131	0, 100, 110, 140	17-May / 26-September	PI, H	26-June, 20-July,
10	2	2011	Kongyu 131	0, 100, 110, 140	10-May / 23-September	PI, H	27-June, 25-July,
11	1	2011	Kongyu 131	0, 70, 100, 130,160	17-May / 21-September	PI, SE, H	30-June, 9-July, 27-July
12	1	2011	Longjing 21	0, 70, 100, 130, 160	19-May / 21-September	PI, SE, H	6-July, 12-July, 31-July
13	1	2011	Kongyu 131	0, 49, 70, 91, 112	17-May / 21-September	H	26-July
14	1	2011	Longjing 21	0, 49, 70, 91, 112	19-May / 21-September	H	1-August
15	1	2012	Kongyu 131	0, 70, 100, 130, 160	18-May / 22-September	PI, SE, H	21-June, 29-June, 23-July
16	1	2012	Longjing 21	0, 70, 100, 130, 160	18-May / 22-September	PI, SE, H	25-June, 2-July, 23-July
17	1	2013	Kongyu 131	0, 70, 100, 130, 160	18-May / 20-September	PI, SE, H	23-June, 2-July, 22-July

<sup>a)</sup>PI: Panicle Initiation; SE: Stem Elongation; B: Booting; H: Heading; F: Flowering; GF: Grain Filling.

### 3.2.4 Data analysis

The data were analyzed to establish the  $N_c$  dilution curve according to Justes *et al.* (1994). In this study, the data from Experiments 1-16 were used to establish the new  $N_c$  dilution curve for Japonica rice in the cold region. The  $N_c$  concentration was determined by identifying the data points for which N does not limit AGB growth or is not in excess. For each site year experiment at each sampling date, all the AGB data were subject to analysis of variance (ANOVA) using the PROC ANOVA of SAS (SAS Institute, USA) and compared using the least significant difference test at  $P \leq 0.01$ . The N-limiting growth treatment is defined as a treatment for which an increase of N application leads to a significant increase in AGB. The non-N-limiting growth treatment is defined as a treatment for which additional N application leads to a significant increase in PNC, but not in AGB (Ata-Ul-Karim *et al.*, 2013). The AGB and their corresponding PNC data of N-limiting treatments were fitted with simple linear regression and the AGB data of non-N-limiting treatments were averaged to calculate maximum AGB. The theoretical critical point was determined by the intersection point of the maximum AGB and PNC as the ordinate in the simple linear regression; and then, all of the maximum AGB values and their corresponding  $N_c$  values were put together in a scatter plot. Regression analysis was performed by fitting a negative power function to the data to generate the  $N_c$  dilution curve.

The data from Experiments 1-16 were used to evaluate the existing  $N_c$  dilution curves of Sheehy *et al.* (1998) and Ata-Ul-Karim *et al.* (2013). The data from Experiment 17 were used to evaluate the new  $N_c$  dilution curve established in this study and to determine its suitability for rice N status diagnosis in Northeast China by calculating NNI and relating it to different N rates. The NNI data from Experiments 9-12 and 15-16 were also related to relative yield (RY). The RY was calculated as the ratio of the grain yield for a given N rate treatment and the highest grain yield in that specific site-year N rate experiment. The linear plus plateau model was used to describe the relationship between RY and NNI using the SAS software.

## 3.3 Results

### 3.3.1 Evaluation of the existing $N_c$ dilution curves

To evaluate the existing  $N_c$  dilution curves developed by Sheehy *et al.* (1998) and Ata-Ul-Karim *et al.* (2013), the data from Experiments 1-16 were grouped into 30 datasets with significant N effect on AGB. Each dataset consisted of AGB and PNC data for all the N rate treatments at a specific site-year and sampling date. For the 30 datasets, 29 datasets were retained because the data of AGB in one dataset were smaller than  $1 \text{ Mg ha}^{-1}$ . The  $N_c$  dilution curve developed by Sheehy *et al.* (1998) was not applicable to such data. The retained data

were divided into two groups: a non-N-limiting group and an N-limiting group. The data were not included if the AGB was classified in more than one group. This analysis resulted in 63 and 64 data points in the non-N-limiting group and the N-limiting group, respectively. These data points were plotted together with the existing  $N_c$  dilution curves (Fig. 3-1). The  $N_c$  curve of Ata-Ul-Karim *et al.* (2013) was lower than that of Sheehy *et al.* (1998) when AGB was less than 5 Mg ha<sup>-1</sup>, but higher after this value (Fig. 3-1). All the N-limiting data points were below these curves; however, about 80% of the non-N-limiting data points were also below the curves, indicating that none of these two curves was suitable for Japonica rice in Northeast China.

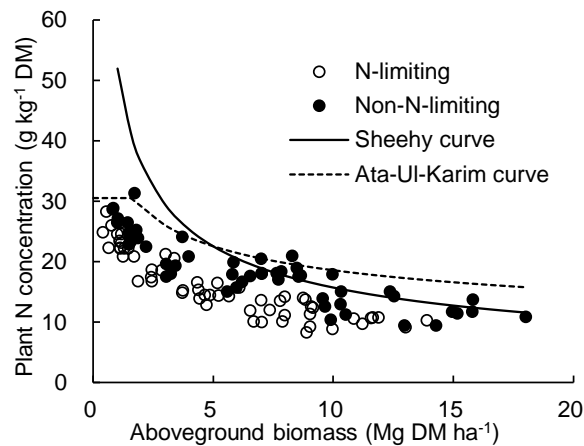


**Fig. 3-1** Evaluation of the previously established critical N ( $N_c$ ) dilution curves using data from short-season Japonica rice grown under N-limiting and non-N-limiting conditions (Experiments 1-16) in Northeast China. The solid line represents the  $N_c$  dilution curve developed for Indica rice by Sheehy *et al.* (1998) ( $N_c = 51.8W^{-0.52}$ , where  $W$  is the aboveground biomass), and the dash line represents the  $N_c$  dilution curve developed for Japonica rice by Ata-Ul-Karim *et al.* (2013) ( $N_c = 35.3W^{-0.28}$  if  $W \geq 1.55$  Mg DM ha<sup>-1</sup>, and  $N_c = 30.5$  g kg<sup>-1</sup> DM if  $W < 1.55$  Mg DM ha<sup>-1</sup>).

### 3.3.2 Development of new $N_c$ dilution curve

From all the data points derived from Experiments 1-16, 22 fulfilled the statistical criteria previously defined to determine  $N_c$  (Table 3-2). The AGB ranged from 0.77 to 18.01 Mg DM ha<sup>-1</sup>, with only two data points being lower than 1 Mg DM ha<sup>-1</sup>. The PNC values ranged from 9.3 to 29.3 g kg<sup>-1</sup> DM. The PNC was not significantly related to AGB and remained more or less constant when AGB was less than 1 Mg ha<sup>-1</sup> (Ata-Ul-Karim *et al.*, 2013). And the  $N_c$  equals to the average of all PNC when aboveground biomass was less than 1 Mg DM ha<sup>-1</sup>, which was close to 27.7 g kg<sup>-1</sup> DM. Therefore, only the data with AGB above 1 Mg DM ha<sup>-1</sup> were retained to develop the new  $N_c$  dilution curve. It was described as  $N_c = 27.7W^{-0.34}$ , with  $R^2$  of 0.91 (Fig. 3-2). And for the AGB less than 1 Mg DM ha<sup>-1</sup>, the  $N_c$  was set to 27.7 g kg<sup>-1</sup> DM.

The new  $N_c$  dilution curve established in this study was used to determine  $N_c$  for each treatment of Experiments 17 at each sampling date and then to calculate NNI. The treatments receiving 0 and 70 kg N ha<sup>-1</sup> had NNI less than or close to 1, while the treatments receiving 100 kg N ha<sup>-1</sup> and higher rates of N applications had NNI greater than or close to 1 (Fig. 3-3). An examination of the final grain yield of each treatment revealed that grain yield was significantly increased by N applications until 100 kg N ha<sup>-1</sup> and reached a plateau (Fig. 3-4). This indicated that the NNI values could be used to diagnose plant N status of short-season rice in Northeast China.

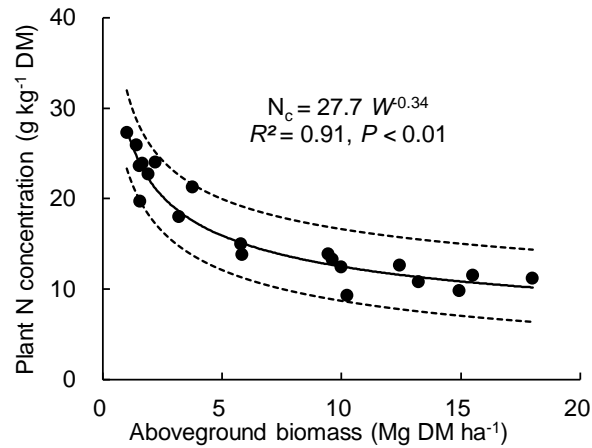


**Fig. 3-2** Critical points used to define the critical N ( $N_c$ ) dilution curve for short-season Japonica rice in Northeast China. The detailed information of these points can be found in Table 3-2. The solid line represents the  $N_c$  dilution curve ( $N_c = 27.7W^{-0.34}$ , where  $W$  is the aboveground biomass), and the dash line represents the 95% confidence bands.

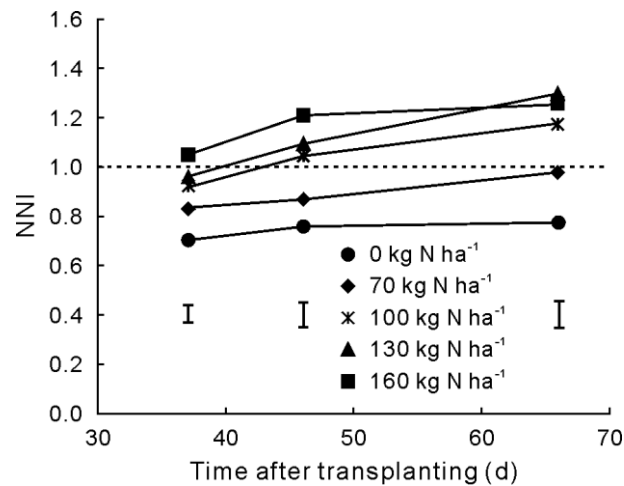


**Fig. 3-3** N nutrition index (NNI) of short-season Japonica rice in Northeast China with different N application rates during the growing season in 2013. The rice cultivar was Kongyu 131 with 11 leaves. The dotted horizontal line represents an NNI of 1.0. The vertical bars represent the pooled standard error of the means for each sampling date.

**Table 3-2** Critical points selected for establishing the critical N dilution curve for short-season Japonica rice in Northeast China

Experiment	Year	Cultivar	Growth Stage	Aboveground biomass (Mg DM ha <sup>-1</sup> )	N concentration, (g kg <sup>-1</sup> DM)
1	2008	Kongyu 131	Panicle initiation	0.77	24.6
10	2011	Kongyu 131	Panicle initiation	0.82	29.3
9	2010	Kongyu 131	Panicle initiation	1.01	27.3
16	2012	Longjing 21	Panicle initiation	1.42	25.9
15	2012	Kongyu 131	Panicle initiation	1.53	23.6
1	2008	Kongyu 131	Stem Elongation	1.55	19.7
12	2011	Longjing 21	Stem Elongation	1.65	23.9
6	2009	Kongyu 131	Stem Elongation	1.91	22.7
11	2011	Kongyu 131	Stem Elongation	2.21	24.0
12	2011	Longjing 21	Stem Elongation	3.18	18.0
16	2012	Longjing 21	Stem Elongation	3.75	21.3
1	2008	Kongyu 131	Heading	5.79	15.0
3	2008	Kongyu 131	Heading	5.83	13.8
10	2011	Kongyu 131	Heading	9.44	13.9
9	2010	Kongyu 131	Heading	9.62	13.3
1	2008	Kongyu 131	Flowering	9.99	12.4
3	2008	Kongyu 131	Flowering	10.24	9.3
4	2008	Kongyu 131	Flowering	12.44	12.6
3	2008	Kongyu 131	Grain Filling	13.22	10.8
1	2008	Kongyu 131	Grain Filling	14.94	9.8
2	2008	Kongyu 131	Grain Filling	15.51	11.5
4	2008	Kongyu 131	Grain Filling	18.01	11.2

The relationship between RY and NNI, expressed by a linear plus plateau model, accounted for 80% of the variation (Fig. 3-5). For  $NNI \geq 1.03$ , RY was close to 1, while for  $NNI < 1.03$ , RY was generally less than 1. This result also indicated that the  $N_c$  dilution curve and the resulting NNI could identify deficient and nondeficient N nutritional status of Japonica rice in Northeast China.

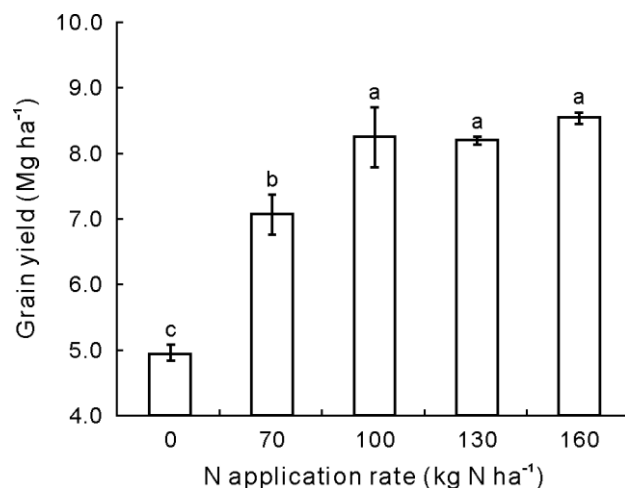


**Fig. 3-4** Grain yield of short-season Japonica rice under different N treatments in Experiment 17 conducted in 2013 in Northeast China. The vertical bars represent standard errors of the means ( $n = 3$ ). Bars with the same letter are not significant differences at  $P \leq 0.05$ .

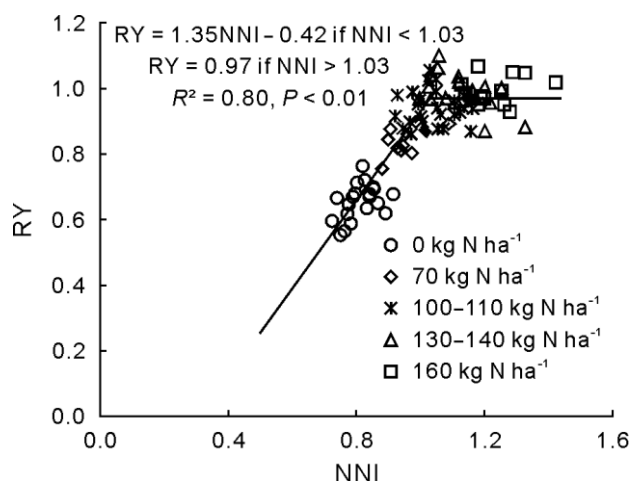


**Fig. 3-5** Relationships between relative grain yield (RY) and N nutrition index (NNI) of short-season Japonica rice in the experiments conducted in 2010-2012 in Northeast China at two sites with two cultivars ( $n = 92$ ). The NNI data were averaged over all sampling dates.

### 3.4 Discussion

Plant-based diagnostic methods for characterizing crop N status are key components of in-season site-specific N management strategies. They can also be used for posteriori diagnosis either in research studies or in farmer's fields to determine the possible reasons for low yields. The concept of NNI is more promising and reliable than PNC itself (Lemaire *et al.*, 2008). The calculation of NNI requires the establishment of  $N_c$  dilution curve.

Previous research has indicated that species-specific  $N_c$  dilution curves were independent of climatic zones for spring maize (Plénet & Lemaire, 1999; Herrmann & Taube, 2004; Ziadi *et al.*, 2008a) and rice (Sheehy *et al.*, 1998). The  $N_c$  dilution curve developed in

this study for Japonica rice in Northeast China was consistently lower than the curves for both Indica rice in the tropical and temperate zones (Sheehy *et al.*, 1998) and Japonica rice in the subtropical-temperate climate zone (Ata-Ul-Karim *et al.*, 2013) (Fig. 3-6). This result agreed with previous findings that Indica rice needed higher N uptake than Japonica rice (Shan *et al.*, 2001), and PNC of Indica rice was significantly higher than Japonica rice during vegetative growth stages (Shan *et al.*, 2001; Yoshida *et al.*, 2006), although climatic zone differences may also be a factor. For the difference between the new  $N_c$  dilution curve and that of Ata-Ul-Karim *et al.* (2013), climatic zone difference may be a major factor. The Ata-Ul-Karim *et al.* (2013) study was conducted in Yangtze River reaches, which are located in a subtropical-temperate climate zone with longer growing seasons. The rice cultivars with 16-17 leaves used in developing their  $N_c$  dilution curve have time to maturity of about 150 d, while the 11- to 12-leaf cultivars in our study have time to maturity of about 130 d or less. The accumulated temperature ( $> 10\text{ }^\circ\text{C}$ ) in the Northeast China region is more than 2000  $^\circ\text{C}$  lower than the Yangtze River reaches during the growing season, which can influence the development rate of rice plant. All these factors may cause the  $N_c$  values to be lower in Northeast China. Ziadi *et al.* (2010a) also found that the  $N_c$  dilution curve for winter wheat in northern France developed by Justes *et al.* (1994) was significantly different from the one for spring wheat in eastern Canada developed by Ziadi *et al.* (2010a). The possible factors causing such difference included climatic conditions, type of wheat, and cultivar (Ziadi *et al.*, 2010a).

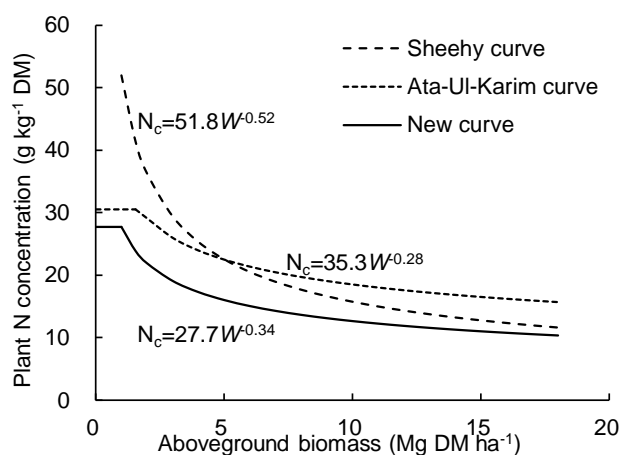


**Fig. 3-6** Comparison of different critical N dilution ( $N_c$ ) curves for rice. The solid line, dash line, and point line represent the new  $N_c$  dilution curve ( $N_c = 27.7W^{0.34}$ , where  $W$  is the aboveground biomass) for short-season Japonica rice in Northeast China, the  $N_c$  dilution curve for Indica rice developed by Sheehy *et al.* (1998) ( $N_c = 51.8W^{0.52}$ ), and the  $N_c$  dilution curve of Ata-Ul-Karim *et al.* (2013) ( $N_c = 35.3W^{0.28}$ ), respectively.

Another possible factor causing differences in  $N_c$  dilution curves is the determination method of PNC. The Kjeldahl method and the Dumas method (or combustion method) are

two commonly used methods for determining PNC. It has been found that the Kjeldahl method produced significantly lower values of soybean protein content than did the Dumas method (Jung *et al.*, 2003). The study of Ata-Ul-Karim *et al.* (2013) also used the Kjeldahl method, while the study of Sheehy *et al.* (1998) used data from published papers and personal communications without reporting the N determination method. We can rule out the possibility that N determination method was a factor causing the differences between the  $N_c$  dilution curves for Yangtze River reaches and for Northeast China.

The NNI is an integrative indicator of plant N status, and it increased with N application rates in this study (Fig. 3-3). The NNI of the 160 kg N ha<sup>-1</sup> treatment was consistently above 1 and reached about 1.2-1.4 at stem elongation and heading stages, indicating luxury N consumption. The grain yield of the 70 kg N ha<sup>-1</sup> treatment was significantly lower than those of the 100 and 160 kg N ha<sup>-1</sup> treatments for cultivar Kongyu 131 (Fig. 3-4), indicating that the 70 kg N ha<sup>-1</sup> treatment was deficient in N supply. The 70 kg N ha<sup>-1</sup> treatment had NNI values lower than 1 at panicle initiation and stem elongation stages (37 and 46 d after transplanting, respectively), but equaled to 1 at heading stage (66 d after transplanting). This could be due to the topdressing N application at the stem elongation stage, and heading stage was about 20 d after the N application, when the applied N was still effective. N could become deficient after heading stage and resulted in reduced grain yield.

The  $N_c$  dilution curve was mainly developed based on the experimental data of the 11-leaf cultivar Kongyu 131, with only 2 years' data of the 12-leaf cultivar Longjing 21. As a result, the NNI may work better for Kongyu 131 than for Longjing 21. Cultivar differences should be taken into consideration when developing  $N_c$  dilution curves. In the study of Ata-Ul-Karim *et al.* (2013), two  $N_c$  dilution curves were developed for two different cultivars, but there were no statistical differences between these two curves; as a result, the two cultivar groups were pooled together, and a general  $N_c$  dilution curve was developed. In our study site, 11- and 12-leaf cultivars were very different, with the latter cultivar being unable to mature properly in certain years. Two different  $N_c$  dilution curves may need to be developed for 11- and 12-leaf cultivars in Northeast China. For potato, Bélanger *et al.* (2001) developed different  $N_c$  dilution curves for different varieties. The new  $N_c$  dilution curve and NNI need to be further evaluated using data from more cultivars and diverse N status.

To reconcile the differences in  $N_c$  dilution curves between regions and cultivars, Zhao *et al.* (2014) proposed a developmental stage-based approach to derive the  $N_c$  concentrations for wheat. The rationale is that the decrease of PNC is due to increased proportion of low N concentration structural tissues (i.e. stems, glumes), the dilution by carbohydrate reserves, and the mutual shading of leaves (Angus & Moncur, 1985), which are more dependent on developmental stage compared with AGB (Zhao *et al.*, 2014). They found that the  $N_c$  dilution curves from different studies tended to converge after stem elongation stage. However, a big difference was observed at early stages (Feekes stages 4-6), which was thought to be due to

difficulties and inconsistencies in recording growth stages and biomass determination when plants were small. Further studies are needed to compare these two approaches to determining  $N_c$  for rice. It will be important to also determine the proportion of leaves and stems in such studies, in addition to their N concentration.

For practical applications across large areas, nondestructive methods are needed to estimate crop NNI. Promising results have been achieved using chlorophyll meters to estimate NNI in wheat (Ziadi *et al.*, 2010b; Cao *et al.*, 2012) and maize (Ziadi *et al.*, 2008b). However, chlorophyll meter is a leaf sensor and is still very time-consuming for large area applications (Miao *et al.*, 2009). Yao *et al.* (2014) used a two-band active crop canopy sensor (GreenSeeker) to estimate rice NNI based on the  $N_c$  dilution curve developed by Ata-Ul-Karim *et al.* (2013) and found that only 25%-34% of the NNI variability could be explained. Cao *et al.* (2013) used a three-band active crop canopy sensor (Crop Circle ACS 470) to estimate NNI based on the  $N_c$  dilution curve developed by Sheehy *et al.* (1998) and found that four red edge-based vegetation indices could explain about 76% of NNI variability. Additional studies are needed to use remote sensing technologies to estimate NNI based on the new  $N_c$  dilution curve developed in this study for in-season site-specific N status diagnosis and management.

### 3.5 Conclusions

The  $N_c$  dilution curves developed for Indica rice in the tropical and temperate zones and for Japonica rice in the subtropical-temperate zone were not suitable for diagnosing short-season Japonica rice N status in Northeast China. A new  $N_c$  dilution curve was developed in this study, which could be described by the equation  $N_c = 27.7W^{-0.34}$  when AGB was 1 Mg DM ha<sup>-1</sup> or above. When AGB was less than 1 Mg DM ha<sup>-1</sup>,  $N_c$  was set to a constant value of 27.7 g kg<sup>-1</sup> DM. This new curve was lower than the previous curves developed in other regions. The validation result indicated that it worked well to diagnose plant N status of the 11-leaf variety rice. Additional studies are needed to further evaluate this new  $N_c$  dilution curve for the diagnosis of N status of different rice cultivars in Northeast China and develop efficient non-destructive methods to estimate NNI for practical applications.

### Acknowledgment

This study was supported by the Key National Research and Development Program (No. 2016YFD0200602), the National Basic Research Program (No. 2015CB150405), the National Natural Science Foundation of China (No. 31421092), and the SINO-GRAIN Project of China (No. CHN-2152, 14-0039).

### 3.6 References

- Angus, J.F., Moncur, M.W., 1985. Models of growth and development of wheat in relation to plant nitrogen. *Aust. J. Agr. Res.* 36, 537–544.
- Ata-Ul-Karim, S.T., Yao, X., Liu, X.J., Cao, W.X., Zhu, Y., 2013. Development of critical nitrogen dilution curve of Japonica rice in Yangtze River Reaches. *Field Crops Res.* 149, 149–158.
- Bélanger, G., Walsh, J.R., Richards, J.E., Milburn, P.H., Ziadi, N., 2001. Critical nitrogen curve and nitrogen nutrition index for potato in eastern Canada. *Am. J. Potato Res.* 78, 355–364.
- Cao, Q., Cui, Z.L., Chen, X.P., Khosla, R., Dao, T.H., Miao, Y.X., 2012. Quantifying spatial variability of indigenous nitrogen supply for precision nitrogen management in small scale farming. *Precis. Agric.* 13, 45–61.
- Cao, Q., Miao, Y.X., Wang, H.Y., Huang, S.Y., Cheng, S.S., Khosla, R., Jiang, R.F., 2013. Non-destructive estimation of rice plant nitrogen status with crop circle multispectral active canopy sensor. *Field Crops Res.* 154, 133–144.
- Chen, C.Q., Qian, C.R., Deng, A.X., Zhang, W.J., 2012. Progressive and active adaptations of cropping system to climate change in Northeast China. *Eur. J. Agron.* 38, 94–103.
- Chen, P.F., Wang, J.H., Huang, W.J., Tremblay, N., Ou, Y.Z., Zhang, Q., 2013. Critical nitrogen curve and remote detection of nitrogen nutrition index for corn in the northwestern plain of Shandong Province, China. *IEEE J. Sel. Topics. Appl. Earth Observ. Remote Sens.* 6, 682–689.
- Fageria, N. K., 2009. *The Use of Nutrients in Crop Plants*. CRC Press, Boca Raton.
- Greenwood, D.J., Lemaire, G., Gosse, G., Cruz, P., Draycott, A., Neeteson, J.J., 1990. Decline in percentage N of C<sub>3</sub> and C<sub>4</sub> crops with increasing plant mass. *Ann. Bot.* 66, 425–436.
- Greenwood, D.J., Neeteson, J.J., Draycott, A., 1986. Quantitative relationships for the dependence of growth rate of arable crops on their nitrogen content, dry weight and aerial environment. *Plant Soil.* 91, 281–301.
- Herrmann, A., Taube, F., 2004. The range of the critical nitrogen dilution curve for maize (*Zea mays L.*) can be extended until silage maturity. *Agron. J.* 96, 1131–1138.
- Jeuffroy, M.H., Recous, S., 1999. Azodyn: A simple model simulating the date of nitrogen deficiency for decision support in wheat fertilization. *Eur. J. Agron.* 10, 129–144.
- Jung, S., Rickert, D.A., Deak, N.A., Aldin, E.D., Recknor, J., Johnson, L.A., Murphy, P.A., 2003. Comparison of Kjeldahl and Dumas methods for determining protein contents of soybean products. *J. Am. Oil Chem. Soc.* 80, 1169–1173.
- Justes, E., Mary, B., Meynard, J.M., Machet, J.M., Thelier-Huche, L., 1994. Determination of a critical nitrogen dilution curve for winter wheat crops. *Ann. Bot.* 74, 397–407.

- Lemaire, G., Avice, J.C., Kim, T.H., Ourry, A., 2005. Developmental changes in shoot N dynamics of lucerne (*Medicago sativa* L.) in relation to leaf growth dynamics as a function of plant density and hierarchical position within the canopy. *J. Exp. Bot.* 56, 935–943.
- Lemaire, G., Gastal, F., 1997. N uptake and distribution in plant canopies. In: Lemaire, G. (Ed.), *Diagnosis of the Nitrogen Status in Crops*. Springer-Verlag, Berlin, pp. 3–43.
- Lemaire G, Jeuffroy M H, Gastal F. 2008. Diagnosis tool for plant and crop N status in vegetative stage: Theory and practices for crop N management. *Eur J Agron.* 28: 614–624.
- Li, W.J., He, P., Jin, J.Y., 2012. Critical nitrogen curve and nitrogen nutrition index for spring maize in North-East China. *J. Plant Nutr.* 35, 1747–1761.
- Miao, Y.X., Mulla, D.J., Randall, G.W., Vetsch, J.A., Vintila, R., 2009. Combining chlorophyll meter readings and high spatial resolution remote sensing images for in-season site-specific nitrogen management of corn. *Precis. Agric.* 10, 45–62.
- Peng, S.B., Tang, Q.Y., Zou, Y.B., 2009. Current status and challenges of rice production in China. *Plant Prod. Sci.* 12, 3–8.
- Plénet, D., Lemaire, G., 1999. Relationships between dynamics of nitrogen uptake and dry matter accumulation in maize crops. Determination of critical N concentration. *Plant Soil.* 216, 65–82.
- Shan, Y.H., Wang, Y.L., Yoshinori, Y., Huang, J.Y., Yang, L.X., Zhang, C.S., 2001. Study on the differences of nitrogen uptake and use efficiency in different types of rice. *J. Yangzhou Univ. Nat. Sci. Ed.* (in Chinese). 4, 42–45, 51.
- Sheehy, J.E., Dionora, M.J.A., Mitchell, P.L., Peng, S., Cassman, K.G., Lemaire, G., Williams, R.L., 1998. Critical nitrogen concentrations: Implications for high-yielding rice (*Oryza sativa* L.) cultivars in the tropics. *Field Crops Res.* 59, 31–41.
- Stockle, C.O., Debaeke, P., 1997. Modeling crop nitrogen requirements: A critical analysis. *Dev. Crop Sci.* 25, 217–225.
- Ulrich, A., 1952. Physiological bases for assessing the nutritional requirements of plants. *Ann. Rev. Plant Physiol.* 3, 207–228.
- Wang, Y.Y., Yang, Y.X., 2001. Effects of agriculture reclamation on the hydrologic characteristics in the Sanjiang Plain, China. *Chin Geogr. Sci.* 11, 163–167.
- Xing, B.S., Dudas, M.J., Zhang, Z.Y., Xu, Q., 1994. Pedogenetic characteristics of albic soils in the three river plain, Heilongjiang Province. *Acta Pedol. Sin.* (in Chinese). 31, 95–104.
- Yan, M.H., Deng, W., Chen, P.Q., 2002. Climate change in the Sanjiang Plain disturbed by large-scale reclamation. *J. Geogr. Sci.* 12, 405–412.
- Yang, X., Lin, E.D., Ma, S.M., Ju, H., Guo, L.P., Xiong, W., Li, Y., Xu, Y.L., 2007. Adaptation of agriculture to warming in Northeast China. *Clim. Change* 84, 45–58.

- Yao, Y.K., Miao, Y.X., Cao, Q., Wang, H.Y., Gnyp, M.L., Bareth, G., Khosla, R., Yang, W., Liu, F.Y., Liu, C., 2014. In-season estimation of rice nitrogen status with an active crop canopy sensor. *IEEE J. Sel. Topics Appl. Earth Observ. Remote Sens.* 7, 4403–4413.
- Yao, Y.K., Miao, Y.X., Huang, S.Y., Gao, L., Ma, X.B., Zhao, G.M., Jiang, R.F., Chen, X.P., Zhang, F.S., Yu, K., Gnyp, M.L., Bareth, G., Liu, C., Zhao, L.Q., Yang, W., Zhu, H.M., 2012. Active canopy sensor-based precision N management strategy for rice. *Agron. Sustain. Dev.* 32, 925–933.
- Yoshida, H., Horie, T., Shiraiwa, T., 2006. A model explaining genotypic and environmental variation of rice spikelet number per unit area measured by cross-locational experiments in Asia. *Field Crops Res.* 97, 337–343.
- Yue, S.C., Meng, Q.F., Zhao, R.F., Li, F., Chen, X.P., Zhang, F.S., Cui, Z.L., 2012. Critical nitrogen dilution curve for optimizing nitrogen management of winter wheat production in the North China Plain. *Agron. J.* 104, 523–529.
- Yue, S.C., Sun, F.L., Meng, Q.F., Zhao, R.F., Li, F., Chen, X.P., Zhang, F.S., Cui, Z.L., 2014. Validation of a critical nitrogen curve for summer maize in the North China Plain. *Pedosphere* 24, 76–83.
- Zhao, G.M., Miao, Y.X., Wang, H.Y., Su, M.M., Fan, M.S., Zhang, F.S., Jiang, R.F., Zhang, Z.J., Liu, C., Liu, P.H., Ma, D.Q., 2013. A preliminary precision rice management system for increasing both grain yield and nitrogen use efficiency. *Field Crops Res.* 154, 23–30.
- Zhao, Z.G., Wang, E.L., Wang, Z.M., Zang, H.C., Liu, Y.P., Angus, J.F., 2014. A reappraisal of the critical nitrogen concentration of wheat and its implications on crop modeling. *Field Crops Res.* 164, 65–73.
- Ziadi, N., Bélanger, G., Claessens, A., Lefebvre, L., Cambouris, A.N., Tremblay, N., Nolin, M.C., Parent, L.É., 2010a. Determination of a critical nitrogen dilution curve for spring wheat. *Agron. J.* 102, 241–250.
- Ziadi, N., Bélanger, G., Claessens, A., Lefebvre, L., Tremblay, N., Cambouris, A.N., Nolin, M.C., Parent, L.É., 2010b. Plant-based diagnostic tools for evaluating wheat nitrogen status. *Crop Sci.* 50, 2580–2590.
- Ziadi, N., Brassard, M., Bélanger, G., Cambouris, A.N., Tremblay, N., Nolin, M.C., Claessens, A., Parent, L.É., 2008a. Critical nitrogen curve and nitrogen nutrition index for corn in eastern Canada. *Agron. J.* 100, 271–276.
- Ziadi, N., Brassard, M., Bélanger, G., Claessens, A., Tremblay, N., Cambouris, A.N., Nolin, M.C., Parent, L.É., 2008b. Chlorophyll measurements and nitrogen nutrition index for the evaluation of corn nitrogen status. *Agron. J.* 100, 1264–1273.

## Chapter 4: Satellite Remote Sensing-Based In-Season Diagnosis of Rice

### Nitrogen Status in Northeast China

SHANYU HUANG<sup>1,2</sup>, YUXIN MIAO<sup>1,\*</sup>, GUANGMING ZHAO<sup>1</sup>, FEI YUAN<sup>1,3</sup>, XIAOBO MA<sup>1</sup>, CHUANXIANG TAN<sup>1</sup>, WEIFENG YU<sup>1</sup>, MARTIN L. GNYP<sup>1,4</sup>, VICTORIA I.S. LENZ-WIEDEMANN<sup>1,2</sup>, UWE RASCHER<sup>1,5</sup>, and GEORG BARETH<sup>1,2</sup>

Published in: *Remote Sens.* 2015, 7, 10646-10667, doi: 10.3390/rs70810646

*Formatting, orthography, and units of the manuscript are adapted to the dissertation style.*

<sup>1</sup> International Center for Agro-Informatics and Sustainable Development, College of Resources and Environmental Sciences, China Agricultural University, Beijing 100193, China

<sup>2</sup> Institute of Geography, University of Cologne, 50923 Cologne, Germany

<sup>3</sup> Department of Geography, Minnesota State University, Mankato, MN 56001, USA

<sup>4</sup> Research Centre Hanninghof, Yara International, 48249 Duellmen, Germany

<sup>5</sup> Forschungszentrum Jülich, Institute of Bio-and Geosciences, IBG-2: Plant Sciences, D-52425 Jülich, Germany

\*Corresponding author. E-mail: ymiao@cau.edu.cn, ymiao2007@gmail.com

#### Abstract

Rice farming in Northeast China is crucially important for China's food security and sustainable development. A key challenge is how to optimize nitrogen (N) management to ensure high yield production while improving N use efficiency and protecting the environment. Handheld chlorophyll meter (CM) and active crop canopy sensors have been used to improve rice N management in this region. However, these technologies are still time-consuming for large-scale applications. Satellite remote sensing provides a promising technology for large-scale crop growth monitoring and precision management. The objective of this study was to evaluate the potential of using FORMOSAT-2 satellite images to diagnose rice N status for guiding topdressing N application at the stem elongation stage in Northeast China. Five farmers' fields (three in 2011 and two in 2012) were selected from the Qixing Farm in Heilongjiang Province of Northeast China. FORMOSAT-2 satellite images were collected in late June. Simultaneously, 92 field samples were collected and six agronomic variables, including aboveground biomass (AGB), leaf area index (LAI), plant N concentration (PNC), plant N uptake (PNU), CM readings and N nutrition index (NNI) defined as the ratio of actual PNC and critical PNC, were determined. Based on the FORMOSAT-2 imagery, a total of 50 vegetation indices were computed and correlated with

the field-based agronomic variables. Results indicated that 45% of NNI variability could be explained using Ratio Vegetation Index 3 (RVI3) directly across years. A more practical and promising approach was proposed by using satellite remote sensing to estimate AGB and PNU at the panicle initiation stage and then using these two variables to estimate NNI indirectly ( $R^2 = 0.52$  across years). Further, the difference between the estimated PNU and the critical PNU can be used to guide the topdressing N application rate adjustments.

#### 4.1 Introduction

Rice (*Oryza sativa* L.) is one of the most important crops in the world, and more than two-thirds of China's population relies on rice as the staple food (Dawe, 2000). Nitrogen (N) is an important element in chlorophyll constitution. Its supply rate affects biomass production and yield to a large extent. Farmers tend to apply high rates of N fertilizer in order to get a high yield. In the past 50 years, Chinese cereal production increased by 3.2 times, mainly due to an increased input of synthetic fertilizers, especially N fertilizer (Zhang *et al.*, 2011). The agronomic efficiency of N fertilizer for rice is only  $11.7 \text{ kg kg}^{-1}$  in China, much lower than those in developed countries ( $20\text{-}25 \text{ kg kg}^{-1}$ ) (Zhang *et al.*, 2008; Jin, 2012). The over-application of N fertilizer increases the risks of environmental pollution due to N loss into the surface water bodies, groundwater or atmosphere, resulting in water eutrophication, increased nitrate content in the groundwater and greenhouse gas emissions (Ju *et al.*, 2009). Precision N management strategies are developed to improve fertilizer N use efficiency by matching the fertilizer N input to crop N demand in proper time and space (Doberman *et al.*, 2002). This requires the development of technologies for real-time and site-specific diagnosis of crop N status in the field for guiding the topdressing N applications (Cao *et al.*, 2015).

Plant N concentration (PNC) and uptake (PNU) have been commonly used as crop N status indicators. To improve crop N status diagnosis, the concept of critical N concentration ( $N_c$ ) has been proposed as the minimum PNC necessary to achieve maximum AGB production (Greenwood *et al.*, 1986; Greenwood *et al.*, 1991).  $N_c$  decreases with increasing biomass. Their relationship can be described using a negative power function, called the critical N dilution curve (Lemaire *et al.*, 2008). Thus, the  $N_c$  at any given biomass value can be calculated by this dilution curve. The actual PNC ( $N_a$ ) can then be compared to  $N_c$ , and their ratio is termed the N nutrition index (NNI). NNI is a better indicator for diagnosing crop N status than PNC or PNU (Lemaire *et al.*, 2008). If  $N_a$  is greater than  $N_c$  ( $\text{NNI} > 1$ ), this indicates an over-supply of N, while the opposite is true if  $N_a$  is smaller than  $N_c$  ( $\text{NNI} < 1$ ) (Lemaire *et al.*, 2008). An NNI value of one indicates an optimal N supply. The calculation of NNI requires destructive sampling and chemical analysis to determine biomass and plant N concentration, which is time and cost consuming and, thus, impractical for in-season site-

specific N management across large areas. Therefore, there is an increasing interest in using proximal and remote sensing technologies to non-destructively estimate the crop NNI (Lemaire *et al.*, 2008; Houlès *et al.*, 2007; Cao *et al.*, 2013; Yao *et al.*, 2014). Several researchers have successfully used chlorophyll meter (CM) data to estimate the NNI of wheat (*Triticum aestivum* L.) (Debaeke *et al.*, 2006; Prost & Jeuffroy, 2007; Ziadi *et al.*, 2010; Cao *et al.*, 2012) and maize (*Zea mays* L.) (Ziadi *et al.*, 2008). However, CM data are point measurements at the leaf level and unsuitable for precision N management across large areas (Miao *et al.*, 2009).

Crop canopy sensors are more efficient and promising than leaf sensors for monitoring crop N status across large fields (Cao *et al.*, 2015; Yao *et al.*, 2014). Mistele and Schmidhalter (2008) used a passive hyperspectral canopy sensor to estimate NNI. They found that the red edge inflection point could explain 95% of winter wheat NNI variability. A passive hyperspectral canopy sensor was also applied to estimate maize NNI by Chen *et al.* (2013). They reported that a model based on principal component analysis and a back propagation artificial neural network approach performed the best by explaining 81% of NNI variability. However, passive canopy sensors are constrained by the time and cloud cover of the acquisition day. Such hyperspectral sensors are also very expensive; therefore, they may be more suitable for research than for on-farm applications.

Active optical crop canopy sensors, unlike passive sensors, have modulated light emitting diodes that irradiate a plant canopy and measure a portion of the reflected radiation, without relying on ambient sunlight (Holland *et al.*, 2012). They are not influenced by environmental light conditions and do not need frequent calibrations. The GreenSeeker active canopy sensor (Trimble Navigation Limited, Sunnyvale, CA, USA) has a red and near-infrared (NIR) band and provides two vegetation indices (VIs), the Normalized Difference Vegetation Index (NDVI) and the Ratio Vegetation Index (RVI). It was found that GreenSeeker NDVI and RVI explained 47% and 44% of winter wheat NNI variability, respectively, across site years and growth stages (Cao *et al.*, 2015). The Crop Circle ACS 470 sensor (Holland Scientific, Inc., Lincoln, NE, USA) is a configurable active crop canopy sensor with three wavebands. It was found that two VIs calculated with the Crop Circle wavebands, the Green Re-normalized Difference Vegetation Index (GRDVI) and the Modified Green Soil Adjusted Vegetation Index (MGSAVI), were effective for estimating winter wheat NNI across site years and growth stages ( $R^2 = 0.77-0.78$ ) (Cao *et al.*, 2015). For rice, the GreenSeeker sensor explained 25%-34% and 30%-31% of NNI variability at the stem elongation and heading stages, respectively (Yao *et al.*, 2014). Using the Crop Circle ACS 470 sensor, four red edge-based indices, including the Red Edge Soil Adjusted Vegetation Index (RESAVI), the Modified RESAVI (MRESAVI), the Red Edge Difference Vegetation Index (REDVI) and the Red Edge Re-normalized Difference Vegetation Index (RERDVI), performed equally well for estimating rice NNI across growth stages ( $R^2 = 0.76$ )

(Cao *et al.*, 2013). Active crop sensors have been mounted on fertilizer applicators, and on-the-go sensing and variable rate N applications have been realized for maize and wheat, but not for rice, considering the challenges for fertilizer application machines to enter paddy fields flooded with water.

Aerial and satellite remote sensing is a promising technology to monitor crop N status for large production fields (Mulla, 2013). Aerial hyperspectral remote sensing and CM data were combined to diagnose maize N status using the N sufficiency index approach (Miao *et al.*, 2009). Cilia *et al.* (2014) applied aerial hyperspectral sensing to estimate maize NNI indirectly. They calculated the Modified Chlorophyll Absorption Ratio Index/Modified Triangular Vegetation Index 2 (MCARI/MTVI2) and MTVI2 to estimate maize PNC ( $R^2 = 0.59$ ) and biomass ( $R^2 = 0.80$ ), respectively. Then, they combined the predicted PNC and biomass maps to generate an NNI map, which agreed well with the NNI obtained by destructive sampling and analysis ( $R^2 = 0.70$ ). The improvements in spatial and temporal resolutions of satellite remote sensing make it possible to monitor crop N status at key crop growth stages. Wu *et al.* (2007) compared QuickBird data with CM readings and petiole nitrate concentration. They found that the QuickBird-VIs differed significantly for different N input treatments at the late growing season. Yang *et al.* (2008) found that the NDVI derived from FORMOSAT-2 satellite imagery was highly correlated to the NDVI calculated from a ground canopy reflectance sensor ( $R^2 = 0.79$ ). Darvishzadeh *et al.* (2012) used the inversion of the PROSAIL model with a lookup table approach and multispectral satellite image data of ALOS AVNIR-2. The method explained 65% of rice plant chlorophyll content variability with a low root mean square error (RMSE) of  $0.45 \text{ g m}^{-2}$ .

So far, little has been reported on rice NNI estimation using satellite remote sensing. Therefore, the objective of this study was to evaluate the potential of using FORMOSAT-2 satellite remote sensing to estimate rice NNI at a key growth stage for guiding panicle N fertilizer application in Northeast China.

## 4.2 Materials and methods

### 4.2.1 Study site

The study site is located at the Qixing Farm in the Sanjiang Plain, Heilongjiang Province, Northeast China. The Sanjiang Plain used to be a wild natural wetland formed by the alluvia of three river systems—Heilong River, Songhua River, and Wusuli River. During the past 50 years, the natural wetland was reclaimed for arable land, especially paddy rice fields. Due to the small population density in this region, each farmer's household has about a 20-30 ha cultivation area, making it the leading large-scale farming region in China. The main soil type is Albic soil, classified as Mollic Planosols in the FAO-UNESCO system, and typical Argialbolls in the Soil Taxonomy (Xing *et al.*, 1994). This area has a typical cool-temperate

sub-humid continental monsoon climate. During the growing season (April-October), the average rainfall is about 400 mm, which accounts for approximately 70% of yearly precipitation. The mean annual temperature is about 2 °C (Wang & Yang, 2001). The annual sunshine duration is 2300-2600 h and the whole year frost-free period ranges from 120-140 days (Yan *et al.*, 2002).

#### 4.2.2 Field information

This study was conducted to diagnose rice N status at a key growth stage to guide panicle fertilizer application based on satellite images. For cold region rice, the crucial period for panicle fertilizer topdressing is during the stem elongation stage. Considering the time, it takes for satellite image acquisition and processing, the best diagnosis stage is at panicle initiation, which is about 7-10 days before the stem elongation stage (Cao *et al.*, 2013; Yao *et al.*, 2012; Zhao *et al.*, 2013). Three farmers' fields in 2011 and two in 2012 were selected for this study. The cultivars and transplanting densities varied (Table 4-1). The seedlings were prepared in greenhouses and then transplanted at the 3.1-3.5 leaf stage into the fields.

The regional optimal N rate recommended by the local extension service was around 100 kg ha<sup>-1</sup>. Field 1 (F1) was managed by an experienced farmer. The best rice management practice of the region, supported by the Jiansanjiang Experiment Station of the China Agricultural University, was applied for this field. Other fields were managed by individual farmers following their own practices.

**Table 4-1** Detailed information about the farmers' fields selected for this study, Heilongjiang Province, China, 2011-2012.

Field	Year	Number of Samples	Area (ha)	N Rate (kg ha <sup>-1</sup> )	Variety	Number of Leaves	Transplanting Date	Plant Density (hills m <sup>-2</sup> )
F 1	2011	33	29.6	97.9	Kendao 6	12	2011/5/17	27
F 2	2011	4	13.1	105.9	Longjing 26	11	2011/5/20	30
F 3	2011	4	31.0	101.0	Kendao 6	12	2011/5/12	27
F 4	2012	14	10.7	120.2	Longjing 31	11	2012/5/16	28
F 5	2012	37	21.6	98.3	Longjing 31	11	2012/5/20	30

#### 4.2.3 Remote sensing images and preprocessing

For this study, we selected the FORMOSAT-2 satellite, which belongs to the National Space Organization of Taiwan (NSPO). It runs on a Sun-synchronous orbit with an orbit altitude of 891 km and collects images at the same local hour with a constant observation angle for the same site (Chern *et al.*, 2006). The multispectral image of FORMOSAT-2 covers four spectral band regions with a ground resolution of 8 m: blue (B) (450-520 nm),

green (G) (520-600 nm), red (R) (630-690 nm) and NIR (760-900 nm) (Liu, 2006). One image scene covers an area of 24 km × 24 km. The panchromatic image with 2-m ground resolution is collected simultaneously. The daily revisit interval makes FORMOSAT-2 one of the most suitable satellites for precision agriculture applications. Images were obtained on 25 June 2011 and 26 June 2012. These two images were almost cloud-free, especially in the study area.

The images were geometrically corrected and radiometrically calibrated using ENVI 4.8 (ENVI, Boulder, CO, USA). The radiometric calibration was performed using the satellite calibration parameters in the following formula for each band:

$$L = DN/a + L_0 \quad (4-1)$$

where  $L$  stands for radiance;  $DN$  is the abbreviation of digital number;  $a$  is the absolute calibration coefficients, which is also called gain; and  $L_0$  stands for the offset. After the linear transformation, the  $DN$  values were converted to radiance values in units of  $W\ m^{-2}\ sr^{-1}\ \mu m^{-1}$ . For geometric correction, high precision ground control points were used. The rectification accuracy was less than 0.5 pixels (< 4 m), which was acceptable for this research.

#### 4.2.4 Field data collection and analysis

A total of 41 and 51 ground samples were collected in 2011 and 2012, respectively. The samples were collected from sites representing different crop growth conditions (N deficient, optimum and surplus conditions), based on visual observations. The sampling dates were 25 June 2011, the same acquisition date as the satellite image, and 28 June 2012, two days after the FORMOSAT-2 image collection. At each sampling site, a hand-held differential Trimble Ag332 GPS was used for geo-referencing. Ground truth data included rice cultivar, plant density, tiller numbers and relative chlorophyll concentration measured with the SPAD-502 instrument (Soil-Plant Analysis Development Section, Minolta, Osaka, Japan). Twenty rice plants were selected at each sampling site for CM measurements in the middle part of the top second leaf for each individual plant. At each sampling site, the AGB was collected destructively by clipping three hills (each hill consisting of 4-6 rice plants). These samples were taken to the laboratory and rinsed with water. The roots were removed, and the samples were separated into leaves and stems. The Leaf Area Index (LAI) was determined by the dry weight method as described by Bei *et al.* (2005). All parts of the samples were put into the oven for deactivation of enzymes at 105 °C for half an hour and then dried at 80 °C until constant weight. After being weighted, the sub-samples were ground to particles smaller than 1 mm and analyzed for N concentration using the Kjeldahl method (Lv *et al.*, 2004; Li, 2006).

For the NNI, the  $N_c$  was calculated by the following equations developed for rice in this region according to Justes *et al.* (1994), based on data from N rate experiments conducted in this region from 2008-2013:

$$N_c = 27.7 W^{-0.34} \quad (4-2)$$

where  $N_c$  is the critical N concentration ( $\text{g kg}^{-1}$ ) in the AGB and  $W$  is the shoot dry weight expressed in  $\text{t ha}^{-1}$ . For AGB larger than  $1 \text{ t ha}^{-1}$ , the  $N_c$  was calculated by the above equation, otherwise, the  $N_c$  was set to 27.7%.

#### 4.2.5 Data analysis

Many spectral VIs have been developed to estimate plant biophysical variables, such as chlorophyll concentration or content, LAI and biomass. However, many of them use narrow bands based on the research results of proximal hyperspectral sensing. In this study, the potential of using broadband satellite remote sensing images for estimating rice N status indicators was evaluated using the broad bands of FORMOSAT-2 satellite images. A total of 50 VIs were evaluated (Table 4-2). The software ENVI and ArcGIS 9 (ESRI, Redlands, CA, USA) were used to extract the pixel values from the FORMOSAT-2 satellite images and to calculate the VIs for corresponding sampling sites.

The regression analysis considered the 50 VIs and each of the 6 field-measured agronomic variables separately. The correlation and regression analyses were performed using SPSS V.20.0 (SPSS, Chicago, IL, USA). The RMSE and relative error ( $\text{RE}_r$ ) were also calculated to evaluate model performances.

**Table 4-2** Vegetation indices evaluated in this study for estimating rice N status indicators, Heilongjiang Province, China, 2011-2012.

Vegetation Index	Formula	Ref.
<b>Two-band vegetation indices</b>		
Ratio Vegetation Index 1 (RVI1)	$\text{NIR}/\text{B}$	Tucker (1979)
Ratio Vegetation Index 2 (RVI2)	$\text{NIR}/\text{G}$	Buschmann & Nagel (1993)
Ratio Vegetation Index 3 (RVI3)	$\text{NIR}/\text{R}$	Tucker (1979)
Difference Index1 (DVI1)	$\text{NIR}-\text{B}$	Tucker (1979)
Difference Index2 (DVI2)	$\text{NIR}-\text{G}$	Tucker (1979)
Difference Index3 (DVI3)	$\text{NIR}-\text{R}$	Tucker (1979)
Normalized Difference Vegetation Index1 (NDVI1)	$(\text{NIR}-\text{R})/(\text{NIR}+\text{R})$	Buschmann & Nagel (1993)
Normalized Difference Vegetation Index2 (NDVI2)	$(\text{NIR}-\text{G})/(\text{NIR}+\text{G})$	Gitelson <i>et al.</i> (1996)
Normalized Difference Vegetation Index3 (NDVI3)	$(\text{NIR}-\text{B})/(\text{NIR}+\text{B})$	Buschmann & Nagel (1993)
Renormalized Difference Vegetation Index1 (RDVI1)	$(\text{NIR}-\text{B})/\text{SQRT}(\text{NIR}+\text{B})$	Roujean & Breon (1995)
Renormalized Difference Vegetation Index2 (RDVI2)	$(\text{NIR}-\text{G})/\text{SQRT}(\text{NIR}+\text{G})$	Roujean & Breon (1995)
Renormalized Difference Vegetation Index3 (RDVI3)	$(\text{NIR}-\text{R})/\text{SQRT}(\text{NIR}+\text{R})$	Roujean & Breon (1995)
Chlorophyll index (CI)	$\text{NIR}/\text{G}-1$	Gitelson <i>et al.</i> (2003)
Wide Dynamic Range Vegetation Index 1(WDRVI1)	$(0.12\text{NIR}-\text{R})/(0.12\text{NIR}+\text{R})$	Gitelson (2004)
Wide Dynamic Range Vegetation Index 2(WDRVI2)	$(0.12\text{NIR}-\text{G})/(0.12\text{NIR}+\text{G})$	Gitelson (2004)
Wide Dynamic Range Vegetation Index 3(WDRVI3)	$(0.12\text{NIR}-\text{B})/(0.12\text{NIR}+\text{B})$	Gitelson (2004)
Soil Adjusted Vegetation Index (SAVI)	$1.5(\text{NIR}-\text{R})/(\text{NIR}+\text{R}+0.5)$	Huete (1988)
Green Soil Adjusted Vegetation Index (GSAVI)	$1.5(\text{NIR}-\text{G})/(\text{NIR}+\text{G}+0.5)$	Huete (1988)
Blue Soil Adjusted Vegetation Index (BSAVI)	$1.5(\text{NIR}-\text{B})/(\text{NIR}+\text{B}+0.5)$	Huete (1988)
Modified Simple Ratio (MSR)	$(\text{NIR}/\text{R}-1)/\text{SQRT}(\text{NIR}/\text{R}+1)$	Chen (1996)
Optimal Soil Adjusted Vegetation Index (OSAVI)	$(1+0.16)[(\text{NIR}-\text{R})/(\text{NIR}+\text{R}+0.16)]$	Rondeaux <i>et al.</i> (1996)
Green Optimal Soil Adjusted Vegetation Index (GOSAVI)	$(1+0.16)[(\text{NIR}-\text{G})/(\text{NIR}+\text{G}+0.16)]$	Rondeaux <i>et al.</i> (1996)
Blue Optimal Soil Adjusted Vegetation Index (BOSAVI)	$(1+0.16)[(\text{NIR}-\text{B})/(\text{NIR}+\text{B}+0.16)]$	Rondeaux <i>et al.</i> (1996)
Modified Soil Adjusted Vegetation Index (MSAVI)	$0.5\{2\text{NIR}+1-\text{SQRT}[(2\text{NIR}+1)^2-8(\text{NIR}-\text{R})]\}$	Qi <i>et al.</i> (1994)
Modified Green Soil Adjusted Vegetation Index (MGSAVI1)	$0.5\{2\text{NIR}+1-\text{SQRT}[(2\text{NIR}+1)^2-8(\text{NIR}-\text{G})]\}$	Qi <i>et al.</i> (1994)
Modified Blue Soil Adjusted Vegetation Index (MBSAVI)	$0.5\{2\text{NIR}+1-\text{SQRT}[(2\text{NIR}+1)^2-8(\text{NIR}-\text{B})]\}$	Qi <i>et al.</i> (1994)
<b>Three-band vegetation indices</b>		
Simple Ratio Vegetation Index (SR)	$\text{R}/\text{G}*\text{NIR}$	Datt (1999)
Modified Normalized Difference Vegetation Index 1 (mNDVI1)	$(\text{NIR}-\text{R}+2\text{G})/(\text{NIR}+\text{R}-2\text{G})$	Wang <i>et al.</i> (2012)
Modified Normalized Difference Vegetation Index 2 (mNDVI2)	$(\text{NIR}-\text{R}+2\text{B})/(\text{NIR}+\text{R}-2\text{B})$	Wang <i>et al.</i> (2012)
New Modified Simple Ratio (mSR)	$(\text{NIR}-\text{B})/(\text{R}-\text{B})$	Sims & Gamon (2002)
Visible Atmospherically Resistant Index (VARI)	$(\text{G}-\text{R})/(\text{G}+\text{R}-\text{B})$	Gitelson <i>et al.</i> (2002)

Table 4-2 continued

Vegetation Index	Formula	Ref.
Structure Insensitive Pigment Index (SIPI)	$(\text{NIR}-\text{B})/(\text{NIR}-\text{R})$	Peñuelas <i>et al.</i> (1995)
Structure Insensitive Pigment Index 1 (SIPI1)	$(\text{NIR}-\text{B})/(\text{NIR}-\text{G})$	Peñuelas <i>et al.</i> (1995)
Normalized Different Index (NDI)	$(\text{NIR}-\text{R})/(\text{NIR}-\text{G})$	Datt (1999)
Plant Senescence Reflectance Index (PSRI)	$(\text{R}-\text{B})/\text{NIR}$	Sims & Gamon (2002)
Plant Senescence Reflectance Index (PSRI1)	$(\text{R}-\text{G})/\text{NIR}$	Sims & Gamon (2002)
Modified Chlorophyll Absorption in Reflectance Index (MCARI)	$[(\text{NIR}-\text{R})-0.2(\text{R}-\text{G})]\times(\text{NIR}/\text{R})$	Daughtry <i>et al.</i> (2000)
Modified Chlorophyll Absorption in Reflectance Index 1 (MCARI1)	$1.2[2.5(\text{NIR}-\text{R})-1.3(\text{NIR}-\text{G})]$	Haboudane <i>et al.</i> (2004)
Modified Chlorophyll Absorption in Reflectance Index 2 (MCARI2)	$1.2[2.5(\text{NIR}-\text{R})-1.3(\text{R}-\text{G})]/\text{SQRT}[(2\text{NIR}+1)^2-(6\text{NIR}-5\text{SQRT}(\text{R})-0.5)]$	Haboudane <i>et al.</i> (2004)
Modified Transformed CARI (MTCARI)	$3[(\text{NIR}-\text{R})-0.2(\text{NIR}-\text{G})]\times(\text{NIR}/\text{R})$	Haboudane <i>et al.</i> (2002)
Triangular Vegetation Index (TVI)	$0.5[1.20(\text{NIR}-\text{G})-200(\text{R}-\text{G})]$	Broge & Leblanc (2000)
Modified Triangular Vegetation Index 1 (MTVI1)	$1.2[1.2(\text{NIR}-\text{G})-2.5(\text{R}-\text{G})]$	Haboudane <i>et al.</i> (2004)
Modified Triangular Vegetation Index 2 (MTVI2)	$1.5[1.2(\text{NIR}-\text{G})-2.5(\text{R}-\text{G})]/\text{SQRT}[(2\text{NIR}+1)^2-(6\text{NIR}-5\text{SQRT}(\text{R})-0.5)]$	Haboudane <i>et al.</i> (2004)
Modified Triangular Vegetation Index 3 (MTVI3)	$1.5[1.2(\text{NIR}-\text{B})-2.5(\text{R}-\text{B})]/\text{SQRT}[(2\text{NIR}+1)^2-(6\text{NIR}-5\text{SQRT}(\text{R})-0.5)]$	Haboudane <i>et al.</i> (2004)
Enhanced Vegetation Index (EVI)	$2.5(\text{NIR}-\text{R})/(1+\text{NIR}+6\text{R}-7.5\text{B})$	Huete <i>et al.</i> (2002)
Triangular Chlorophyll Index (TCI)	$1.2(\text{NIR}-\text{G})-5(\text{R}-\text{G})(\text{NIR}/\text{R})^{0.5}$	Haboudane <i>et al.</i> (2008)
MTCARI/OSAVI	MTCARI/OSAVI	Haboudane <i>et al.</i> (2002)
MCARI/MTVI2	MCARI/MTVI2	Eitel <i>et al.</i> (2007)
MTCARI/MSAVI	MTCARI/MSAVI	Haboudane <i>et al.</i> (2002)
TCI/OSAVI	TCI/OSAVI	Haboudane <i>et al.</i> (2008)

#### 4.2.6 The estimation of NNI

The rice NNI can be estimated directly and indirectly. The direct method is to use the selected VI to estimate NNI directly based on the established relationships. The indirect method is to first use the selected VIs to estimate rice biomass and PNU. With the critical N dilution curve developed for rice in this region, the  $N_c$  can be derived for each biomass value. The estimated biomass and  $N_c$  can then be used together to calculate critical PNU ( $AGB \times N_c$ ). The NNI can then be estimated using PNU and critical PNU, because PNU/critical PNU equals to  $(AGB \times N_a)/(AGB \times N_c)$ , which can be further simplified to  $N_a/N_c$ . Considering practical applications, we classified the rice N status into three categories based on NNI values: deficient N status (NNI < 0.95), optimal N status (NNI = 0.95-1.05) and surplus N status (NNI > 1.05).

The indirect method was used in this study to create NNI maps of selected fields at the

pixel-level. For irrigation purpose, each rice field was divided into many smaller plots, which were also used as management units for fertilizer application. Therefore, the pixel-level NNI values were averaged for each small plot to create plot-level NNI maps using ArcGIS 9.

### 4.3 Results

#### 4.3.1 Variability of rice N status indicators

The variability of rice biomass, LAI and PNU (CV = 23%-28%) was consistently larger than that of PNC, SPAD values and NNI (CV = 4%-14%) (Table 4-3). In addition, larger variability of PNC and NNI was found in 2012 (CV = 11% and 14%, respectively) than in 2011 (CV = 5%). Likewise, the values of biomass, LAI and PNU were significantly higher in 2012 than in 2011. The NNI ranged from 0.89-1.17 in 2011, with an average of 1.01. This indicated that in general, the N status of these fields was optimal. In 2012, the NNI ranged from 0.83-1.50, with an average of 1.15, revealing a surplus N status (Table 4-3).

**Table 4-3** Descriptive statistics of rice N status indicators for 2011 (41 field samples) and 2012 (51 field samples), Heilongjiang Province, China.

N status indicator	Mean	Minimum	Maximum	SD	CV (%)
2011					
Biomass (t ha <sup>-1</sup> )	0.87	0.50	1.55	0.22	25
Leaf area index	0.84	0.52	1.51	0.20	23
Plant N concentration (g kg <sup>-1</sup> )	27.6	24.5	30.6	0.14	5
SPAD Value	42.30	37.03	44.08	1.80	4
Plant N uptake (kg ha <sup>-1</sup> )	23.86	12.97	43.25	5.80	24
N Nutrition Index	1.01	0.89	1.17	0.05	5
2012					
Biomass (t ha <sup>-1</sup> )	2.91	1.45	4.68	0.79	27
Leaf area index	3.34	1.77	5.66	0.86	26
Plant N concentration (g kg <sup>-1</sup> )	22.4	17.5	27.7	0.25	11
SPAD Value	40.60	37.07	43.40	1.68	4
Plant N uptake (kg ha <sup>-1</sup> )	65.00	30.11	114.9	17.93	28
N Nutrition Index	1.15	0.83	1.50	0.16	14

SD: standard deviation; CV: coefficient of variation (%).

An examination of each individual field indicated that the average PNC and SPAD values were the highest in Filed 1 (F1), the biomass value was the lowest, while the average NNI was optimal. In contrast, F4 had the lowest PNC, but the highest average NNI and biomass, indicating a surplus N status (Table 4-4). These results indicated the importance of using NNI for N status diagnosis, rather than PNC.

**Table 4-4** Descriptive statistics of rice N status indicators for different fields, Heilongjiang Province, China, 2011-2012.

Field	Biomass (t ha <sup>-1</sup> )	Plant N Concentration (g kg <sup>-1</sup> )	SPAD Value	NNI
F1	0.81±0.16	27.7±1.40	43.07±0.62	1.00±0.05
F2	1.27±0.25	26.3±1.44	37.89±0.89	1.03±0.10
F3	0.97±0.17	27.4±1.13	39.83±0.65	1.00±0.04
F4	3.89±0.41	21.2±2.82	40.90±1.08	1.21±0.16
F5	2.53±0.53	22.9±2.26	40.49±1.85	1.13±0.16

#### 4.3.2 Vegetation index analysis

The performance of the VIs differed with N status indicators. The top 10 VIs for estimating different N status indicators in each year are listed in Table 4-5.

For aboveground biomass, the top 10 VIs performed similarly in 2011 ( $R^2 = 0.63-0.67$ ) and 2012 ( $R^2 = 0.63-0.64$ ). This was also true for PNU for both years. For LAI, the top 10 VIs performed slightly better in 2011 ( $R^2 = 0.63-0.67$ ) than in 2012 ( $R^2 = 0.58-0.60$ ). Four VIs that are based on the combinations of NIR and red bands, including Ratio Vegetation Index 3 (RVI3), Wide Dynamic Range Vegetation Index 1 (WDRVI1), Soil Adjusted Vegetation Index (SAVI) and Modified Simple Ratio (MSR), were consistently among the top 10 indices for biomass, PNU and LAI. The MCARI index, based on the combination of NIR, red and green bands, had the highest correlation with aboveground biomass ( $R^2 = 0.67$ ) and LAI ( $R^2 = 0.67$ ) in 2011. Four VIs, which included MCARI1, Triangular Vegetation Index (TVI), Modified TVI1 (MTVI1) and Transformed Chlorophyll Absorption in Reflectance Index (TCARI), were also among the top 10 indices for both aboveground biomass and PNU.

Lower correlations were found between the VIs and NNIs, with  $R^2$  of 0.15-0.18 in 2011 and 0.33-0.35 in 2012 for the 10 best models. None of the VIs was significantly correlated with PNC in a specific year, although 30%-55% of the PNC variability was explained across the two years (Table 4-5). The relationships between VIs and SPAD values were also weak, with  $R^2$  being 0.10-0.27 and 0.14-0.23 in 2011 and 2012, respectively.

Fig. 4-1 shows selected VI models with the best performance in estimating rice aboveground biomass, LAI, PNU and NNI across years. The values for 2011 samples were all smaller than those of 2012. Most samples in 2011 had NNI values close to optimum, and the variability was very small, with CV being only 5%. As a result, a cluster was formed at the lower end of Fig. 4-1d. This may explain why the relationships between VIs and NNI were quite weak in 2011 (Table 4-5).

### 4.3.3 Nitrogen status diagnosis

According to the above results, an indirect NNI estimation method was used in this study. The NNI values estimated this way were moderately correlated with measured NNI across 2011 and 2012 ( $R^2 = 0.52$ ,  $RMSE = 0.10$  and  $RE_r = 9.14\%$ ) (Fig. 4-2). By comparing the regression line to the 1:1 line in Fig. 4-2, a systematic bias can be identified in the regression model. In particular, when the observed NNI was less than 1.08, the model overestimated the NNI, while the opposite was true when the NNI was greater than 1.08.

The NNI maps created using the indirect method for two farmers' fields are shown in Fig. 4-3 as an example. Fig. 4-3a,b shows the NNI maps at the pixel level and the plot level, respectively. The first (Fig. 4-3, left) is a well-managed field, with 92% of the field being in the optimal N status category. In contrast, the second field (Fig. 4-3, right) had only 35% in the optimal N category and about 51% in the deficient N category.

A more quantitative and preferable approach is to produce a PNU difference map ( $\Delta PNU$ ) by subtracting the critical PNU map from the predicted PNU map. This  $\Delta PNU$  map can not only tell us if the N status is deficient, optimal or surplus, but also the amount of deficiency or surplus. This further can be used to produce a prescription map for topdressing N application rates (NR) at the stem elongation stage. Specifically, the prescription map will be the planned topdressing panicle NR map based on regional best management practice minus the  $\Delta PNU$  map. Fig. 4-4 displays a  $\Delta PNU$  map of the second field shown in Fig. 4-3. About 12% of the field had an N surplus of over  $5 \text{ kg ha}^{-1}$ , while 20% of the field had an N deficiency of over  $5 \text{ kg ha}^{-1}$ .

**Table 4-5** The top 10 coefficients of determination ( $R^2$ ) for the relationships between vegetation indices based on the FORMOSAT-2 satellite images and rice N status indicators in Heilongjiang Province, China, 2011-2012. Only significant  $R^2$  values were listed.

Indices	2011	2012	2011+2012	Indices	2011	2012	2011+2012
<b>Aboveground biomass (t ha<sup>-1</sup>)</b>				<b>LAI</b>			
MCARI	0.67**	0.62**	0.90**	MCARI	0.67**	0.58**	0.90**
DVI3	0.65**	0.63**	0.90**	DVI2	0.67**	0.58**	0.91**
TVI	0.64**	0.64**	0.90**	RVI3	0.65**	0.60**	0.90**
RVI3	0.64**	0.63**	0.90**	DVI3	0.65**	0.60**	0.91**
MTVI1	0.63**	0.64**	0.90**	RDVI2	0.65**	0.58**	0.90**
MCARI1	0.63**	0.64**	0.90**	WDRVI1	0.65**	0.60**	0.90**
MTCARI	0.63**	0.64**	0.89**	MSR	0.65**	0.60**	0.90**
WDRVI1	0.63**	0.64**	0.89**	RDVI3	0.64**	0.60**	0.90**
MSR	0.63**	0.64**	0.90**	SAVI	0.63**	0.61**	0.88**
SAVI	0.61**	0.64**	0.87**	NDVI1	0.63**	0.61**	0.88**
<b>Plant N concentration (g kg<sup>-1</sup>)</b>				<b>SPAD Values</b>			
DVI4			0.55**	TCI	0.27**	0.17**	0.13**
RDVI4			0.53**	PSRI	0.19**		0.10**
NDVI4			0.49**	MTVI2	0.18**	0.22**	0.16**
RDVI2			0.49**	MTCARI	0.16**	0.22**	0.14**
RVI4			0.49**	MCARI2	0.15*	0.23**	0.15**
MGSAVI			0.48**	WDRVI1	0.14*	0.20**	0.12**
NDVI2			0.48**	MTVI3	0.10*	0.25**	0.13**
GOSAVI			0.48**	MTCARI/OSAVI		0.14**	
WDRVI2			0.47**	EVI		0.14**	
mNDVI1			0.30**	DVI	0.13*		0.19**
<b>Plant N uptake (kg ha<sup>-1</sup>)</b>				<b>NNI</b>			
RVI3	0.66**	0.61**	0.87**	RDVI1	0.18**	0.32**	0.41**
TVI	0.66**	0.61**	0.87**	DVI2	0.17**	0.33**	0.43**
WDRVI1	0.66**	0.62**	0.87**	RVI2	0.17**	0.33**	0.44**
RDVI3	0.66**	0.62**	0.87**	WDRVI2	0.16**	0.34**	0.43**
MTCARI	0.65**	0.63**	0.86**	DVI3	0.16**	0.34**	0.43**
MSR	0.65**	0.62**	0.87**	RDVI2	0.16**	0.34**	0.42**
MCARI1	0.65**	0.62**	0.87**	RVI3	0.16**	0.34**	0.45**
MTVI1	0.65**	0.62**	0.87**	WDRVI1	0.15*	0.35**	0.44**
SAVI	0.64**	0.62**	0.85**	RDVI3	0.15*	0.35**	0.43**
OSAVI	0.64**	0.62**	0.85**	TVI	0.15*	0.34**	0.44**

\*\* . Correlation is significant at the 0.01 level; \* . Correlation is significant at the 0.05 level.

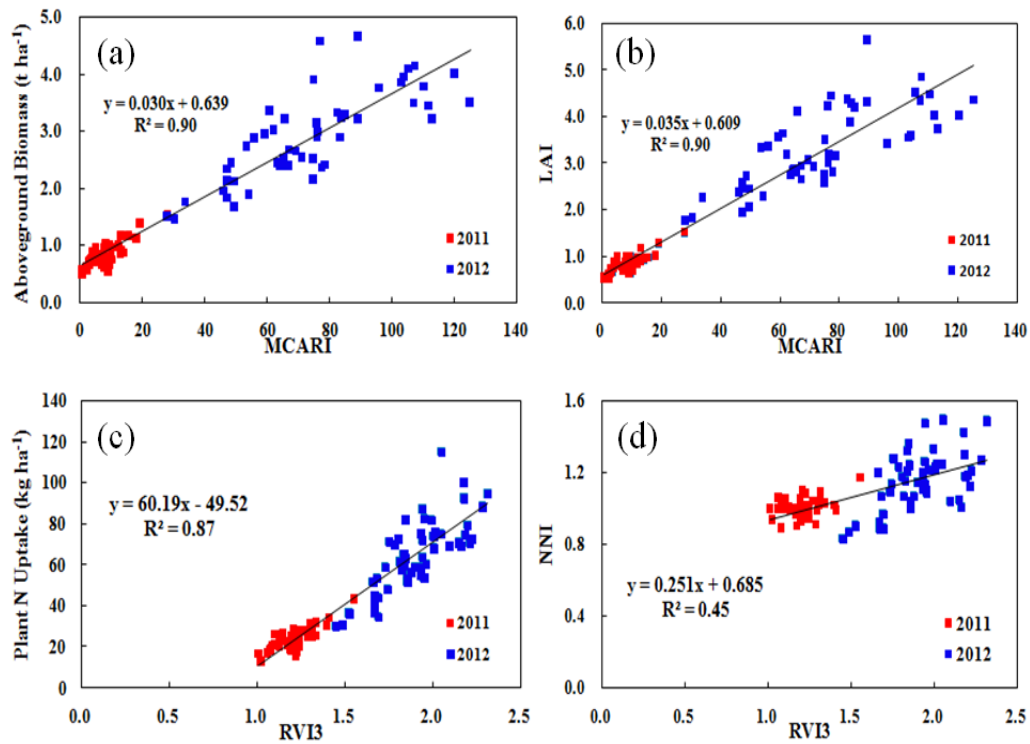


**Fig. 4-1** Selected VI regression vs. rice aboveground biomass (a), LAI (b), PNU (c), and NNI (d), Heilongjiang Province, China, 2011-2012.

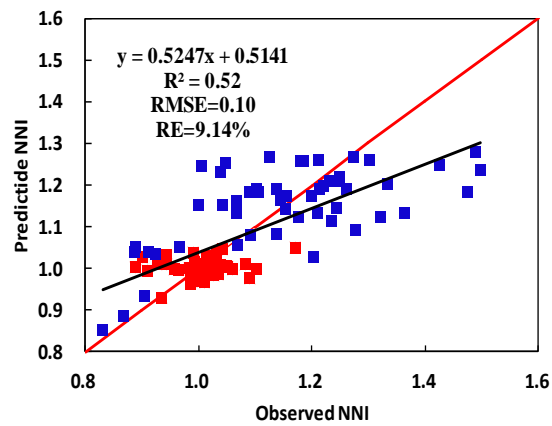


**Fig. 4-2** Relationship between observed and predicted NNI using MCARI-estimated biomass and RVI3-estimated plant N uptake in 2011 and 2012, Heilongjiang Province, China. The red line is the 1:1 line.

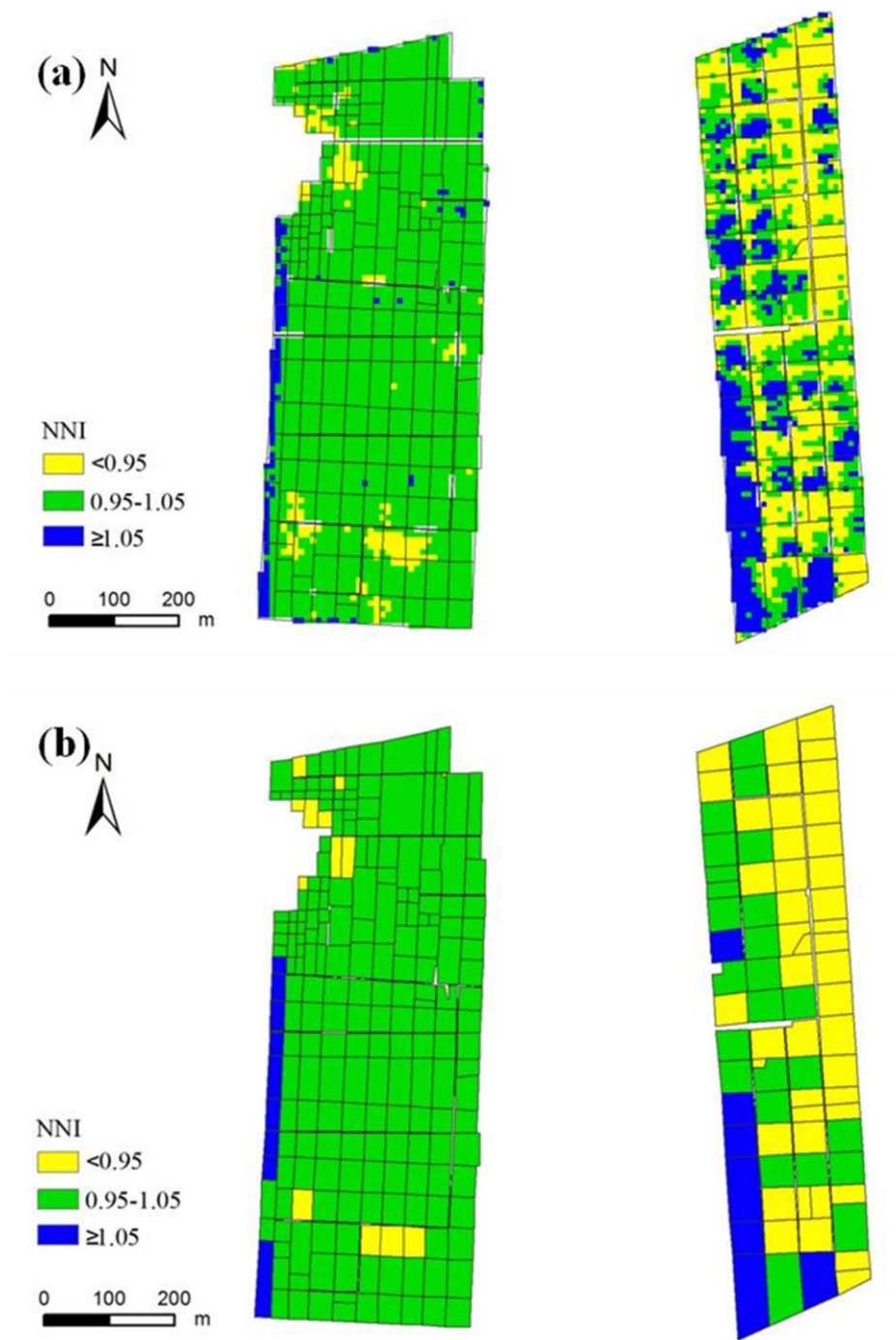


**Fig. 4-3** Examples of predicted rice N nutrition index (NNI) maps of two fields at pixel-level (a) and plot-level (b), Heilongjiang Province, China.

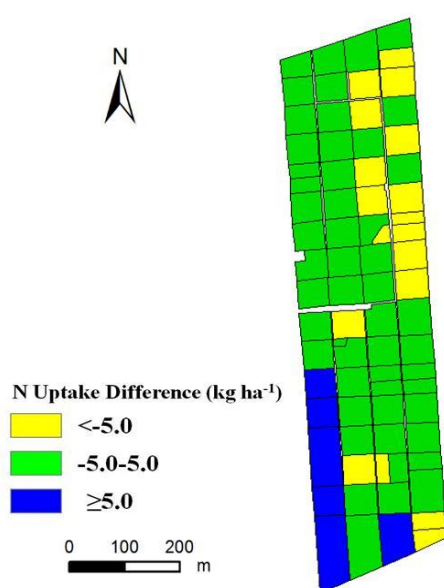


**Fig. 4-4** Example of a plant N uptake difference map of a farmer's field, Heilongjiang Province, China.

## 4.4 Discussion

### 4.4.1 Direct estimation of NNI

Using satellite remote sensing to estimate rice plant NNI for diagnosing rice N status and guiding in-season site-specific N management across large areas is an attractive idea. How well can we estimate NNI directly using FORMOSAT-2 satellite data? The results of this study indicated that all of the top 10 VIs were significantly correlated with NNI, explaining 18% and 35% of the NNI variability in 2011 and 2012, respectively. Across years, 45% of NNI variability was explained with RVI3. This result is slightly better than what Yao *et al.* (2014) found using the handheld GreenSeeker NDVI and RVI, which explained 25% and 34% of rice NNI variability at the stem elongation stage, respectively. It was found that the top 10 VIs obtained with the three-band Crop Circle ACS 470 sensor explained 61%-69% of rice NNI variability across the panicle initiation and stem elongation stages (Cao *et al.*, 2013). However, our study only used data from the panicle initiation stage in 2011, which was expected to be more influenced by the water background than the stem elongation stage. In general, it is not satisfactory to use satellite images to directly estimate rice plant NNI at this stage. At later stages when the rice plants reach canopy closure, this approach may work better. However, it may then be too late for guiding in-season N application.

### 4.4.2 Indirect estimation of NNI

An alternative approach is to use remote sensing to estimate key parameters and indirectly estimate NNI. Cilia *et al.* (2014) used aerial hyperspectral remote sensing to

estimate maize N concentration and biomass and then estimated NNI indirectly. Our study indicated that biomass could be reliably estimated using satellite remote sensing at the panicle initiation and stem elongation stages, with over 60% of its variability being explained by the top 10 VIs in both 2011 and 2012. We selected MCARI for further analysis. This index was initially developed for estimating leaf chlorophyll variation, but it was also significantly related to LAI (Daughtry *et al.*, 2000; Haboudane *et al.*, 2004). In this study, the MCARI index was highly correlated with rice aboveground biomass and LAI ( $R^2 = 0.58-0.67$ ). The results agree with those of Cao *et al.* (2013), who also identified a modified MCARI as the best index for estimating rice biomass ( $R^2 = 0.79$ ) and plant N uptake ( $R^2 = 0.83$ ) across growth stages. The top 10 Crop Circle VIs in their study explained 50%-54% of rice biomass variability across the panicle initiation and stem elongation stages. Our results were comparable to the results ( $R^2 = 0.68-0.69$ ) of Gnyp *et al.* (2014) that were obtained with optimized narrow band RVI and NDVI for estimating rice biomass at the stem elongation stage. However, estimating rice PNC before canopy closure is a great challenge. We did not find any significant correlation between VIs and rice PNC in this study. This was also stated by Yao *et al.* (2014). They found that the GreenSeeker NDVI and RVI were not significantly correlated with rice PNC at the stem elongation stage. Cao *et al.* (2013) found that the three-band Crop Circle ACS 470 sensor at best explained 33% of rice PNC across the panicle initiation and stem elongation stages using the Red Edge Green Difference Vegetation Index (REGDVI). Even with hyperspectral remote sensing, Yu *et al.* (2013) only explained 39% of rice PNC variability across the tillering and heading stages using the Optimized Simple Ratio or Normalized Difference Index. Before canopy closure, soil and water backgrounds in paddy rice fields can influence plant reflectance (Van Niel & McVicar, 2004). In addition, plant biomass dominates canopy reflectance before the heading stage, making the estimation of chlorophyll and N concentration at early growth stages difficult (Mistele & Schmidhalter, 2008). Therefore, the approach adopted by Cilia *et al.* (2014) did not work for rice monitoring at the panicle initiation and stem elongation stages in our study.

A practical approach is to use satellite remote sensing to estimate rice biomass and PNU. From the estimated biomass and the critical N dilution curve, the critical PNU can be determined, and NNI will be calculated using the estimated PNU and the critical PNU. The results of this study supported this idea. Over 60% of rice PNU variability was explained by RVI3 in both years. This was even better than the result obtained with the GreenSeeker sensor for estimating rice PNU at the stem elongation stage ( $R^2 = 0.40-0.41$ ) by Yao *et al.* (2014) and similar to the results ( $R^2 = 0.63-0.65$ ) obtained with the Crop Circle ACS 470 sensor for estimating rice PNU across the panicle initiation and stem elongation stages by Cao *et al.* (2013). The estimated NNI obtained this way explained 52% of the measured NNI variability across 2011 and 2012, which was slightly better than the direct estimation of NNI using VIs obtained from satellite images ( $R^2 = 0.45$ ).

#### 4.4.3 Applications for rice N status diagnosis and topdressing N recommendation

After the NNI map is generated, it is necessary to define the NNI thresholds for N status diagnosis. The current thresholds (NNI < 1: deficient; NNI = 1: optimal; NNI > 1: surplus) may need to be further refined for practical applications. For example, the NNI values of 0.99 and 1.01 are very close to each other and are all quite optimal, but they will be classified as deficient and surplus N status, respectively, based on current thresholds. Cilia *et al.* (2014) proposed to classify NNI into five classes (NNI  $\leq$  0.7, 0.7 < NNI  $\leq$  0.9, 0.9 < NNI  $\leq$  1.1, 1.1 < NNI  $\leq$  1.3, NNI > 1.3) and regarded NNI  $\leq$  0.9 as N deficient, 0.9 < NNI  $\leq$  1.1 as N optimal and NNI > 1.1 as N surplus. Based on the rice N management situations in the study region, we proposed the following thresholds for rice: NNI  $\leq$  0.95 as N deficient, 0.95 < NNI  $\leq$  1.05 as N optimal and NNI > 1.05 as N surplus. These threshold values can be used to delineate a field into three regions with different N nutritional status. The diagnosis results are shown in Fig. 4-3 indicated that the first field (Fig. 4-3 left) was well managed, with the majority of the field having an optimal N status, while about 51% of the second field (Fig. 4-3, right) was deficient in N. These agreed quite well with the two farmers' management practices. However, these threshold values are empirical, and more studies are needed to further test and refine these thresholds by relating NNI to relative grain yield.

The NNI-based rice N status map can be used to guide in-season topdressing N application. For the optimal N zone, 30 kg N ha<sup>-1</sup> was recommended based on the regional best N management practice. For the deficient N zone, 35 or 40 kg ha<sup>-1</sup> can be recommended, and for the surplus N zone 25 or 20 kg ha<sup>-1</sup>. This approach is commonly used in site-specific N management of rice based on CM diagnosis developed by the International Rice Research Institute (Peng *et al.*, 2010). It is empirical, but very practical for on-farm applications in small-scale farming areas of Asia. A more quantitative approach is to produce a PNU difference map using the estimated PNU map minus the critical PNU map. The recommended N topdressing application rate can be determined using the regional optimum topdressing N application rate minus the PNU difference. This approach is different from the variable rate N application strategy proposed by Cilia *et al.* (2014). They first computed the average PNU from the optimal NNI pixels and then used this average value together with the estimated PNU to calculate the difference, and for N deficient pixels, the deficient amounts were used as variable N application rates. For pixels with optimal and surplus N, no N fertilizers were recommended. In our approach, we did not analyze the pixel scale, because, in rice farming, the field is divided into many small plots for irrigation purpose. These plots also serve as management units. We applied plot-average NNI values to diagnose the rice N status of each plot. Our precision N management strategy takes the regional optimal N rate as the initial total N rate, with 40% and 30% being applied as basal and tillering N fertilizers, respectively. For topdressing N application at the stem elongation stage,

30% of the initial total N rate should be applied if the N status is optimal. Otherwise, the topdressing N rates can be adjusted based on deficient or surplus N amounts. Even if the N status is optimal at the stem elongation stage, it only indicates the N status at that stage, which is more than two months prior to harvest, and a certain amount of N fertilizers should still be recommended to meet the N requirements from stem elongation to harvest.

#### 4.4.4 Challenges and future research needs

The proposed approach discussed above requires the satellite imagery to be collected in a narrow time window, preferably one week before topdressing N application at the stem elongation stage for rice in the study region. If the image is collected too early, the diagnosis result may not match the true rice N status at the stem elongation stage. In addition, rice plants will be too small, and the water background will strongly influence the plant reflectance. If the image is collected too close to the stem elongation stage, it may be too late to use the diagnosis result for guiding the topdressing N application. Therefore, a satellite with a high temporal resolution is required. The daily revisit time of the FORMOSAT-2 satellite makes it ideal for this purpose. Its 8-m spatial resolution may be too coarse for small-scale farming in other parts of China, such as in the North China Plain (Shen *et al.*, 2013), but is good enough for large-scale farming in the Sanjiang Plain of Northeast China.

It should be noted that there are 7-10 days between the panicle initiation and stem elongation stages and the rice plants are fast developing, so the rice biomass and plant N uptake determined at the panicle initiation stage are smaller than the values at the stem elongation stage. Studies are needed to determine the influence of this difference on the recommended topdressing N application rates.

Year to year weather variability poses a challenge to use satellite remote sensing for in-season rice N status diagnosis and guiding topdressing application. The satellite imageries were collected at similar times in both years. However, the temperature in 2012 was higher than 2011. The accumulated temperature from transplanting date to the sampling date of 2012 was about 100 °C higher than that in 2011. As a result, rice plants grew faster in 2012 and already reached the stem elongation stage when the image was collected on 26 June 2012. This was reflected by the larger biomass, LAI, and plant N uptake values in 2012 than 2011 (Table 4-3). Another factor to consider is that there are many cloudy and rainy days during the growing season in many parts of the major rice planting regions, which can prevent us from getting the needed satellite images within the narrow time window in some years. Such uncertainty in year to year weather variability makes it very difficult to collect the satellite images at the right time for guiding in-season N management.

To overcome this limitation, multi-temporal and dual-polarimetric TerraSAR-X satellite data were evaluated for monitoring rice crop growth, and very promising results were

obtained for rice biomass estimation (Koppe *et al.*, 2013). Low-altitude remote sensing based on unmanned aerial vehicles (UAVs) may also be an alternative way for diagnosing in-season rice N status and guiding variable rate N management (Zhang & Kovacs, 2012; Huang *et al.*, 2013; Uto *et al.*, 2013). Due to the quick turn-around time, UAV-based remote sensing images can be collected 1-2 days before the topdressing N application, and the diagnosis result will be more representative. Nevertheless, due to the much smaller coverage and bigger data volume of UAV images, they are still not very practical for regional studies over large areas.

The FORMOSAT-2 satellite images only have four commonly-used wavebands (B, G, R, and NIR). Previous research indicated that red edge-based VIs performed better for estimating crop N status NNI than traditional red light-based indices (Cao *et al.*, 2015; Mistele & Schmidhalter, 2008; Li *et al.*, 2014). According to Li *et al.* (2014), the red edge-based Canopy Chlorophyll Content Index (CCCI) was reported to have the best performance among all of the indices evaluated for estimating summer maize N concentration and uptake at V6, V7 and V10-V12 stages, based on the simulation of Crop Circle ACS 470 active sensor, RapidEye and WorldView 2 satellite images. It is necessary to evaluate the potential improvements in estimating rice NNI using RapidEye and WorldView 2 satellite images. Hyperspectral sensing has the potential to further improve the estimation of crop NNI, as demonstrated in winter wheat (Mistele & Schmidhalter, 2008) and summer maize (Chen *et al.*, 2013), and more studies are needed to explore the potential of hyperspectral sensing for monitoring crop NNI.

In summary, the proposed satellite remote sensing approach can achieve comparable performance as ground-based active canopy sensors for estimating rice N status and is applicable to other rice planting regions. It is more efficient for large area applications, but is more influenced by weather conditions, while active canopy sensors are independent of environmental light conditions. It requires special training to process satellite remote sensing data, while active canopy sensors are easy to use, but are not suitable for large area applications. The UAV-based approach, coupled with red edge-based indices and hyperspectral remote sensing, has the potential to overcome the disadvantages of the ground active sensing and satellite remote sensing approaches. Therefore, it deserves further studies.

#### 4.5 Conclusions

This study evaluated the potential of using FORMOSAT-2 satellite images to estimate rice NNI at the panicle initiation stage for guiding topdressing N application at the stem elongation stage in Northeast China. Across years, 45% of NNI variability could be explained using the RVI3 index directly. On the other hand, the indirect approach using FORMOSAT-2 images to estimate the aboveground biomass, PNU and, consequently, NNI

achieved slightly better results ( $R^2 = 0.52$  across years). Moreover, the calculated difference between the estimated PNU and the critical PNU based on the indirect method can be used to guide the topdressing N application rate adjustments, which demonstrated that FORMOSAT-2 images have the potential to estimate rice N status for guiding panicle N fertilizer applications in Northeast China. However, more studies are needed to further evaluate and improve the proposed method of in-season rice N status diagnosis and precision N management strategy under different on-farm conditions using different types of satellite data. The potential of UAV-based remote sensing, coupled with red edge-based indices and hyperspectral sensors, for improving rice NNI monitoring also needs to be studied in future research.

### Acknowledgment

This study was financially supported by the National Basic Research Program (2015CB150405), the Natural Science Foundation of China (31071859), the Innovative Group Grant of the Natural Science Foundation of China (31421092), the European Aeronautic Defense and Space Company (EADS), the CHN-2152, 14-0039 SINOGRain project and the Sino-UK Newton AgriTech Remote Sensing for Sustainable Intensification project. We thank the staff of the Jiansanjiang Bureau of Agricultural Land Reclamation, Qixing Farm, and the Jiansanjiang Institute of Agricultural Sciences for their support. We also would like to thank all of the farmers for their cooperation in this research, and Prasad Thenkabail, Tao Cheng and the anonymous reviewers for their suggestions to improve the manuscript.

### Conflicts of Interest

The authors declare no conflict of interest.

### 4.6 References

- Bei, J.H., Wang, K.R., Chu, Z.D., Chen, B., Li, S.K., 2005. Comparative study on the measurement methods of the leaf area. *J. Shihezi Uni. (Nat. Sci.)*. 23, 216–218.
- Broge, N.H., Leblanc, E., 2000. Comparing prediction power and stability of broadband and hyperspectral vegetation indices for estimation of green leaf area index and canopy chlorophyll density. *Remote Sens. Environ.* 76, 156–172.
- Buschmann, C., Nagel, E., 1993. In vivo spectroscopy and internal optics of leaves as basis for remote sensing of vegetation. *Int. J. Remote Sens.* 14, 711–722.

- Cao, Q., Cui, Z., Chen, X., Khosla, R., Dao, T.H., Miao, Y., 2012. Quantifying spatial variability of indigenous nitrogen supply for precision nitrogen management in small scale farming. *Precis. Agric.* 13, 45–61.
- Cao, Q., Miao, Y., Feng, G., Gao, X., Li, F., Liu, B., Yue, S., Cheng, S., Ustin, S., Khosla, R., 2015. Active canopy sensing of winter wheat nitrogen status: An evaluation of two sensor systems. *Comput. Electron. Agric.* 112, 54–67.
- Cao, Q., Miao, Y., Wang, H., Huang, S., Cheng, S., Khosla, R., Jiang, R., 2013. Non-destructive estimation of rice plant nitrogen status with Crop Circle multispectral active canopy sensor. *Field Crops Res.* 154, 133–144.
- Chen, J.M., 1996. Evaluation of vegetation indices and a modified simple ratio for boreal applications. *Can. J. Remote Sens.* 22, 229–242.
- Chen, P., Wang, J., Huang, W., Tremblay, N., Ouyang, Z., Zhang, Q., 2013. Critical nitrogen curve and remote detection of nitrogen nutrition index for corn in the Northwestern Plain of Shandong Province, China. *IEEE J. Sel. Topics Appl. Earth Observ. Remote Sens.* 6, 682–689.
- Chern, J.S., Wu, A.M., Lin, S.F., 2006. Lesson learned from FORMOSAT-2 mission operations. *Acta Astronaut.* 59, 344–350.
- Cilia, C., Panigada, C., Rossini, M., Meroni, M., Busetto, L., Amaducci, S., Boschetti, M., Picchi, V., Colombo, R., 2014. Nitrogen status assessment for variable rate fertilization in maize through hyperspectral imagery. *Remote Sens.* 6, 6549–6565.
- Darvishzadeh, R., Matkan, A.A., Ahangar, A.D., 2012. Inversion of a radiative transfer model for estimation of rice canopy chlorophyll content using a lookup-table approach. *IEEE J. Sel. Topics Appl. Earth Observ. Remote Sens.* 5, 1222–1230.
- Datt, B., 1999. Visible/near infrared reflectance and chlorophyll content in Eucalyptus leaves. *Int. J. Remote Sens.* 20, 2741–2759.
- Daughtry, C.S.T., Walthall, C.L., Kim, M.S., Colstoun, E.B., McMurtrey III, J.E., 2000. Estimating corn leaf chlorophyll concentration from leaf and canopy reflectance. *Remote Sens. Environ.* 74, 229–239.
- Dawe, D., 2000. The contribution of rice research to poverty alleviation. In: Sheehy, J.E., Mitchell, P.L., Hardy, B. (Eds.), *Redesigning rice photosynthesis to increase yield, Proceedings of the Workshop on the Quest to Reduce Hunger: Redesigning Rice Photosynthesis*, 30 November–3 December 1999. Elsevier Science, Amsterdam and IRRI, Los Baños, Philippines, pp. 3–12.
- Debaeke, P., Rouet, P., Justes, E., 2006. Relationship between the normalized SPAD index and the nitrogen nutrition index: Application to durum wheat. *J. Plant Nutr.* 29, 75–92.

- Doberman, A., Witt, C., Dawe, D., Abdurachman, S., Gines, H.C., Nagarajan, R. et al. 2002. Site-specific nutrient management for intensive rice cropping systems in Asia. *Field Crops Res.* 74, 37–66.
- Eitel, J.U.H., Long, D.S., Gessler, P.E., Smith, A.M.S., 2007. Using in-situ measurements to evaluate the new RapidEye™ satellite series for prediction of wheat nitrogen status. *Int. J. Remote Sens.* 28, 4183–4190.
- Gitelson, A.A., 2004. Wide dynamic range vegetation index for remote quantification of biophysical characteristics of vegetation. *J. Plant Physiol.* 161, 165–173.
- Gitelson, A.A., Gritz, Y., Merzlyak, M.N., 2003. Relationships between leaf chlorophyll content and spectral reflectance and algorithms for non-destructive chlorophyll assessment in higher plant leaves. *J. Plant Physiol.* 160, 271–282.
- Gitelson, A.A., Kaufman, Y.J., Merzlyak, M.N., 1996. Use of a green channel in remote sensing of global vegetation from EOS-MODIS. *Remote Sens. Environ.* 58, 289–298.
- Gitelson, A.A., Kaufman, Y.J., Stark, R., Rundquist, D., 2002. Novel algorithms for remote estimation of vegetation fraction. *Remote Sens. Environ.* 80, 76–87.
- Gnyp, M.L., Miao, Y., Yuan, F., Ustin, S.L., Yu, K., Yao, Y., Huang, S., Bareth, G., 2014. Hyperspectral canopy sensing of paddy rice aboveground biomass at different growth stages. *Field Crops Res.* 155, 42–55.
- Greenwood, D.J., Gastal, F., Lemaire, G., Draycott, A., Millard, P., Neeteson, J.J., 1991. Growth rate and % N of field grown crops: theory and experiments. *Ann. Bot.* 67, 181–190.
- Greenwood, D.J., Neeteson, J.J., Draycott, A., 1986. Quantitative relationships for the dependence of growth rate of arable crops on their nitrogen content, dry weight and aerial environment. *Plant Soil* 91, 281–301.
- Haboudane, D., Miller, J.R., Pattey, E., Zarco-Tejada, P.J., Strachan, I.B., 2004. Hyperspectral vegetation indices and novel algorithms for predicting green LAI of crop canopies: Modeling and validation in the context of precision agriculture. *Remote Sens. Environ.* 90, 337–352.
- Haboudane, D., Miller, J.R., Tremblay, N., Zarco-Tejada, P.J., Dextraze, L., 2002. Integrated narrow-band vegetation indices for prediction of crop chlorophyll content for application to precision agriculture. *Remote Sens. Environ.* 81, 416–426.
- Haboudane, D., Tremblay, N., Miller, J.R., Vigneault, P., 2008. Remote estimation of crop chlorophyll content using spectral indices derived from hyperspectral data. *IEEE Trans. Geosci. Remote. Sens.* 46, 423–437.
- Holland, K.H., Lamb, D.W., Schepers, J.S., 2012. Radiometry of proximal active optical sensors (AOS) for agricultural sensing. *IEEE J. Sel. Topics Appl. Earth Observ. Remote Sens.* 5, 1793–1802.

- Houlès, V., Guerif, M., Mary, B., 2007. Elaboration of a nitrogen nutrition indicator for winter wheat based on leaf area index and chlorophyll content for making nitrogen recommendations. *Eur. J. Agron.* 27, 1–11.
- Huang, Y., Thomson, S. J., Hoffmann, W. C., Lan, Y., Fritz, B. K., 2013. Development and prospect of unmanned aerial vehicle technologies for agricultural production management. *Int. J. Agric. Biol. Eng.* 6, 1–10.
- Huete, A., Didan, K., Miura, T., Rodriguez, E.P., Gao, X., Ferreira, L.G., 2002. Overview of the radiometric and biophysical performance of the MODIS vegetation indices. *Remote Sens. Environ.* 83, 195–213.
- Huete, A.R., 1988. A soil-adjusted vegetation index (SAVI). *Remote Sens. Environ.* 25, 295–309.
- Jin, J., 2012. Changes in the efficiency of fertiliser use in China. *J. Sci. Food Agric.* 92, 1006–1009.
- Ju, X., Xing, G., Chen, X., Zhang, S., Zhang, L., Liu, X., Cui, Z., Yin, B., Christie, P., Zhu, Z., Zhang, F., 2009. Reducing environmental risk by improving N management in intensive Chinese agricultural systems. *Proc. Natl. Acad. Sci. USA (PNAS)* 106, 3041–3046.
- Justes, E., Mary, B., Meynard, J.M., Machet, J. M., Thelier-Huche, L., 1994. Determination of a critical nitrogen dilution curve for winter wheat crops. *Ann. Bot.* 74, 397–407.
- Koppe, W., Gnyp, M.L., Hütt, C., Yao, Y., Miao, Y., Chen, X., Bareth, G., 2013. Rice monitoring with multi-temporal and dual-polarimetric TerraSAR-X data. *Int. J. Appl. Earth Observ. Geoinfo.* 21, 568–576.
- Lemaire, G., Jeuffroy, M.H., Gastal, F., 2008. Diagnosis tool for plant and crop N status in vegetative stage: Theory and practices for crop N management. *Eur. J. Agron.* 28, 614–624.
- Li, F., Miao, Y., Feng, G., Yuan, F., Yue, S., Gao, X., Liu, Y., Liu, B., Ustin, S. L., Chen, X., 2014. Improving estimation of summer maize nitrogen status with red edge-based spectral vegetation indices. *Field Crops Res.* 157, 111–123.
- Li, N., 2006. The comparison on various methods for determining different proteins. *J. Shanxi Agric. Univ. (Natural Science Edition)*. 26, 132–134.
- Liu, C.C., 2006. Processing of FORMOSAT-2 daily revisit imagery for site surveillance. *IEEE Trans. Geosci. Remote Sens.* 44, 3206–3214.
- Lv, W., Ge, Y., Wu, J., Chang, J., 2004. Study on the method for the determination of nitric nitrogen, ammoniacal nitrogen and total nitrogen in plant. *Spectrosc. Spect. Anal.* 24, 204–206.
- Miao, Y., Mulla, D. J., Randall, G. W., Vetsch, J. A., Vintila, R., 2009. Combining chlorophyll meter readings and high spatial resolution remote sensing images for in-season site-specific nitrogen management of corn. *Precis. Agric.* 10, 45–62.

- Mistele, B., Schmidhalter, U., 2008. Estimating the nitrogen nutrition index using spectral canopy reflectance measurements. *Eur. J. Agron.* 29, 184–190.
- Mulla, D.J., 2013. Twenty five years of remote sensing in precision agriculture: Key advances and remaining knowledge gaps. *Biosyst. Eng.* 114, 358–371.
- Peng, S., Buresh, R.J., Huang, J., Zhong, X., Zou, Y., Yang, J., Wang, G., Liu, Y., Hu, R., Tang, Q., Cui, K., Zhang, F., Dobermann, A., 2010. Improving nitrogen fertilization in rice by site-specific N management. A review. *Agron. Sustain. Dev.* 30, 649–656.
- Peñuelas, J., Baret, F., Filella, I., 1995. Semi-empirical indices to assess carotenoids/chlorophyll a ratio from leaf spectral reflectance. *Photosynthetica* 32, 221–230.
- Prost, L., Jeuffroy, M. H., 2007. Replacing the nitrogen nutrition index by the chlorophyll meter to assess wheat N status. *Agron. Sustain. Dev.* 27, 321–330.
- Qi, J., Chehbouni, A., Huete, A.R., Kerr, Y.H, Sorooshian, S., 1994. A modified soil adjusted vegetation index. *Remote Sens. Environ.* 48, 119–126.
- Rondeaux, G., Steven, M., Baret, F., 1996. Optimization of soil-adjusted vegetation indices. *Remote Sens. Environ.* 55, 95–107.
- Roujean, J.L., Breon, F.M., 1995. Estimating PAR absorbed by vegetation from bidirectional reflectance measurements. *Remote Sens. Environ.* 51, 375–384.
- Shen, J., Cui, Z., Miao, Y., Mi, G., Zhang, H., Fan, M., Zhang, C., Jiang, R., Zhang, W., Li, H., Chen, X., Li, X., Zhang, F., 2013. Transforming agriculture in China: from solely high yield to both high yield and high resource use efficiency. *Global Food Sec.* 2, 1–8.
- Sims, D.A., Gamon, J.A., 2002. Relationships between leaf pigment content and spectral reflectance across a wide range of species, leaf structures and developmental stage. *Remote Sens. Environ.* 81, 337–354.
- Tucker, C.J., 1979. Red and photographic infrared linear combinations for monitoring vegetation. *Remote Sens. Environ.* 8, 127–150.
- Uto, K., Seki, H., Saito, G., Kosugi, Y., 2013. Characterization of rice paddies by a UAV-mounted miniature hyperspectral sensor system. *IEEE J. Sel. Topics Appl. Earth Observ. Remote Sens.* 6, 851–860.
- Van Niel, T.G., McVicar, T.R., 2004. Current and potential uses of optical remote sensing in rice-based irrigation systems: A review. *Aust. J. Agric. Res.* 55, 155–185.
- Wang, W., Yao, X., Yao, X.F., Tian, Y.C., Liu, X.J., Ni, J., Cao, W.X., Zhu, Y., 2012. Estimating leaf nitrogen concentration with three-band vegetation indices in rice and wheat. *Field Crops Res.* 129, 90–98.
- Wang, Y., Yang, Y., 2001. Effects of agriculture reclamation on hydrologic characteristics in the Sanjiang Plain. *Chin. Geogr. Sci.* 11, 163–167.

- Wu, J., Wang, D., Rosen, C.J., Bauer, M.E., 2007. Comparison of petiole nitrate concentrations, SPAD chlorophyll readings, and QuickBird satellite imagery in detecting nitrogen status of potato canopies. *Field Crops Res.* 101, 96–103.
- Xing, B., Dudas, M.J., Zhang, Z., Qi, X., 1994. Pedogenetic characteristics of albic soils in the three river plain, Heilongjiang Province. *Acta Pedolog. Sin.* 31, 95–104.
- Yan, M., Deng, W., Chen, P., 2002. Climate change in the Sanjiang Plain disturbed by large-scale reclamation. *J. Geogr. Sci.* 12, 405–412.
- Yang, C.M., Liu, C.C., Wang, Y.W., 2008. Using FORMOSAT-2 satellite data to estimate leaf area index of rice crop. *J. Photogram. Remote Sens.* 13, 253–260.
- Yao, Y., Miao, Y., Cao, Q., Wang, H., Gnyp, M.L., Bareth, G., Khosla, R., Yang, W., Liu, F., Liu, C., 2014. In-season estimation of rice nitrogen status with an active crop canopy sensor. *IEEE J. Sel. Topics Appl. Earth Observ. Remote Sens.* 7, 4403–4413.
- Yao, Y., Miao, Y., Huang, S., Gao, L., Ma, X., Zhao, G., Jiang, R., Chen, X., Zhang, F., Yu, K., Gnyp, M.L., Bareth, G., Liu, C., Zhao, L., Yang, W., Zhu, H., 2012. Active canopy sensor-based precision N management strategy for rice. *Agron. Sustain. Dev.* 32, 925–933.
- Yu, K., Li, F., Gnyp, M.L., Miao, Y., Bareth, G., Chen, X., 2013. Remotely detecting canopy nitrogen concentration and uptake of paddy rice in the Northeast China Plain. *ISPRS J. Photogramm. Remote Sens.* 78, 102–115.
- Zhang, C., Kovacs, J.M., 2012. The application of small unmanned aerial systems for precision agriculture: A review. *Precis. Agric.* 13, 693–712.
- Zhang, F., Cui, Z., Fan, M., Zhang, W., Chen, X., Jiang, R., 2011. Integrated soil-crop system management: reducing environmental risk while increasing crop productivity and improving nutrient use efficiency in China. *J. Environ. Qual.* 40, 1051–1057.
- Zhang, F., Wang, J., Zhang, W., Cui, Z., Ma, W., Chen, X., Jiang, R., 2008. Nutrient use efficiencies of major cereal crops in China and measures for improvement. *Acta Pedolog. Sin.* 5, 915–924.
- Zhao, G., Miao, Y., Wang, H., Su, M., Fan, M., Zhang, F., Jiang, R., Zhang, Z., Liu, C., Liu, P., Ma, D., 2013. A preliminary precision rice management system for increasing both grain yield and nitrogen use efficiency. *Field Crops Res.* 154, 23–30.
- Ziadi, N., Bélanger, G., Claessens, A., Lefebvre, L., Tremblay, N., Cambouris, A.N., Nolin, M.C., Parent, L.É., 2010. Plant-based diagnostic tools for evaluating wheat nitrogen status. *Crop Sci.* 50, 2580–2590.
- Ziadi, N., Brassard, M., Bélanger, G., Claessens, A., Tremblay, N., Cambouris, A.N., Nolin, M.C., Parent, L.É., 2008. Chlorophyll measurements and nitrogen nutrition index for the evaluation of corn nitrogen status. *Agron. J.* 100, 1264–1273.

## Chapter 5: Potential of RapidEye and WorldView-2 Satellite Data for Improving Rice Nitrogen Status Monitoring at Different Growth Stages

SHANYU HUANG<sup>1,2</sup>, YUXIN MIAO<sup>1,\*</sup>, FEI YUAN<sup>3</sup>, MARTIN L. GNYP<sup>1,4</sup>, YINKUN YAO<sup>1</sup>, QIANG CAO<sup>5</sup>, HONGYE WANG<sup>1</sup>, VICTORIA I.S. LENZ-WIEDEMANN<sup>1,2</sup>, and GEORG BARETH<sup>1,2</sup>

Published in: *Remote Sens.* 2017, 9, 227, doi:10.3390/rs9030227

*Formatting, orthography, and units of the manuscript are adapted to the dissertation style.*

- <sup>1</sup> International Center for Agro-Informatics and Sustainable Development, College of Resources and Environmental Sciences, China Agricultural University, Beijing 100193, China
- <sup>2</sup> Institute of Geography, University of Cologne, 50923 Cologne, Germany
- <sup>3</sup> Department of Geography, Minnesota State University, Mankato, MN 56001, USA
- <sup>4</sup> Research Centre Hanninghof, Yara International, 48249 Duellen, Germany
- <sup>5</sup> National Engineering and Technology Center for Information Agriculture, Nanjing Agricultural University, Nanjing 210095, China

\*Corresponding author. E-mail: ymiao@cau.edu.cn, ymiao2007@gmail.com

### Abstract

For in-season site-specific nitrogen (N) management of rice to be successful, it is crucially important to diagnose rice N status efficiently across large areas within a short time frame. In recent studies, the FORMOSAT-2 satellite images with traditional blue (B), green (G), red (R), and near-infrared (NIR) wavebands have been used to estimate rice N status due to its high spatial resolution, daily revisit capability, and relatively lower cost. This study aimed to evaluate the potential improvements of RapidEye and WorldView-2 data over FORMOSAT-2 for rice N status monitoring, as the former two sensors provide additional wavelengths besides the traditional four wavebands. Ten site-year N rate experiments were conducted in Jiansanjiang, Heilongjiang Province of Northeast China from 2008 to 2011. Plant samples and field hyperspectral data were collected at three growth stages: panicle initiation (PI), stem elongation (SE), and heading (HE). The canopy-scale hyperspectral data were upscaled to simulate the satellite bands. Vegetation index (VI) analysis, stepwise multiple linear regression (SMLR), and partial least squares regression (PLSR) were performed to derive plant N status indicators. The results indicated that the best-performed VIs calculated from the simulated RapidEye and WorldView-2 bands, especially those based on the red edge (RE) band, explained significantly more variability for aboveground biomass

(AGB), plant N uptake (PNU), and nitrogen nutrition index (NNI) estimations than their FORMOSAT-2-based counterparts did, especially at the PI and SE stages. The SMLR and PLSR models based on the WorldView-2 bands generally had the best performance, followed by the ones based on the RapidEye bands. The SMLR results revealed that both the NIR and RE bands were important for N status estimation. In particular, the NIR1 band (760-900 nm from RapidEye or 770-895 nm from WorldView-2) was most important for estimating all the N status indicators. The RE band (690-730 nm or 705-745 nm) improved AGB, PNU, and NNI estimations at all three stages, especially at the PI and SE stages. AGB and PNU were best estimated using data across the stages while plant N concentration (PNC) and NNI were best estimated at the HE stage. The PLSR analysis confirmed the significance of the NIR1 band for AGB, PNU, and NNI estimations at all stages except for the HE stage. It also showed the importance of including extra bands (coastal, yellow, and NIR2) from the WorldView-2 sensor for N status estimation. Overall, both the RapidEye and WorldView-2 data with RE bands improved the results relative to FORMOSAT-2 data. However, the WorldView-2 data with three extra bands in the visible and NIR regions showed the highest potential in estimating rice N status.

## 5.1 Introduction

Precision nitrogen (N) management of rice (*Oryza sativa* L.) is crucially important for food security and sustainable development, especially for Asian countries like China (Yao *et al.*, 2012; Zhao *et al.*, 2013; Huang *et al.*, 2015). Non-destructive technologies are needed for in-season site-specific diagnosis of rice plant N status and making topdressing N recommendations. During the past decade, active canopy sensors (ACS), such as GreenSeeker (Trimble Navigation Limited, Sunnyvale, CA, USA) and Crop Circle (Holland Scientific, Lincoln, NE, USA) sensors, have been developed and have gained popularity for diagnosing crop N status and guiding in-season N management of wheat (*Triticum aestivum* L.), maize (*Zea mays* L.), and rice (Yao *et al.*, 2012; Yao *et al.*, 2014; Li *et al.*, 2009; Cao *et al.*, 2015; Cao *et al.*, 2016; Xia *et al.*, 2016). For large production field applications, such sensors have been installed on variable rate fertilizer application machines for real-time sensing, diagnosis of crop N status, topdressing or side-dressing N recommendation, and variable rate application (Schmidt *et al.*, 2009; Diacono *et al.*, 2013; Holland & Schepers, 2013). However, such systems are not common for rice, as it is difficult for variable rate application machines to enter flooded paddy fields. It is also very challenging and time-consuming to carry active canopy sensors and walk across large paddy fields.

Alternatively, satellite remote sensing offers a promising non-intrusive solution to monitor rice N status and to guide site-specific N recommendations over large areas (Huang *et al.*, 2015; Mulla, 2013; Mulla & Miao, 2016). For in-season site-specific N management,

a satellite sensor with relatively high spatial resolution is required because rice canopy plots are small. In addition, high temporal resolution is also crucially important, as cloudy weather conditions are quite common in rice planting regions. There is only a narrow time window to collect and process remote sensing images, produce topdressing fertilization prescription, and implement fertilizer applications. Therefore, to date, studies of using satellite instruments for crop N monitoring are still limited due to the restricted sensor resolutions of most satellites.

The FORMOSAT-2 is the first earth observation satellite developed by the National Space Organization (NSPO) of Taiwan in 2004. The FORMOSAT-2 data have a spatial resolution of 8 m for the four multispectral bands (Blue (B), Green (G), Red (R), and Near-Infrared (NIR)) and 2 m for the panchromatic band. The daily revisit capability with a constant view angle and the medium-high spatial resolution make FORMOSAT-2 one of the most suitable satellites for regional precision agriculture applications (Huang *et al.*, 2015; Zhao *et al.*, 2015). Particularly, Huang *et al.* (2015) found that FORMOSAT-2 images could be used to estimate rice aboveground biomass (AGB), leaf area index (LAI), plant N uptake (PNU) and N nutrition index (NNI) at the early growth stage. In addition, the IKONOS and QuickBird satellite sensors have higher spatial resolutions but lower temporal resolutions than FORMOSAT-2 with the same band settings. They also have been used in previous studies for monitoring crop N status, green LAI (GLAI), and yield (Beeri *et al.*, 2005; Claverie *et al.*, 2012; Tang *et al.*, 2004).

Launched in August of 2008, RapidEye was the first commercial satellite with red edge (RE) band in addition to traditional B, G, R, and NIR bands, with an improved 5 m spatial resolution (Magney *et al.*, 2016). Many studies evaluated the applicability of the RE wavebands. Eitel *et al.* (2007) used hyperspectral data to simulate RapidEye wavebands and found that the RE-based vegetation index (VI), Modified Chlorophyll Absorption Ratio Index/Modified Triangular Vegetation Index 2 (MCARI/MTVI2), performed the best for chlorophyll content and leaf N concentration estimations. Eitel *et al.* (2011) stated that the RE-based VI, Normalized Difference Red Edge (NDRE), could identify plant N stress earlier than Normalized Difference Vegetation Index (NDVI) and Green NDVI (GNDVI). The RE-based indices from the RapidEye images improved the LAI and plant N status estimations compared with the R radiation-based VIs (Asam *et al.*, 2013; Kim & Yeom, 2012; Ramoelo *et al.*, 2012).

In addition to RapidEye, the WorldView-2 satellite was launched in October of 2009 with a further increased spatial resolution of 2 m. Besides the traditional four and the RE wavebands, three additional ones are included: coastal (C), yellow (Y), and an extra NIR band (NIR2). Mutanga *et al.* (2012) found that the NDRE using WorldView-2 imagery could solve the saturation problem encountered with high-density biomass estimation for wetland

vegetation.

The FORMOSAT-2, RapidEye, and WorldView-2 satellites are ideal choices for crop N status estimation since they all have short revisit time with 2-8 m spatial resolutions. Notably, both the RapidEye and WorldView-2 satellite sensors with additional wavelengths have the potential to further improve crop N monitoring. The first crucial question addresses how to define the expected improvements of RapidEye data for rice N status monitoring compared with FORMOSAT-2 data. Second, can WorldView-2 data further improve the estimation of rice N status with three extra spectral bands compared with RapidEye? Comparing these three satellite datasets directly proves difficult because of the lacking of archived images from these satellite sensors at multiple growth stages for this study site on our sampling dates. To evaluate and quantify the potential benefits of the RE band or the additional three bands, a practical approach is to use hyperspectral canopy reflectance data to simulate the spectral bands of the three satellite sensors. This approach has been widely used in remote sensing studies in recent years. Yang *et al.* (2008) found that the NDVI values calculated with a hyperspectral canopy sensor were highly correlated ( $R^2 = 0.79$ ) with NDVIs derived from broadband FORMOSAT-2 images. Bsaibes *et al.* (2009) compared the ground measured albedo and FORMOSAT-2 retrievals for five crops and found their albedo values were closely related. Bausch and Khosla (2010) compared several normalized VIs based on QuickBird imagery with the ones calculated from simulated QuickBird bands using hyperspectral data, and confirmed their high levels of similarity.

In previous studies, VIs have been widely used to estimate crop N status. While numerous VIs have been developed, the most commonly used VIs are based on R and NIR bands, such as the NDVI. However, the NDVI may saturate under moderate-to-high biomass conditions at later growth stages (Thenkabail *et al.*, 2000; Mutanga & Skidmore, 2004; Gnyp *et al.*, 2014). The RE-based VIs have been proven to be sensitive to crop canopy chlorophyll and N variation, even under the high biomass condition (Cao *et al.*, 2016; Van Niel & McVicar, 2004; Nguy-Robertson *et al.*, 2012; Cao *et al.*, 2013; Kanke *et al.*, 2016). Since both RapidEye and WorldView-2 have the RE band, the question of how RE-based indices could improve the estimation of rice N status needed to be answered. In addition to VI analysis, the stepwise multiple linear regression (SMLR) and partial least squares regression (PLSR) were applied as well since it was noted that multivariate techniques have usually allowed slightly better N prediction than the VI method (Stroppiana *et al.*, 2012). The PLSR analysis combines the methods of principal component analysis and multiple linear regression that cut the predictors to a smaller and uncorrelated subset. Therefore, it can efficiently deal with the multi-collinearity issue in predicting variables (Wold *et al.*, 2001). PLSR has been used successfully to estimate canopy biomass and N status in wheat crops (Hansen & Schjoerring, 2003) and to assess rice leaf growth and N status (Nguyen & Lee, 2006).

Therefore, the objective of this study was to evaluate the potential of using RapidEye and WorldView-2 satellite data to improve rice N status monitoring over commonly used four-band satellite data such as FORMOSAT-2 at different growth stages based on ground hyperspectral canopy data and VI analysis, SMLR as well as PLSR.

## 5.2 Materials and methods

### 5.2.1 Study area

The study area is located at the Qixing Farm in the Sanjiang Plain, Heilongjiang Province, Northeast China. The Sanjiang Plain used to be a wild natural wetland formed by the alluvium of three river systems—Heilong River, Songhua River, and Wusuli River. This area has a typical cool-temperate sub-humid continental monsoon climate. During the growing season (April-October), the average rainfall is around 400 mm, which accounts for approximately 70% of yearly precipitation. The mean annual temperature is about 2 °C (Wang & Yang, 2001), and the average daily temperature is 19.9 °C during the growing season (from mid-May to mid-September). The annual sunshine duration is 2300-2600 h and the whole year frost-free period is about 120-140 days (Yan *et al.*, 2002). The main soil type in the region is Albic soil, classified as Mollic Planosols in the FAO-UNESCO system and Typical Argialbolls in Soil Taxonomy (Xing *et al.*, 1994).

### 5.2.2 Experiment design

Ten N rate experiments were conducted in 2008, 2009, and 2011, involving two Japonica rice cultivars: Kongyu 131 (11 leaves) and Longjing 21 (12 leaves) (Table 5-1). All of the experiments adopted the randomized complete block design with 3-4 replications. The N fertilizer was applied in three splits for Experiments 1-6: 40%-45% as the basal application before transplanting, 20%-30% at the tillering stage, and 30%-35% at the stem elongation (SE) stage. For Experiments 7-10, the N fertilizer was applied in two splits: 60% as the basal application and 40% at the tillering stage. In each experiment, 45-60 kg ha<sup>-1</sup> phosphate (P<sub>2</sub>O<sub>5</sub>) and 90-105 kg ha<sup>-1</sup> potash (K<sub>2</sub>O) fertilizers were applied to ensure sufficient phosphorus (P) and potassium (K) nutrients. The P fertilizer was applied as a basal application before transplanting while the K fertilizer was applied in two splits, with 50% as the basal fertilizer and 50% as the panicle fertilizer at the SE stage.

**Table 5-1** Details of the N rate experiments conducted from 2008 to 2011 in Jiansanjiang, Heilongjiang Province, Northeast China.

Experiment	Site	Year	Cultivar	N Rates (kg ha <sup>-1</sup> )	Transplanting/Harvesting Date	Sampling Stage
1	1	2008	Kongyu 131	0, 35, 70, 105, 140	29 May/21 September	PI, SE, HE
2	2	2008	Kongyu 131	0, 35, 70, 105, 140	13 May/22 September	PI, SE, HE
3	1	2009	Kongyu 131	0, 35, 70, 105, 140	24 May/27 September	SE, HE
4	2	2009	Kongyu 131	0, 35, 70, 105, 140	20 May/27 September	PI, SE, HE
5	1	2011	Kongyu 131	0, 70, 100, 130, 160	17 May/21 September	PI
6	1	2011	Longjing 21	0, 70, 100, 130, 160	19 May/21 September	PI
7	1	2008	Kongyu 131	0, 23, 45, 68, 91	29 May/21 September	HE
8	2	2008	Kongyu 131	0, 23, 45, 68, 91	13 May/22 September	HE
9	1	2009	Kongyu 131	0, 23, 45, 68, 91	24 May/27 September	SE, HE
10	2	2009	Kongyu 131	0, 23, 45, 68, 91	20 May/27 September	SE, HE

PI: panicle initiation stage; SE: stem elongation stage; HE: heading stage.

### 5.2.3 Determining N status indicators with plant sampling and analysis

Plant samples were collected at several critical growth stages, including the panicle initiation (PI), SE and heading (HE) stages, to determine the values of four N status indicators—AGB, plant N concentration (PNC), PNU, and NNI. Growth stages have significant impacts on estimating N status indicators. The AGB and PNU increase with the advancement of growth stages, and they have positive correlations with N nutritional status. As explained by the dilution effect (Greenwood *et al.*, 1986; Lemaire *et al.*, 2008), the PNC declines during the growth period within dense canopies. It is positively correlated with N nutritional status but inversely related to growth stages.

The detailed sampling dates and related information were listed in Table 5-1. Before plant sampling, the average tiller number per hill for each treatment plot was determined, and then 3 to 6 representative hills with average tiller numbers were randomly selected and cut at the ground surface. All the plant samples were rinsed with water and the roots were removed to determine the AGB. Then the samples were separated into leaves, stems, and panicles (for samples collected at the HE stage). The separated samples were put into an oven at 105 °C for half an hour for deactivation of enzymes, and then dried at 70-80 °C until constant weight. After being weighed, the samples were ground into powders and sub-samples were put through 1 mm sieve for PNC analysis using the standard Kjeldahl-N method. The PNU was determined by multiplying PNC with dry AGB. Both PNC and PNU have been widely used as N status indicators in former studies.

NNI is defined as the ratio of the actual PNC ( $N_a$ ) and the critical N concentration ( $N_c$ ), which was calculated using the equation developed for rice in Northeast China based on data

from N rate experiments conducted in this region from 2008 to 2013 following the method of Justes *et al.* (1994). More details about the method can be found in Huang *et al.* (2015). NNI is a unitless parameter. It increases with increasing N rates. This trend remains constant during the growth period (Gastal *et al.*, 2001; Farruggia *et al.*, 2004). If  $N_a$  is greater than  $N_c$  ( $NNI > 1$ ), it indicates a surplus of N while the opposite is true if  $N_a$  is smaller than  $N_c$  ( $NNI < 1$ ). An NNI value of 1 indicates an optimal N supply (Huang *et al.*, 2015; Lemaire *et al.*, 2008). NNI has advantages as a specific, sensitive, memorable, and predictive tool for crop N diagnosis (Lemaire *et al.*, 2008; Chen *et al.*, 2010). Therefore, NNI is a better indicator for diagnosing crop N status than PNC and PNU (Lemaire *et al.*, 2008). The NNI map can be used directly to guide in-season topdressing N applications (Huang *et al.*, 2015; Cilia *et al.*, 2014).

#### 5.2.4 Field spectral measurements and re-sampling

The rice canopy spectra were collected using portable hyperspectral instruments FieldSpec3 (Analytical Spectral Devices Inc., Boulder, CO, USA) for Experiments 1-4 and 7-10, and QualitySpec Pro (Analytical Spectral Devices Inc., Boulder, CO, USA) for Experiments 5 and 6. The QualitySpec Pro collects reflectance from 350 to 1800 nm while the FieldSpec 3 provides spectra across 350 to 2500 nm. Both of them have a spectral resolution of 1.2 nm from 350 to 1100 nm and a 2 nm spectral resolution beyond 1100 nm.

All spectra were obtained under sunny cloudless conditions during local mid-day (9:00 a.m.-1:00 p.m.). The measurements were taken 0.3 m above the canopy with a 25° field of view, which gave a sample diameter of 0.14 m. The sensors were carried along the north side of the rice plant rows to minimize the disturbance of the canopy structure and avoid the creation of shadows. The reflectance values were calibrated by a barium sulfate ( $BaSO_4$ ) reference panel at least every 10-15 min. Five to six scans were taken randomly for each plot. The average value was calculated subsequently and used as the plot reflectance.

Next, the FORMOSAT-2 (F2), RapidEye (RY), and WorldView-2 (WV2) bands were simulated and evaluated. Detailed sensor characteristics for the three satellite systems were shown in Table 5-2. The field hyperspectral data were resampled in order to simulate the satellite wavebands based on the theory of band equivalent reflectance explained as Equation (5-1):

$$r_i = \frac{\sum_{\lambda u_i}^{\lambda l_i} r(\lambda) \varphi_i(\lambda)}{\sum_{\lambda u_i}^{\lambda l_i} \varphi_i(\lambda)} \quad (5-1)$$

where  $r_i$  stands for the reflectance of band  $i$ ;  $\lambda u_i$  is the starting wavelength of band  $i$ ;  $\lambda l_i$  is the termination wavelength of band  $i$ ;  $r(\lambda)$  is the reflectance value at wavelength  $\lambda$ ;  $\varphi_i(\lambda)$  is the band response function of band  $i$  at wavelength  $\lambda$ . The band response function data of

FORMOSAT-2 was provided by the NSPO while the corresponding data for RapidEye and WorldView-2 were supplied by the ENVI 4.8 software (Harris Geospatial Solutions, Broomfield, CO, USA) (Fig. 5-1).

**Table 5-2** The properties of the FORMOSAT-2, RapidEye, and WorldView-2 satellite sensors.

Properties	FORMOSAT-2 (F2)	RapidEye (RY)	WorldView-2 (WV2)
Type	Sun-synchronous	Sun-synchronous	Sun-synchronous
Launch time	4 May 2004	8 August 2008	9 October 2009
Orbit altitude (km)	891	620	770
Spatial Resolution for Multispectral bands (m)	8	6.5	2
Spatial Resolution for Panchromatic bands (m)	2	-	0.5
Revisit time (Day)	1	< 1	1.1
Swath width (km)	24	80	16.4
Band settings	450–520 nm (Blue: B) 520–600 nm (Green: G) 630–690 nm (Red: R) 760–900 nm (NIR1: NIR1)	440–510 nm (Blue: B) 520–590 nm (Green: G) 630–685 nm (Red: R) 690–730 nm (Red edge: RE) 760–900 nm (NIR1: NIR1)	400–450 nm (Coastal: C) 450–510 nm (Blue: B) 510–581 nm (Green: G) 585–625 nm (Yellow: Y) 630–690 nm (Red: R) 705–745 nm (Red Edge: RE) 770–895 nm (NIR1: NIR1) 860–1040 nm (NIR2: NIR2)

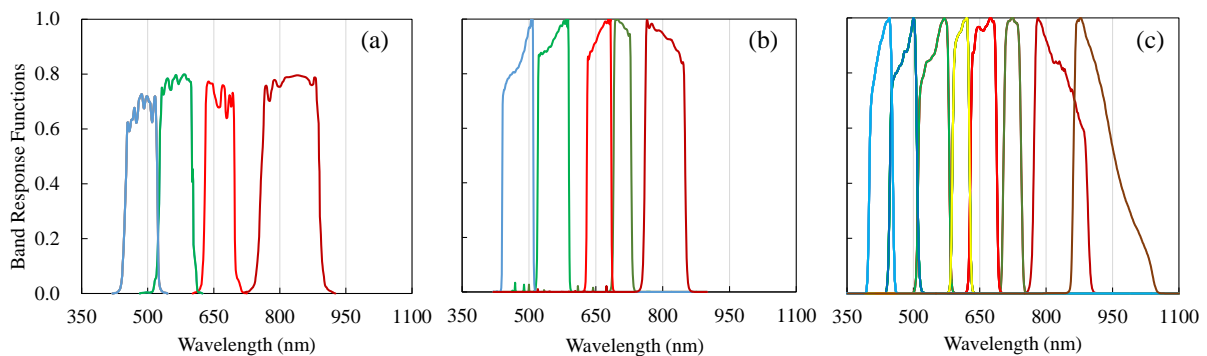


**Fig. 5-1** Band response functions for: FORMOSAT-2 (a); RapidEye (b); and WorldView-2 (c) satellite sensors used in this study.

### 5.2.5 Data analysis

All 369 in-situ samples were divided into two groups by a stratified random sampling method, with approximately 2/3 of the data used for model calibration and the rest for model validation.

In total, 21 different VIs were calculated (Table 5-3) and correlated with the four N status indicators separately. To evaluate the band effects of simulated satellite data on the relationships between VIs and N status indicators over the growing season, the same VIs were calculated for all three types of satellite data when possible. Linear regression models were then constructed for the three individual growth stages and across the stages. The relationships between each of the VIs and each of the indicators were determined. The coefficient of determination ( $R^2$ ) was used to assess and compare the performance of the VI models. According to the  $R^2$  ranking, the top 5 VIs were listed, and the best VIs were shown in scatter plots. The Root Mean Square Error (RMSE) and relative error (REr) were also calculated to evaluate the model performance.

In addition, SMLR using SPSS V.20.0 (IBM SPSS Statistics, Armonk, NY, USA) and PLSR using Matlab 7.10 (MathWorks, Natick, MA, USA) were implemented to estimate the four variables. In order to evaluate the relative importance of each waveband in each of the PLSR models, the Variable Importance in Projection (VIP) values were computed. The VIP is a variable selection method in PLSR. It calculates the influence of the independent variables to the dependent variable, and selects the most influential predictors for a PLSR model. The VIP value for a variable is a weighted sum of squares of the PLSR weights that take into account the explained variance of each PLSR dimension. A variable with a VIP value greater than one is considered important in the PLSR model. The larger the VIP score, the greater the contribution of the variable. The VIP values can be used to identify individual waveband importance and the most effective spectral regions (Chong & Jun, 2005; Li *et al.*, 2014b).

**Table 5-3** Vegetation indices evaluated in this study for estimating rice N status indicators.

Vegetation Indices	Formula	Satellite Sensors	Reference
Ration Vegetation Index (RVI)	$NIR/R$	F2, RY, WV2	Jordan (1969)
Chlorophyll Index (CI)	$(NIR/G) - 1$	F2, RY, WV2	Gitelson <i>et al.</i> (2005)
Normalized Difference Vegetation Index (NDVI)	$(NIR - R)/(NIR + R)$	F2, RY, WV2	Rouse <i>et al.</i> (1973)
Green NDVI (GNDVI)	$(NIR - G)/(NIR + G)$	F2, RY, WV2	Gitelson <i>et al.</i> (1996)
Optimized Soil Adjusted Vegetation Index (OSAVI)	$(1 + 0.16) \times ((NIR - R)/(NIR + R + 0.16))$	F2, RY, WV2	Rondeaux <i>et al.</i> (1996)
Modified Chlorophyll Absorption in Reflectance Index (MCARI)	$((NIR - R) - 0.2(R - G)) \times (NIR/R)$	F2, RY, WV2	Daughtry <i>et al.</i> (2000)
Triangular Vegetation Index (TVI)	$0.5 \times (120(NIR - G) - 200(R - G))$	F2, RY, WV2	Broge & Leblanc (2000)
Modified Transformed Chlorophyll Absorption in Reflectance Index (TCARI)	$3 \times ((NIR - R) - 0.2(NIR - G))(NIR/R)$	F2, RY, WV2	Haboudane <i>et al.</i> (2002)
MCARI/OSAVI	MCARI/OSAVI	F2, RY, WV2	Haboudane <i>et al.</i> (2002)
TCARI/OSAVI	TCARI/OSAVI	F2, RY, WV2	Haboudane <i>et al.</i> (2002)
Red Edge Chlorophyll Index (RECI)	$(NIR/RE) - 1$	RY, WV2	Broge & Leblanc (2000)
Normalized difference Red Edge Index (NDRE)	$(NIR - RE)/(NIR + RE)$	RY, WV2	Fitzgerald <i>et al.</i> (2010)
MERIS Terrestrial Chlorophyll Index (MTCI)	$(NIR - RE)/(RE - R)$	RY, WV2	Dash & Curran (2004)
Canopy Chlorophyll Content Index (CCCI)	$(NDRE - NDRE_{min})/(NDRE_{max} - NDRE_{min})$	RY, WV2	Fitzgerald <i>et al.</i> (2010)
Nitrogen Planar Domain Index (NDPI)	$(RECI - RECI_{min})/(RECI_{max} - RECI_{min})$	RY, WV2	Clarke <i>et al.</i> (2001)
Red Edge OSAVI (REOSAVI)	$(1 + 0.16) \times ((NIR - RE)/(NIR + RE + 0.16))$	RY, WV2	Wu <i>et al.</i> (2008)
Red Edge MCARI (REMCARI)	$((NIR - RE) - 0.2(RE - G)) \times (NIR/RE)$	RY, WV2	Wu <i>et al.</i> (2008)
Red Edge Triangular Vegetation Index (RETVI)	$0.5 \times (120(NIR - G) - 200(RE - G))$	RY, WV2	Broge & Leblanc (2000)
Red Edge TCARI (RETCARI)	$3 \times ((NIR - RE) - 0.2(NIR - G))(NIR/RE)$	RY, WV2	Wu <i>et al.</i> (2008)
REMCARI/REOSAVI	REMCARI/REOSAVI	RY, WV2	Wu <i>et al.</i> (2008)
RETCARI/REOSAVI	RETCARI/REOSAVI	RY, WV2	Wu <i>et al.</i> (2008)

## 5.3 Results

### 5.3.1 Variability of the N status indicators

The descriptive statistics of the four N status indicators at different growth stages for both of the calibration and validation datasets were listed in Table 5-4. In the calibration dataset, both AGB and PNU increased moderately from the PI stage to the SE stage, and dramatically to the HE stage. In contrast, PNC decreased slightly from the PI stage to the SE stage, and declined sharply to the HE stage, affected by the “dilution effect” described by Plénet and Lemaire (1999). The NNI indicated a slightly under-supply of N at the PI stage, but a nearly optimal N supply at the SE stage and an over-supply at the HE stage. The AGB and PNU had larger coefficients of variation (CVs) than PNC and NNI (Table 5-4). Similar trends were observed for the validation dataset. The mean values of the four N indicators across stages were similar for both datasets.

**Table 5-4** Descriptive statistics of the measured aboveground biomass (AGB), N concentration (PNC), plant N uptake (PNU), and N nutrition index (NNI) for the model estimation and validation at the panicle initiation (PI), stem elongation (SE), heading (HE) and across stages (All).

Stage	Statistical indicator	Calibration Dataset				Validation Dataset			
		AGB (t ha <sup>-1</sup> )	PNC (g kg <sup>-1</sup> )	PNU (kg ha <sup>-1</sup> )	NNI	AGB (t ha <sup>-1</sup> )	PNC (g kg <sup>-1</sup> )	PNU (kg ha <sup>-1</sup> )	NNI
PI	<i>n</i>	57	57	57	57	28	28	28	28
	Mean	1.11	24.7	27.53	0.96	1.05	24.6	26.09	0.94
	SD	0.50	1.72	12.71	0.11	0.48	2.08	11.84	0.10
	CV	45.02	6.97	46.17	11.4	45.79	8.45	45.4	10.63
SE	<i>n</i>	92	92	92	92	45	45	45	45
	Mean	1.78	23.6	40.13	1.01	1.83	23.9	41.32	1.02
	SD	0.88	3.57	16.96	0.14	0.99	3.50	18.25	0.12
	CV	49.36	15.11	42.26	13.74	54.17	14.64	44.17	12.04
HE	<i>n</i>	98	98	98	98	49	49	49	49
	Mean	6.28	16.2	103.34	1.09	5.93	16.0	95.41	1.05
	SD	1.49	2.76	36.20	0.24	1.45	2.90	31.09	0.22
	CV	23.75	17.06	35.03	21.97	24.46	18.11	32.59	21.18
All	<i>n</i>	247	247	247	247	122	122	122	122
	Min	0.20	8.3	4.39	0.53	0.14	9.6	3.17	0.65
	Max	9.92	31.5	205.64	1.63	9.21	33.5	195.37	1.63
	Mean	3.41	20.9	62.30	1.03	3.30	20.9	59.55	1.02
	SD	2.59	4.84	42.36	0.19	2.45	4.98	37.94	0.17
	CV	75.95	22.97	67.99	18.45	74.24	23.92	63.71	16.67

*n*: number of observations; SD: standard deviation; CV: coefficient of variation (%).

### 5.3.2 Correlation between N indicators and vegetation indices

For VI models derived from RapidEye and WorldView-2 bands, all the top five ones for AGB (Table 5-5) and PNU (Table 5-6) estimations were based on RE indices—MERIS Terrestrial Chlorophyll Index (MTCI), Canopy Chlorophyll Content Index (CCCI), N Planar Domain Index (NDPI), Red Edge Chlorophyll Index (RECI), and NDRE. Comparatively, the top five FORMOSAT-2-based VI models showed significantly lower performance at the PI and SE stages and slightly lower performance at the HE stage and across the stages, demonstrating the importance of using RE band in AGB and PNU estimations at early and middle growth stages. From the PI through the HE stages, the best performed RE VI models showed  $R^2$  values ranging from 0.62 to 0.65 for PNU estimation (Table 5-6). Across the stages, the RE-based NDPI, RECI, MTCI and the traditional Chlorophyll Index (CI) explained the most variability for AGB and PNU estimations with  $R^2$  ranging from 0.80 to 0.83 (Fig. 5-2).

In contrast, as shown in Table 5-5, PNC did not have any significant relationships with most of the VIs at the PI and SE stages, indicating the difficulty of estimating N concentrations at early and middle stages using VIs. However, at the HE stage, the model performance was significantly improved with the highest  $R^2$  ranging from 0.42 to 0.57. Again, the RE-based indices performed better at this stage. Across the stages, similar performance was obtained for both groups of indices. In addition, Table 5-6 revealed an improved NNI estimation using RE-based VIs relative to the non-RE ones. The performance gap between the two groups of indices was the smallest at the SE stage. Likewise, the best RE-based VI models ( $R^2 = 0.60-0.62$ ) for NNI estimation were found to be at the HE stage, slightly better than the original CI ( $R^2 = 0.58$ ) and GNDVI ( $R^2 = 0.57$ ) models. These results demonstrated that the best stage for PNC and NNI estimations based on these satellite sensor bands was the HE stage. For FORMOSAT-2-based indices, the CI was the best for estimating these N indicators in most cases (Fig. 5-2).

## Different Growth Stages

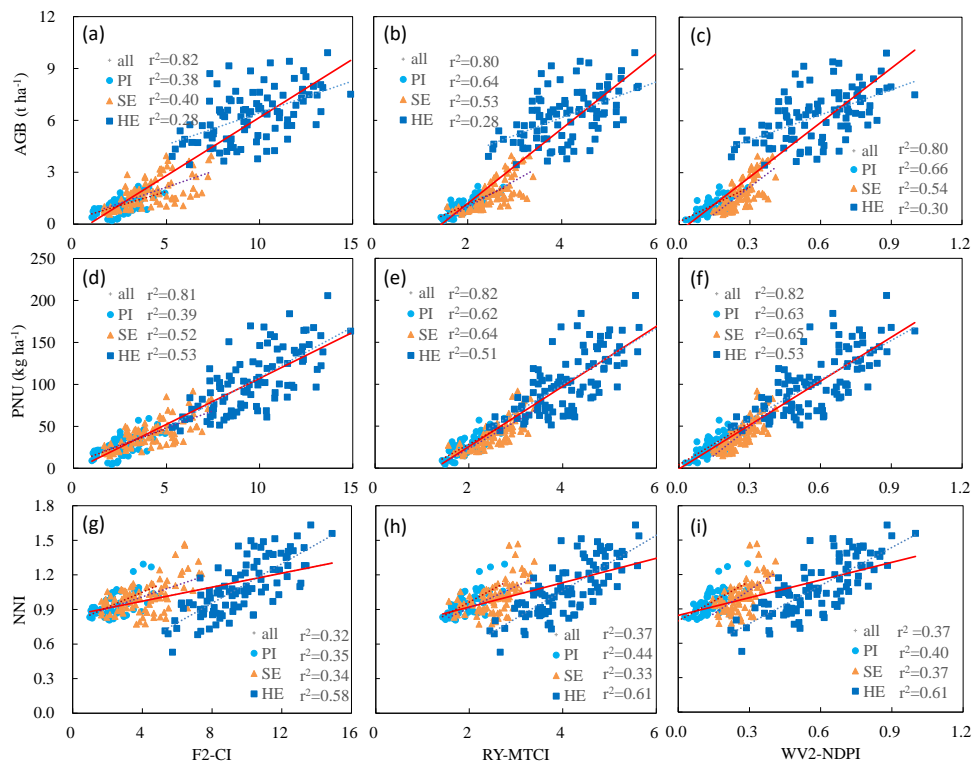


**Fig. 5-2** Relationships between: FORMOSAT-2-based Chlorophyll Index (CI) (a); RapidEye-based MERIS Terrestrial Chlorophyll Index (MTCI) (b); WorldView-2-based Nitrogen Planar Domain Index (NDPI) (c), and aboveground biomass (AGB); FORMOSAT-2-based CI (d); RapidEye-based MTCI (e); WorldView-2-based NDPI (f), and plant N uptake (PNU); and FORMOSAT-2-based CI (g); RapidEye-based MTCI (h); WorldView-2-based NDPI (i), and N nutrition index (NNI), at the panicle initiation (PI), stem elongation (SE), heading (HE), and across all stages. The relationships between VIs and N status indicators across growth stages are indicated by the red lines.

**Table 5-5** The top five coefficients of determination ( $R^2$ ) for the relationships between vegetation indices based on the wavebands of FORMOSAT-2 (F2), RapidEye (RY), WorldView-2 (WV2) and aboveground biomass (AGB), plant N concentration (PNC) at the panicle initiation (PI), stem elongation (SE), heading (HE), and across stages (All), respectively. Only significant  $R^2$  values were listed.

PI Stage		SE Stage		HE Stage		All	
Index	AGB	Index	AGB	Index	AGB	Index	AGB
F2-CI	0.39 **	F2-GNDVI	0.41 **	F2-CI	0.28 **	F2-CI	0.82 **
F2-GNDVI	0.35 **	F2-OSAVI	0.41 **	F2-GNDVI	0.27 **	F2-RVI	0.80 **
F2-MCARI/OSAVI	0.33 **	F2-NDVI	0.41 **	F2-RVI	0.21 **	F2-MCARI/OSAVI	0.77 **
F2-TCARI/OSAVI	0.34 **	F2-CI	0.40 **	F2-NDVI	0.20 **	F2-TCARI/OSAVI	0.77 **
F2-RVI	0.33 **	F2-TVI	0.39 **	F2-TCARI/OSAVI	0.18 **	F2-MCARI	0.75 **
RY-MTCI	0.64 **	RY-MTCI	0.53 **	RY-MTCI	0.28 **	RY-CI	0.82 **
RY-CCCI	0.61 **	RY-CCCI	0.51 **	RY-CCCI	0.28 **	RY-RECI	0.81 **
RY-NDPI	0.59 **	RY-NDPI	0.50 **	RY-NDPI	0.28 **	RY-NDPI	0.81 **
RY-RECI	0.46 **	RY-RECI	0.47 **	RY-RECI	0.28 **	RY-RVI	0.80 **
RY-NDRE	0.43 **	RY-NDRE	0.46 **	RY-NDRE	0.28 **	RY-MTCI	0.80 **
WV2-NDPI	0.65 **	WV2-MTCI	0.57 **	WV2-NDPI	0.30 **	WV2-CI	0.82 **
WV2-MTCI	0.62 **	WV2-NDPI	0.54 **	WV2-MTCI	0.30 **	WV2-RECI	0.82 **
WV2-RETVI	0.57 **	WV2-RECI	0.51 **	WV2-RECI	0.30 **	WV2-MTCI	0.81 **
WV2-RECI	0.54 **	WV2-NDRE	0.50 **	WV2-NDRE	0.30 **	WV2-RETVI	0.81 **
WV2-NDRE	0.53 **	WV2-RETVI	0.47 **	WV2-CCCI	0.30 **	WV2-NDPI	0.80 **
Index	PNC	Index	PNC	Index	PNC	Index	PNC
F2-CI		F2-NDVI	0.06 *	F2-CI	0.53 **	F2-OSAVI	0.42 **
F2-GNDVI		F2-GNDVI		F2-GNDVI	0.52 **	F2-TVI	0.41 **
F2-RVI		F2-OSAVI		F2-NDVI	0.46 **	F2-NDVI	0.39 **
F2-TCARI/OSAVI		F2-CI		F2-RVI	0.44 **	F2-RVI	0.39 **
F2-TCARI		F2-RVI		F2-TCARI/OSAVI	0.42 **	F2-GNDVI	0.39 **
RY-RETCARI/REOSAVI		RY-RETCARI	0.09 **	RY-RECI	0.57 **	RY-OSAVI	0.42 **
RY-GNDVI		RY-NDVI	0.06 *	RY-MTCI	0.56 **	RY-REOSAVI	0.42 **
RY-RECI		RY-NDRE	0.05 *	RY-NDPI	0.56 **	RY-TVI	0.41 **
RY-NDPI		RY-MTCI		RY-NDRE	0.55 **	RY-GNDVI	0.40 **
RY-MTCI		RY-GNDVI		RY-RETCARI/REOSAVI	0.55 **	RY-RETVI	0.40 **
WV2-GNDVI		WV2-MTCI	0.07 *	WV2-REOSAVI	0.57 **	WV2-RETCARI	0.44 **
WV2-RECI		WV2-NDVI	0.06 *	WV2-RECI	0.56 **	WV2-OSAVI	0.42 **
WV2-NDPI		WV2-NDRE	0.05 *	WV2-MTCI	0.56 **	WV2-REOSAVI	0.41 **
WV2-NDRE		WV2-GNDVI		WV2-NDRE	0.56 **	WV2-TVI	0.41 **
WV2-CI		WV2-RECI		WV2-NDPI	0.55 **	WV2-GNDVI	0.39 **

\*\* Correlation is significant at the  $P \leq 0.01$  level; \* Correlation is significant at the  $P \leq 0.05$  level.

**Table 5-6** The top five coefficients of determination ( $R^2$ ) for the relationships between vegetation indices based on the wavebands of FORMOSAT-2 (F2), RapidEye (RY), WorldView-2 (WV2) and plant N uptake (PNU), N nutrition index (NNI) at the panicle initiation (PI), stem elongation (SE), heading (HE), and across stages (All), respectively. Only significant  $R^2$  values were listed.

PI Stage		SE Stage		HE Stage		All	
Index	PNU	Index	PNU	Index	PNU	Index	PNU
F2-CI	0.39 **	F2-CI	0.52 **	F2-CI	0.50 **	F2-CI	0.81 **
F2-GNDVI	0.35 **	F2-TVVI	0.52 **	F2-GNDVI	0.48 **	F2-RVI	0.77 **
F2-TCARI/OSAVI	0.34 **	F2-GNDVI	0.50 **	F2-RVI	0.40 **	F2-MCARI/OSAVI	0.76 **
F2-RVI	0.33 **	F2-OSAVI	0.50 **	F2-NDVI	0.39 **	F2-TCARI/OSAVI	0.76 **
F2-MCARI/OSAVI	0.33 **	F2-MCARI/OSAVI	0.49 **	F2-TCARI/OSAVI	0.36 **	F2-MCARI	0.75 **
RY-MTCI	0.62 **	RY-MTCI	0.64 **	RY-NDPI	0.52 **	RY-NDPI	0.83 **
RY-CCCI	0.59 **	RY-CCCI	0.62 **	RY-RECI	0.52 **	RY-MTCI	0.82 **
RY-NDPI	0.58 **	RY-NDPI	0.61 **	RY-MTCI	0.51 **	RY-CI	0.81 **
RY-RECI	0.46 **	RY-RECI	0.57 **	RY-RETCARI	0.51 **	RY-RECI	0.81 **
RY-NDRE	0.43 **	RY-RETVI	0.56 **	RY-RETCARI/REOSAVI	0.51 **	RY-REMCARI	0.79 **
WV2-NDPI	0.63 **	WV2-NDPI	0.65 **	WV2-RECI	0.62 **	WV2-NDPI	0.82 **
WV2-MTCI	0.60 **	WV2-MTCI	0.64 **	WV2-NDPI	0.61 **	WV2-MTCI	0.82 **
WV2-RETVI	0.54 **	WV2-RETVI	0.61 **	WV2-MTCI	0.61 **	WV2-RECI	0.82 **
WV2-RECI	0.53 **	WV2-RECI	0.60 **	WV2-NDRE	0.61 **	WV2-CI	0.81 **
WV2-NDRE	0.52 **	WV2-NDRE	0.59 **	WV2-REOSAVI	0.61 **	WV2-REMCARI	0.81 **
Index	NNI	Index	NNI	Index	NNI	Index	NNI
F2-CI	0.35 **	F2-TCARI	0.34 **	F2-CI	0.58 **	F2-CI	0.32 **
F2-TCARI/OSAVI	0.32 **	F2-TCARI/OSAVI	0.33 **	F2-GNDVI	0.57 **	F2-TCARI	0.30 **
F2-RVI	0.31 **	F2-MCARI	0.33 **	F2-NDVI	0.48 **	F2-MCARI	0.29 **
F2-GNDVI	0.31 **	F2-MCARI/OSAVI	0.32 **	F2-RVI	0.47 **	F2-TCARI/OSAVI	0.29 **
F2-MCARI/OSAVI	0.29 **	F2-CI	0.30 **	F2-TCARI/OSAVI	0.44 **	F2-RVI	0.28 **
RY-MTCI	0.44 **	RY-REMCARI	0.35 **	RY-NDPI	0.61 **	RY-RETCARI/REOSAVI	0.37 **
RY-NDPI	0.44 **	RY-CCCI	0.34 **	RY-RECI	0.61 **	RY-MTCI	0.37 **
RY-RECI	0.38 **	RY-TCARI	0.34 **	RY-MTCI	0.61 **	RY-NDPI	0.35 **
RY-CCCI	0.36 **	RY-MTCI	0.33 **	RY-NDRE	0.60 **	RY-CCCI	0.35 **
RY-NDRE	0.36 **	RY-REMCARI/REOSAVI	0.33 **	RY-RETCARI/REOSAVI	0.60 **	RY-RETCARI	0.34 **
WV2-MTCI	0.41 **	WV2-NDPI	0.37 **	WV2-RECI	0.62 **	WV2-NDPI	0.37 **
WV2-RECI	0.41 **	WV2-REMCARI	0.36 **	WV2-NDPI	0.61 **	WV2-MTCI	0.35 **
WV2-NDRE	0.41 **	WV2-RETVI	0.36 **	WV2-MTCI	0.61 **	WV2-CCCI	0.35 **
WV2-NDPI	0.40 **	WV2-TCARI	0.34 **	WV2-NDRE	0.61 **	WV2-RECI	0.34 **
WV2-RETVI	0.38 **	WV2-TCARI/OSAVI	0.33 **	WV2-REOSAVI	0.61 **	WV2-REMCARI	0.33 **

\*\* Correlation is significant at the  $P \leq 0.01$  level; \* Correlation is significant at the  $P \leq 0.05$  level.

The improvements of RE-based VIs over traditional ones (B, G, R, and NIR bands) were also demonstrated in Fig. 5-3. It is evident that most of the RE-based indices derived from the WorldView-2 bands had the best performance, followed by the RapidEye RE-based indices, and the FORMOSAT-2-based VIs had the worst performance. The slightly better performance of WorldView-2 RE-based indices relative to those of RapidEye might be attributed to the different RE band settings of the two satellite sensors. Particularly, the RE-based Transformed Chlorophyll Absorption Reflectance Index (RETCARI) and RETCARI/RE-based Optimized Soil Adjusted Vegetation Index (REOSAVI) based on RapidEye bands underperformed than the same indices with WorldView-2 bands at the PI stage, but the opposite was true at the HE stage (Fig. 5-3).

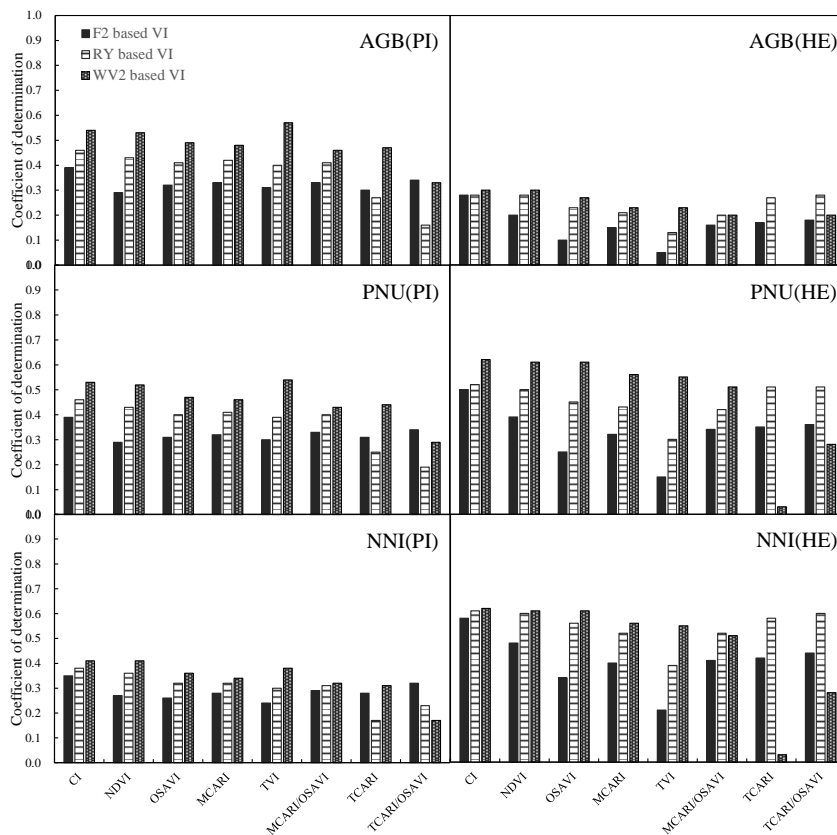


**Fig. 5-3** Comparison of different vegetation indices (VIs) calculated using FORMOSAT-2 (F2), RapidEye (RY) and WorldView-2 (WV2) satellite data for the relationships with aboveground biomass (AGB), plant N uptake (PNU), and N nutrition index (NNI) at the panicle initiation (PI) and heading (HE) stages, respectively.

### 5.3.3 Stepwise multiple linear regression analysis

The SMLR analysis indicated that models using the simulated RapidEye and WorldView-2 bands explained more variability than the ones using FORMOSAT-2 bands at the PI and SE stages (Table 5-7). The regression results showed that the NIR1 band was the

most important band for estimating these N status indicators as it was selected in all the models except the FORMOSAT-2 AGB estimation model at the SE stage. In addition, the RE bands of RapidEye and WorldView-2 were important for AGB, PNU, and NNI estimations at the PI and SE stages (Table 5-7).

At the HE stage, the  $R^2$  values for all the SMLR AGB models were similar (0.29-0.31) based on the three sensor datasets (Table 5-7). Better  $R^2$  values were achieved for PNU ( $R^2 = 0.50-0.52$ ), PNC ( $R^2 = 0.51-0.57$ ) and NNI ( $R^2 = 0.57-0.61$ ) estimations at this stage than previous ones. The SMLR models outperformed the VI-based models for estimating PNC; however, none of the models performed satisfactorily at the PI and SE stages (Table 5-7). Compared to the best-performed VI models for estimating all four N indicators, the SMLR models yielded higher  $R^2$  at the PI and SE stages, but similar  $R^2$  at the HE stage and across the stages (Tables 5-5, 5-6, 5-7).

In general, AGB and PNU were best estimated at the early growth stage (PI) and across the stages while NNI and PNC were best estimated at the later stage (HE). In most cases, the regression models based on the simulated WorldView-2 bands had the highest performance for AGB, PNU, and NNI estimations at a specific growth stage.

#### 5.3.4 Partial least squares regression modeling

Table 5-8 presents the  $R^2$  and RMSE of Calibration (RMSEC) values of the PLSR models for the four N indicators using the entire spectra of the three simulated satellite bands. According to the  $R^2$  and RMSEC values, the WorldView-2 band-based PLSR models significantly outperformed all the FORMOSAT-2-based ones while the RapidEye-based PLSR models achieved slightly better results than the FORMOSAT-2 ones. However, the performance gaps were much smaller at the HE stage and across the three stages.

**Table 5-7** Stepwise multiple linear regression (SMLR) models based on simulated multi-spectral FORMOSAT-2 (F2), RapidEye (RY), WorldView-2 (WV2) wavebands for estimating aboveground biomass (AGB), plant N uptake (PNU), N nutrition index (NNI), and plant N concentration (PNC) at the panicle initiation (PI), stem elongation (SE), heading (HE) and across stages. The wavebands were ranked by the entered order.

	AGB				PNU				NNI				PNC			
	PI	SE	HE	All												
<b>Based on F2 bands</b>																
R <sup>2</sup>	0.61**	0.51**	0.29**	0.82**	0.60**	0.66**	0.50**	0.81**	0.45**	0.30**	0.57**	0.36**	0.08*	0.22**	0.51**	0.43**
Band	NIR1	R	G	NIR1	NIR1	NIR1	R	NIR1	NIR1	NIR1	R	NIR1	G	R	R	NIR1
	G	B	NIR1	G	G	G	NIR1	G	G		NIR1	G		B	NIR1	R
	B			B	B	B	G	B	B		G	B		NIR1	G	
	R				R	R								G		
<b>Based on RY bands</b>																
R <sup>2</sup>	0.68**	0.55**	0.29**	0.82**	0.66**	0.68**	0.50**	0.82**	0.46**	0.50**	0.59**	0.38**	0.07*	0.20**	0.57**	0.43**
Band	NIR1	NIR1	G	NIR1	NIR1	NIR1	R	NIR1	R	NIR1	R	NIR1	G	R	NIR1	NIR1
	RE	RE	NIR1	RE	RE	RE	NIR1	RE	NIR1	RE	NIR1	RE		B	RE	R
	R	G			R	B	RE	R	RE	R	RE	R		NIR1	G	
	B				B									G		
<b>Based on WV2 bands</b>																
R <sup>2</sup>	0.76**	0.63**	0.31**	0.82**	0.71**	0.69**	0.52**	0.82**	0.52**	0.49**	0.61**	0.38**	0.09**	0.10**	0.56**	0.43**
Band	NIR1	NIR1	Y	NIR1	Y	R	R	NIR2								
	RE	RE	NIR1	RE		B	NIR2	R								
	NIR2	G	G	R	R	G			NIR2	R		G			RE	
	C	R			NIR2					Y						
	Y	Y			C											

\*\* Correlation is significant at the  $P \leq 0.01$  level; \* Correlation is significant at the  $P \leq 0.05$  level.

**Table 5-8** Aboveground biomass (AGB), plant N uptake (PNU), N nutrition index (NNI), and plant N concentration (PNC) modeling (calibration subset) by partial least square regression (PLSR) analysis using the wavelengths based on the FORMOSAT-2 (F2), RapidEye (RY), WorldView-2 (WV2) datasets at the panicle initiation (PI), stem elongation (SE), heading (HE) and across stages (All). RMSEC stands for the RMSE of calibration subset.

	AGB				PNU				NNI				PNC			
	PI	SE	HE	All	PI	SE	HE	All	PI	SE	HE	All	PI	SE	HE	All
<b>Based on F2 bands</b>																
R <sup>2</sup>	0.64	0.56	0.31	0.82	0.62	0.68	0.50	0.81	0.46	0.50	0.58	0.36	0.09	0.22	0.54	0.43
RMSEC	0.3	0.58	1.23	1.11	7.76	9.61	25.5	18.32	0.08	0.1	0.15	0.15	1.62	3.14	1.87	3.64
<b>Based on RY bands</b>																
R <sup>2</sup>	0.71	0.57	0.3	0.82	0.69	0.69	0.5	0.82	0.49	0.52	0.59	0.36	0.11	0.23	0.56	0.44
RMSEC	0.26	0.57	1.24	1.11	7.02	9.44	25.44	18.05	0.08	0.10	0.15	0.15	1.62	3.12	1.81	3.63
<b>Based on WV2 bands</b>																
R <sup>2</sup>	0.78	0.67	0.38	0.84	0.75	0.78	0.55	0.83	0.55	0.56	0.62	0.43	0.24	0.31	0.6	0.43
RMSEC	0.23	0.5	1.17	1.02	6.24	7.87	24.22	17.56	0.07	0.09	0.15	0.14	1.48	2.94	1.73	3.33

Similar to the SMLR analysis, AGB and PNU were best estimated at the PI stage and across the stages by the PLSR method, whereas NNI and PNC were best estimated at the HE stage. The PLSR and SMLR methods had similar performance for the AGB and PNU estimations while better  $R^2$  and RMSEC values were found in the PLSR models for NNI and PNC estimations in most cases. Especially for the PNC estimation, the PLSR models based on the WorldView-2 bands explained significantly more variability ( $R^2 = 0.24-0.31$ ) compared to the counterparts of SMLR models ( $R^2 = 0.09-0.10$ ) at the PI and SE stages.

In addition, the calculated VIP values revealed that for AGB and PNU estimation, the NIR bands, especially the NIR1 centered at 830 nm was the most important one in the PLSR models in most cases (Figs. 5-4, 5-5). In contrast, for PNC estimation, the VIP scores indicated that the most important band changed from G band (for FORMOSAT-2 and RapidEye) at the PI stage to R band at the SE stage, and finally to NIR1 band at the HE stage (Fig. 5-6a-c). For NNI estimation, the NIR1 band was consistently important (Fig. 5-6d-f). The R band at the PI stage (Fig. 5-6d), G band at the SE stage (Fig. 5-6e) and both G and R bands at the HE stage were important for NNI estimation. The RE band showed relatively high VIP values at the SE stage for both AGB and PNU estimations and at the PI stage for PNC estimation. The Y band of WorldView-2 demonstrated its importance at the HE stage for AGB, PNU, and NNI estimations. Notably, the Y band had high VIP values for PNC estimation from PI thru HE stages. The C band of WorldView-2 also had VIP values close to or above “1” for AGB and PNU estimations at the SE stage (Figs. 5-4, 5-5, 5-6).

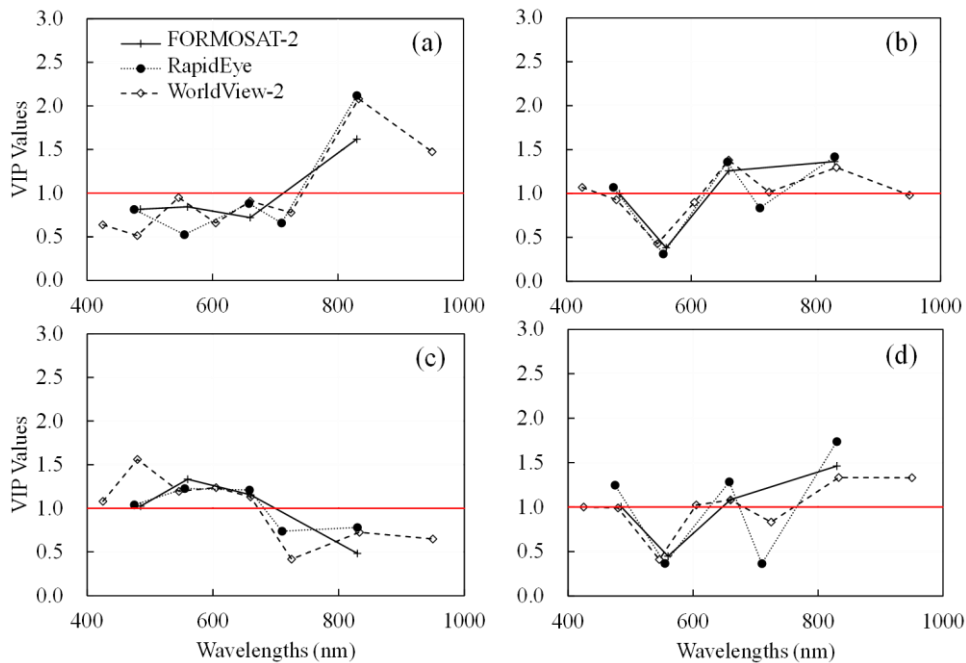


**Fig. 5-4** Variable Importance in Projection (VIP) values as function of wavelengths formatted to FORMOSAT-2, RapidEye, and WorldView-2 spectra for aboveground biomass (AGB) estimation at: the panicle initiation (PI) (a); stem elongation (SE) (b); heading (HE) (c); and across stages (d).

### 5.3.5 Validation of the estimation models

The validation results of the three types of models were summarized in Table 5-9. The VI-based PNC model validation for the PI stage was excluded since no significant relationship was identified. For AGB and PNU estimations, the RapidEye and WorldView-2 band-based VI models had significantly higher  $R^2$  than those based on FORMOSAT-2 bands while the validation results of the former two types of models were more comparable at the PI and SE stages (Table 5-9). The SMLR and PLSR validation models showed similar results. However, the FORMOSAT-2-based SMLR and PLSR models had significantly higher  $R^2$  and lower RMSE and REr compared to the counterparts of VI models. For PNC estimation, the WorldView-2 band-based PLSR models had significantly higher  $R^2$  than those of FORMOSAT-2-based models at the PI and SE stages (Table 5-9). In most cases, the SMLR and PLSR models showed better performance for estimating the four N indicators than the VI models.

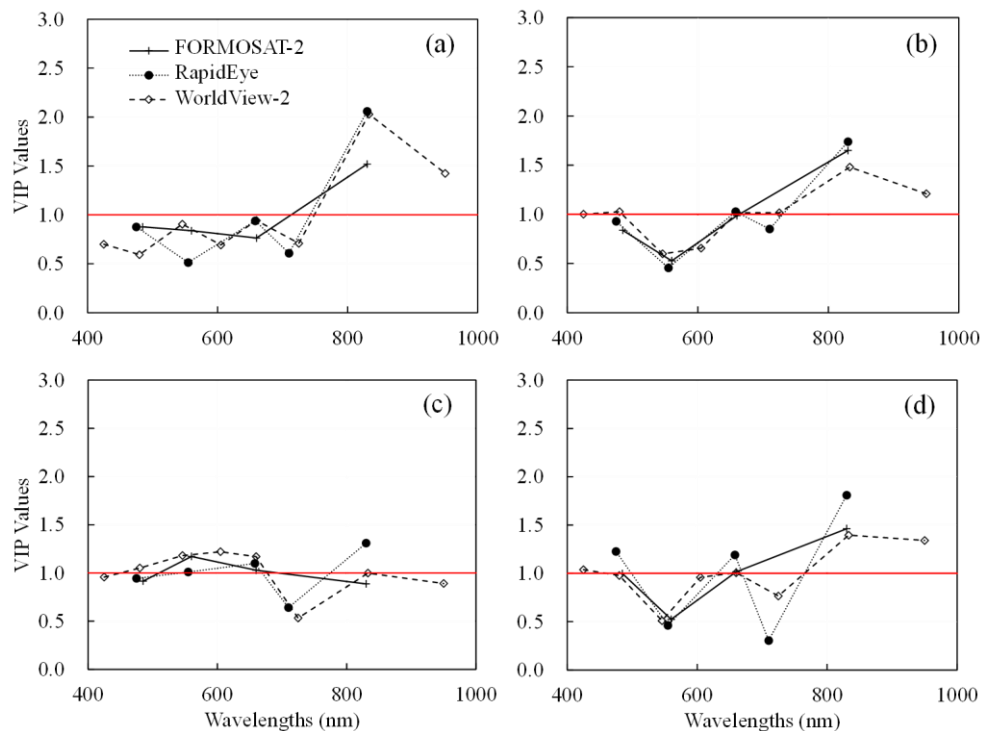


**Fig. 5-5** Variable Importance in Projection (VIP) values as function of wavelengths formatted to FORMOSAT-2, RapidEye, and WorldView-2 spectra for plant N uptake (PNU) estimation at: the panicle initiation (PI) (a); stem elongation (SE) (b); heading (HE) (c); and across stages (d).

Different Growth Stages

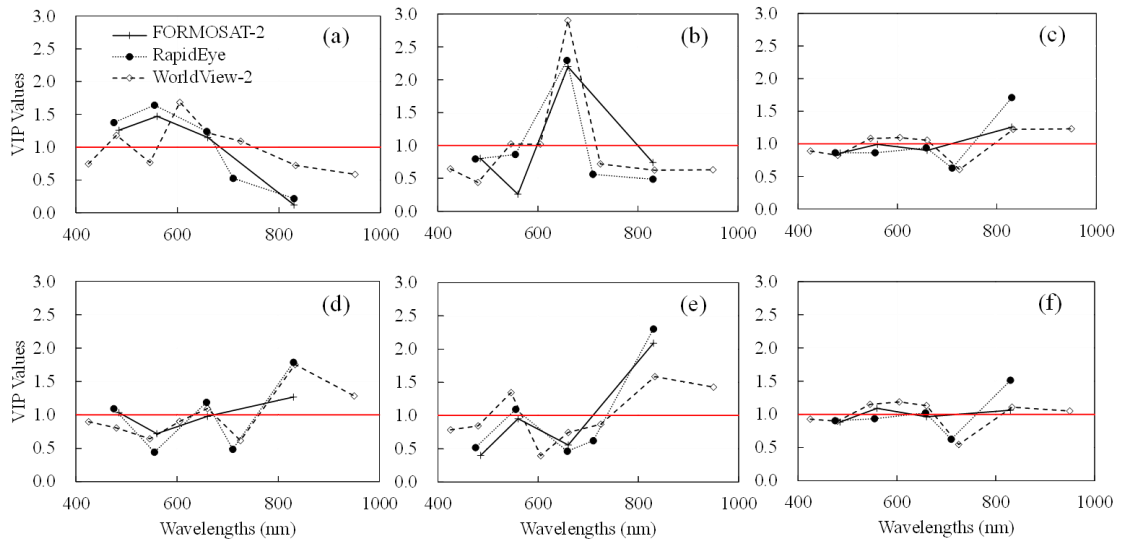


**Fig. 5-6** Variable Importance in Projection (VIP) values as function of wavelengths formatted to FORMOSAT-2, RapidEye, and WorldView-2 spectra for plant N concentration (PNC) estimation at: the panicle initiation (PI) (a); stem elongation (SE) (b); and heading (HE) (c) stages; and for N nutrition index (NNI) estimation at: the PI (d); SE (e); and HE (f) stages.

**Table 5-9** Comparison of the validation results for the best performed vegetation indices (VIs), the stepwise multiple linear regression (SMLR) models, and the partial least squares regression (PLSR) models for biomass (AGB), plant N uptake (PNU), N nutrition index (NNI), and plant N concentration (PNC) estimations at the panicle initiation (PI), stem elongation (SE), and heading (HE) stages. RMSEP stands for the RMSE of validation subset.

	AGB									PNU								
	PI			SE			HE			PI			SE			HE		
	F2	RY	WV2															
<b>Best performed VI-based models</b>																		
R <sup>2</sup>	0.36	0.76	0.64	0.57	0.73	0.75	0.26	0.28	0.32	0.37	0.73	0.62	0.66	0.78	0.72	0.47	0.46	0.45
RMSEP	0.39	0.24	0.29	0.67	0.53	0.70	1.27	1.25	1.23	9.33	6.16	7.27	10.92	8.71	9.73	23.77	24.06	24.20
REr (%)	36.56	22.73	27.40	36.90	29.08	38.35	21.46	21.13	20.66	35.75	23.61	27.88	26.43	21.08	23.54	24.91	25.22	25.36
<b>SMLR-based models</b>																		
R <sup>2</sup>	0.69	0.77	0.85	0.65	0.77	0.82	0.39	0.39	0.39	0.73	0.78	0.84	0.76	0.78	0.76	0.49	0.50	0.49
RMSEP	0.27	0.23	0.19	0.62	0.53	0.45	1.19	1.19	1.18	6.27	5.56	4.74	9.83	9.28	9.36	23.04	22.98	23.14
REr (%)	25.56	21.95	17.81	33.90	28.87	24.78	19.98	19.99	19.83	24.03	21.30	18.16	23.79	22.45	22.66	24.14	24.08	24.25
<b>PLSR-based models</b>																		
R <sup>2</sup>	0.65	0.77	0.84	0.76	0.79	0.78	0.38	0.39	0.33	0.70	0.77	0.81	0.76	0.77	0.72	0.50	0.49	0.47
RMSEP	0.28	0.23	0.19	0.55	0.52	0.48	1.18	1.18	1.23	6.49	5.59	5.12	9.76	9.34	9.92	23.07	23.14	23.54
REr (%)	26.79	21.62	18.10	30.27	28.45	26.17	19.91	19.93	20.72	24.88	21.43	19.64	23.63	22.59	24.01	24.18	24.26	24.68
	NNI									PNC								
	PI			SE			HE			PI			SE			HE		
	F2	RY	WV2															
<b>Best performed VI-based models</b>																		
R <sup>2</sup>	0.37	0.45	0.41	0.28	0.32	0.27	0.43	0.41	0.38	-	-	-	0.13	0.02	0.24	0.26	0.24	0.20
RMSEP	0.08	0.07	0.08	0.11	0.10	0.11	0.17	0.18	0.18	-	-	-	0.33	0.34	0.31	0.25	0.26	0.27
REr (%)	8.41	7.79	8.14	10.31	10.06	10.94	16.28	16.81	17.29	-	-	-	13.77	14.44	13.1	15.67	16.17	16.67
<b>SMLR-based models</b>																		
R <sup>2</sup>	0.55	0.52	0.44	0.28	0.25	0.30	0.46	0.48	0.46	0.12	0.11	0.09	0.25	0.21	0.37	0.30	0.36	0.30
RMSEP	0.07	0.07	0.07	0.11	0.11	0.11	0.17	0.16	0.17	0.19	0.20	0.20	0.30	0.31	0.29	0.24	0.23	0.24
REr (%)	7.18	7.28	7.86	10.34	11.05	10.44	15.81	15.48	15.89	7.92	7.94	7.97	12.58	12.98	12.36	15.19	14.48	15.17
<b>PLS-based models</b>																		
R <sup>2</sup>	0.62	0.56	0.54	0.28	0.27	0.24	0.48	0.47	0.44	0.14	0.21	0.34	0.25	0.30	0.48	0.36	0.35	0.30
RMSEP	0.06	0.07	0.07	0.11	0.11	0.11	0.16	0.16	0.17	1.93	1.87	1.71	3.02	2.93	2.52	2.31	2.35	2.47
REr (%)	6.68	7.00	7.14	10.53	10.70	10.81	15.44	15.64	16.12	7.85	7.62	6.96	12.64	12.27	10.56	14.43	14.65	15.41

## 5.4 Discussion

### 5.4.1 Impacts of growth stages on N status monitoring

The AGB increased notably while the PNC decreased steadily over the growth stages in this study (Table 5-4), which confirmed to many previous studies (Lemaire *et al.*, 2008; Justes *et al.*, 1994; Plénet & Lemaire, 1999; Ata-Ul-Karim *et al.*, 2013). Because PNU is a product of AGB and PNC, plants with high PNC and low AGB at earlier growth stages may have similar PNU as those with low PNC and higher biomass at later growth stages (Chen *et al.*, 2010). Thus, the growth stage is an important reference factor, which must be taken into account when using PNU as an indicator for crop N diagnosis.

Our VI models revealed that rice AGB and PNU were best estimated at the early growth stage while the opposite was true for NNI and PNC. Similarly, Yu *et al.* (2013) found the VIs performed better for estimating rice PNC after the HE stage. Li *et al.* (2014a) also noted that PNC was better estimated at later growth stages for maize. This is because that before the HE stage, the N accumulation rate is lower than that of biomass; therefore, the later dominates canopy reflectance (Yu *et al.*, 2013; Mistele & Schmidhalter, 2008). After the HE stage, the increase in AGB gains slower, and plant N starts to dominate canopy reflectance (Yu *et al.*, 2013). Huang *et al.* (2015) proposed an indirect approach to estimate NNI at the PI stage based on the AGB and PNU values derived from FORMOSAT-2 satellite images for guiding topdressing N application at the SE stage. This indirect method might be tested using RE-based VI models derived from RapidEye and WorldView-2 images in the future.

### 5.4.2 Importance of the red edge and other bands for N status estimation

The use of canopy spectra for N assessment mostly depends on the close relationship between N and chlorophylls in the cell metabolism (Shiratsuchi *et al.*, 2011). The R band-based VIs like NDVI, RVI, and OSAVI are the most common indices in N status estimation. However, the R band can be easily influenced by soil background reflectance at early growth stage when vegetation coverage is small. The NDRE and RECI indices significantly improved the estimation results compared to NDVI and RVI in our research (Tables 5-5, 5-6). This is because the RE reflectance is highly correlated with chlorophyll content (Cho & Skidmore, 2006; Clevers *et al.*, 2002), and is responsive to variation in LAI or biomass (Gnyp *et al.*, 2014; Haboudane *et al.*, 2008). In addition, it is insensitive to background effects (Zarco-Tejada *et al.* 2004). Our results also confirmed the findings by Li *et al.* (2014a), who found that the NDRE and RECI improved the PNC and PNU estimations of summer maize. They also proved that the broader bandwidth led to decreased performance of NDVI and RVI while no significant effect was identified for NDRE and RECI.

The RE-based index, MTCI, had the best performance in this study. According to Li *et al.* (2014a), the broadband MTCI performed slightly better than the narrow ones. In our study, the broadband MTCI calculated using the simulated RapidEye and WorldView-2 bands was among the top five indices for AGB, PNU, and NNI estimation models. MTCI was also proven to be highly correlated with the PNC in maize (Li *et al.*, 2014a) and in rice (Yu *et al.*, 2013). It would not saturate at high N treatments (Li *et al.*, 2014a; Shiratsuchi *et al.*, 2011). Nevertheless, the relationship between MTCI and PNC might be more influenced by soil background at early stages relative to CCCI (Li *et al.*, 2014a).

The two RE-based indices, CCCI and NDPI, are both two-dimensional indices (Clarke *et al.*, 2001). The CCCI is calculated based on NDVI and NDRE, while the NDPI is based on NDVI and RECI. Ramoelo *et al.* (2012) evaluated the CCCI for wheat canopy N content estimation using simulated RapidEye bands, and proved the CCCI performed well for estimating N status indicators. Li *et al.* (2014a) simulated the WorldView-2 wavebands and reported that the CCCI and NDPI improved the estimation results. In our study, the CCCI and NDPI based on RapidEye, and NDPI based on WorldView-2 bands yielded high  $R^2$  for AGB (Table 5-5), PNU (Table 5-6), and NNI (Table 5-6) estimations, similar to previous research. However, the CCCI based on WorldView-2 bands yielded slightly lower  $R^2$  than that of RapidEye at early stages. Different RE band settings might lead to the discrepancies of model results. In particular, the RE band of WorldView-2 ranges from 705 to 745 nm, peaking at 725 nm, while the RE band of RapidEye is set to 690-730 nm, peaking at 710 nm. As the crop develops, the RE position moves to longer wavelength due to higher crop biomass and plant pigment content. Thus, at early growth stages, the RE-based indices using both satellite bands yielded similar  $R^2$ , while the RE indices of WorldView-2 achieved slightly higher  $R^2$  for AGB and PNU estimations than the ones of RapidEye at the HE stage (Tables 5-5, 5-6).

The G band-based GNDVI and CI performed slightly better than the R band-based NDVI and RVI. These results confirmed previous findings by Carter (1993) and Carter and Knapp (2001), who found that G and RE spectra were sensitive to a wider range of chlorophyll levels than R reflectance. Bausch and Khosla (2010) also reported that G band-based VIs improved N status evaluation compared with R band-based indices. Yu *et al.* (2013) found two “hot zones” related to N status: RE bands (700-760 nm) paired with RE to NIR spectral region (700-1100 nm) and G bands (500-590 nm) paired with RE to NIR region (700-1100nm), which confirmed the importance of RE, NIR, and G bands for N status estimation.

The NIR1 waveband explained the most variability compared with other wavebands. This was also observed in wheat LAI estimation using PLSR analysis by Herrmann *et al.* (2011), who revealed different VIP values of NIR band between wheat and potato. For rice

LAI, leaf dry weight, leaf N concentration, and leaf N density estimations, PLSR models demonstrated that the bands > 760 nm and at 687 nm were most important (Nguyen & Lee, 2006). The RE band (707 nm) was only important for leaf N concentration as the third latent variable (Nguyen & Lee, 2006). In our study, the VIP scores indicated it was important to include the RE band at the PI stage for PNC estimation and at the SE stage for AGB and PNU estimations. The Y band of WorldView-2 demonstrated high importance for PNC estimation from PI thru HE stages. In addition, the Y band was significant for estimating all four N status variables at the HE stage whereas the C band was valuable for AGB and PNU estimations at the SE stage. Such results demonstrated the value of having the additional C and Y bands in WorldView-2 sensor for crop N status monitoring. While WorldView-2 data with extra spectral bands have higher potential for improving N status monitoring, considering the cost factor, RapidEye data might be more practical than WorldView-2 data for large-scale studies.

#### 5.4.3 Limitations of this study

Physically based canopy reflectance models were not applied in this study because they are complex to design, parameterize, and implement, especially in wet rice paddies. Furthermore, those models can only be inverted to retrieve canopy parameters that are directly involved in physical processes of radiative transfer, such as photosynthetic pigments, instead of N (Stroppiana *et al.*, 2012). The VI, SMLR, and PLSR models generated from this study were not validated using actual satellite images. We were able to obtain several FORMOSAT-2 images during our sampling period, but they cannot be used for validation purpose due to their relatively coarse resolution (8 m) and the relatively small size of our experimental fields in this research. However, in our previous research, we have demonstrated the application of using FORMOSAT-2 satellite imagery for monitoring rice N status in this region (Huang *et al.*, 2015). Given the frequent cloudy and rainy days during the growing season in major rice planting regions, it is difficult to obtain satellite images within a narrow time window. We could not find any archived RapidEye and WorldView-2 images that matched our field sampling dates for this remote study site. Some new remote sensing technologies, such as all-weather dual-polarimetric TerraSAR-X satellite data (Koppe *et al.*, 2013) and low-altitude remote sensing based on unmanned aerial vehicles (UAVs) (Mulla & Miao, 2016), may be incorporated to overcome the limitations.

#### 5.5 Conclusions and future outlooks

This study simulated the band settings of FORMOSAT-2, RapidEye, and WorldView-2 satellite images to evaluate the potentials of using satellite remote sensing with RE and additional bands to improve estimation of rice N status. The major findings are summarized

as follows:

For VI analysis, the best-performed RE-based VIs explained 53%-64% AGB variability and 62%-65% PNU variability, compared to 30%-40% AGB and 39%-52% PNU variability using the CI at the PI and SE stages.

For the NNI estimation, the NPDI based on WorldView-2 bands and MTCI based on RapidEye bands explained 14%-26% more variability than FORMOSAT-2-based indices.

The SMLR analysis indicated the NIR1 band was most important for estimating all four N status indicators. In addition, the RE band improved AGB, PNU, and NNI estimations at all the three stages, especially at the early PI and SE stages.

The PLSR analysis confirmed the significance of NIR band for PNU estimation at all stages. It also revealed that it was important to include RE band for AGB and PNU estimation at the SE stage and for PNC estimation at the PI stage. Similar to the RE band, the C band of WorldView-2 was also valuable for AGB and PNU estimations at the SE stage. Notably, the Y band of Worldview-2 was found to be significant at the later stage (HE) for estimations of all four N status variables. Especially for PNC estimation, Y band showed consistent importance at all three growth stages.

Both the SMLR and PLSR models, especially those based on the WorldView-2 bands, improved the estimations of all variables in most cases compared to the VI approach.

The PLSR method had slightly better performance than the SMLR approach for NNI and PNC estimations in most cases.

Biomass and PNU were best estimated at the PI and across the stages while NNI and PNC were best assessed at the HE stage.

Overall, the analyses based on the simulated WorldView-2 data showed the best results for estimating rice N status, followed by the ones based on the RapidEye data.

In conclusion, this study demonstrated the values of having the RE as well as the additional visible and NIR bands for rice N status monitoring. The VI and linear regression methods used have been proven suitable. Satellite remote sensing with high spatial and temporal resolution provides a promising technology for large-scale crop N monitoring. In the future, the potential of shortwave infrared (SWIR) bands for N status monitoring can be further investigated using WorldView-3 data with eight SWIR bands. Other methods such as artificial neural networks (ANNs) and support vector machines (SVMs) can be tested in order to reveal possible nonlinear relationships in the data. Moreover, airborne or UAV-based hyperspectral images should be explored in future studies as some most important reflectance features related to N content can only be measured by hyperspectral sensors.

## Acknowledgment

This research was financially supported by National Basic Research Program (2015CB150405), National Key Research Program (2016YFD0200602), the Innovative Group Grant of Natural Science Foundation of China (31421092), the Sino-Norwegian Cooperative SINOGRain project (CHN-2152, 14-0039), and the GIS and RS Group of the University of Cologne, Germany. We thank the staff of Jiansanjiang Bureau of Agricultural Land Reclamation, Qixing Farm and Jiansanjiang Institute of Agricultural Research for their support. We also would like to thank Kang Yu, Lei Gao, Christoph Hütt for their field work and contributions in spectral data collection.

## Conflicts of Interest

The authors declare no conflict of interest.

## 5.6 References

- Asam, S., Fabritius, H., Klein, D., Conrad, C., Dech, S., 2013. Derivation of leaf area index for grassland within alpine upland using multi-temporal RapidEye data. *Int. J. Remote Sens.* 34, 8628–8652.
- Ata-Ul-Karim, S.T., Yao, X., Liu, X., Cao, W., Zhu, Y., 2013. Development of critical nitrogen dilution curve of Japonica rice in Yangtze River Reaches. *Field Crops Res.* 149, 49–158.
- Bausch, W.C., Khosla, R., 2010. QuickBird satellite versus ground-based multi-spectral data for estimating nitrogen status of irrigated maize. *Precis. Agric.* 11, 274–290.
- Beeri, O., Phillips, R., Carson, P., Leibig, M., 2005. Alternate satellite models for estimation of sugar beet residue nitrogen credit. *Agric. Ecosyst. Environ.* 107, 21–35.
- Broge, N.H., Leblanc, E., 2000. Comparing prediction power and stability of broadband and hyperspectral vegetation indices for estimation of green leaf area index and canopy chlorophyll density. *Remote Sens. Environ.* 76, 156–172.
- Bsaibes, A., Courault, D., Baret, F., Weiss, M., Oliso, A., Jacob, F., Hagolle, O., Marloie, O., Bertrand, N., Desfond, V., Kzemipour, F., 2009. Albedo and LAI estimates from FORMOSAT-2 data for crop monitoring. *Remote Sens. Environ.* 113, 716–729.
- Cao, Q., Miao, Y., Feng, G., Gao, X., Li, F., Liu, B., Yue, S., Cheng, S., Ustin, S., Khosla, R., 2015. Active canopy sensing of winter wheat nitrogen status: An evaluation of two sensor systems. *Comput. Electron. Agric.* 112, 54–67.
- Cao, Q., Miao, Y., Shen, J., Yu, W., Yuan, F., Cheng, S., Huang, S., Wang, H., Yang, W., Liu, F., 2016. Improving in-season estimation of rice yield potential and responsiveness

- to topdressing nitrogen application with Crop Circle active canopy sensor. *Precis. Agric.* 17, 136–154.
- Cao, Q., Miao, Y., Wang, H., Huang, S., Chen, S., Khosla, R., Jiang, R., 2013. Non-destructive estimation of rice plant nitrogen status with Crop Circle multispectral active canopy sensor. *Field Crops Res.* 154, 133–144.
- Carter, G.A., 1993. Responses of leaf spectral reflectance to plant stress. *Am. J. Bot.* 80, 239–243.
- Carter, G.A., Knapp, A.K., 2001. Leaf optical properties in higher plants: Linking spectral characteristics to stress and chlorophyll concentration. *Am. J. Bot.* 88, 677–684.
- Chen, P., Haboudane, D., Tremblay, N., Wang, J., Vigneault, P., Li, B., 2010. New spectral indicator assessing the efficiency of crop nitrogen treatment in corn and wheat. *Remote Sens. Environ.* 114, 1987–1997.
- Cho, M.A., Skidmore, A.K., 2006. A new technique for extracting the red edge position from hyperspectral data: The linear extrapolation method. *Remote Sens. Environ.* 101, 181–193.
- Chong, I., Jun, C., 2005. Performance of some variable selection methods when multicollinearity is present. *Chemom. Intell. Lab.* 78, 103–112.
- Cilia, C., Panigada, C., Rossini, M., Meroni, M., Busetto, L., Amaducci, S., Boschetti, M., Picchi, V., Colombo, R., 2014. Nitrogen status assessment for variable rate fertilization in maize through hyperspectral imagery. *Remote Sens.* 6, 6549–6565.
- Clarke, T.R., Moran, M.S., Barnes, E.M., Pinter, P.J., Qi, J., 2001. Planar domain indices: a method for measuring a quality of a single component in two-component pixels. In: *Proc. IEEE International Geosci. Remote Sens. Sympos. [CD ROM]*, Sydney, Australia, 9–13 July.
- Claverie, M., Demarez, V., Duchemin, B., Hagolle, O., Ducrot, D., Marais-Sicre, C., Dejoux, J.F., Huc, M., Keravec, P., Béziat, P., Fieuzal, R., Ceschia, E., Dedieu, G., 2012. Maize and sunflower biomass estimation in southwest France using high spatial and temporal resolution remote sensing data. *Remote Sens. Environ.* 124, 844–857.
- Clevers, J.G.P.W., De Jong, S.M., Epema, G.F., Van Der Meer, F.D., Bakker, W.H., Skidmore, A.K., Scholte, K.H., 2002. Derivation of the red edge index using the MERIS standard band setting. *Int. J. Remote Sens.* 23, 3169–3184.
- Dash, J., Curran, P.J., 2004. The MERIS terrestrial chlorophyll index. *Int. J. Remote Sens.* 31, 5513–5532.
- Daughtry, C.S.T., Walthall, C.L., Kim, M.S., Colstoun, E.B., McMurtrey, J.E.I., 2000. Estimating corn leaf chlorophyll concentration from leaf and canopy reflectance. *Remote Sens. Environ.* 74, 229–239.

- Diacono, M., Rubino, P., Montemurro, F., 2013. Precision nitrogen management of wheat: A review. *Agron. Sustain. Dev.* 33, 219–241.
- Eitel, J.U.H., Long, D.S., Gessler, P.E., Smith, A.M.S., 2007. Using in-situ measurements to evaluate the new RapidEye™ satellite series for prediction of wheat nitrogen status. *Int. J. Remote Sens.* 28, 4183–4190.
- Eitel, J.U.H., Vierling, L.A., Litvak, M.E., Long, D.S., Schulth, U., Ager, A.A., Krofcheck, D.J., Stoscheck, L., 2011. Broadband, red edge information from satellites improves early stress detection in a New Mexico conifer woodland. *Remote Sens. Environ.* 115, 3640–3646.
- Farruggia, A., Gastal, F., Scholefield, D., 2004. Assessment of the nitrogen status of grassland. *Grass Forage Sci.* 59, 113–120.
- Fitzgerald, G., Rodriguez, D., O’Leary, G., 2010. Measuring and predicting canopy nitrogen nutrition in wheat using a spectral index-The canopy chlorophyll content index (CCCI). *Field Crops Res.* 116, 318–324.
- Gastal, F., Farrugia, A., Hacquet, J., 2001. The nitrogen nutrition index of grass can be evaluated through determination of N concentration of upper leaves. In: *Proceedings of the 2001 11th Nitrogen Workshop, Reims, France*, pp. 449–450.
- Gitelson, A.A., Kaufman, Y.J., Merzlyak, M.N., 1996. Use of a green channel in remote sensing of global vegetation from EOS-MODIS. *Remote Sens. Environ.* 58, 289–298.
- Gitelson, A.A., Viña, A., Ciganda, V., Rundquist, D.C., Arkebauer, T.J., 2005. Remote estimation of canopy chlorophyll content in crops. *Geophys. Res. Lett.* 32, L08403.
- Gnyp, M.L., Miao, Y., Yuan, F., Ustin, S.L., Yu, K., Yao, Y., Huang, S., Bareth, G., 2014. Hyperspectral canopy sensing of paddy rice aboveground biomass at different growth stages. *Field Crops Res.* 155, 42–55.
- Greenwood, D.J., Neeteson, J.J., Draycott, A., 1986. Quantitative relationships for the dependence of growth rate of arable crops on their nitrogen content, dry weight and aerial environment. *Plant Soil* 91, 281–301.
- Haboudane, D., Miller, J.R., Tremblay, N., Zarco-Tejada, P.J., Dextraze, L., 2002. Integrated narrow-band vegetation indices for prediction of crop chlorophyll content for application to precision agriculture. *Remote Sens. Environ.* 81, 416–426.
- Haboudane, D., Tremblay, N., Miller, J.R., Vigneault, P., 2008. Remote estimation of crop chlorophyll content using spectral indices derived from hyperspectral data. *IEEE Trans. Geosci. Remote Sens.* 46, 423–437.
- Hansen, P.M., Schjoerring, J.K., 2003. Reflectance measurement of canopy biomass and nitrogen status in wheat crops using normalized difference vegetation indices and partial least squares regression. *Remote Sens. Environ.* 86, 542–553.

- Herrmann, I., Pimstein, A., Karnieli, A., Cohen, Y., Alchanatis, V., Bonfil, D.J., 2011. LAI assessment of wheat and potato crops by VEN $\mu$ S and Sentinel-2 bands. *Remote Sens. Environ.* 115, 2141–2151.
- Holland, K.H., Schepers, J.S., 2013. Use of a virtual-reference concept to interpret active crop canopy sensor data. *Precis. Agric.* 14, 71–85.
- Huang, S., Miao, Y., Zhao, G., Yuan, F., Ma, X., Tan, C., Yu, W., Gnyp, M., Lenz-Wiedemann, V.I.S., Rascher, U., Bareth, G., 2015. Satellite remote sensing-based in-season diagnosis of rice nitrogen status in Northeast China. *Remote Sens.* 7, 10646–10667.
- Jordan, C.F., 1969. Derivation of leaf-area index from quality of light on the forest floor. *Ecology* 50, 663–666.
- Justes, E., Mary, B., Meynard, J.M., Machet, J.M., Thelier-Huche, L., 1994. Determination of a critical nitrogen dilution curve for winter wheat crops. *Ann. Bot.* 74, 397–407.
- Kanke, Y., Tubaña, B., Dalen, M., Harrell, D., 2016. Evaluation of red and red-edge reflectance-based vegetation indices for rice biomass and grain yield prediction models in paddy fields. *Precis. Agric.* 17, 507–530.
- Kim, H.O., Yeom, J.M., 2012. Multi-temporal spectral analysis of rice fields in South Korea using MODIS and RapidEye satellite imagery. *J. Astron. Space Sci.* 29, 407–411.
- Koppe, W., Gnyp, M.L., Hütt, C., Yao, Y., Miao, Y., Chen, X., Bareth, G., 2013. Rice monitoring with multi-temporal and dual-polarimetric TerraSAR-X data. *Int. J. Appl. Earth Obs. Geoinf.* 21, 568–576.
- Lemaire, G., Jeuffroy, M.H., Gastal, F., 2008. Diagnosis tool for plant and crop N status in vegetative stage: Theory and practices for crop N management. *Eur. J. Agron.* 28, 614–624.
- Li, F., Miao, Y., Feng, G., Yuan, F., Yue, S., Gao, X., Liu, Y., Liu, B., Ustin, S.L., Chen, X., 2014a. Improving estimation of summer maize nitrogen status with red edge-based spectral vegetation indices. *Field Crops Res.* 157, 111–123.
- Li, F., Miao, Y., Zhang, F., Cui, Z., Li, R., Chen, X., Zhang, H., Schroder, J., Raun, W.R., Jia, L., 2009. In-season optical sensing improves nitrogen-use efficiency for winter wheat. *Soil Sci. Soc. Am. J.* 73, 1566–1574.
- Li, X., Zhang, Y., Bao, Y., Luo, J., Jin, X., Xu, X., Song, X., Yang, G., 2014b. Exploring the best hyperspectral features for LAI estimation using partial least squares regression. *Remote Sens.* 6, 6221–6241.
- Magney, T.S., Eitel, J.U., Vierling, L.A., 2016. Mapping wheat nitrogen uptake from RapidEye vegetation indices. *Precis. Agric.* doi: 10.1007/s11119-016-9463-8.
- Mistele, B., Schmidhalter, U., 2008. Estimating the nitrogen nutrition index using spectral canopy reflectance measurements. *Eur. J. Agron.* 29, 184–190.

- Mulla, D.J., 2013. Twenty-five years of remote sensing in precision agriculture: Key advances and remaining knowledge gaps. *Biosyst. Eng.* 114, 358–371.
- Mulla, D.J., Miao, Y., 2016. Precision Farming. In: Thenkabail, P.S. (Ed.), *Land Resources Monitoring, Modeling, and Mapping with Remote Sensing*. CRC Press, FL, USA, pp. 161–178.
- Mutanga, O., Adam, E., Cho, M.A., 2012. High density biomass estimation for wetland vegetation using WorldView-2 imagery and random forest regression algorithm. *Int. J. Appl. Earth Obs. Geoinf.* 18, 399–406.
- Mutanga, O., Skidmore, A.K., 2004. Narrow band vegetation indices overcome the saturation problem in biomass estimation. *Int. J. Remote Sens.* 25, 3999–4014.
- Nguyen, H.T., Lee, B.W., 2006. Assessment of rice leaf growth and nitrogen status by hyperspectral canopy reflectance and partial least square regression. *Eur. J. Agron.* 24, 349–356.
- Nguy-Robertson, A., Gitelson, A., Peng, Y., Viñaet, A., Arkebauer, T., Rundquist, D., 2012. Green leaf area index estimation in maize and soybean: Combining vegetation indices to achieve maximal sensitivity. *Agron. J.* 104, 1336–1347.
- Plénet, D., Lemaire, G., 1999. Relationships between dynamics of nitrogen uptake and dry matter accumulation in maize crops. Determination of critical N concentration. *Plant Soil* 216, 65–82.
- Ramoelo, A., Skidmore, A.K., Cho, M.A., Schlerf, M., Mathieu, R., Heitkönig, I.M.A., 2012. Regional estimation of savanna grass nitrogen using the red-edge band of the spaceborne RapidEye sensor. *Int. J. Appl. Earth Obs. Geoinf.* 19, 151–162.
- Rondeaux, G., Steven, M., Baret, F., 1996. Optimization of soil-adjusted vegetation indices. *Remote Sens. Environ.* 55, 95–107.
- Rouse, J.W., Haas, R.H., Schell, J.A., Deering, D.W., 1973. Monitoring vegetation systems in the Great Plains with ERTS. *Earth Res. Techn. Satellite-1 Symp.*, Goddard Space Hight Center. Washington D.C., pp. 309-317.
- Schmidt, J.P., Dellinger, A.E., Beegle, D.B., 2009. Nitrogen recommendations for corn: An on-the-go sensor compared with current recommendation methods. *Agron. J.* 101, 916–924.
- Shiratsuchi, L., Ferguson, R., Shanahan, J., Adamchuk, V., Rundquist, D., Marx, D., Slater, G., 2011. Water and nitrogen effects on active canopy sensor vegetation indices. *Agron. J.* 103, 1815–1826.
- Stroppiana, D., Fava, F., Boschetti, M., Brivio, P.A., 2012. Estimation of nitrogen content in crops and pastures using hyperspectral vegetation indices. In: Thenkabail, P.S., Lyon, J.G., Huete, A., (Ed.), *Hyperspectral Remote Sensing of Vegetation*, CRC Press, FL, USA, pp. 245–262.

- Tang, Y.L., Huang, J.F., Wang, R.C., Wang, F.M., 2004. Comparison of yield estimation simulated models of rice by remote sensing. *Trans. Chin. Soc. Agric. Eng.* 20, 166–171.
- Thenkabail, P.S., Smith, R.B., Pauw, E.D., 2000. Hyperspectral vegetation indices and their relationships with agricultural crop characteristics. *Remote Sens. Environ.* 71, 158–182.
- Van Niel, T.G., McVicar, T.R., 2004. Current and potential uses of optical remote sensing in rice-based irrigation systems: A review. *Aust. J. Agric. Res.* 55, 155–185.
- Wang, Y., Yang, Y., 2001. Effects of agriculture reclamation on hydrologic characteristics in the Sanjiang Plain. *China Geogr. Sci.* 11, 163–167.
- Wold, S., Trygg, J., Berglund, A., Antti, H., 2001. Some recent developments in PLS modeling. *Chemometr. Intell. Lab.* 58, 131–150.
- Wu, C., Niu, Z., Tang, Q., Huang, W., 2008. Estimating chlorophyll content from hyperspectral vegetation indices: Modeling and validation. *Agric. Forest Meteorol.* 148, 1230–1241.
- Xia, T., Miao, Y., Wu, D., Shao, H., Khosla, R., Mi, G., 2016. Active optical sensing of spring maize for in-season diagnosis of nitrogen status based on nitrogen nutrition index. *Remote Sens.* 8, 605.
- Xing, B., Dudas, M.J., Zhang, Z., Qi, X., 1994. Pedogenetic characteristics of albic soils in the three river plain, Heilongjiang Province. *Acta Pedolog. Sin.* 31, 95–104.
- Yan, M., Deng, W., Chen, P., 2002. Climate change in the Sanjiang Plain disturbed by large-scale reclamation. *J. Geogr. Sci.* 12, 405–412.
- Yang, C.M., Liu, C.C., Wang, Y.W., 2008. Using FORMOSAT-2 satellite data to estimate leaf area index of rice crop. *J. Photogram. Remote Sens.* 13, 253–260.
- Yao, Y., Miao, Y., Huang, S., Gao, L., Ma, X., Zhao, G., Jiang, R., Chen, X., Zhang, F., Yu, K., Gnyp, M.L., Bareth, G., Liu, C., Zhao, L., Yang, W., Zhu, H., 2012. Active canopy sensor-based precision N management strategy for rice. *Agron. Sustain. Dev.* 32, 925–933.
- Yao, Y., Miao, Y., Cao, Q., Wang, H., Gnyp, M.L., Bareth, G., Khosla, R., Yang, W., Liu, F., Liu, C., 2014. In-season estimation of rice nitrogen status with an active crop canopy sensor. *IEEE J. Sel. Top. Appl. Earth Obs. Remote Sens.* 7, 4403–4413.
- Yu, K., Li, F., Gnyp, M.L., Miao, Y., Bareth, G., Chen, X., 2013. Remotely detecting canopy nitrogen concentration and uptake of paddy rice in the Northeast China Plain. *ISPRS J. Photogramm. Remote Sens.* 78, 102–115.
- Zarco-Tejada, P.J., Miller, J.R., Morales, A., Berjon, A., Aguera, J., 2004. Hyperspectral indices and model simulation for chlorophyll estimation in open-canopy tree crops. *Remote Sens. Environ.* 90, 463–476.

- Zhao, G., Miao, Y., Wang, H., Su, M., Fan, M., Zhang, F., Jiang, R., Zhang, Z., Liu, C., Liu, P., Ma, D., 2013. A preliminary precision rice management system for increasing both grain yield and nitrogen use efficiency. *Field Crops Res.* 154, 23–30.
- Zhao, Q., Lenz-Wiedemann, V.I.S., Yuan, F., Jiang, R., Miao, Y., Zhang, F., Bareth, G., 2015. Investigating within-field variability of rice from high resolution satellite imagery in Qixing Farm County, Northeast China. *ISPRS Int. J. Geo-Inf.* 4, 236–261.

## Chapter 6: Proximal Fluorescence Sensing for In-Season Diagnosis of Rice

### Nitrogen Status

SHANYU HUANG<sup>1,2</sup>, YUXIN MIAO<sup>1,3,\*</sup>, FEI YUAN<sup>4</sup>, QIANG CAO<sup>5</sup>, HUICHUN YE<sup>6</sup>, VICTORIA I.S. LENZ-WIEDEMANN<sup>1,2</sup>, and GEORG BARETH<sup>1,2</sup>

Manuscript submitted to the Journal of Field Crops Research

*Formatting and orthography of the manuscript are adapted to the dissertation style.*

<sup>1</sup> International Center for Agro-Informatics and Sustainable Development, College of Resources and Environmental Sciences, China Agricultural University, Beijing 100193, China

<sup>2</sup> Institute of Geography, University of Cologne, 50923 Cologne, Germany

<sup>3</sup> Precision Agriculture Center, Department of Soil, Water and Climate, University of Minnesota, St. Paul 55108, USA

<sup>4</sup> Department of Geography, Minnesota State University, Mankato, MN 56001, USA

<sup>5</sup> National Engineering and Technology Center for Information Agriculture, Nanjing Agricultural University, Nanjing 210095, China

<sup>6</sup> Key Laboratory of Digital Earth Science, Institute of Remote Sensing and Digital Earth, Chinese Academy of Sciences, Beijing 100094, China

\*Corresponding author. E-mail: ymiao@cau.edu.cn, ymiao2014@126.com

#### Abstract

Precision nitrogen (N) management requires accurate and timely in-season site-specific assessment of the crop N status. The proximal fluorescence sensor Multiplex<sup>®</sup>3 is a promising tool for monitoring crop N status. It performs non-destructive estimation of N sensitive indicators such as chlorophyll and flavonols contents. The objective of this study was to evaluate the potential of proximal fluorescence sensing for N status estimation at different growth stages for rice in cold regions. In 2012 and 2013, paddy rice field experiments with five N supply rates and two varieties were conducted in Northeast China. Field samples and fluorescence data in three modes of measurement were collected using Multiplex<sup>®</sup>3 at the panicle initiation (PI), stem elongation (SE), and heading (HE) stages. The Multiplex indices and their normalized N sufficient indices (NSI) were then used to estimate the five N status indicators: aboveground biomass (AGB), leaf N concentration (LNC), plant N concentration (PNC), plant N uptake (PNU), and N nutrition index (NNI), were determined. Results indicated that most of the fluorescence indices, especially the simple fluorescence ratios (SFR\_G, SFR\_R), blue-green to red fluorescence ratio

(BRR\_FRF), flavonols (FLAV), and N balance index (NBI\_G, NBI\_R), were highly sensitive to different N application rates. Strong relationships between some fluorescence indices (SFR\_G, SFR\_R, BRR\_FRF, FLAV, NBI\_G, and NBI\_R) and three N indicators (LNC, PNC, NNI) were found, with coefficients of determination ( $R^2$ ) ranging from 0.40 and 0.78. The N diagnostic results indicated that the NSI based on NBI\_R (NBI-R<sub>NSI</sub>) and FLAV achieved the highest diagnosis accuracy rate (90%) at the stem elongation and heading stages, respectively, while NBI\_R<sub>NSI</sub> showed the highest diagnostic consistency across growth stages. It is concluded that the Multiplex sensor can be used to reliably estimate N nutritional status for rice in cold regions, especially for the estimation of LNC, PNC and NNI. The normalized sufficiency indices based on Multiplex indices can further improve the accuracy of N nutrition diagnosis by reducing the inter-annual variations and changes caused by different varieties.

## 6.1 Introduction

Nitrogen (N) is an essential nutrient for plant growth and development. However, excessive N fertilizer applications have led to severe environmental impacts in China (Guo *et al.*, 2010; Miao *et al.*, 2011). Therefore, there has been a growing interest in developing precision N management strategies in agricultural research for many years. This requires the development of efficient and timely crop N status diagnosis strategies and technologies (Samborski *et al.*, 2009).

Plant or leaf N concentration is the direct indicator of N nutrition status. The traditional N testing method in the laboratory is time consuming and impractical for characterizing spatial and temporal variability in crop N status in precision N management. Alternatively, it is known that there is a strong relationship between plant chlorophyll content and N content (Evans, 1983; Blackmer & Schepers, 1995). Therefore, various instruments based on measuring chlorophyll have been developed to give indirect, nondestructive, and real-time estimations of leaf N content (Schlemmer *et al.*, 2005; Samborski *et al.*, 2009). For example, the Soil Plant Analysis Development chlorophyll meter (SPAD, Minolta Camera Co., Osaka, Japan) is a widely used portable instrument for measuring chlorophyll in leaves. The SPAD meter measures the difference in absorption in the red (660 nm) and near-infrared (940 nm) wavelengths (Schröder *et al.*, 2000; Schepers *et al.*, 1992a). Leaf chlorophyll absorbs red light but not infrared, therefore, the SPAD reading indicate plant chlorophyll concentration and N content (Schepers *et al.*, 1992b; Markwell *et al.*, 1995; Lin *et al.*, 2010). However, the reliability of SPAD results is affected by factors such as growth stage, irradiance, water status, and leaf thickness (Samborski *et al.*, 2009; Schepers *et al.*, 1992b; Blackmer & Schepers, 1995).

Optical non-destructive methods based on canopy reflectance measurements have also

been widely used (Ali *et al.*, 2017; Mulla & Miao, 2016). The high measuring efficiency of reflectance spectroscopy sensors and the strong correlation between their measurements and crop physiological and biochemical parameters offer a high potential for N management (Gitelson *et al.*, 2003; Heege *et al.*, 2008). Proximal active sensors, such as GreenSeeker (NTech Industries, Inc., Ukiah, CA) and Crop Circle (Holland Scientific, NE, USA), have been used to diagnose N nutritional status in real-time and to guide in-season precision management for rice N fertilization (Yao *et al.*, 2012; Cao *et al.*, 2016). However, the results based on the canopy reflectance are affected by various factors, such as soil characteristics, crop growth stage, and saturation under high biomass conditions (Olfs *et al.*, 2005; Yao *et al.*, 2012). In addition, it is more difficult to estimate chlorophyll or N status using optical remote sensing methods as the contribution of leaf area index and biomass to canopy reflectance is much greater than that of chlorophyll or N concentration (Yu *et al.*, 2013b; Huang *et al.*, 2015).

Contrary to reflectance indices, the fluorescence spectra are less affected by biomass or leaf area index (Bredemeier & Schmidhalter, 2005; Heege *et al.*, 2008). At different N nutritional levels, the fluorescence intensities of leaves are significantly different near the 440 nm (Blue, B), 525 nm (Green, G), 685-690 nm (Red, R), and 735-740 nm (Near infrared, NIR) wavelengths (McMurtrey *et al.*, 1994; Langsdorf *et al.*, 2000). Studies have shown that the fluorescence ratio  $F(\text{NIR})/F(\text{R})$  has a high correlation with chlorophyll concentration (Gitelson *et al.* 1999; Cerovic *et al.* 2009) and the leaf N concentration (Yang *et al.*, 2016). Because the fluorescence ratio is only related to chlorophyll concentration or photosynthetic activity, soil background will not affect the spectra under low coverage or at early growth stages. Longchamps and Khosla (2014) observed that N supply levels in corn could be differentiated as early as the V5 phenological stage using proximal fluorescence sensors. In contrast, the test results only became reliable starting from the V8 growth stage based on the reflectance sensors (Teal *et al.*, 2006; Martin *et al.*, 2007). Therefore, chlorophyll fluorescence sensing is a powerful tool to address the shortcoming of proximal reflectance sensors in crop N status monitoring.

The fluorescence hand-held instruments Multiplex 3 (FORCE-A, Orsay, Paris, France) and Dualex (FORCE-A, Orsay, Paris, France) are developed for real-time fluorescence measurements in the field. Multiplex 3 and Dualex can detect not only chlorophyll fluorescence but also polyphenolics (mainly flavonols). When N is deficient, polyphenolics increase significantly due to the carbon and N balance regulation mechanism (Jones & Hartley, 1999). These compounds are mainly concentrated in epidermal cells, and have typical absorption peaks in the ultraviolet region (Knogge & Weissenboeck, 1986; Burchard *et al.*, 2000; Cerovic *et al.*, 2002). Thus, N status diagnosis is improved by combining the polyphenolics and chlorophyll fluorescence (Tremblay *et al.*, 2007, 2009). Lejealle *et al.* (2010) demonstrated that the N balance index (NBI), which is the chlorophyll-to-flavonols

ratio, had a better and more stable correlation with leaf N concentration. The Multiplex 3 sensor uses more indices than Dualex (Cerovic *et al.*, 2008) and therefore can detect physiological and biochemical plant parameters in addition to N, such as anthocyanins (Cerovic *et al.*, 2008), or plant diseases (Yu *et al.*, 2013a). In addition, it is a canopy sensor and is more efficient than a leaf sensor, like Dualex. It allows rapid large-area measurements with simultaneous GPS data recording for generating field maps (Diago *et al.*, 2016; Song *et al.*, 2017). However, studies based on the fluorescence instrument Multiplex 3 are still limited, especially for rice N status diagnosis and precision N management. Li *et al.* (2013) reported a preliminary study estimating rice N status using the Multiplex sensor. Therefore, it is necessary to further systematically and comprehensively study methods and application potential of Multiplex fluorescence canopy sensor for in-season rice N status diagnosis.

The main objectives of this study were to: 1) determine the optimal measurement mode of Multiplex sensor; 2) evaluate the potential of Multiplex sensor for N diagnosis in paddy rice; and 3) establish and validate estimation models for N indicators based on Multiplex indices. Particularly, to reduce the influences of varieties, years, sites and other factors, the normalized N sufficiency index (NSI) was calculated and included in the analysis of the fluorescence indices. Well-fertilized reference plots were used to normalize the reflectance measurements as more stable rice N diagnostic results might be obtained when calculating the NSI (Lu *et al.*, 2017).

## 6.2 Materials and methods

### 6.2.1 Experiment design

Two field trials were conducted at the Jiansanjiang Experiment Station of the China Agricultural University (47°15'N, 132°39'E), Sanjiang Plain, Heilongjiang Province, Northeast China. The field experiments in 2012 and 2013 included five different N rates (0, 70, 100, 130, 160 kg N ha<sup>-1</sup>) and two Japonica rice varieties, Kongyu 131 (KY 131) and Longjing 21 (LJ 21). These two represent the main varieties in this region: KY 131 has 11 leaves, four elongation nodes and about 127 maturity days, while LJ 21 has 12 leaves and needs 133 maturity days. Planting density was approximately 30 hills m<sup>-2</sup> for KY 131 and 28 hills m<sup>-2</sup> for LJ 21, with an identical row spacing of 0.3 m. The plot size was 4.5 m×9 m. The N fertilizer applications were split into 40%, 30%, 30%, and applied before transplanting, at the active tillering stage, and at the stem elongation (SE) stage, respectively. Phosphate (50 kg P<sub>2</sub>O<sub>5</sub> ha<sup>-1</sup>) fertilizers were applied before transplanting, and potash (100 kg K<sub>2</sub>O ha<sup>-1</sup>) fertilizers were applied as two splits, 50% as basal fertilizer and 50% as panicle fertilizer at the SE stage. The two experiments were carried out in a randomized complete block design with three replicates. More details of the two experiments are listed in Table 6-1.

**Table 6-1** Details of N rates experiments with two rice cultivars conducted during 2012-2013.

Experiment	Year	Cultivar	Transplanting Date	Sampling Date/ Sampling Stage
1	2012	KY 131	18-May	21-Jun (PI), 29-Jun (SE), 23-Jul (HE)
1	2012	LJ 21	18-May	25-Jun (PI), 2-Jul (SE), 23-Jul (HE)
2	2013	KY 131	17-May	23-Jun (PI), 2-Jul (SE), 22-Jul (HE)
2	2013	LJ 21	17-May	28-Jun (PI), 6-Jul (SE), 27-Jul (HE)

PI: Panicle Initiation; SE: Stem Elongation; HE: Heading

### 6.2.2 Fluorescence measurements

The portable fluorescence sensor Multiplex 3 was used in this study. It is an active sensor involving four emission light sources (UV\_A, green, red or blue) to excite the fluorescence in plant tissues. Generally, the UV\_A (375 nm), green (530 nm), and red (630 nm) emission light sources are used for plant monitoring, and the blue emission light source is used for calibration. The sensor has three filtered detectors for fluorescence recording including blue-green fluorescence (447 nm) (BGF), red fluorescence (665 nm) (RF) and far-red fluorescence (735 nm) (FRF). All the variables provided by the Multiplex sensor and their explanations are listed in Table 6-2. There are nine measured single fluorescence variables under three excitations, and ten calculated indices.

The Simple Fluorescence Ratio (SFR) index is the ratio of the FRF and RF emission under red (SFR\_R) or green (SFR\_G) illumination. SFR is related to the leaf chlorophyll content. Due to the chlorophyll absorption waveband overlapping with its fluorescence emission red band, the chlorophyll re-absorption occurs at shorter wavelengths (RF) rather than at FRF wavelengths. Therefore, using the FRF wavelengths as a reference, the absorption of the RF wavelengths reflects the content of chlorophyll. (Gitelson *et al.*, 1999; Pedrós *et al.*, 2010). SFR increases with chlorophyll content. The Flavonols (FLAV) index compares the fluorescence emission density of the far-red fluorescence under ultraviolet (FRF\_UV) and red excitation (FRF\_R). It is related to the flavonoid concentration of the epidermal layer (Ounis *et al.*, 2001; Agati *et al.*, 2011). The N Balance Index (NBI) is defined as the ratio of SFR and FLAV (Cartelat *et al.*, 2005). Therefore, NBI is proportional to both chlorophyll and flavonoid concentration. Blue-green to Far-red Fluorescence Ratio (BRR\_FRF) index is the ratio of BGF and FRF under UV excitation. The ratio of fluorescence emission at 440 nm and 740 nm ( $F_{440}/F_{740}$ ) wavelength was proven to be sensitive to environmental changes and growth conditions, and can detect plant stress before visible symptoms occur (Lichtenthaler, 1996; Yu *et al.*, 2013a). The Anthocyanins (ANTH) index and Fluorescence Excitation Ratio Anthocyanin Relative Index (FERARI) are both proven to correlated with skin anthocyanin content (Ghozlen *et al.*, 2010).

The Multiplex sensor readings were obtained right before the field samples were

collected at three growth stages. The Multiplex was put deeply into the canopy in two representative rows in the center of each plot. This mode was named “measuring in movement” or “on-the-go” (OG) mode, as shown in Huang *et al.* (2017). Finally, the collected data were averaged for the two rows to represent the plot. The following analysis was mainly based on results obtained with this measurement mode. For comparison, another two common measurement modes were applied, one measuring “above the canopy” (AC) and the other “at the leave scale” (LS). The measurements above the canopy were conducted in the field by randomly selecting ten representative hills and the average was used to represent the plot. The measurements based on the leaves were conducted in the laboratory taking ten leaves at the second position from the top.

### 6.2.3 Plant sampling and measurements

At the PI, SE and HE stages, for each plot three to six plant samples were collected from the same rows where fluorescence sensor measurements were acquired. Various N status indicators, including above ground biomass (AGB), plant N concentration (PNC), leaf N concentration (LNC), plant N uptake (PNU), and N nutrition index (NNI), were determined. The detailed sampling dates and related information are listed in Table 6-1. Roots from all the plant samples were removed and the samples were cleansed with water and then separated into leaves, stems, and panicles (e.g. HE stage). All samples were dried at 105 °C for half an hour to reduce plant metabolic activities. After being dried in an oven at 70-80 °C to constant weight, the samples were weighted. N concentration for leaves, stems, and panicles was determined using the standard Kjeldahl method. The PNC is the sum of the products of each organ’s N concentration and their proportional weight. The PNU was determined by multiplying PNC by AGB. The NNI is defined as the ratio of the actual PNC ( $N_a$ ) and the critical N concentration ( $N_c$ ), with  $N_c$  being calculated following the equation developed for rice in this region (Huang *et al.*, 2018).

**Table 6-2** Description of the variables and indices recorded by the Multiplex sensor (modified from Table 1 by Zhang *et al.*, 2012).

Variables	Formula	Explanation
BGF_UV	/	Blue-green Fluorescence under UV excitation
RF_UV	/	Red Fluorescence under UV excitation
FRF_UV	/	Far-Red Fluorescence under UV excitation
BGF_G	/	Reflected Blue-Green light under Green excitation
RF_G	/	Red Fluorescence under Green excitation
FRF_G	/	Far-Red Fluorescence under Green excitation
BGF_R <sup>#</sup>	/	Blue-green Fluorescence under Red excitation
RF_R	/	Red Fluorescence under Red excitation
FRF_R	/	Far-Red Fluorescence under Red excitation
SFR_G	FRF_G/RF_G	Simple Fluorescence Ratio under Green excitation
SFR_R	FRF_R/RF_R	Simple Fluorescence Ratio under Red excitation
BRR_FRF	BGF_UV/FRF_UV	Blue-green to Far-Red Fluorescence Ratio under UV excitation
FER_RUV	FRF_R/FRF_UV	Flavonols under Red and UV excitation
FLAV	Log (FRF_R/FRF_UV)	Flavonols under Red and UV excitation
FER_RG	FRF_R/FRF_G	Anthocyanins under Red and Green excitation
ANTH	Log (FRF_R/FRF_G)	Anthocyanins under Red and Green excitation
NBI_G	FRF_UV/RF_G	Nitrogen Balance Index under UV and Green excitation
NBI_R	FRF_UV/RF_R	Nitrogen Balance Index under UV and Red excitation
FERARI <sup>#</sup>	Log (5000/FRF_R)	Fluorescence Excitation Ratio Anthocyanin Relative Index

# The variable is not measured in the “on-the-go” mode

#### 6.2.4 Statistical analysis

The Multiplex data of the three measurement modes at each sampling stage, year, and cultivar obtained under the varied N supply were subjected to analysis of variance (ANOVA) using SAS software (SAS Institute, Cary, NC, USA). Moreover, the means for each treatment were compared using the least significant difference (LSD) test at the 95% level of significance. Relationships between the Multiplex indices and N status indicators were determined. All of the in-situ samples were divided into two groups by a stratified random sampling method, with approximately 2/3 of the data used for model calibration and the remaining for model validation. Simple linear regression analyses were performed with SPSS 20.0 (SPSS Inc., Chicago, Illinois, USA). The coefficient of determination ( $R^2$ ) was calculated for comparison. The relationships between Multiplex indices and N status indicators established at different growth stages was validated. The root mean square error (RMSE) and the relative error ( $RE_r$ ), shown in equations (6-1) and (6-2), between the predicted and observed values were used for evaluation.

$$RMSE = \sqrt{\frac{1}{n} \sum_{i=1}^n (y_i - \hat{y}_i)^2} \quad (6-1)$$

$$RE_r(\%) = \frac{RMSE}{\bar{y}} \times 100 \quad (6-2)$$

where  $y_i$ ,  $\hat{y}_i$ , and  $\bar{y}$  were the observed, predicted and mean value, respectively.

In order to evaluate normalized vegetation indices for improving the estimation of N nutrition indicators, the well-fertilized plots were used as N sufficient reference to calculate the NSI index. The NSI index equals to the ratio of Multiplex indices of the plots receiving normal N rates and the well-fertilized plots. In this study, the treatment with the largest shoot dry matter was defined as the well-fertilized plot, corresponding to the treatment of 130 or 160 kg N ha<sup>-1</sup>.

Finally, the NNI diagnosis results of validation data using Multiplex indices were compared to the observed NNI by areal agreement and kappa statistics (Xia *et al.*, 2016). Both used the same diagnostic criteria: N deficient when NNI < 0.95, N optimal when NNI is between 0.95-1.05, and N surplus when NNI > 1.05. The areal agreement (%) and Kappa statistics were used to determine the accuracy of the diagnosis results. The areal agreement indicates the percentage of two groups sharing a common category or diagnosis class, for example N deficient, N optima or N surplus. The Kappa statistic is a more robust measure of the agreement of two classifications by correcting the agreement that occurs by chance. When Kappa equals 1, it indicates that the two categorization systems are identical. A Kappa value  $\geq 0.60$  indicates a satisfactory agreement, while < 0.4 indicates weak agreement (Landis & Koch, 1977).

## 6.3 Results

### 6.3.1 Comparison of the different measurement modes of the Multiplex sensor

Most researchers applied Multiplex sensor using the AC mode, while some chose the LS or OG modes (Zhang *et al.*, 2012; Diago *et al.*, 2016). These three measurement modes were adopted for each treatment plot. The results were compared to determine the best measurement mode. The abbreviation of the measurement mode is added to the variable as a prefix. For example, AC\_SFR\_G represents the Multiplex index SFR\_G obtained from above the canopy.

Fig. 6-1 shows box plots of Multiplex indices obtained from the three measuring modes at two phenological stages. Since FLAV and ANTH are the log transformation values of FER\_RUV and FER\_RG, only FLAV and ANTH were selected for analysis. At the PI growth stage, the mean value of the Multiplex indices (except for the BBR\_FRF) obtained with the OG mode were significantly higher ( $P \leq 0.05$ ) than the corresponding indices obtained under

LS mode, which were significantly higher than those obtained under the AC mode. Similar results were found at the SE stage. In addition, larger data ranges were found in the measured NBI\_G and NBI\_R indices under the OG mode.

The distribution interval (or range) of most measurements was greater in the OG mode than in the AC and LS mode, especially for NBI\_G and NBI\_R (Fig. 6-1). The ANOVA results for the five N rates (0, 70, 100, 130, and 160 kg N ha<sup>-1</sup>) are listed in Table 6-3, which indicated the sensitivity of each Multiplex variable. N fertilization treatment effects were significant for most Multiplex variables measured in the OG and the AC modes, but not for most variables obtained in the LS mode. The N treatment effects were more significant for the OG mode than for the AC mode at the PI and SE growth stages or for the LS mode at the HE stage.

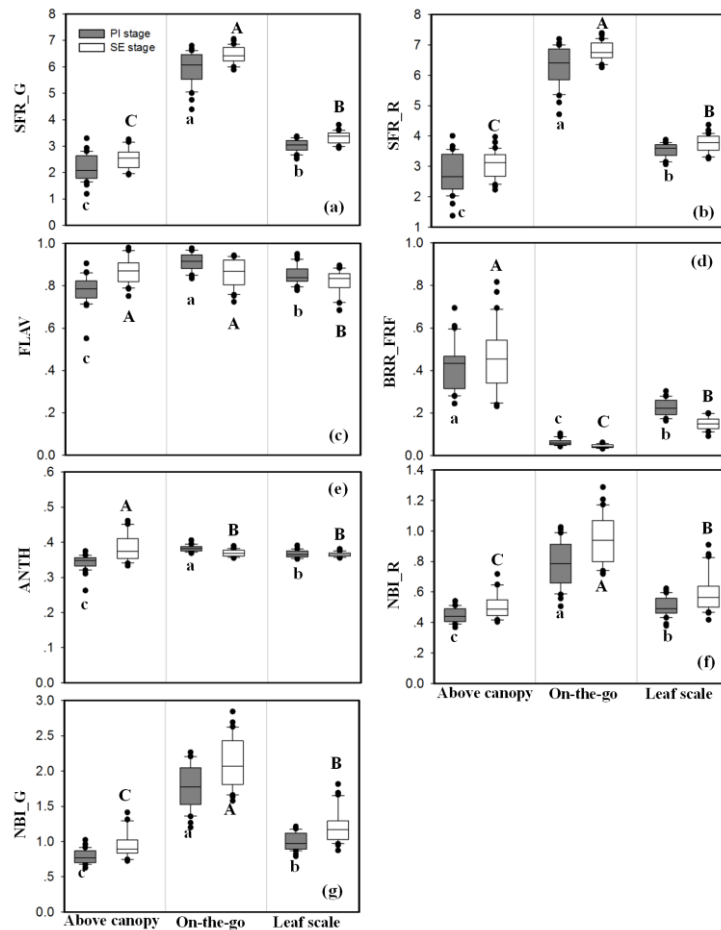


**Fig. 6-1** Box plots of selected Multiplex indices values for the above canopy, on-the-go, and leaf scale measuring modes at the panicle initiation and stem elongation stages in 2013: SFR\_G (a), SFR\_R (b), FLAV (c), BRR\_FRF (d), ANTH (e), NBI\_R (f) and NBI\_G (g). Within the same growth stage, different lowercase (panicle initiation stage) or uppercase letters (stem elongation stage) above or below the boxes indicate that the Multiplex index values differed significantly according to least significant difference test at  $P \leq 0.05$ .

**Table 6-3** Significance test (ANOVA) of Multiplex variables measured in three modes: above canopy (AC), on-the-go (OG), and leaf scale (LS) at the panicle initiation (PI), stem elongation (SE), and heading (HE) growth stages for the rice varieties Kongyu 131 (KY 131) and Longjing 21 (LJ 21) in 2013.

Variety	Stage	BGF_UV	RF_UV	FRF_UV	BGF_G	RF_G	FRF_G	BGF_R	RF_R	FRF_R	SFR_G	SFR_R	BRR_FRF	FLAV	ANTH	NBL_G	NBL_R	FERARI		
<b>AC measurement mode</b>																				
KY 131	PI	NS	*	*	NS	*	*	NS	*	*	**	**	NS	NS	NS	NS	NS	**		
	SE	NS	NS	NS	NS	NS	NS	NS	NS	NS	NS	*	NS	NS	NS	*	NS	NS		
	<b>OG measurement mode</b>																			
	PI	***	**	**	**	***	***		***	***	***	***	**	*	*	**	**			
	SE	**	***	***	NS	**	***		**	**	**	**	**	**	**	**	**	**		
	HE	NS	***	***	NS	**	**		*	**	**	**	**	**	**	**	***	***		
	<b>LS measurement mode</b>																			
	PI	NS	NS	NS	NS	NS	NS	NS	NS	NS	*	*	*	NS	NS	NS	NS	NS	NS	
	SE	NS	NS	NS	NS	NS	NS	*	NS	NS	*	***	**	NS	NS	NS	**	*	*	
HE	NS	NS	NS	**	NS	*	NS	NS	NS	*	**	*	*	NS	NS	*	*	*		
<b>AC measurement mode</b>																				
LJ 21	PI	NS	*	*	NS	*	*	*	*	*	**	**	**	*	*	**	*	**		
	SE	NS	*	*	NS	*	*	NS	*	*	*	*	**	NS	NS	NS	NS	*		
	<b>OG measurement mode</b>																			
	PI	NS	*	*	NS	NS	*		NS	*	**	**	*	*	*	**	**			
	SE	NS	**	**	NS	NS	**		NS	**	***	***	*	*	*	**	**			
	HE	NS	***	***	NS	**	***		NS	***	***	***	***	***	***	NS	***	***		
	<b>LS measurement mode</b>																			
	PI	NS	NS	NS	NS	NS	NS	NS	NS	NS	NS	*	**	NS	NS	NS	*	NS	NS	
	SE	NS	**	**	NS	NS	*	NS	NS	NS	NS	*	NS	**	NS	NS	*	*	*	
HE	NS	NS	NS	NS	NS	NS	NS	NS	NS	NS	NS	NS	NS	NS	NS	NS	NS	NS		

\*\*\*. Correlation is significant at the 0.001 level; \*\*. Correlation is significant at the 0.01 level; \*. Correlation is significant at the 0.05 level; NS. Correlation is not significant.

Fig. 6-2 demonstrates the comparison results for selected Multiplex indices at each N application rate for cultivar KY 131 in 2013 (as an example). According to the P level results in Table 6-3, the indices measured in the OG mode could better distinguish effects of N supply compared to the other two modes. For the differentiation of the high N-application treatment (100 and 130 kg ha<sup>-1</sup>) effects, the Multiplex indices under the OG mode performed consistently better than others did. Their values showed an increase from the N rate treatment of 130 kg ha<sup>-1</sup> to 160 kg N ha<sup>-1</sup>, although their difference was not significant. For the variety LJ 21, or for the experiments conducted in 2012, the indices under OG mode are most sensitive for N rate treatment compared to the other two modes (data not shown).

In conclusion, the ANOVA analysis results showed that most of the Multiplex variables obtained under the OG mode were more sensitive to N supply than the ones obtained under the other two modes. Measurements taken under the AC mode were more strongly influenced by N supply than the ones taken under the LS mode (Table 6-3, Fig. 6-2). Thus, only results of the “on-the-go” mode were used for further analysis and discussion.

### 6.3.2 Changes in Multiplex indices (“on-the-go” mode) over growth stages under varied N supply

For the variety KY 131 in 2013, SFR\_G, SFR\_R, NBI\_G, and NBI\_R values were significantly higher at high N rate plots (100-160 kg N ha<sup>-1</sup>) than 0 kg N ha<sup>-1</sup> plots across growth stages (Fig. 6-2). These indices could differentiate more N rates at the medium to late stages, which may be due to the larger variation of the LNC, PNC, and NNI at these stages than at the early stage (data not shown). The values of these indices increased from the PI to SE stage but decreased from the SE to HE stage, because the panicle formation decreased the chlorophyll/N concentration in the upper layer at the HE stage. The opposite was true for the BRR\_FRF, FLAV and ANTH. NBI\_G and NBI\_R could differentiate different N application rates the best, followed by SFR\_G, SFR\_R, BRR\_FRF, and FLAV. The performance of ANTH was the worst (Fig. 6-2).

**1) Panicle initiation**

N Rate	AC_SFR_G				AC_SFR_R				AC_BRR_FRF				AC_FLAV				AC_ANTH				AC_NBI_G				AC_NBI_R				AC_FERARI							
0	1.48	0.22			1.75	0.30			0.61	0.07			0.66	0.07			0.30	0.03			0.67	0.03			0.40	0.00			1.92	0.06			2.10	0.10		
70	1.77	0.14			2.21	0.17			0.51	0.07			0.76	0.02			0.34	0.01			0.70	0.05			0.39	0.02			1.87	0.08			1.92	0.06		
100	1.93	0.29			2.38	0.25			0.48	0.06			0.77	0.04			0.34	0.02			0.73	0.04			0.41	0.02			1.87	0.08			1.89	0.04		
130	1.90	0.10			2.37	0.15			0.47	0.03			0.75	0.01			0.34	0.01			0.74	0.03			0.43	0.01			1.89	0.04			1.89	0.04		
160		2.28	0.08			2.83	0.08		0.41	0.03			0.84	0.05			0.36	0.01			0.77	0.07			0.42	0.02			1.74	0.04			1.74	0.04		

**2) Stem elongation**

N Rate	OG_SFR_G				OG_SFR_R				OG_BRR_FRF				OG_FLAV				OG_ANTH				OG_NBI_G				OG_NBI_R				OG_FERARI							
0	4.72	0.25			5.05	0.26			0.10	0.01			0.97	0.00			0.40	0.01			1.27	0.07			0.55	0.03			0.67	0.03			1.58	0.05		
70	5.46	0.19			5.77	0.08			0.07	0.01			0.94	0.02			0.39	0.00			1.54	0.07			0.67	0.03			1.47	0.02			1.47	0.02		
100	5.57	0.20			5.89	0.19			0.07	0.01			0.96	0.01			0.39	0.00			1.49	0.10			0.65	0.04			1.48	0.02			1.48	0.02		
130	5.91	0.24			6.20	0.23			0.06	0.01			0.93	0.02			0.39	0.01			1.69	0.11			0.73	0.06			1.48	0.02			1.48	0.02		
160	5.99	0.21			6.30	0.21			0.06	0.01			0.91	0.01			0.38	0.00			1.78	0.11			0.78	0.05			1.44	0.02			1.44	0.02		

**3) Heading**

N Rate	LS_SFR_G				LS_SFR_R				LS_BRR_FRF				LS_FLAV				LS_ANTH				LS_NBI_G				LS_NBI_R				LS_FERARI							
0	2.63	0.08			3.15	0.01			0.28	0.02			0.83	0.01			0.37	0.01			0.91	0.02			0.47	0.01			1.49	0.05			1.49	0.05		
70	2.82	0.17			3.27	0.17			0.24	0.02			0.85	0.03			0.37	0.01			0.94	0.04			0.47	0.02			1.49	0.05			1.49	0.05		
100	2.93	0.13			3.43	0.15			0.26	0.01			0.92	0.03			0.38	0.01			0.85	0.02			0.42	0.02			1.47	0.02			1.47	0.02		
130	2.91	0.10			3.45	0.14			0.25	0.02			0.88	0.05			0.38	0.01			0.92	0.11			0.45	0.02			1.48	0.02			1.48	0.02		
160	3.13	0.05			3.63	0.05			0.22	0.01			0.87	0.01			0.37	0.01			1.00	0.08			0.50	0.05			1.44	0.02			1.44	0.02		

**Fig. 6-2** Mean value comparisons for each Multiplex index at the three growth stages and each N application rate (kg N ha<sup>-1</sup>) for variety KY 131 in 2013. Differentiation patterns for N rate treatment at each sampling stage are depicted for the three measurement modes (above canopy, AC; on-the-go, OG; leaf scale, LS). Different lowercase letters at the bottom of the plot at each stage indicate significant differences according to the least significant difference test at  $P \leq 0.05$ . The two numbers in the cells are the mean value and standard deviation (italic).

### 6.3.3 Correlations between Multiplex indices (“on-the-go” mode) and N status indicators

The linear regression results of the seven Multiplex indices and the five N status indicators at three growth stages across the two rice varieties are shown in Table 6-4. The SFR\_G, SFR\_R, NBI\_G, and NBI\_R indices were positively correlated with the N indicators whereas the opposite was true for BRR\_FRF, ANTH, and FLAV. The ANTH parameter showed no significant correlation with AGB and PNU at the SE stage. The  $R^2$  varied widely for these indices ( $R^2 = 0.03-0.78$ ). For each N indicator, the SFR\_G, SFR\_R, and ANTH showed a high variability in the regression models at different growth stages. Lower coefficients of determination were found at the SE stage. The BRR\_FRF, FLAV, NBI\_G and NBI\_R indices showed stable relationships at the three growth stages. The best performing index across varieties at the PI, SE, and HE stages differed, but NBI\_G and NBI\_R showed high correlations with LNC ( $R^2 = 0.52-0.68$ ), PNC ( $R^2 = 0.52-0.71$ ) and NNI ( $R^2 = 0.69-0.78$ ). The second-best performing indices were BRR\_FRF and FLAV. The SFR\_G and SFR\_R indices only showed high correlations at the PI stage. The normalized sufficiency indices SFR\_G<sub>NSI</sub>, SFR\_R<sub>NSI</sub>, and ANTH<sub>NSI</sub> showed more stable relationships with LNC, PNC, and NNI than SFR\_G, SFR\_R and ANTH indices, especially at the SE and HE stages. The other four normalized sufficiency indices BRR\_FRF<sub>NSI</sub>, FLAV<sub>NSI</sub>, NBI\_G<sub>NSI</sub>, NBI\_R<sub>NSI</sub> showed similar  $R^2$  values regarding the LNC, PNC, and NNI estimation.

For the AGB estimation, all standard and normalized indices showed lower  $R^2$  values than those for PNC at the SE and HE stages. For the PNU estimation, most of the indices and NSIs showed high  $R^2$  values (0.39-0.72). Compared to other N status indicators, the best performing indices for NNI estimation explained the most variations ( $R^2 = 0.72$  for PI,  $R^2 = 0.78$  for SE,  $R^2 = 0.76$  for HE), and the best performing NSIs also showed the highest relationships with NNI at SE ( $R^2 = 0.77$ ) and HE ( $R^2 = 0.82$ ) stages.

### 6.3.4 Validation of the estimation models for N status indicators

In order to diagnose rice N status, linear regression models between Multiplex indices and N indicators were established. The regression models varied across growth stages. Table 6-5 lists the best performing models at the PI, SE, and HE stages. The best performing indices differed across the stages. However, the relationships of NBI\_G and NBI\_R with N indicators were relatively more stable. After normalization, the NBI\_R<sub>NSI</sub> showed an absolute advantage for N indicator estimation at the PI and SE growth stages.

Fig. 6-3 shows the  $RE_r$  values of the validation models for six Multiplex indices (SFR\_G, SFR\_R, BRR\_FRF, FLAV, NBI\_G, and NBI\_R) and the N status indicators. The  $RE_r$  values for AGB and PNU estimations based on these indices decreased steadily with advancing growth stages, while a slightly increasing trend was observed for LNC and PNC estimation models from the SE to HE stages. The  $RE_r$  values for LNC (4.50%-10.24%), PNC (5.87%-

10.87%) models were much smaller than those for AGB (15.49%-30.18%) and PNU (19.31%-31.25%). The  $RE_r$  of NNI remained similar during the three growth stages. At the earlier to middle growth stages, NBI\_R and NBI\_G presented a lower  $RE_r$  than the other four indices for all the six N indicators. At the HE stage, however, the prediction accuracies of the six indices were similar.

**Table 6-4** The coefficients of determination ( $R^2$ ) for the linear relationships between standard and normalized Multiplex indices and N status indicators (leaf N concentration (LNC), plant N concentration (PNC), N nutrition index (NNI), aboveground biomass (AGB) and plant N uptake (PNU)) for two varieties at the panicle initiation (PI), stem elongation (SE), and heading (HE) growth stages.

Multiplex indices	LNC (g kg <sup>-1</sup> )			PNC (g kg <sup>-1</sup> )			NNI			AGB (t ha <sup>-1</sup> )			PNU (kg ha <sup>-1</sup> )		
	PI	SE	HE	PI	SE	HE	PI	SE	HE	PI	SE	HE	PI	SE	HE
<b>Standard indices</b>															
SFR_G	0.63**	0.30**	0.49**	0.64**	0.34**	0.46**	0.72**	0.31**	0.59**	0.60**	0.14*	0.41**	0.66**	0.21**	0.58**
SFR_R	0.59**	0.28**	0.42**	0.58**	0.34**	0.38**	0.66**	0.29**	0.54**	0.56**	0.13*	0.45**	0.61**	0.19**	0.57**
BRR_FRF	0.53**	0.52**	0.67**	0.47**	0.48**	0.66**	0.57**	0.48**	0.72**	0.50**	0.26**	0.33**	0.54**	0.39**	0.59**
FLAV	0.40**	0.64**	0.55**	0.39**	0.64**	0.55**	0.58**	0.73**	0.67**	0.55**	0.50**	0.38**	0.59**	0.68**	0.59**
ANTH	0.38**	0.12*	0.27**	0.41**	0.14*	0.33**	0.60**	0.10*	0.47**	0.60**	0.03NS	0.36**	0.61**	0.06NS	0.48**
NBI_G	0.54**	0.68**	0.62**	0.52**	0.71**	0.61**	0.69**	0.78**	0.76**	0.63**	0.50**	0.47**	0.68**	0.71**	0.71**
NBI_R	0.52**	0.67**	0.58**	0.52**	0.71**	0.56**	0.70**	0.77**	0.74**	0.64**	0.47**	0.51**	0.69**	0.68**	0.72**
<b>Normalized indices</b>															
SFR_G <sub>NSI</sub>	0.58**	0.39**	0.67**	0.65**	0.42**	0.70**	0.55**	0.54**	0.69**	0.35**	0.45**	0.24**	0.43**	0.50**	0.52**
SFR_R <sub>NSI</sub>	0.57**	0.42**	0.62**	0.61**	0.46**	0.67**	0.52**	0.57**	0.68**	0.33**	0.45**	0.25**	0.40**	0.52**	0.52**
BRR_FRF <sub>NSI</sub>	0.49**	0.34**	0.63**	0.48**	0.41**	0.74**	0.41**	0.56**	0.76**	0.26**	0.50**	0.28**	0.33**	0.56**	0.58**
FLAV <sub>NSI</sub>	0.42**	0.51**	0.70**	0.44**	0.60**	0.76**	0.41**	0.74**	0.82**	0.26**	0.55**	0.34**	0.33**	0.70**	0.64**
ANTH <sub>NSI</sub>	0.51**	0.40**	0.57**	0.64**	0.40**	0.65**	0.54**	0.57**	0.56**	0.34**	0.52**	0.11*	0.42**	0.58**	0.35**
NBI_G <sub>NSI</sub>	0.59**	0.53**	0.69**	0.61**	0.63**	0.75**	0.55**	0.76**	0.78**	0.35**	0.55**	0.31**	0.43**	0.71**	0.61**
NBI_R <sub>NSI</sub>	0.60**	0.55**	0.69**	0.65**	0.64**	0.75**	0.58**	0.77**	0.79**	0.36**	0.56**	0.31**	0.46**	0.72**	0.61**

\*\* . Correlation is significant at the 0.01 level; \* . Correlation is significant at the 0.05 level; NS. Correlation is not significant.

**Table 6-5** Equations and coefficients of determination of linear regression models ( $n = 40$ ) at different growth stages based on the best performing Multiplex index and crop N indicators (LNC, PNC, NNI, PNU, AGB).

Growth stage	Standard Indices	Model	R <sup>2</sup>	Normalized Indices	Model	R <sup>2</sup>
PI	SFR_G	LNC = 4.468x+5.932	0.63	NBI_R <sub>NSI</sub>	LNC = 23.918x+10.413	0.60
PI	SFR_G	PNC = 2.912x+4.961	0.64	NBI_R <sub>NSI</sub>	PNC = 15.323x+8.247	0.65
PI	SFR_G	NNI = 0.2442x-0.5188	0.72	NBI_R <sub>NSI</sub>	NNI = 1.1412x - 0.1116	0.58
PI	NBI_R	PNU = 88.184x-33.56	0.69	NBI_R <sub>NSI</sub>	PNU = 85.908x-43.67	0.46
PI	NBI_G	AGB = 1.5268x - 1.1565	0.64	NBI_R <sub>NSI</sub>	AGB = 2.905x - 1.1184	0.36
SE	NBI_G	LNC = 8.707x + 14.352	0.68	NBI_R <sub>NSI</sub>	LNC = 17.96x + 16.279	0.55
SE	NBI_G	PNC = 5.544x + 9.082	0.71	NBI_R <sub>NSI</sub>	PNC = 12.317x + 9.542	0.64
SE	NBI_G	NNI = 0.5003x + 0.0582	0.78	NBI_R <sub>NSI</sub>	NNI = 1.1571x + 0.0601	0.77
SE	NBI_G	PNU = 51.494x - 40.873	0.71	NBI_R <sub>NSI</sub>	PNU = 120.8x - 42.157	0.72
SE	NBI_G	AGB = 1.7391x - 0.4502	0.50	NBI_R <sub>NSI</sub>	AGB = 4.1975x - 0.5961	0.56
HE	BRR_FRF	LNC = -210.31x + 47.452	0.67	NBI_G <sub>NSI</sub>	LNC = 21.646x + 15.473	0.69
HE	BRR_FRF	PNC = -131.79x + 24.313	0.66	FLAV <sub>NSI</sub>	PNC = -31.59x + 49.591	0.76
HE	NBI_G	NNI = 0.5942x - 0.054	0.76	FLAV <sub>NSI</sub>	NNI = -3.0631x + 4.3956	0.82
HE	NBI_R	PNU = 213.07x - 67.623	0.72	FLAV <sub>NSI</sub>	PNU = -462.81x + 612.19	0.64
HE	NBI_R	AGB = 8.3363x + 0.0609	0.51	FLAV <sub>NSI</sub>	AGB = -15.729x + 24.131	0.34

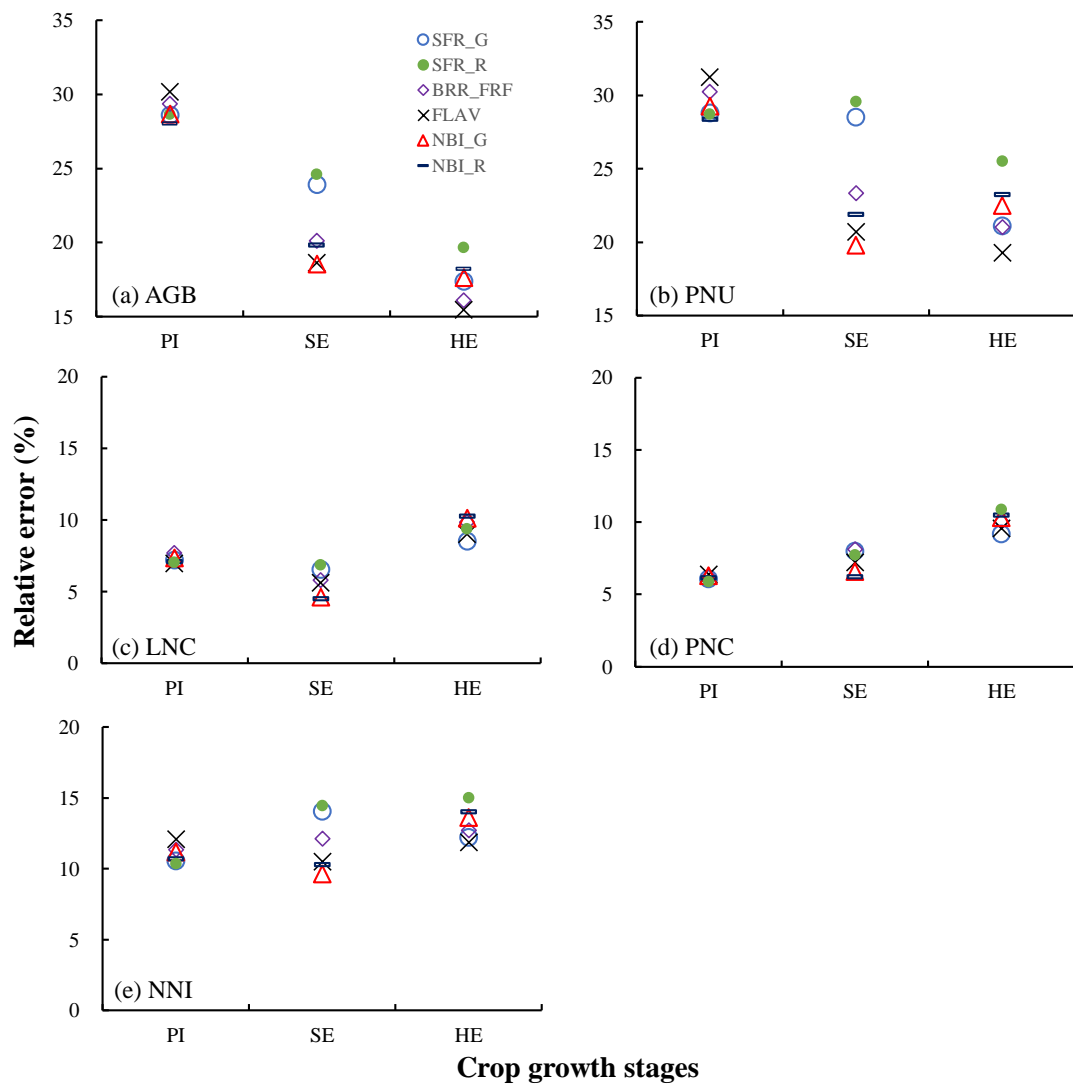


**Fig. 6-3** The relative error ( $RE_r$ ) values of the validation analysis based on the regression models of the six Multiplex indices and the N status indicators for (a) above ground biomass (AGB), (b) plant N uptake (PNU), (c) leaf N concentration (LNC), (d) plant N concentration (PNC), and (e) N nutrition index (NNI) at the panicle initiation (PI), stem elongation (SE), and heading (HE) stages.

### 6.3.5 Comparing the Multiplex index-based and the normalized sufficiency index-based N nutrition status diagnosis results

The best performing indices SFR\_G, BRR\_FRF, NBI\_G, NBI\_R, NBI\_G<sub>NSI</sub>, NBI\_R<sub>NSI</sub> and FLAV<sub>NSI</sub> shown in Table 6-5 were validated using independent data sets. Moderate model performance with  $R^2$  ranging from 0.34 to 0.82 were obtained. Higher estimation potential was observed for LNC, PNC, and NNI than AGB based on most Multiplex indices and the normalized sufficiency indices. Considering the NNI as an ideal indicator for N status diagnosis, the NNI models were further verified. The diagnostic results of the indices SFR\_G, SFR\_R, BRR\_FRF, FLAV, ANTH, NBI\_G, and NBI\_R were compared at the

critical N fertilizer application stages (SE and HE). According to the previous research (Huang *et al.*, 2015), the experimental plots were divided into N deficient, N optimal and N surplus groups based on the NNI threshold values of 0.95, 0.95-1.05, and 1.05. Their Kappa statistics were analyzed to evaluate the diagnostic accuracies of the different indices. The results confirmed that the NNI models based on BRR\_FRF, NBI\_R, NBI\_G performed highly consistent at the SE and HE growth stages, and their corresponding NSI indices further improved the results (Table 6-6). At the SE stage, the NBI\_R<sub>NSI</sub> achieved the highest diagnostic accuracy rate (90%), while the FLAV achieved the same accuracy rate at the HE stage. Across the two growth stages, the NBI\_R<sub>NSI</sub> showed the highest diagnostic consistency.

**Table 6-6** Agreement and Kappa statistics for different indices (SFR\_G, SFR\_R, BRR\_FRF, FLAV, ANTH, NBI\_G, and NBI\_R) and corresponding normalized indices (SFR\_G<sub>NSI</sub>, SFR\_R<sub>NSI</sub>, BRR\_FRF<sub>NSI</sub>, FLAV<sub>NSI</sub>, ANTH<sub>NSI</sub>, NBI\_G<sub>NSI</sub> and NBI\_R<sub>NSI</sub>) regarding diagnostic results (N Nutrition Index) at different growth stages.

Comparison	Agreement (%)		Kappa statistics		Comparison	Agreement (%)		Kappa statistics	
	SE	HE	SE	HE		SE	HE	SE	HE
SFR_G and NNI	75	65	0.554***	0.310*	SFR_G <sub>NSI</sub> and NNI	70	85	0.494**	0.661***
SFR_R and NNI	70	70	0.510***	0.322*	SFR_R <sub>NSI</sub> and NNI	75	85	0.583***	0.661***
BRR_FRF and NNI	60	70	0.363*	0.409**	BRR_FRF <sub>NSI</sub> and NNI	80	80	0.655***	0.538***
FLAV and NNI	75	90	0.605***	0.763***	FLAV <sub>NSI</sub> and NNI	75	80	0.558***	0.570***
ANTH and NNI	55	75	0.283 <sup>NS</sup>	0.355*	ANTH <sub>NSI</sub> and NNI	80	65	0.669***	0.227 <sup>NS</sup>
NBI_G and NNI	75	80	0.595***	0.590***	NBI_G <sub>NSI</sub> and NNI	75	85	0.673***	0.698***
NBI_R and NNI	75	80	0.595***	0.590***	NBI_R <sub>NSI</sub> and NNI	90	85	0.840***	0.698***

\*\*\*. Correlation is significant at the 0.001 level; \*\*. Correlation is significant at the 0.01 level; \*. Correlation is significant at the 0.05 level; NS. Correlation is not significant.

## 6.4 Discussion

### 6.4.1 Estimation of crop N indicators by fluorescence indices

Strong relationships between the Multiplex indices SFR\_G, SFR\_R, BRR\_FRF, FLAV, NBI\_G, NBI\_R and the five N indicators were achieved with low RE<sub>r</sub> and high R<sup>2</sup> values (Table 6-4, Fig. 6-3). These results conform to previous research results in this field (Li *et*

*al.*, 2013; Padilla *et al.*, 2016; Agati *et al.*, 2015; Yang *et al.*, 2016). Many studies confirmed SFR was a good fluorescence index for chlorophyll content monitoring (Buschmann, 2007; Gitelson *et al.*, 1999; Yu *et al.*, 2013). However, it was found in this study that the  $R^2$  of the SFR\_G, SFR\_R for LNC, PNC, and NNI estimation decreased steadily from early stage to mid to late stages, while an opposite trend was observed for FLAV. Padilla *et al.* (2016) found that the NNI estimation relationships changed for SFR\_G with the phenological stage of cucumber (*Cucumis sativus* L.). Firstly, the consistency of the relationship between chlorophyll content and N concentration varied with crop development, leading to different performances of SFR for N concentration estimation. For example, at the SE stage, the linear correlation between LNC and chlorophyll meter readings of rice was weaker than at other growth stages (Yuan *et al.*, 2016). Secondly, the lower distinguishing ability for SFR under the N non-limiting conditions may also be a reason (Padilla *et al.*, 2016). The performance of FLAV increased from the PI to HE stages, which was also confirmed by Padilla *et al.* (2016), who found the relationship of FLAV and NNI increased at the middle to late growth stages. The better performance of FLAV at the later stage can be interpreted as a consequence of the accumulation of the flavonols content in leaves under light radiation (Ounis *et al.*, 2001; Barthod *et al.*, 2007). The NBI\_G and NBI\_R indices were the best indices according to the strength and consistency of the relationships with N indicators (Table 6-5). Confirmed by many studies, the NBI indices appeared to be the most efficient in estimating the N status (Cartelat *et al.*, 2005; Goulas *et al.*, 2004; Agati *et al.*, 2015; Padilla *et al.*, 2016). This is because the NBI is a ratio of SFR and FLAV, which makes it more robust than using FLAV or SFR alone to reduce the effects of leaf age or other factors (Cartelat *et al.*, 2005; Tremblay *et al.*, 2007; Lejealle *et al.*, 2010). The NBI\_G performed very similarly as NBI\_R in this study, as demonstrated by Longchamps and Khosla (2010). Moreover, they found that SFR was less sensitive to N application than NBI. This is consistent with our results, as shown in Fig. 6-2. In most cases, the SFR\_G and SFR\_R indices could not distinguish between the 100 and 130 kg N ha<sup>-1</sup> treatments, but NBI could. The BRR\_FRF index was significantly correlated with the N nutritional status, and was especially sensitive to N deficiency in this research. When there is N stress, the fluorescence ratio of blue-green/far-red will increase after exposure to UV radiation to avoid or alleviate the damage of the photosynthetic apparatus (Lichtenthaler & Schweiger, 1998). Generally, the UV-protection response takes place before the chlorophyll damage can be seen, so the BRR\_FRF can also be considered as a potential index that can realize early N deficiency detection (Buschmann *et al.*, 1998). The BRR\_FRF was also proved to be very sensitive to environmental stresses, such as disease and drought (Buschmann *et al.*, 1998; Yu *et al.*, 2013a; Burling *et al.*, 2013). The ANTH index provided by Multiplex is commonly used to reflect anthocyanin content, which corresponds to the maturation degree of fruit (Ghozlen *et al.*, 2010; Agati *et al.*, 2005). In this research, the low values of ANTH were due to the low anthocyanin content in the rapid

vegetative growth phase for rice (Chen *et al.*, 2015). Nevertheless, ANTH was also found to be closely related to the leaf chlorophyll concentration in some studies (Yu *et al.*, 2013a; Zhang *et al.*, 2012). This study revealed that ANTH was significantly related to N status indicators in some growth stages, although the  $R^2$  value was not very high.

#### 6.4.2 Normalized nitrogen sufficiency fluorescence indices

Our research involved two years and two varieties of experiments. The normalized N sufficiency index approach has been suggested to reduce the influence of the varieties, developmental stages on SPAD values or spectral data (Lin *et al.*, 2010; Zubillaga & Urricariet, 2005; Samborski *et al.*, 2009). From the results of this study, in most cases, the normalized NSIs were more closely associated with the LNC, PNC, and NNI (Table 6-4). The  $R^2$  of the index  $ANTH_{NSI}$  was the most improved, followed by  $NBI_{G_{NSI}}$  and  $NBI_{R_{NSI}}$ . However, the improvement in  $R^2$  for  $BRR_{FRF_{NSI}}$  was minimal. The variance analysis of this study showed consistent results, which demonstrated that NSI indices could reduce the influence of inter-annual and growth stage differences (data not shown). Since NNI itself is a diagnostic criterion, it represents an optimal N status when NNI equals to one (Lemaire *et al.*, 2008). From Table 6-6, according to the predicted NNI values, the NSI indices improved the accuracy of diagnosis at the critical topdressing (SE and HE) stages. Similarly, Lu *et al.* (2017) observed NNI inversion through the normalized sufficiency vegetation indices further improved the N nutrition diagnosis results of rice. Hussain *et al.* (2000) proposed a critical NSI value of 0.90 for rice. However, in this study, when the NSI indices were 0.90, different optimal NNI values were derived by different indices at different development stages (ranging from 0.85 to 2.14). Only the corresponding optimal NNI values for the  $NBI_{G_{NSI}}$  and  $NBI_{R_{NSI}}$  indices were closest to one (ranging from 0.91 to 1.19) (data not shown). Therefore, it is not suitable to use the NSI threshold as a diagnostic criterion directly, which has a relatively large risk to result in misdiagnosis. Another possible reason is that the N fertilizer application rate in this study was only 1.3-1.6 times higher than the optimal amount instead of 1.8-2.0 times higher than recommended for the well-fertilized N plot as Hussain *et al.* (2000) suggested.

Furthermore, all of the Multiplex indices were divided by the readings of the N rate with the largest shoot dry matter at each sampling date to obtain a sufficiency index. However, Varvel *et al.* (2007) suggested that the maximum readings within each cropping system, variety, year, should be considered as the normalized criterion. Obviously, with different normalization criteria, different sufficient indices will be obtained, which will affect the corresponding analysis results. More in-depth and systematic research is expected in the future.

### 6.4.3 The application potential and limitations of Multiplex sensor

The Multiplex indices presented high  $R^2$  values for LNC and PNC estimation at the earlier growth stages (Table 6-4). In particular, the validation data showed that the  $RE_r$  values for LNC and PNC estimations were as low as 6%-7% (Fig. 6-3c, d). This is consistent with the results of Cerovic *et al.* (2015) and Agati *et al.* (2015), who have shown a high correlation between the fluorescence index and LNC. NBI and LNC had a fairly linear relationship. Therefore, the NBI indices can be used to more accurately estimate a wider range of LNC. Agati *et al.* (2015) also found the results based on reflectance imaging (camera picture) are less sensitive to N application than fluorescence-based indices. Research by Stroppiana *et al.* (2009) and Yu *et al.* (2013b) on rice showed unsatisfactory results for the estimation of LNC and PNC based on reflectance spectroscopy. This is due to the fact that the effect of N on the leaf area index and biomass is much greater than its effect on chlorophyll content. Second, near-infrared radiation is hardly absorbed in the canopy and is highly transmissive, so its correlation with leaf area index or biomass is extremely high; while visible light, especially the blue and red radiation, is easily absorbed by chlorophyll and its transmittance is low, so it is highly correlated with chlorophyll content (Heege *et al.*, 2008; Stroppiana *et al.*, 2009). On the other hand, changes in plant metabolism indicators are fast or slow due to changes in response to the environment. However, the sensitivity of reflectance-based parameters does not always provide satisfactory monitoring results (Tremblay *et al.*, 2012). Demotes-Mainard *et al.* (2008) observed that changes in N concentration took precedence over changes in biomass. Thus, fluorescence-based techniques that are highly sensitive to plant N status information may address the limitation of reflectance-based methods (Tremblay *et al.*, 2012; Longchamps & Khosla, 2014). Similarly, the Multiplex indices showed a very good estimation for NNI, with  $R^2$  reaching a maximum of 0.72-0.78, and the validation results also showed a low inversion error for NNI ( $RMSE \leq 0.16$ ,  $RE_r \leq 15\%$ ), especially with the NBI\_G and NBI\_R indices (Table 6-4). Many studies have confirmed that NBI has a strong estimation potential for NNI (Cartelat *et al.*, 2005; Padilla *et al.*, 2014, 2016). This is because NBI is the ratio of SFR to FLAV. The SFR index was considered to be an important parameter for estimating chlorophyll concentration, which was often used as an index of surface-based N (Agati *et al.*, 2013), while the FLAV parameter directly reflects flavonols content, which is controlled by light as well as leaf mass per area (LMA), and has a very good correlation with leaf mass (Meyer *et al.*, 2006). Therefore, NBI as the SFR/ FLAV ratio is the best N nutrition diagnostic index.

The fluorescence-based indices are more sensitive to chlorophyll or N content than the reflectance-based indices, and can detect the difference in N nutrition status earlier. However, the difference of the stage based-models between the vegetation indices and the N nutrition indicators based on the canopy reflectance instrument is smaller than that based on

fluorescence (Padilla *et al.*, 2014). The surface area of the crop involved in each test, i.e. the viewing angle of the reflectance spectroscopy sensors (e.g. the Crop Circle ACS 470 is 55,000 cm<sup>2</sup>) compared to the fluorescence sensors (e.g. the Multiplex is 50 cm<sup>2</sup> and the Dualex is 3.2 cm<sup>2</sup>) is larger (Padilla *et al.*, 2014). Therefore, canopy reflectance measurements are more representative, while fluorescence instruments require increasing the number of tests to obtain sufficiently representative data. The small size of the test window for Multiplex may be the main reason for its poor ability to estimate plant biomass in the middle to late stages (Table 6-4). It has been suggested to combine the fluorescence and reflectance data to improve the estimation of plant N status (Samborski *et al.*, 2009; Tremblay *et al.*, 2012). This may be one of the important research directions in the future.

## 6.5 Conclusions

This study compared three measurement modes for the fluorescence instrument Multiplex<sup>®</sup>3 and determined that the “on-the-go” mode was most suitable for application in rice fields. Using this measurement mode, stable test results were obtained and crop growth information was best derived. The results of this study proved that the fluorescence indices of chlorophyll content (SFR), the ratio of blue-green to far-red fluorescence (BRR\_FRF), flavonols content (FLAV) and the ratio of the chlorophyll-to-flavonols contents (NBI) were significantly correlated to all five N status indicators at the PI through HE growth stages. Among them, NBI\_G and NBI\_R were the best performing indices and highly correlated to LNC ( $R^2 = 0.52-0.68$ ), PNC ( $R^2 = 0.52-0.71$ ), NNI ( $R^2 = 0.69-0.78$ ), AGB ( $R^2 = 0.47-0.64$ ), PNU ( $R^2 = 0.68-0.72$ ) at the three growth stages. The normalized sufficiency indices (NSI) of the Multiplex parameters could improve the LNC, PNC and NNI estimation ability for most indices, especially at the HE stage. Among them, the ANTH<sub>NSI</sub> was improved the most. The validation results show that the relative error values for the estimation of LNC, PNC, NNI, AGB, and PNU were 4.50%-10.24%, 5.87%-10.87%, 9.64%-14.08%, 15.49%-30.18%, and 19.30%-31.25%, respectively. The N diagnostic results indicated that the NBI\_R<sub>NSI</sub> and FLAV achieved the highest diagnosis accuracy rate (90%) at the stem elongation and heading stages, respectively, while NBI\_R<sub>NSI</sub> showed the highest diagnostic consistency across growth stages. It is concluded that the Multiplex sensor can be used to reliably estimate N nutritional status for rice in cold regions, especially for the estimation of LNC, PNC, and NNI. The normalized sufficiency indices based on Multiplex indices can further improve the accuracy of N nutrition diagnosis by reducing the differences between years and varieties.

## Acknowledgment

This study was financially supported by the National Basic Research Program (2015CB150405), National Key Research and Development Program of China (2016

YFD0200600, 2016YFD0200602), and the Norwegian Ministry of Foreign Affairs (SINOGRAIN II, CHN-17/0019). The supports by Mrs. Wen Yang, Huamin Zhu and Fengyan Liu at Jiansanjiang Institute of Agricultural Sciences are highly appreciated.

## 6.6 References

- Agati, G., Cerovic, Z.G., Pinelli, P., Tattini, M., 2011. Light-induced accumulation of ortho-dihydroxylated flavonoids as non-destructively monitored by chlorophyll fluorescence excitation techniques. *Environ. Exp. Bot.* 73(11), 3–9.
- Agati, G., Foschi, L., Grossi, N., Guglielminetti, L., Cerovic, Z. G., Volterrani, M., 2013. Fluorescence-based versus reflectance proximal sensing of nitrogen content in *Paspalum vaginatum*, and *Zoysia matrella*, turfgrasses. *Eur. J. Agron.* 45(1), 39–51.
- Agati, G., Foschi, L., Grossi, N., Volterrani, M., 2015. In field non-invasive sensing of the nitrogen status in hybrid bermudagrass (*Cynodon dactylon*, × *C. transvaalensis* Burt Davy) by a fluorescence-based method. *Eur. J. Agron.* 63, 89–96.
- Agati, G., Pinelli, P., Cortés, E. S., Romani, A., Cartelat, A., Cerovic, Z.G., 2005. Nondestructive evaluation of anthocyanins in olive (*Olea europaea*) fruits by in situ chlorophyll fluorescence spectroscopy. *J. Agric. Food Chem.* 53(5), 1354–1363.
- Ali, M.M., Al-Ani, A., Eamus, D., Tan, D.K.Y., 2017. Leaf nitrogen determination using non-destructive techniques-A review. *J. Soil Sci. Plant Nut.* 40(7), 928–953.
- Barthod, S., Cerovic, Z., Epron, D., 2007. Can dual chlorophyll fluorescence excitation be used to assess the variation in the content of UV-absorbing phenolic compounds in leaves of temperate tree species along a light gradient? *J. Exp. Bot.* 58(7), 1753–1760.
- Blackmer, T.M., Schepers J.S., 1995. Use of a chlorophyll meter to monitor nitrogen status and schedule fertigation for corn. *J. Prod. Agric.* 8(1), 56–60.
- Bredemeier, C., Schmidhalter, U., 2005. Laser-induced chlorophyll fluorescence sensing to determine biomass and nitrogen uptake of winter wheat under controlled environment and field condition. In: J. V. Stafford (Eds.), *Proceedings of the 5th European Conference on Precision Agriculture*, Wageningen Academic Publishers, The Netherlands, pp. 273–280.
- Burchard, P., Bilger W., Weissenböck, G., 2000. Contribution of hydroxycinnamates and flavonoids to epidermal shielding of UV-A and UV-B radiation in developing rye primary leaves as assessed by ultraviolet-induced chlorophyll fluorescence measurements. *Plant Cell Environ.* 23(12), 1373 – 1380.
- Buschmann, C., 2007. Variability and application of the chlorophyll fluorescence emission ratio red/far-red of leaves. *Photosynth. Res.* 92(2), 261–271.
- Buschmann, C., Lichtenthaler, H.K., 1998. Principles and characteristics of multi-colour fluorescence imaging of plants. *J. Plant Physiol.* 152(2–3), 297–314.

- Cao, Q., Miao, Y., Shen, J., Yu, W., Yuan, F., Cheng, S., Huang, S., Wang, H., Yang, W., Liu, F., 2016. Improving in-season estimation of rice yield potential and responsiveness to topdressing nitrogen application with Crop Circle active crop canopy sensor. *Precision Agric.* 17, 136–154.
- Cartelat, A., Cerovic, Z.G., Goulas, Y., Meyer, S., Lelarge, C., Prioul, J.L., Barbottin, A., Jeuffroy, M.H., Gate, P., Agati, G., 2005. Optically assessed contents of leaf polyphenolics and chlorophyll as indicators of nitrogen deficiency in wheat (*Triticum aestivum* L.). *Field Crops Res.* 91(1), 35–49.
- Cerovic, Z.G., Ghazlen, N.B., Milhade, C., Obert, M., Debuisson, S., Le Moigne M., 2015. Nondestructive Diagnostic Test for Nitrogen Nutrition of Grapevine (*Vitis vinifera* L.) Based on Dualex Leaf-Clip Measurements in the Field. *J. Agr. Food Chem.* 63(14), 3669–3680.
- Cerovic, Z.G., Goutouly, J.P., Hilbert, G., Destrac-Irvine, A., Martinon, V., Moise, N., 2009. Mapping winegrape quality attributes using portable fluorescence-based sensors. *Frutic* 9, 301–310.
- Cerovic, Z.G., Moise, N., Agati, G., Latouche, G., Ghazlen, N.B., Meyer, S., 2008. New portable optical sensors for the assessment of winegrape phenolic maturity based on berry fluorescence. *J. Food Compos. Anal.* 21(8), 650–654.
- Cerovic, Z.G., Ounis, A., Cartelat, A., Latouche, G., Goulas, Y., Meyer, S., Moya, I., 2002. The use of chlorophyll fluorescence excitation spectra for the non-destructive in situ assessment of UV-absorbing compounds in leaves. *Plant Cell Environ.* 25(12), 1663–1676.
- Chen, Y., Chen, J., Yan, B., Cui, L., Pan, J., Kai, G., 2015. Agronomic traits of a new characteristic rice line ‘Huxuan 102’. *Acta Agriculturae Shanghai* 2, 60–64.
- Demotes-Mainard, S., Boumaza, R., Meyer, S., Cerovic, Z.G., 2008. Indicators of nitrogen status for ornamental woody plants based on optical measurements of leaf epidermal polyphenol and chlorophyll contents. *Sci. Hortic-Amsterdam* 115(4), 377–385.
- Diago, M.P., Rey-Carames, C., Le Moigne, M., Fadaili, E.M., Tardaguila, J., Cerovic, Z.G., 2016. Calibration of non-invasive fluorescence-based sensors for the manual and on-the-go assessment of grapevine vegetative status in the field. *Aust. J. Grape Wine R.* 22(3), 438–449.
- Evans, J.R., 1983. Nitrogen and photosynthesis in the flag leaf of wheat (*Triticum aestivum* L.). *Plant Physiol.* 72(2), 297–302.
- Ghazlen, N.B., Cerovic, Z.G., Germain, C., Toutain, S., Latouche, G., 2010. Non-destructive optical monitoring of grape maturation by proximal sensing. *Sensors* 10(11), 10040–10068.
- Gitelson, A.A., Buschmann, C., Lichtenthaler, H.K., 1999. The chlorophyll fluorescence ratio F-735/F-700 as an accurate measure of the chlorophyll content in plants. *Remote*

- Sens. Environ. 69(3), 296–302.
- Gitelson, A.A., Gritz, Y., Merzlyak, M.N., 2003. Relationships between leaf chlorophyll content and spectral reflectance and algorithms for non-destructive chlorophyll assessment in higher plant leaves. *J. Plant Physiol.* 160(3), 271–82.
- Goulas, Y., Cerovic, Z. G., Cartelat, A., Moya, I., 2004. Dualex: a new instrument for field measurements of epidermal ultraviolet absorbance by chlorophyll fluorescence. *Appl. Opt.* 43(23), 4488–4496.
- Guo, J.H., Liu, X.J., Zhang, Y., Shen, J.L., Han, W.X., Zhang, W.F., Christie, P., Goulding, K.W., Vitousek, P.M., Zhang, F.S., 2010. Significant acidification in major Chinese croplands. *Science* 327(5968), 1008–1010.
- Heege, H.J., Reusch, S., Thiessen, E., 2008. Prospects and results for optical systems for site-specific on-the-go control of nitrogen-top-dressing in Germany. *Precis. Agric.* 9(3), 115–131.
- Huang, S., Miao, Y., Cao, Q., Yao, Y., Zhao, G., Yu, W., Shen, J., Yu, K., Bareth, G., 2018. Critical nitrogen dilution curve for rice nitrogen status diagnosis in Northeast China. *Pedosphere* 28(5), 814–822.
- Huang, S., Miao, Y., Yuan, F., Cao, Q., Ye, H., Lenz-Wiedemann, V., Khosla, R., Bareth, G., 2017. Proximal fluorescence sensing for in-season diagnosis of rice nitrogen status. *Adv. Anim. Biosci.* 8(2), 343–348.
- Huang, S., Miao, Y., Zhao, G., Yuan, F., Ma, X., Tan, C., Yu, W., Gnyp, M., Lenz-Wiedemann, V., Rascher, U., 2015. Satellite Remote Sensing-Based In-Season Diagnosis of Rice Nitrogen Status in Northeast China. *Remote Sens.* 7(8), 10646–10667.
- Hussain, F., Bronson, K.F., Peng, S., 2000. Use of chlorophyll meter sufficiency indices for nitrogen management of irrigated rice in Asia. *Agron. J.* 92(5), 875–879.
- Jones, C.G., Hartley, S.E., 1999. A protein competition model of phenolic allocation. *Oikos* 86(1), 27–44.
- Knogge, W., Weissenböck, G., 1986. Tissue-distribution of secondary phenolic biosynthesis in developing primary leaves of *Avena sativa* L. *Planta* 167(2), 196–205.
- Landis, R. J., Koch, G. G., 1977. The measurement of observer agreement for categorical data. *Biometrics* 33, 159–174.
- Langsdorf, G., Buschmann, C., Sowinska, M., Babani, F., Mokry, M., Timmermann, F., Lichtenthaler, H.K., 2000. Multicolor fluorescence imaging of sugar beet leaves with different nitrogen status by flash lamp UV-excitation. *Photosynthetica* 38(4), 539–551.
- Lejealle, S., Evain, S., Cerovic, Z.G., 2010. Multiplex: a new diagnostic tool for management of nitrogen fertilization of turfgrass. In: Proceedings of the 10th International Conference on Precision Agriculture, [CD ROM], Denver, Colorado, USA, 18–21 July.
- Lemaire, G., Jeuffroy, M.H., Gastal, F., 2008. Diagnosis tool for plant and crop N status in

- vegetative stage: theory and practices for crop N management. *Eur. J. Agron.* 28(4), 614–624.
- Li, J.W., Zhang, J.X., Zhao, Z., Lei, X.D., Xu, X.L., Lu, X.X., Weng, D.L., Gao, Y., Cao, L.K., 2013. Use of fluorescence-based sensors to determine the nitrogen status of paddy rice. *J. Agr. Sci.* 151(06), 862–871.
- Lichtenthaler, H.K., 1996. Vegetation Stress: an Introduction to the Stress Concept in Plants. *J Plant Physiol.* 148(1–2), 4–14.
- Lichtenthaler, H.K., Schweiger, J., 1998. Cell wall bound ferulic acid, the major substance of the blue-green fluorescence emission of plants. *J. Plant Physiol.* 152(2), 272–282.
- Lin, F.F., Qiu, L.F., Deng, J.S., Shi, Y.Y., Chen, L.S., Wang, K., 2010. Investigation of spad meter-based indices for estimating rice nitrogen status. *Comput. Electron. Agr.* 71, S60–S65.
- Longchamps, L., Khosla, R., 2014. Early detection of nitrogen variability in maize using fluorescence. *Agron. J.* 106(2), 511–518.
- Lu, J., Miao, Y., Wei, S., Li, J., Yuan, F. 2017. Evaluating different approaches to non-destructive nitrogen status diagnosis of rice using portable RapidScan active canopy sensor. *Sci. Rep.* 7(1), 14073.
- Markwell, J., Osterman, J.C., Mitchell, J.L., 1995. Calibration of the Minolta SPAD-502 leaf chlorophyll meter. *Photosynth. Res.* 46(3), 467–472.
- Martin, K.L., Girmaa, K., Freemana, K.W., Teala, R.K., Tubañaa, B., Arnalla, D.B., Chunga, B., Walsh, O., Solieb, J.B., Stoneb M.L., Raun W.R., 2007. Expression of variability in corn as influenced by growth stage using optical sensor measurements. *Agron. J.* 99(2), 384–389.
- McMurtrey, J.E. III., Chappelle, E.W., Kim, M.S., Meisinger, J.J., Corp, L.A., 1994. Distinguishing nitrogen fertilization levels in field corn (*Zea mays L.*) with actively induced fluorescence and passive reflectance measurements. *Remote Sens. Environ.* 47(1), 36–44.
- Meyer, S., Cerovic, Z.G., Goulas, Y., Montpied, P., Demotes-Mainard, S., Bidet, L.P., Moya, I., Dreyer, E., 2006. Relationships between optically assessed polyphenols and chlorophyll contents, and leaf mass per area ratio in woody plants: a signature of the carbon-nitrogen balance within leaves? *Plant Cell Environ.* 29(7), 1338–1348.
- Miao, Y., B. A. Stewart, F. Zhang. 2011. Long-term experiments for sustainable nutrient management in China. A review. *Agron. Sustain. Dev.* 31(2), 397-414.
- Mulla, D.J., Y. Miao. 2016. Precision Farming. In P. S. Thenkabail (Ed.). *Land Resources Monitoring, Modeling, and Mapping with Remote Sensing*. CRC Press: Boca Raton, FL, USA.
- Olf, H.W., Blankenau, K., Brentrup, F., Jasper, J., Link, A., Lammel, J. 2005. Soil-and plant-based nitrogen-fertilizer recommendations in arable farming. *J. Soil Sci. Plant Nut.*

- 168(4), 414–431.
- Ounis, A., Cerovic, Z.G., Briantais, J.M., Moya, I., 2001. Dual-excitation FLIDAR for the estimation of epidermal UV absorption in leaves and canopies. *Remote Sens. Environ.* 76(1), 33–48.
- Padilla, F. M., Peña-Fleitas, M. T., Gallardo, M., Thompson, R.B., 2016. Proximal optical sensing of cucumber crop N status using chlorophyll fluorescence indices. *Eur. J. Agron.* 73, 83–97.
- Padilla, F.M., Peña-Fleitas, M.T., Gallardo, M., Thompson, R.B., 2014. Evaluation of optical sensor measurements of canopy reflectance and of leaf flavonols and chlorophyll contents to assess crop nitrogen status of muskmelon. *Eur. J. Agron.* 58, 39–52.
- Pedrés, R., Goulas, Y., Jacquemoud, S., Louis, J., Moya, I., 2010. FluorMODleaf: A new leaf fluorescence emission model based on the PROSPECT model. *Remote Sens. Environ.* 114(1), 155–167.
- Samborski, S.M., Tremblay N., Fallon E., 2009. Strategies to make use of plant sensors-based diagnostic information for nitrogen recommendations. *Agron. J.* 101(4), 800–816.
- Schepers, J.S., Blackmer, T.M., Francis, D.D., 1992a. Predicting N fertilizer needs for corn in humid regions: using chlorophyll meters. In: Bock, B.R., Kelley, K.R. (Ed.), *Predicting N fertilizer needs for corn in humid regions*. Bull. Y-226. Natl. Fert. and Environ. Res. Ctr., Tennessee Valley Authority, Muscle Shoals, AL. pp. 105–114.
- Schepers, J.S., Francis, D.D., Vigil, M., Below, F.E., 1992b. Comparison of corn leaf nitrogen concentration and chlorophyll meter readings. *Commun. Soil Sci. Plan.* 23(17–20), 2173–2187.
- Schlemmer, M.R., Francis, D.D., Shanahan, J.F., 2005. Remotely measuring chlorophyll content in corn leaves with differing nitrogen levels and relative water content. *Agron. J.* 97(1), 106–112.
- Schröder, J.J., Neeteson, J.J., Oenema, O., Struik, P.C., 2000. Does the crop or the soil indicate how to save nitrogen in maize production? Reviewing the state of the art. *Field Crops Res.* 66(2), 151–164.
- Song, X., Yang, G., Yang, C., Wang, J., Cui, B., 2017. Spatial variability analysis of within-field winter wheat nitrogen and grain quality using canopy fluorescence sensor measurements. *Remote Sens.* 9(3), 237.
- Stroppiana, D., Boschetti, M., Brivio, P. A., Bocchi, S., 2009. Plant nitrogen concentration in paddy rice from field canopy hyperspectral radiometry. *Field Crops Res.* 111(1–2), 119–129.
- Teal, R.K., Tubana, B., Girma, K., Freeman, K.W., Arnall, D.B., Walsh, O., Raun, W.R., 2006. In-season prediction of corn grain yield potential using normalized difference vegetation index. *Agron. J.* 98(6), 1488–1494.
- Tremblay, N., Wang, Z., Bélec, C., 2007. Evaluation of the Dualex for the assessment of corn

- nitrogen status. *J. Soil Sci. Plant Nut.* 30(9), 1355–1369.
- Tremblay, N., Wang, Z., Belec, C., 2009. Performance of Dualex in spring wheat for crop nitrogen status assessment, yield prediction and estimation of soil nitrate content. *J. Soil Sci. Plant Nut.* 33(1), 57–70.
- Tremblay, N., Wang, Z., Cerovic, Z.G., 2012. Sensing crop nitrogen status with fluorescence indicators. a review. *Agron. Sustain. Dev.* 32(2), 451–464.
- Varvel, G. E., Wilhelm, W.W., Shanahan, J.F., Schepers, J.S., 2007. An Algorithm for Corn Nitrogen Recommendations Using a Chlorophyll Meter Based Sufficiency Index. *Agron. J.* 99(3), 701–706.
- Xia, T., Miao, Y., Wu, D., Shao, H., Khosla, R., Mi, G. 2016. Active Optical Sensing of Spring Maize for In-Season Diagnosis of Nitrogen Status Based on Nitrogen Nutrition Index. *Remote Sens.* 8(7), 605, doi:10.3390/rs8070605
- Yang, J., Wei, G., Shi, S., Lin, D., Sun, J., Song, S., Chen, B., Zhang, Z. 2016. Analyzing the performance of fluorescence parameters in the monitoring of leaf nitrogen content of paddy rice. *Sci. Rep.* 6, 28787.
- Yao, Y., Miao, Y., Huang, S., Gao, L., Ma, X., Zhao, G., Jiang, R., Chen, X., Zhang, F., Yu, K., Gnyp, M.L., Bareth, G., Liu, C., Zhao, L., Yang, W., Zhu, H., 2012. Active canopy sensor-based precision n management strategy for rice. *Agron. Sustain. Dev.* 32(4), 925–933.
- Yu, K., Leufen, G., Hunsche, M., Noga, G., Chen, X., Bareth, G., 2013a. Investigation of leaf diseases and estimation of chlorophyll concentration in seven barley varieties using fluorescence and hyperspectral indices. *Remote Sens.* 6(1), 64–86.
- Yu, K., Li, F., Gnyp, M. L., Miao, Y., Bareth, G., Chen, X., 2013b. Remotely detecting canopy nitrogen concentration and uptake of paddy rice in the Northeast China Plain. *ISPRS J. Photogramm.* 78, 102–115.
- Yuan, Z., Ata-Ul-Karim, S.T., Cao, Q., Lu, Z., Cao, W., Zhu, Y., Liu, X., 2016. Indicators for diagnosing nitrogen status of rice based on chlorophyll meter readings. *Field Crops Res.* 185, 12–20.
- Zhang, Y.P., Tremblay, N., Zhu, J.J., 2012. A first comparison of Multiplex (R) for the assessment of corn nitrogen status. *J. Food Agric. Environ.* 10(12), 1008–1016.
- Zubillaga, M., Urricariet, S., 2005. Assessment of Nitrogen Status in Wheat Using Aerial Photography. *Commun. Soil Sci. Plan.* 36(13–14), 1787–1798.

## Chapter 7: General Discussion

In order to achieve modern agricultural production that guarantees food production and environmental friendliness simultaneously, remote sensing-based crop N nutrition diagnosis and precision N management are important. In this dissertation, a new N nutrition diagnostic indicator was constructed ( $N_c$  dilution curve) from the relationship between biomass and N concentration in cold region rice. Based on this new diagnostic indicator, this research studied how to use satellite remote sensing images to diagnose N nutrition for rice in large scale farmland. Comparing sensitive bands and vegetation indices (VIs) for the estimation of N nutrition indicators confirmed the importance of red edge band for estimating N nutrition indicators. Further, a stepwise multiple linear regression (SMLR), and a partial least square regression (PLSR) were used to evaluate the potential of new-satellite remote sensing system for monitoring N nutrition. Accordingly, the regression models for N nutrition indicators were established. To further improve the accuracy of N nutrition status diagnosis, a fluorescence sensor was evaluated. This chapter focuses on discussing the advantages of N nutrition diagnosis based on the  $N_c$  dilution curve as well as the application potential and limitations of satellite and fluorescence remote sensing technologies. In addition, some discussions will focus on how to resolve the limitations and how to apply the diagnostic results for precision N management.

### 7.1 N concentration and NNI remote sensing estimation

The  $N_c$  dilution curve was established in Chapter 3 ( $N_c = 27.7W^{-0.34}$  when AGB was 1 Mg DM ha<sup>-1</sup> or above, and  $N_c$  was set to a constant value of 27.7 g kg<sup>-1</sup> when AGB was less than 1 Mg DM ha<sup>-1</sup>). According to the “-3/2 self thinning rule” in plant ecology, due to the light competition among individual plants, plants develop the height (the third dimension) in order to position their leaves within the top layers for well illumination (Hamilton *et al.*, 1995; Lemaire *et al.*, 2007). Therefore, the coefficient  $b$  ( $b = 0.34$  for the new curve in this study) equals to the theoretical value of 1/3, which indicates isometric plant growth (similar relative rate in all three dimensions) (Hamilton *et al.*, 1995; Lemaire *et al.*, 2007). And the  $N_c$  dilution curve established for rice in Northeast China was close to that established for flooded rice in Japan ( $N_c = 29.8W^{-0.34}$  in Tokyo,  $N_c = 26.9W^{-0.36}$  in Osaka) (Katsura *et al.*, 2010). This is because the climatic conditions in Northeast China are very close to Japan. Previous research has indicated that species-specific  $N_c$  dilution curves were widely suitable for spring maize (Plénet & Lemaire, 1999; Herrmann & Taube, 2004; Ziadi *et al.*, 2008a). On the other hand, the  $N_c$  dilution curve is more stable than the PNU inter years (Lemaire & Gastal, 1997). The dilution curve between N concentration and biomass is relatively stable

between years, while crop PNU is variable over years due to the variations in light and temperature production potential. NNI is an integrative indicator of plant N status. It increases with N application rates. The dilution curve and NNI can also be used in research or posterior diagnosis in farm fields to determine possible causes of low yield. Therefore, NNI is a more promising and reliable diagnostic tool than PNC (Lemaire *et al.*, 2008).

From the perspective of remote sensing estimation, N concentration is estimated based on empirical relationships with chlorophyll concentration, while NNI has more estimation methods (Houlès *et al.*, 2007). During vegetative growth stages, the contribution of LAI to canopy reflectance spectra is much greater than that of chlorophyll concentration (Yu *et al.*, 2013b). Therefore, the N concentration and NNI are difficult to estimate by empirical relationships with chlorophyll concentration. The analysis results of Chapters 4 and 5 also confirmed that direct estimation of PNC and NNI performed worse than the estimation of PNU before the heading stage using the broadband satellite remote sensing data. Research showed that the red edge-based VIs and optimized narrow band RVI and NDVI explained more NNI variability (Cao *et al.*, 2013; Mistele & Schmidhalter, 2008). The indirect estimation methods, which first use remote sensing to estimate key parameters such as biomass, PNC, and PNU, and then indirectly estimate NNI have demonstrated to be effective (Cilia *et al.*, 2014). The indirect estimation method that uses PNU and critical PNU are covered in Chapter 4 of this thesis. The fact that PNU is linearly related and strictly proportional to LAI during the vegetation growth stage, and it is strictly proportional to LAI explains its better performance for the NNI estimation (Lemaire *et al.*, 2007).

## 7.2 Satellite remote sensing application potential

In Chapter 5, 9 of the 10 VIs calculated based on the simulated wavebands of FORMOSAT-2 satellite were the same as those derived from actual satellite remote sensing images included in Chapter 4. For both cases, the CI, RVI (RVI3 in Chapter 4, RVI in Chapter 5), MCARI, TCARI, TVI, GNDVI (NDVI2 in Chapter 4, GNDVI in Chapter 5), OSAVI, and NDVI (NDVI3 in Chapter 4, NDVI in Chapter 5) were very stable in estimating the AGB ( $R^2 = 0.87-0.90$  for actual FORMOSAT-2 data,  $R^2 = 0.60-0.82$  for simulated wavebands) (Tables 4-5, 5-5, 5-6). Among them, the CI and RVI (RVI3 in Chapter 4) were the VIs that explained the most variation in both cases. And they were also the best and most stable VIs for estimating PNU (Tables 4-5, 5-5, 5-6). The performance of MCARI and TCARI closely followed the CI and RVI. The MCARI and TCARI are highly related to leaf chlorophyll variation and LAI (Daughtry *et al.*, 2000; Haboudane *et al.*, 2004). The OSAVI and RVI can weaken the effects of background reflectance, while the MCARI and CI can enhance the response to chlorophyll concentrations in addition to weakening the background noise and avoiding the saturation effect because of their linearity with chlorophyll content

(Daughtry *et al.*, 2000; Gitelson *et al.*, 2003, 2005). Previous studies have also observed high linear correlations between the MCARI and N indicators such as AGB ( $R^2 = 0.68-0.79$ ) and PNU ( $R^2 = 0.83$ ) (Cao *et al.*, 2013; Gnyp *et al.*, 2014). The wavebands of FORMOSAT-2 include the traditional blue (450-520 nm), green (520-600 nm), red (630-690 nm), and near-infrared (760-900 nm), which are the commonly used wavebands in many operational satellites (Table 2-2). Therefore, VIs based on the traditional bands have high potential in applications over large-area.

Crop growth stages not only affect the relationships between VIs and N nutrition indicators but also affect the selection of sensitive bands (Li *et al.*, 2010). For the estimation of AGB in Chapter 5, the  $R^2$  of the estimation models across the growth stages were very high ( $> 0.80$ ). However, the root mean square error (RMSE) and the relative error ( $RE_r$ ) obtained in the validation data using the models of across stages were greater than those based on each growth stage (PI and SE). Similar results were observed for the PNU estimation. This is because the clusters of different growth stages in the scatter plot were not evenly distributed on both sides of the regression curve, which led to a high coefficient of determination of the fitted regression model, but higher RMSE and  $RE_r$  were obtained for validation (Gnyp, 2014). Considering precision N management is often only for critical key growth stages, estimating agronomic parameters at different growth stages are important.

However, at the early crop growth stage, the performance of VIs based on the visible wavebands was poorer than that based on the red edge waveband for the estimation of N nutrition indicators (Tables 5-5, 5-6). The small vegetation coverage at this growth stage is the dominant factor. The red edge waveband has been shown to be insensitive to background effects (Zarco-Tejada *et al.* 2004). The results of Chapter 5 show that the VIs based on the red edge waveband can increase the coefficient of determination by more than 20% when estimating AGB and PNU at the early stages (Tables 5-5, 5-6). Previous studies showed that red edge reflectance was highly correlated with chlorophyll content (Cho & Skidmore, 2006; Clevers *et al.*, 2002). This is because red edge position changes with the chlorophyll content (Buschmann & Nagel, 1993; Dawson & Curran, 1998) and the spectral characteristic of red edge band mainly account for N and chlorophyll content, while the visible reflectance is affected by the spectral features of multiple pigments (Haboudane *et al.*, 2004; Hansen & Schjoerring, 2003). Chlorophyll absorbs more in the red band than in the red edge band, which is an important reason for the red edge band-VIs to be unsaturated under high chlorophyll concentrations (Gitelson & Merzlyak, 1996). It has been reported that the red edge-VIs improved the estimations of N nutrition indicators in many studies (Wu *et al.*, 2008; Li *et al.*, 2014a; Cao *et al.*, 2013; Dong *et al.*, 2015). In this study, the estimation of NNI was also improved by introducing the red edge-VIs, and the SMLR analysis proved that the red edge band was the most important one for NNI estimation except for the near-infrared band (760-900 nm) (Table 5-7). However, it was difficult to estimate PNC in the early stage of

crop growth based on satellite remote sensing according to our results. Eitel *et al.* (2007) also showed the difficulty of estimating leaf N concentration by using simulated RapidEye bands.

Numerous studies have shown that high spatial and temporal satellite and aerial imagery data are useful for precision N management (Bausch & Khosla, 2010; Nigon *et al.*, 2014; Magney *et al.*, 2017). The advantage of satellite imagery to quickly acquire large-area data is still unmatched by drone platforms or ground-based systems. The low-cost and maintenance-free means based on satellite and aerial imagery are very helpful for accurate agricultural decision-making. Providing spatial distribution maps of in-season N uptake can help develop precision fertilization and maximize the efficiency of N use (Diacono *et al.* 2013; Long *et al.* 2015). The N recommendation approach developed in this thesis requires the satellite imagery to be collected in a narrow time window, preferably one week before topdressing N application at the stem elongation stage for rice in the study region. The satellites evaluated in this thesis all have short revisit capability and high spatial resolutions. The 8-m spatial resolution of FORMOSAT-2, 5-m for RapidEye, and 2-m for WorldView-2 can meet the requirements of agricultural production models at different scales, for instance, the large-scale farming in the Sanjiang Plain of Northeast China, and the small-scale farming in other parts of China (Shen *et al.*, 2013). The reason for using the satellites with high temporal resolution is to minimize the impact of cloudy and rainy weather. Alternatively, Radar images and unmanned aerial vehicles (UAVs) may also be used.

### 7.3 Fluorescence remote sensing application potential

From the analysis results of Chapter 6, it can be seen that the best performing fluorescence index explains more variation of PNC and NNI, compared to those indices based on the satellite-based wavebands, in the early stage of crop growth (Tables 4-5, 5-5, 5-6, 6-4). The difficulty of estimating the PNC based on reflectance spectroscopy at the early growth stages for rice has been reported by Stroppiana *et al.* (2009) and Yu *et al.* (2013). This is because the reflectance spectrum is mainly determined by LAI and biomass, and the effect of chlorophyll is a secondary cause. In addition, most existing VIs based on reflectance spectrum contain the near-infrared band, which is highly reflected by the canopy, so its correlation with LAI or biomass is extremely high, whereas visible light irradiation is easily absorbed by chlorophyll and its transmittance is low (Heege *et al.*, 2008; Stroppiana *et al.*, 2009). When N supplement status changes, the N concentration changes before appearance parameters (e.g. biomass or LAI) for crops (Demotes-Mainard *et al.*, 2008). Therefore, the reflectance-based remote sensing may not provide satisfactory monitoring results in some cases, while the fluorescence-based remote sensing is more sensitive (Tremblay *et al.*, 2011; Agati *et al.*, 2015; Longchamps & Khosla, 2014). The best performing Multiplex index-the

NBI was highly correlated with NNI ( $R^2 = 0.72-0.78$ ), and the validation results also showed that the index had a low inversion error for NNI ( $RMSE \leq 0.16$ ,  $RE_r \leq 15\%$ ) (Table 6-4). This result is in conformity with previous studies by Agati *et al.* (2015) and Padilla *et al.* (2016). The NBI is defined as the ratio of SFR to FLAV, which is a surface-based indicator with unit as Chl/g DM (Agati *et al.*, 2013). The NNI, defined as the ratio of  $N_a$  to  $N_c$ , therefore equals  $N_a / (aW^{-b}) = a^{-1}N_aW^{-b}$ , which is also related to N concentration and dry matters like the NBI.

The good fit of the regression curve between the NBI and NNI resulted in highly accurate diagnostic results based on NNI (Table 6-6). Many studies agreed that it was the best to estimate NNI for different crop growth stages (Mistele & Schmidhalter, 2008; Ravier *et al.*, 2017). However, the interception and slope coefficients of the NBI-NNI regression curves established in this research are similar and consistent at different stages (Table 6-5). Ravier *et al.* (2017) suggested that establishing a model for NNI estimation that is independent of biomass or cultivar effects is very useful for farmers. However, N status diagnosis and precision N fertilizer management based on fluorescence remote sensing are still at the initial stage, and there are many problems to be solved. For example, how to collect fluorescence remote sensing data effectively over large areas?

#### 7.4 Remote sensing-based in-season N management strategies

Based on the critical N uptake curve (Eq. 2-3), Chapter 4 proposes an N topdressing recommendation algorithm based on remote sensing. Our methodology combined the information of the AGB and PNU retrieved from their best performing VIs. Conforming to many studies on N management strategies based on remote sensing technique, the indicator PNU was chosen (Magney *et al.*, 2017; Cilia *et al.*, 2014; Villodre *et al.*, 2017). The PNU is an alternative indicator of the N or chlorophyll content. Because the N or chlorophyll content is largely a factor of LAI, and strongly affects the near-infrared reflectance (Eitel *et al.* 2008), VIs-based PNU estimations can often achieve very high  $R^2$ . However, PNU maps cannot provide the recommendations for N fertilizer topdressing. One approach is to diagnose the N status based on NNI. According to the diagnostic results, the best N recommendation rate of the region can be increased or decreased N. Another approach is to produce a PNU difference map using the estimated PNU map minus the critical PNU map. Then the recommended N topdressing application rate can be determined by using the regional optimum topdressing N application rate to minus the PNU difference. Those are all very simple and feasible approaches. However, some problems need to be noted. When the crop population is too small to reach the maximal yield potential, the algorithm fails to adjust the recommendation rate accordingly, excessive supply of N fertilizer will eventually accumulate in the soil and increase the risk of discharge to the environment. The range of

the recommended fertilization rates set in the algorithm was not very big, resulting in only small adjustments based on the optimal rate. Therefore, it may lose its sensitivity to yield changes. In addition, whether it is possible to provide recommendations successfully in an extreme climate year remains questionable. However, due to other stress factors (such as water, pests, and diseases), the effects of recommended N fertilizer will be affected (Cilia *et al.*, 2014). This issue occurs frequently in N experiments. Therefore, the N recommendation approaches need further verification and improvement in the future.

### 7.5 Limitations of the thesis

The results of this study show that remote sensing technique can be used to monitor crop N status. As a result, remote sensing diagnostic models for rice N nutrition in cold regions were established, which could be used to guide precision fertilization in the farms. However, these models are empirical and lack a certain mechanism. The geographical transferability of the models is also an important issue to be considered (Foody *et al.*, 2003; Eitel *et al.*, 2007). Wu *et al.* (2008) suggested that relationships between physiological parameters and VIs for all conditions were not a single correlation curve, but a series of correlation curves.

Many studies have shown that VIs constructed from simulated satellite band data can be used to estimate crop N status well. However, due to the differences in observation conditions caused by sensor resolution and target azimuth angle, there are some differences between the actual and simulated band reflectance of the same target. For instance, Bausch and Khosla (2010) pointed out that different view angles of satellites may affect the VI values. Jackson *et al.* (1990) stated that the use of oblique imagery in temporal studies to calculate the NIR/R ratio from wheat canopy reflectance could lead to serious misinterpretations of the data, and NDVI also varied with view angles but not as drastically as the NIR/R ratio. Pinter *et al.* (1990) showed that if a radiometer was pointed toward a canopy in the direction of the sun, it would perceive a greater reduction in visible light than in the NIR when compared with data collected from a nadir view.

Different remote sensing methods have different abilities to monitor crop agronomic parameters, even the same remote sensing methods have different monitoring capabilities at different growth stages. For example, most of the multispectral satellites data have some limitations in estimating PNC at the early crop growth stage due to their limited bands, broad bandwidth, and rough spectral information expression. The proximal fluorescence sensor Multiplex<sup>®</sup>3 can effectively solve this problem and further improve the accuracy of NNI estimation. However, due to its small view angle, the ability of fluorescence to estimate biomass is weak. How to monitor N status in the entire process of crop growth by combining various remote sensing methods is the key issue to be solved urgently in future research.

## Chapter 8: Conclusions and future outlook

### 8.1 Conclusions

This thesis focused on the research of N nutrition diagnosis and N fertilizer management strategy for cold region paddy rice in Northeast China. Experiments were conducted based on multi-source remote sensing technologies. Diagnostic criteria of N nutrition in cold paddy rice was clarified. N nutrition diagnosis methods based on proximal and satellite remote sensing technologies were established to promote the precision N management strategies. The major findings are summarized as follows:

Regarding the  $N_c$  dilution curve analysis, the  $N_c$  dilution curves developed for Indica rice in the tropical and temperate zones and for Japonica rice in the subtropical-temperate zone were not suitable for diagnosing short-season Japonica rice N status in Northeast China. A new  $N_c$  dilution curve was developed and could be described by the equation:  $N_c = 27.7W^{-0.34}$  if  $W \geq 1$  Mg dry matter (DM) ha<sup>-1</sup> or  $N_c = 27.7$  g kg<sup>-1</sup> DM if  $W < 1$  Mg DM ha<sup>-1</sup>, where  $W$  is the aboveground biomass. The gradient of this new curve was lower than the previous curves developed in other regions. The validation results indicated that it worked well for diagnosing plant N status of the 11-leaf variety rice.

For the evaluation of the potentials of using FORMOSAT-2 satellite remote sensing to estimate rice NNI, while it was found that 45% of NNI variability could be explained using the Ratio Vegetation Index 3 (RVI3) directly across years, a more practical and promising approach was proposed. That is, using satellite remote sensing to estimate aboveground biomass (AGB) and plant N uptake (PNU) at the panicle initiation stage and then using these two variables to estimate NNI indirectly ( $R^2 = 0.52$  across years). Moreover, the calculated difference between the estimated PNU and the critical PNU based on the indirect method were used to guide the topdressing N application rate adjustments, which demonstrated that FORMOSAT-2 images have the potential to estimate rice N status for guiding panicle N fertilizer applications in Northeast China.

Pertaining to the potentials of red edge and additional bands for rice N status estimation, the results indicated that, the best-performed red edge-based VIs explained 53%–64% AGB variability and 62%–65% PNU variability, compared to 30%–40% AGB and 39%–52% PNU variability using the chlorophyll index (CI) at the panicle initiation and stem elongation stages. In addition, for the NNI estimation, the N planar domain index (NDPI) based on the WorldView-2 bands and MERIS terrestrial chlorophyll index (MTCI) based on the RapidEye bands explained 14%–26% more variability than the FORMOSAT-2-based indices. Overall, compared to the FORMOSAT-2 satellite data, both the RapidEye and WorldView-2 data with

red edge band improved the results. However, the WorldView-2 data with three extra bands in the visible and NIR regions showed the highest potential in estimating rice N status.

About the potentials of the proximal fluorescence sensor Multiplex<sup>®</sup>3 for N status estimation at different growth stages for rice in cold regions, it was found that different N application rates significantly affected most of the fluorescence indices, especially the simple fluorescence ratios (SFR\_G, SFR\_R), blue-green to red fluorescence ratio (BRR\_FRF), flavonols (FLAV), and N balance index (NBI\_G, NBI\_R). There were strong relationships between some fluorescence indices (BRR\_FRF, FLAV, NBI\_G, and NBI\_R) and N indicators (LNC, PNC, and NNI) with  $R^2$  between 0.40 and 0.78. In particular, NNI was well estimated using these fluorescence indices. These results indicated that most of the Multiplex indices were reliable indicators of N nutritional status for rice in cold regions.

## 8.2 Future outlook

In this study, the N critical curve established was mainly based on 11-leaf cold rice variety, which still should be further validated using other varieties (e.g., 12-leaf and 13-leaf varieties) to improve its regional universality. Meanwhile, the N fertilizer recommendation model established based on the critical N uptake curve is a simple and operable N fertilizer recommendation algorithm, which is suitable for fertilization recommendation for different farmers in large areas. However, this N fertilizer recommendation approach did not consider the impact of climate conditions (e.g., light-temperature potential productivity). Its sensitivity to climate still needs further research and improvement.

For the application of remote sensing technology in precision agriculture, at present, a new earth observation system with high frequency, high spatial resolution, multiple bands, and full coverage is being constructed by newly launched satellites globally. Vegetation chlorophyll fluorescence remote sensing theory and technology have also been developed rapidly. Agricultural UAV and internet technology have made new breakthroughs. These bring new opportunities for regional crop N nutrition monitoring and the development of precision agriculture. In the future, modern agricultural remote sensing technology integrated with multi-platform and multi-scale "satellite-airborne-ground" remote sensing data is an important development direction of modern precision agriculture under the condition of large-scale planting.

The remote sensing diagnostic model for N nutrition in cold rice is still based on empirical statistical method, and the remote sensing information reflects the instantaneous state of surface parameters. This makes the crop growth monitoring process by remote sensing method only lack a certain mechanism and time continuity. In contrast, crop growth model can continuously simulate the daily growth and development of crops by considering the meteorological, soil, crop varieties and crop planting factors. Therefore, future research

will focus on the integration of remote sensing information and crop growth models, and thus forming a nutrient monitoring and decision-making system for the entire process of crop growth.

## General References (chapters 1, 2, 7)

- Abdallah, F.B., Olivier, M., Goffart, J.P., Minet, O., 2016. Establishing the nitrogen dilution curve for potato cultivar bintje in Belgium. *Potato Res.* 59(3), 241–258.
- Agati, G., Foschi, L., Grossi, N., Guglielminetti, L., Cerovic, Z. G., Volterrani, M., 2013. Fluorescence-based versus reflectance proximal sensing of nitrogen content in *Paspalum vaginatum* and *Zoysia matrella*, turfgrasses. *Eur. J. Agron.* 45(1), 39–51.
- Agati, G., Foschi, L., Grossi, N., Volterrani, M., 2015. In field non-invasive sensing of the nitrogen status in hybrid bermudagrass (*Cynodon dactylon* × *C. transvaalensis* Burt Davy) by a fluorescence-based method. *Eur. J. Agron.* 63, 89–96.
- Ata-Ul-Karim, S. T., Liu, X., Lu, Z., Zheng, H., Cao, W., Zhu, Y., 2017. Estimation of nitrogen fertilizer requirement for rice crop using critical nitrogen dilution curve. *Field Crops Res.* 201, 32–40.
- Ata-Ul-Karim, S.T., Cao, Q., Zhu, Y., Tang, L., Rehman, M.A.R., Cao, W., 2016a. Non-destructive assessment of plant nitrogen parameters using leaf chlorophyll measurements in rice. *Front. Plant Sci.* 7, 1829.
- Ata-Ul-Karim, S.T., Liu, X., Lu, Z., Yuan, Z., Zhu, Y., Cao, W., 2016b. In-season estimation of rice grain yield using critical nitrogen dilution curve. *Field Crops Res.* 195, 1–8.
- Ata-Ul-Karim, S.T., Yao, X., Liu, X., Cao, W., Zhu, Y., 2013. Development of critical nitrogen dilution curve of japonica rice in Yangtze river reaches. *Field Crops Res.* 149, 149–158.
- Baret, F., Houles, V., Guerif, M., 2006. Quantification of plant stress using remote sensing observations and crop models, the case of nitrogen management. *J. Exp. Bot.* 58(4), 869–880.
- Barnes, E.M., Clarke, T.R., Richards, S.E., Colaizzi, P.D., Haberland, J., Kostrzewski, M., Waller, P., Choi, C., Riley, E., Thompson, T., Lascano, R.J., Li, H., Moran, M.S., 2000. Coincident detection of crop water stress, nitrogen status and canopy density using ground-based multispectral data. In: *Proceedings of the Fifth International Conference on Precis. Agric.* Bloomington MN, USA.
- Bausch, W.C, Khosla, R., 2010. QuickBird satellite versus ground-based multi-spectral data for estimating nitrogen status of irrigated maize. *Precis. Agric.* 11(3), 274–290.
- Bélanger, G., Walsh, J.R., Richards, J.E., Milburn, P.H., Ziadi, N., 2001. Critical nitrogen curve and nitrogen nutrition index for potato in eastern Canada. *Am. J. Potato Res.* 78(5), 355–364.
- Bsaibes, A., Courault, D., Baret, F., Weiss, M., Olioso, A., Jacob, F., Hagolle, O., Marloie, O., Bertrand, N., Desfond, V., Kzemipour, F., 2009. Albedo and LAI estimates from

- FORMOSAT-2 data for crop monitoring. *Remote Sens. Environ.* 113, 716–729.
- Burchard, P., Bilger, W., Weissenbock, G., 2000. Contribution of hydroxycinnamates and flavonoids to epidermal shielding of UV-A and UV-B radiation in developing rye primary leaves as assessed by ultraviolet-induced chlorophyll fluorescence measurements. *Plant Cell Environ.* 23(12), 1373–1380.
- Buschmann, C., Lichtenthaler, H.K., 1998. Principles and characteristics of multi-colour fluorescence imaging of plants. *J. Plant Physiol.* 152(2–3), 297–314.
- Buschmann, C., Nagel, E., 1993. In vivo spectroscopy and internal optics of leaves as basis for remote sensing of vegetation. *Int. J. Remote Sens.* 14, 711–722.
- Caldwell, M.M., Gold, W.G., Harris, G., Ashurst, C.W., 1983. A modulated lamp system for solar UV-b (280–320 nm). supplementation studies in the field. *Photochem. Photobiol.* 37(4), 479–485.
- Cao, Q., Cui, Z., Chen, X., Khosla, R., Dao, T. H., Miao, Y., 2012. Quantifying spatial variability of indigenous nitrogen supply for precision nitrogen management in small scale farming. *Precis. Agric.* 2012. 13(1), 45–61.
- Cao, Q., Miao, Y., Shen, J., Yu, W., Yuan, F., Cheng, S., Huang, S., Wang, H., Yang, W., Liu, F., 2016. Improving in-season estimation of rice yield potential and responsiveness to topdressing nitrogen application with crop circle active crop canopy sensor. *Precis. Agric.* 17(2), 136–154.
- Cao, Q., Miao, Y., Wang, H., Huang, S., Cheng, S., Khosla, R., Jiang, R., 2013. Non-destructive estimation of rice plant nitrogen status with crop circle multispectral active canopy sensor. *Field Crops Res.* 154(3), 133–144.
- Cartelat, A., Cerovic, Z.G., Goulas, Y., Meyer, S., Lelarge, C., Prioul, J.L., Barbottin, A., Jeuffroy, M.H., Gate, P., Agati, G., Moya, I., 2005. Optically assessed contents of leaf polyphenolics and chlorophyll as indicators of nitrogen deficiency in wheat (*Triticum aestivum L.*). *Field Crops Res.* 91(1), 35–49.
- Cassman, K.G., Dobermann, A., Walters, D.T., 2002. Agroecosystems, nitrogen-use efficiency, and nitrogen management. *Ambio.* 31(2), 132–40.
- Cassman, K.G., Gines, G.C., Dizon, M.A., Samson, M.I., Alcantara, J.M., 1996. Nitrogen-use efficiency in tropical lowland rice systems: contributions from indigenous and applied nitrogen. *Field Crops Res.* 47(1), 1–12.
- Cerovic, Z.G., Goutouly, J.P., Hilbert, G., Destrac-Irvine, A., Moise, N., 2009. Mapping winegrape quality attributes using portable fluorescence-based sensors. In: Best, S. (Ed.), *FRUTIC 09*, Concepcion, Chile, pp. 301–310.
- Cerovic, Z.G., Moise, N., Agati, G., Latouche, G., Ghazlen, N. B., Meyer, S., 2008. New portable optical sensors for the assessment of winegrape phenolic maturity based on berry fluorescence. *J. Food Compos. Anal.* 21(8), 650–654.
- Cerovic, Z.G., Ounis, A., Cartelat, A., Latouche, G., Goulas, Y., Meyer, S., Moya, I., 2002.

- The use of chlorophyll fluorescence excitation spectra for the non-destructive in situ assessment of UV-absorbing compounds in leaves. *Plant Cell Environ.* 25(12), 1663–1676.
- Chakwizira, E., Ruiter, J.M.D., Maley, S., Teixeira, E., 2016. Evaluating the critical nitrogen dilution curve for storage root crops. *Field Crops Res.* 199, 21–30.
- Chan, C.W., Schueller, J.K., Miller, W.M., Whitney, J.D., Cornell, J.A.M., 2004. Error sources affecting variable rate application of nitrogen fertilizer. *Precis. Agric.* 5(6), 601–616.
- Chappelle, E.W., Kim, M.S., McMurtrey, J.E., 1992. Ratio analysis of reflectance spectra (RARS), An algorithm for the remote estimation of the concentrations of chlorophyll A, chlorophyll B, and carotenoids in soybean leaves. *Remote Sens. Environ.* 39(3), 239–247.
- Chen, P., Wang, J., Huang, W., Tremblay, N., Ou, Y., Zhang, Q., 2013. Critical nitrogen curve and remote detection of nitrogen nutrition index for corn in the northwestern plain of Shandong Province, China. *IEEE J. Sel. Top. Appl. Earth Obs. Remote Sens.* 6(2), 682–689.
- Chen, X., Cui, Z., Fan, M., Vitousek, P., Zhao, M., Ma, W., Wang, Z., Zhang, W., Yan, X., Yang, J., Deng, X., Gao, Q., Zhang, Q., Guo, S., Ren, J., Li, S., Ye, Y., Wang, Z., Huang, J., Tang, Q., Sun, Y., Peng, X., Zhang, J., He, M., Zhu, Y., Xue, J., Wang, G., Wu, L., An, N., Wu, L., Ma, L., Zhang, W., Zhang, F., 2014. Producing more grain with lower environmental costs. *Nature*, 514(7523), 486.
- Cho, M.A., Skidmore, A.K., 2006. A new technique for extracting the red edge position from hyperspectral data, The linear extrapolation method. *Remote Sens. Environ.* 101(2), 181–193.
- Cilia, C., Panigada, C., Rossini, M., Meroni, M., Busetto, L., Amaducci, S., Boschetti, M., Picchi, V., Colombo, R., 2014. Nitrogen status assessment for variable rate fertilization in maize through hyperspectral imagery. *Remote Sens.* 6(7), 6549–6565.
- Clevers, J.G.P.W., Gitelson, A.A., 2013. Remote estimation of crop and grass chlorophyll and nitrogen content using red-edge bands on Sentinel-2 and -3. *Int. J. Appl. Earth Obs.* 23, 344–351.
- Clevers, J.G.P.W., Jong, S.M.D., Epema, G.F., Meer, F.D.V.D., Bakker, W.H., Skidmore, A.K., Scholte, K.H., 2002. Derivation of the red edge index using the MERIS standard band setting. *Int. J. Remote Sens.* 23(16), 3169–3184.
- Clevers, J.G.P.W., Kooistra, L., 2012. Using hyperspectral remote sensing data for retrieving canopy chlorophyll and nitrogen content. *IEEE J. Sel. Top. Appl. Earth Obs. Remote Sens.* 5(2), 574–583.
- Clevers, J.G.P.W., Kooistra, L., van den Brande, M.M.M., 2017. Using Sentinel-2 Data for Retrieving LAI and Leaf and Canopy Chlorophyll Content of a Potato Crop. *Remote*

- Sens. 9(5), 405.
- Colenne, C., Meynard, J.M., Reau, R., Justes, E., Merrien, A., 1998. Determination of a critical nitrogen dilution curve for winter oilseed rape. *Ann. Bot.* 81(2), 311–317.
- Coquil, B, Bordes, J.P., 2005. FARMSTAR: an efficient decision support tool for near real time crop management from satellite images. *Precis. Agric.* 05, 873–880.
- Cui, Z., Chen, X., Miao, Y., Fei, L., Zhang, F., Li, J., Ye, Y., Yang, Z., Zhang, Q., Liu, C., 2008. On-farm evaluation of winter wheat yield response to residual soil nitrate-N in north China plain. *Agron. J.* 100(6), 1527–1534.
- Dash, J., Curran, P.J., 2004. The MERIS terrestrial chlorophyll index. *Int. J. Remote Sens.* 25(23), 5403–5413.
- Daughtry, C.S.T., Walthall, C.L., Kim, M.S., Colstoun, E.B., McMurtrey III, J.E., 2000. Estimating corn leaf chlorophyll concentration from leaf and canopy reflectance. *Remote Sens. Environ.* 74, 229–239.
- Dawson, T. P., Curran, P. J., 1998. Technical note a new technique for interpolating the reflectance red edge position. *Int. J. Remote Sens.* 19(11), 2133–2139.
- Day, T.A., Howells B.W., Rice, W.J., 1994. Ultraviolet absorption and epidermal-transmittance spectra in foliage. *Physiol. Plantarum.* 92(2), 207–218.
- Demotes-Mainard, S., Boumaza, R., Meyer, S., Cerovic, Z.G., 2008. Indicators of nitrogen status for ornamental woody plants based on optical measurements of leaf epidermal polyphenol and chlorophyll contents. *Sci. Hortic.* 115(4), 377–385.
- Diacono, M., Rubino, P., Montemurro, F., 2013. Precision nitrogen management of wheat: A review. *Agron. Sustain. Dev.* 33, 219–241.
- Doberman, A., Witt, C., Dawe, D., Abdulrachman, S., Gines, H.C., Nagarajan, R. et al. 2002. Site-specific nutrient management for intensive rice cropping systems in Asia. *Field Crops Res.* 74, 37–66.
- Dobermann, A., 2007. Nutrient use efficiency-measurement and management. In: A Drauss et al. (Eds.), *Fertilizer Best Management Practices. General Principles, Strategy for their Adoption and Voluntary Initiatives vs Regulations.* IFA, Paris.
- Dong, T., Meng, J., Shang, J., Liu, J., Wu, B., 2015. Evaluation of chlorophyll-related vegetation indices using simulated sentinel-2 data for estimation of crop fraction of absorbed photosynthetically active radiation. *IEEE J. Sel. Top. Appl. Earth Obs. Remote Sens.* 8(8), 4049–4059.
- Ecartot, M., Compan, F., Roumet, P., 2013. Assessing leaf nitrogen content and leaf mass per unit area of wheat in the field throughout plant cycle with a portable spectrometer. *Field Crops Res.* 140(140), 44–50.
- Eitel, J.U.H., Long, D.S., Gessler, P.E., Hunt, E.R., 2008. Combined spectral index to improve ground-based estimates of nitrogen status in dryland wheat. *Agron. J.* 100(6), 1694–1702.

- Eitel, J.U.H., Long, D.S., Gessler, P.E., Smith, A.M.S., 2007. Using in-situ measurements to evaluate the new RapidEye™ satellite series for prediction of wheat nitrogen status. *Int. J. Remote Sens.* 28, 4183–4190.
- Fageria, N.K., Baligar, V.C., 2005. Enhancing Nitrogen Use Efficiency in Crop Plants. *Adv. Agron.* 88, 97–185.
- Fageria, N. K., 2009. *The Use of Nutrients in Crop Plants*. CRC Press, Boca Raton.
- Farruggia, A., Gastal, F., Scholefield, D., 2004. Assessment of the nitrogen status of grassland. *Grass Forage Sci.* 59(2), 113–120.
- Fitzgerald, G., Rodriguez, D., Leary, G.O., 2010. Measuring and predicting canopy nitrogen nutrition in wheat using a spectral index—The canopy chlorophyll content index (CCCI). *Field Crops Res.* 116(3), 318–324.
- Footy, G.M., Boyd, D.S., Cutler, M.E.J., 2003. Predictive relations of tropical forest biomass from Landsat™ data and their transferability between regions. *Remote Sens. Environ.* 85(4), 463–474.
- Gao, C., Zhang, S., Liu, H., Cong, J., Li, Y., Wang, G., 2018. The impacts of land reclamation on the accumulation of key elements in wetland ecosystems in the Sanjiang Plain, Northeast China. *Environ. Pollut.* 237, 487–498.
- Gastal, F., Lemaire, G., 2002. N uptake and distribution in crops, an agronomical and ecophysiological perspective. *J. Exp. Bot.* 53(370), 789–799.
- Gianquinto, G., Orsini, F., Fecondini, M., Mezzetti, M., Sambo, P., Bona, S., 2011. A methodological approach for defining spectral indices for assessing tomato nitrogen status and yield. *Eur. J. Agron.* 35(3), 135–143.
- Gitelson, A., Merzlyak, M.N., 1994. Quantitative estimation of chlorophyll-a using reflectance spectra, Experiments with autumn chestnut and maple leaves. *J. Photoch. Photobio. B.* 22(3), 247–252.
- Gitelson, A.A., 2013. Remote estimation of crop fractional vegetation cover, the use of noise equivalent as an indicator of performance of vegetation indices. *Int. J. Remote Sens.* 34(17), 6054–6066.
- Gitelson, A.A., Buschmann, C., Lichtenthaler, H.K., 1999. The chlorophyll fluorescence ratio F-735/F-700 as an accurate measure of the chlorophyll content in plants. *Remote Sens. Environ.* 69(3), 296–302.
- Gitelson, A.A., Gritz, Y., Merzlyak, M.N., 2003. Relationships between leaf chlorophyll content and spectral reflectance and algorithms for non-destructive chlorophyll assessment in higher plant leaves. *J. Plant Physiol.* 160, 271–282.
- Gitelson, A.A., Peng, Y., Masek, J.G., Rundquist, D.C., Verma, S., Suyker, A., Baker, J.M., Hatfield, J.L., Meyers, T., 2012. Remote estimation of crop gross primary production with Landsat data. *Remote Sens. Environ.* 121(138), 404–414.
- Gitelson, A.A., Signature, M., 1996. *Analysis of Leaf Reflectance Spectra, Algorithm*

- Development for Remote Sensing of Chlorophyll. *J. Plant Physiol.* 148(3–4), 494–500.
- Gitelson, A.A., Viña, A., Ciganda, V., Rundquist, D.C., Arkebauer, T.J., 2005. Remote estimation of canopy chlorophyll content in crops. *Geophys. Res. Lett.* 32, L08403.
- Gnyp, M.L., 2014. Evaluating and developing methods for non-destructive monitoring of biomass and nitrogen in wheat and rice using hyperspectral remote sensing. University of Cologne, Cologne.
- Gnyp, M.L., Miao, Y., Yuan, F., Ustin, S.L., Yu, K., Yao, Y., Huang, S., Bareth, G., 2014. Hyperspectral canopy sensing of paddy rice aboveground biomass at different growth stages. *Field Crops Res.* 155, 42–55.
- Godfray, H.C., Beddington, J.R., Crute, I.R., Haddad, L., Lawrence, D., Muir, J.F., Pretty, J., Robinson, S., Thomas, S.M., Toulmin, C., 2010. Food security: the challenge of feeding 9 billion people. *Science*, 327(5967), 812–818.
- González-Piqueras, J., Lopez-Corcoles, H., Sánchez, S., Carrilero, J.V., Bodas, V., Campos, I., Osann, A., Calera, A., 2017. Monitoring crop N status by using red edge-based indices. *Adv. Anim. Biosci.* 8(2), 338–342.
- Goulas, Y., Cerovic, Z.G., Cartelat, A., Moya, I., 2004. Dualex: a new instrument for field measurements of epidermal ultraviolet absorbance by chlorophyll fluorescence. *Appl. Opt.* 43(23), 4488–4496.
- Greenwood, D.J., Lemaire, G., Gosse, G., Cruz, P., Draycott, A., Neeteson, J.J., 1990. Decline in percentage N of C3 and C4 crops with increasing plant mass. *Ann. Bot.* 66(4), 425–436.
- Greenwood, D.J., Neeteson, J.J., Draycott, A., 1986. Quantitative relationships for the dependence of growth rate of arable crops on their nitrogen content, dry weight and aerial environment. *Plant Soil.* 91(3), 281–301.
- Guo, J.H., Liu, X.J., Zhang, Y., Shen, J.L., Han, W.X., Zhang, W.F., Christie, P., Goulding, K.W.T., Vitousek, P.M., Zhang, F.S., 2010 Significant acidification in major Chinese croplands. *Science* 327, 1008–1010.
- Haboudane, D., Miller, J.R., Pattey, E., Zarco-Tejada, P.J., Strachan, I.B., 2004. Hyperspectral vegetation indices and novel algorithms for predicting green LAI of crop canopies: Modeling and validation in the context of precision agriculture. *Remote Sens. Environ.* 90, 337–352.
- Hahlbrock, K., Scheel, D., 1989. Physiology and molecular biology of phenylpropanoid metabolism. *Annu. Rev. Plant Phys.* 40, 347–369.
- Hamilton, N.R.S., Matthew, C., Lemaire, G., 1995. In defence of the  $-3/2$  boundary rule: a re-evaluation of self-thinning concepts and status. *Ann. Bot.* 76(6), 569–577.
- Hansen, P.M., Schjoerring, J.K., 2003. Reflectance measurement of canopy biomass and nitrogen status in wheat crops using normalized difference vegetation indices and partial least squares regression. *Remote Sens. Environ.* 86(4), 542–553.

- Hatfield, J.L., Gitelson, A.A., Schepers, J.S., Walthall, C.L., 2008. Application of spectral remote sensing for agronomic decisions. *Agron. J.* 100(3), 117–131.
- Heege, H.J., Reusch, S., Thiessen, E., 2008. Prospects and results for optical systems for site-specific on-the-go control of nitrogen-top-dressing in Germany. *Precis. Agric.* 9(3), 115–131.
- Heffer, P., 2009. Assessment of fertilizer use by crop at the global level 2006/07-2007/08. International Fertilizer Industry Association, Paris, France.
- Herrmann, A., Taube, F., 2004. The range of the critical nitrogen dilution curve for maize (*Zea mays L.*) can be extended until silage maturity. *Agron. J.* 96, 1131–1138.
- Hirose, T., Werger, M.J.A., 1987. Maximizing daily canopy photosynthesis with respect to the leaf nitrogen allocation pattern in the canopy. *Oecologia* 72(4), 520–526.
- Horler, D., Dockray, M., Barber, J., 1983. The red edge of plant leaf reflectance. *Int. J. Remote Sens.* 4(2), 273–288.
- Houlès, V., Guérif, M., Mary, B., 2007. Elaboration of a nitrogen nutrition indicator for winter wheat based on leaf area index and chlorophyll content for making nitrogen recommendations. *Eur. J. Agron.* 27(1), 1–11.
- Inamura, T., Goto, K., Iida, M., Nonami, K., Inoue, H., Umeda, M., 2004. Geostatistical analysis of yield, soil properties and crop management practices in paddy rice fields. *Plant Prod. Sci.* 7(2), 230–239.
- Indahl, U., 2005. A twist to partial least squares regression. *J. Chemometr.* 19(1), 32–44.
- Jackson, R.D., Teillet, P.M., Slater, P.N., Fedosejevs, G., Jasinski, M.F., Aase, J.K., Moran, M.S., 1990. Bidirectional measurements of surface reflectance for view angle corrections of oblique imagery. *Remote Sens. Environ.* 32(2), 189–202.
- Jacquemoud, S., Verdebout, J., Schmuck, G., Andreoli, G., Hosgood, B., 1995. Investigation of leaf biochemistry by statistics. *Remote Sens. Environ.* 1995. 54(3), 180–188.
- Jeuffroy, M.H., Bouchard, C., 1999. Intensity and duration of nitrogen deficiency on wheat grain number. *Crop Sci.* 39(5), 1385–1393.
- Jiang, X.H., Yang, S.Y., Ren, J.Q., Tian, S.N., Jiang, J.X., 2014. Analysis of climatic conditions in the cold rice region in North China. *Heilongjiang Meteorol.* 31(4), 16–18 (in Chinese).
- Jin, J., 2012. Changes in the efficiency of fertiliser use in China. *J. Sci. Food Agric.* 92, 1006–1009.
- Jones, C.G., Hartley, S.E., 1999. A protein competition model of phenolic allocation. *Oikos* 86(1), 27–44.
- Jordan, C.F., 1969. Derivation of leaf-area index from quality of light on the forest floor. *Ecology* 50(4), 663–666.
- Justes, E., Mary, B., Meynard, J.M., Machet, J.M., Thelierhuche, L., 1994. Determination of a critical nitrogen dilution curve for winter wheat crops. *Ann. Bot.* 74(4), 397–407.

- Justes, E., Meynard, J.M., Mary, B., Plénet, D., 1997. Diagnosis using stem base extract, JUBIL method. In: Lemaire, G. (Ed.), *Diagnosis of the nitrogen status in crops*. Springer-Verlag, Heidelberg, Germany, pp. 163–187
- Katsura, K., Okami, M., Mizunuma, H., Kato, Y., 2010. Radiation use efficiency, N accumulation and biomass production of high-yielding rice in aerobic culture. *Field Crops Res.* 117(1), 81–89.
- Kiraly, Z., 1964. Effect of nitrogen fertilization on phenol metabolism and stem rust susceptibility of wheat. *J. Phytopathol.* 51, 252–261.
- Knogge, W., Weissenböck, G., 1986. Tissue-distribution of secondary phenolic biosynthesis in developing primary leaves of *Avena sativa* L. *Planta.* 167(2), 196–205.
- Ksouri, R., Megdiche, W., Debez, A., Falleh, H., Grignon, C., Abdelly, C., 2007. Salinity effects on polyphenol content and antioxidant activities in leaves of the halophyte *Cakile maritima*. *Plant Physiol. Bioch.* 45(3), 244–249.
- Kusnierek, K., Korsath, A., 2015. Simultaneous identification of spring wheat nitrogen and water status using visible and near infrared spectra and Powered Partial Least Squares Regression. *Comput. Electron. Agr.* 117, 200–213.
- Langsdorf, G., Buschmann, C., Sowinska, M., Babani, F., Mokry, M., Timmermann, F., Lichtenthaler, H.K., 2000. Multicolour fluorescence imaging of sugar beet leaves with different nitrogen status by flash lamp UV-excitation. *Photosynthetica* 38(4), 539–551.
- Le, C., Zha, Y., Li, Y., Sun, D., Lu, H., Yin, B., 2010. Eutrophication of lake waters in China: cost, causes, and control. *Environ. Manage.* 45(4), 662–668.
- Leff, B., Ramankutty, N., Foley, J.A., 2004. Geographic distribution of major crops across the world. *Global Biogeochem. Cy.* 18, GB1009.
- Lemaire, G., Avice, J.C., Kim, T.H., Ourry, A., 2005. Developmental changes in shoot n dynamics of lucerne (*Medicago sativa* L.) in relation to leaf growth dynamics as a function of plant density and hierarchical position within the canopy. *J. Exp. Bot.* 56(413), 935–943.
- Lemaire, G., Cruz, P., Gosse, G., Chartier, M., 1985. Relationship between dynamics of nitrogen uptake and dry matter growth for Lucerne (*Medicago sativa* L.). *Agronomie* 5, 685–692.
- Lemaire, G., Gastal, F., 1997. N uptake and distribution in plant canopies. In: Lemaire, G. (Ed.), *Diagnosis of the nitrogen status in crops*. Springer-Verlag, Heidelberg, Germany, pp. 3–43
- Lemaire, G., Gastal, F., Salette, J., 1989. Analysis of the effect of N nutrition on dry matter yield of a sward by reference to potential yield and optimum N content. In: *Proceedings of the XVth International Grassland Congress, Nice, France*, pp. 179–180.
- Lemaire, G., Jeuffroy, M.H., Gastal, F., 2008. Diagnosis tool for plant and crop N status in vegetative stage, theory and practices for crop N management. *Eur. J. Agron.* 28(4),

614–624.

- Lemaire, G., Meynard, J.M., 1997. Use of the nitrogen nutrition index for the analysis of agronomical data. In: Lemaire, G. (Ed.), *Diagnosis of the nitrogen status in crops*. Springer-Verlag, Heidelberg, Germany, pp. 45–55.
- Lemaire, G., Salette, J., 1984a. Relationship between growth and nitrogen uptake in a pure grass stand. I. Environmental effects [nitrogen nutrition, nitrogen content, allometric relations, variability between years, tall fescue]. *Agronomie* 4(5), 423–430
- Lemaire, G., Salette, J., 1984b. Relationship between growth and nitrogen uptake in a pure grass stand. II. variability in different genotypes. *Agronomie* 4(5), 431–436.
- Lemaire, G., Van, O. E., Sheehy, J., Jeuffroy, M. H., Massignam, A., Rossato, L., 2007. Is crop N demand more closely related to dry matter accumulation or leaf area expansion during vegetative growth. *Field Crops Res.* 99(1), 91–106.
- Lenk, S., Chaerle, L., Pfündel, E.E., Langsdorf, G., Hagenbeek, D., Lichtenthaler, H.K., Van Der Straeten, D., Buschmann, C., 2007. Multispectral fluorescence and reflectance imaging at the leaf level and its possible applications. *J. Exp. Bot.* 58(4), 807–814.
- Li, F., 2008. Nitrogen management for winter wheat based on remote sensing and soil-plant testing. China Agricultural University, Beijing (in Chinese with English abstract).
- Li, F., Miao, Y., Feng, G., Yuan, F., Yue, S., Gao, X., Liu, Y., Liu, B., Ustin, S.L., Chen, X., 2014a. Improving estimation of summer maize nitrogen status with red edge-based spectral vegetation indices. *Field Crops Res.* 157, 111–123.
- Li, F., Miao, Y., Hennig, S. D., Gnyp, M. L., Chen, X., Jia, L., Bareth, G., 2010. Evaluating hyperspectral vegetation indices for estimating nitrogen concentration of winter wheat at different growth stages. *Precis. Agric.* 11(4), 335–357.
- Li, F., Mistele, B., Hu, Y., Chen, X., Schmidhalter, U., 2014b. Reflectance estimation of canopy nitrogen content in winter wheat using optimised hyperspectral spectral indices and partial least squares regression. *Eur. J. Agron.* 52(1), 198–209.
- Li, J.W., Zhang, J.X., Zhao, Z., Lei, X.D., Xu, X.L., Lu, X.X., Weng, D.L., Gao, Y., Cao, L.K., 2013. Use of fluorescence-based sensors to determine the nitrogen status of paddy rice. *J. Agr. Sci.* 151(06), 862–871.
- Li, Y.J., Zhao, H.M., Ren, F.W., 2005. Northern area winter-rice seedling of two stages ultrahigh yield methods. *Heilongjiang Agr. Sci.* (4), 50, 11 (in Chinese with English abstract).
- Lichtenthaler, H.K., 1996. Vegetation Stress, an Introduction to the Stress Concept in Plants. *J. Plant Physiol.* 148(1–2), 4–14.
- Liu, J., Pattey, E., Jégo, G., 2012. Assessment of vegetation indices for regional crop green LAI estimation from Landsat images over multiple growing seasons. *Remote Sens. Environ.* 123, 347–358.
- Liu, L., Gitz, D.C., McClure, J.W., 1995. Effects of UV-B on flavonoids, ferulic acid, growth

- and photosynthesis in barley primary leaves. *Physiol. Plantarum* 93(4), 725–733.
- Liu, X., Zhang, Y., Han, W., Tang, A., Shen, J., Cui, Z., Vitousek, P., Erisman, J.W., Goulding, K., Christie, P., Fangmeier, A. Zhang, F., 2013. Enhanced nitrogen deposition over China. *Nature* 494(7438), 459–462.
- Long, D.S., Whitmus, J.D., Engel, R.E., Brester, G.W., 2015. Net returns from terrain-based variable-rate nitrogen management on dryland spring wheat in Northern Montana. *Agron. J.* 107(3), 1055–1067.
- Longchamps, L., Khosla, R., 2014. Early detection of nitrogen variability in maize using fluorescence. *Agron. J.* 106(2), 511–518.
- Ly, D., Chenu, K., Gauffreteau, A., Rincint, R., Huet, S., Gouache, D., Martre, P., Bordes, J., Charmet, G., 2017. Nitrogen nutrition index predicted by a crop model improves the genomic prediction of grain number for a bread wheat core collection. *Field Crops Res.* 214, 331–340.
- Magney, T.S., Eitel, J.U.H., Vierling, L.A., 2017. Mapping wheat nitrogen uptake from RapidEye vegetation indices. *Precis. Agric.* 18(4), 429–451.
- Maresma, Á., Lloveras, J., Martínez-Casasnovas, J.A., 2018. Use of multispectral airborne images to improve in-season nitrogen management, predict grain yield and estimate economic return of maize in irrigated high yielding environments. *Remote Sens.* 10(4), 543.
- Martin, M.E., Plourde, L.C., Ollinger, S.V., Smith, M.L., McNeil, B.E., 2008. A generalizable method for remote sensing of canopy nitrogen across a wide range of forest ecosystems. *Remote Sens. Environ.* 112(9), 3511–3519.
- Meyer, S., Cerovic, Z. G., Goulas, Y., Montpied, P., Demotes-Mainard, S., Bidet, L.P.R., Moya, I., Dreyer, E., 2006. Relationships between optically assessed polyphenols and chlorophyll contents, and leaf mass per area ratio in woody plants: a signature of the carbon-nitrogen balance within leaves? *Plant Cell Environ.* 29(7), 1338–1348.
- Miao, Y., Mulla, D.J., Randall, G.W., Vetsch, J.A., Vintila, R., 2009. Combining chlorophyll meter readings and high spatial resolution remote sensing images for in-season site-specific nitrogen management of corn. *Precis. Agric.* 10(1), 45–62.
- Mistele, B., Schmidhalter, U., 2008. Estimating the nitrogen nutrition index using spectral canopy reflectance measurements. *Eur. J. Agron.* 29(4), 184–190.
- Moulin, S., 1999. Impacts of model parameter uncertainties on crop reflectance estimates, A regional case study on wheat. *Int. J. Remote Sens.* 20(1), 213–218.
- Mulla, D.J., 2013. Twenty-five years of remote sensing in *Precis. Agric.* Key advances and remaining knowledge gaps. *Biosyst. Eng.* 114(4), 358–371.
- Mulla, D.J., Miao, Y., 2016. Precision Farming. In: Thenkabail, P.S. (Ed.), *Land Resources Monitoring, Modeling, and Mapping with Remote Sensing*. CRC Press, FL, USA, pp. 161–178.

- National Bureau of Statistics PRC. China Statistical Yearbook 2017. China Statistics Press, 2017.
- Nigon, T. J., Mulla, D. J., Rosen, C. J., Cohen, Y., Alchanatis, V., Rud, R., 2014. Evaluation of the nitrogen sufficiency index for use with high resolution, broadband aerial imagery in a commercial potato field. *Precis. Agric.* 15(2), 202–226.
- Noura, Z., Gilles, B., François, G., Annie, C., Gilles, L., Nicolas, T., 2009. Leaf nitrogen concentration as an indicator of corn nitrogen status. *Agron. J.* 101(4), 947–957.
- Orych, A., Walczykowski, P., Dąbrowski, R., Kutyna, E., 2014. Using plant spectral response curves in detecting plant stress. *Ecol. Quest.* 17, 67–74.
- Osborne, S.L., Schepers, J.S., Francis, D.D., Schlemmer, M.R., 2002. Use of spectral radiance to estimate in-season biomass and grain yield in nitrogen- and water-stressed corn. *Crop Sci.* 42(1), 165–171.
- Padilla, F.M., Peña-Fleitas, M.T., Gallardo, M., Thompson, R.B., 2014. Evaluation of optical sensor measurements of canopy reflectance and of leaf flavonols and chlorophyll contents to assess crop nitrogen status of muskmelon. *Eur. J. Agron.* 58, 39–52.
- Padilla, F.M., Peña-Fleitas, M.T., Gallardo, M., Thompson, R.B., 2016. Proximal optical sensing of cucumber crop N status using chlorophyll fluorescence indices. *Eur. J. Agron.* 73, 83–97.
- Peng, S., Garcia, F.V., Laza, R.C., Sanico, A.L., Visperas, R.M., Cassman, K.G., 1996. Increased N-use efficiency using a chlorophyll meter on high-yielding irrigated rice. *Field Crops Res.* 47(2–3), 243–252.
- Peng, S., Huang, J., Zhong, X., Yang, J., Wang, G., Zou, Y., Zhang, F. Zhu, Q., Buresh, R., Christian, W., 2002. Challenge and opportunity in improving fertilizer-nitrogen use efficiency of irrigated rice in China. *Agr. Sci. China* 1(7), 67–76.
- Peng, X., Yang, Y., Yu, C., Chen, L., Zhang, M., Liu, Z., Sun, Y., Luo, S., Liu, Y., 2015. Crop management for increasing rice yield and nitrogen use efficiency in Northeast China. *Agro. J.* 107(5), 1682–1690.
- Peng, Y., Nguy-Robertson, A., Arkebauer, T., Gitelson, A., 2017. Assessment of canopy chlorophyll content retrieval in maize and soybean, implications of hysteresis on the development of generic algorithms. *Remote Sens.* 9(3), 226.
- Pinter, P.J.Jr., Jackson, R.D., Moran, M.S., 1990. Bidirectional reflectance factors of agricultural targets: A comparison of ground-, aircraft-, and satellite-based observations. *Remote Sens. Environ.* 32, 215–228.
- Plénet, D., Lemaire, G., 1999. Relationships between dynamics of nitrogen uptake and dry matter accumulation in maize crops. Determination of critical N concentration. *Plant Soil* 216(1), 65–82.
- Pons, T.L., Percy, R.W., 1994. Nitrogen reallocation and photosynthetic acclimation in response to partial shading in soybean plants. *Physiol. Plantarum* 92(4), 636–644.

- Prost, L., Jeuffroy, M.H., 2007. Replacing the nitrogen nutrition index by the chlorophyll meter to assess wheat N status. *Agron. Sustain. Dev.* 27(4), 321–330.
- Ravier, C., Quemada, M., Jeuffroy, M., 2017. Use of a chlorophyll meter to assess nitrogen nutrition index during the growth cycle in winter wheat. *Field Crops Res.* 214, 73–82.
- Rodriguez, D., Fitzgerald, G.J., Belford, R., Christensen, L., 2006. Detection of nitrogen deficiency in wheat from spectral reflectance indices and basic crop eco-physiological concepts. *Aust. J. Agric. Res.* 57, 781–789.
- Rouse, J.W., Haas, R.H., Schell, J.A., Deering, D.W., 1973. Monitoring vegetation systems in the Great Plains with ERTS. *Earth Res. Techn. Satellite-1 Symp.*, Goddard Space Hight Center. Washington D.C., pp. 309-317.
- Samson, G., Tremblay, N., Dudelzak, A.E., Babichenko, S.M., Dextraze, L., Wollring, J., 2000. Nutrient stress of corn plants: early detection and discrimination using a compact multiwavelength fluorescent lidar. In: Reuter, R. (Ed.), *Proceedings of the 20th EARSeL Symposium*, Dresden, Germany. pp. 214–223.
- Scharf, P.C., Kitchen, N.R., Schmidt, J.P., Sudduth, K.A., 2002. Remote sensing for nitrogen management. *J. Soil Water Conserv.* 57(6), 518–523.
- Schlemmer, M., Gitelson, A., Schepers, J., Ferguson, R., Peng, Y., Shanahan, J., Rundquist, D., 2013. Remote estimation of nitrogen and chlorophyll contents in maize at leaf and canopy levels. *Int. J. Appl. Earth Obs.* 25(1), 47–54.
- Sheehy, J.E., Mja, D., Mitchell, P.L., Peng, S., Cassman, K.G., Lemaire, G., Williams, R.L., 1998. Critical nitrogen concentrations, implications for high-yielding rice (*Oryza sativa* L.) cultivars in the tropics. *Field Crops Res.* 59(1), 31–41.
- Shen, J., Cui, Z., Miao, Y., Mi, G., Zhang, H., Fan, M., Zhang, C., Jiang, R., Zhang, W., Li, H., Chen, X., Li, X., Zhang, F., 2013. Transforming agriculture in China: From solely high yield to both high yield and high resource use efficiency. *Glob. Food Secur.* 2(1), 1–8.
- Stroppiana, D., Boschetti, M., Brivio, P. A., Bocchi, S., 2009. Plant nitrogen concentration in paddy rice from field canopy hyperspectral radiometry. *Field Crops Res.* 111(1–2), 119–129.
- Thenkabail, P.S., Smith, R.B., Pauw, E.D., 2000. Hyperspectral vegetation indices and their relationships with agricultural crop characteristics. *Remote Sens. Environ.* 71(2), 158–182.
- Thenkabail, P.S., Ward, A.D., Lyon, J.G., 1994. Landsat-5 thematic mapper models of soybean and corn crop characteristics. *Int. J. Remote Sens.* 15(1), 49–61.
- Thind, H.S., Gupta, R.K., 2010. Need based nitrogen management using the chlorophyll meter and leaf color chart in rice and wheat in South Asia: a review. *Nutr. Cycl. Agroecosys.* 88(3), 361–380.
- Thorp, K.R., Wang, G., Bronson, K.F., Badaruddin, M., Mon, J., 2017. Hyperspectral data

- mining to identify relevant canopy spectral features for estimating durum wheat growth, nitrogen status, and grain yield. *Comput. Electron. Agr.* 136, 1–12.
- Tilman, D., Balzer, C., Hill, J., Befort, B.L., 2011. Global food demand and the sustainable intensification of agriculture. *Proc. Nat. Acad. Sci. U.S.A.* 108(50), 20260–20264.
- Tremblay, N., Fallon, E., Ziadi, N., 2011. Sensing of crop nitrogen status: opportunities, tools, limitations, and supporting information requirements. *HortTechnology* 21(3), 274–281.
- Tremblay, N., Wang, Z., Bélec, C., 2007. Evaluation of the Dualex for the assessment of corn nitrogen status. *J. Plant. Nutr.* 30(9), 1355–1369.
- Tucker, C.J., 1979. Red and photographic infrared linear combinations for monitoring vegetation. *Remote Sens. Environ.* 8(2), 127–150.
- Ulrich, A., 1952. Physiological bases for assessing the nutritional requirements of plants. *Annu. Rev. Plant Phys.* 3(1), 207–228.
- Villodre, J., Campos, I., Lopez–Corcoles, H., Gonzalez-Piqueras, J., González, L., Bodas, V., Sanchez-Prieto, S., Osann, A., Calera, A., 2017. Mapping optimum nitrogen crop uptake. *Adv. Anim. Biosci.* 8(2), 322–327.
- Vuolo, F., Essl, L., Zappa, L., Sandén, T., Spiegel, H., 2017. Water and nutrient management, the Austria case study of the FATIMA H2020 project. *Adv. Anim. Biosci.* 8(2), 400–405.
- Wiegand, C. L., Maas, S. J., Aase, J. K., Hatfield, J. L., Pinter, P. J., Jackson, R. D., Kanemasu, E.T., Lapitan, R.L., 1992. Multisite analyses of spectral-biophysical data for wheat. *Remote Sens. Environ.* 42, 1–21.
- Wu, C., Niu, Z., Tang, Q., Huang, W., 2008. Estimating chlorophyll content from hyperspectral vegetation indices: Modeling and validation. *Agric. Forest Meteorol.* 148, 1230–1241.
- Xia, T., Miao, Y., Wu, D., Shao, H., Khosla, R., Mi, G., 2016. Active optical sensing of spring maize for in-season diagnosis of nitrogen status based on nitrogen nutrition index. *Remote Sens.* 8(7), 605
- Xue, X., Wang, J., Wang, Z., Zhou, Z., 2007. Determination of a critical dilution curve for nitrogen concentration in cotton. *J. Plant Nutr. Soil. Sc.* 170(6), 811–817.
- Yang, C.M., Liu, C.C., Wang, Y.W., 2008. Using FORMOSAT-2 satellite data to estimate leaf area index of rice crop. *ISPRS J. Photogramm. Remote Sens.* 13(4), 253–260.
- Yao, Y., Miao, Y., Cao, Q., Wang, H., Gnyp, M. L., Bareth, G., Khosla, R., Wang, W., Liu, F., Liu, C., 2014. In-Season Estimation of Rice Nitrogen Status With an Active Crop Canopy Sensor. *IEEE J. Sel. Top. Appl. Earth Obs. Remote Sens.* 7(11), 1–11.
- Yoshida, S., 1981. *Fundamentals of Rice Crop Science*. International Rice Research Institute, Los Baños, Philippines, pp. 4–9
- Yu, K., Li, F., Gnyp, M.L., Miao, Y., Bareth, G., Chen, X., 2013. Remotely detecting canopy nitrogen concentration and uptake of paddy rice in the Northeast China plain. *ISPRS J.*

- Photogramm. Remote Sens. 78(1), 102–115.
- Yu, Q., 2014. Research of rice yield quality and plant type in different accumulated temperature zone in Heilongjiang Province. Shenyang Agricultural University, Shenyang, China (in Chinese with English abstract).
- Yuan, Z., Ata-Ul-Karim, S.T., Cao, Q., Lu, Z., Cao, W., Zhu, Y., Liu, X., 2016. Indicators for diagnosing nitrogen status of rice based on chlorophyll meter readings. *Field Crops Res.* 185(185), 12–20.
- Yue, S., Meng, Q., Zhao, R., Li, F., Chen, X., Zhang, F., Cui, Z.L., 2012. Critical nitrogen dilution curve for optimizing nitrogen management of winter wheat production in the North China Plain. *Agron. J.* 104(2), 523–529.
- Yue, S.C., Sun, F.L., Meng, Q.F., Zhao, R.F., Fei, L.I., Chen, X.P., Zhang, F.S., Cui, Z.L., 2014. Validation of a critical nitrogen curve for summer maize in the North China Plain. *Pedosphere* 24(1), 76–83.
- Zarco-Tejada, P.J., Catalina, A., González, M.R., Martín, P., 2013. Relationships between net photosynthesis and steady-state chlorophyll fluorescence retrieved from airborne hyperspectral imagery. *Remote Sens. Environ.* 136, 247–258.
- Zarco-Tejada, P.J., Miller, J.R., Morales, A., Berjon, A., Aguera, J., 2004. Hyperspectral indices and model simulation for chlorophyll estimation in open-canopy tree crops. *Remote Sens. Environ.* 90, 463–476.
- Zhang, F., Cui, Z., Chen, X., Ju, X., Shen, J., Chen, Q., Liu, X., Zhang, W., Mi, G., Fan, M., Jiang, R. 2012. Chapter one - Integrated nutrient management for food security and environmental quality in China. *Adv. Agron.* 116, 1–40.
- Zhang, F., Cui, Z., Fan, M., Zhang, W., Chen, X., Jiang, R., 2011. Integrated soil-crop system management: reducing environmental risk while increasing crop productivity and improving nutrient use efficiency in China. *J. Environ. Qual.* 40(4), 1051–1057.
- Zhang, F., Shen, J., Li, L., Liu, X., 2004. An overview of rhizosphere processes related with plant nutrition in major cropping systems in China. *Plant Soil* 260(1/2), 89–99.
- Zhang, F., Wang, J., Zhang, W., Cui, Z., Ma, W., Chen, X., Jiang, R., 2008. Nutrient use efficiencies of major cereal crops in China and measures for improvement. *Acta Pedolog. Sin.* 5, 915–924.
- Zhao, B., 2014. Determining of a critical dilution curve for plant nitrogen concentration in winter barley. *Field Crops Res.* 160(4), 64–72.
- Zhao, B., Ata-Ul-Karim, S.T., Liu, Z., Zhang, J., Xiao, J., Liu, Z., Qin, A., Ning, D., Yang, Q., Zhang, Y., Duan, A., 2018. Simple Assessment of Nitrogen Nutrition Index in Summer Maize by Using Chlorophyll Meter Readings. *Front Plant Sci.* 2018. 9(11).
- Zhu, Z.L. 1998. The present situation of nitrogen fertilizer use, and the problems and strategies in China, in: Li Q.K. (EDs.), *Fertilizer problems in sustainable development of agriculture in China.* Jiangxi Science and Technology Publishers, Nanchang. pp. 38–

51 (In Chinese.).

- Ziadi, N., Bélanger, G., Claessens, A., Lefebvre, L., Cambouris, A. N., Tremblay, N., Nolin, M.C., Parent, L.E., 2010a. Determination of a critical nitrogen dilution curve for spring wheat. *Agron. J.* 102(1), 241–250.
- Ziadi, N., Bélanger, G., Claessens, A., Lefebvre, L., Tremblay, N., Cambouris, A., Nolin, M., Parent, L., 2010b. Plant-based diagnostic tools for evaluating wheat nitrogen status. *Crop Sci.* 50(50), 2580–2590.
- Ziadi, N., Bélanger, G., Gastal, F., Claessens, A., Lemaire, G., Tremblay, N., 2009. Leaf nitrogen concentration as an indicator of corn nitrogen status. *Agron. J.* 101(4), 947–957.
- Ziadi, N., Brassard, M., Bélanger, G., Cambouris, A.N., Tremblay, N., Nolin, M.C., Claessens, A., Parent, L., 2008a. Critical nitrogen curve and nitrogen nutrition index for corn in eastern Canada. *Agron. J.* 100(2), 271–276.
- Ziadi, N., Brassard, M., Bélanger, G., Claessens, A., Tremblay, N., Cambouris, A., Nolin, M., Parent, L., 2008b. Chlorophyll measurements and nitrogen nutrition index for the evaluation of corn nitrogen status. *Agron. J.* 100(5), 1264–1273.

## Appendix A: Eigenanteil

### Chapter 3

Title	A New Critical Nitrogen Dilution Curve for Rice Nitrogen Status Diagnosis in Northeast China
Authors	<b>Huang, S.</b> , Miao, Y., Cao, Q., Yao, Y., Zhao, G., Yu, W., Shen, J., Yu, K. and Bareth, G. (First Author)
Status	Published
Journal	Pedosphere
Publication time	2018
Volume and Pages	28: 814-822
DOI	10.1016/S1002-0160(17)60392-8
Author Contributions	Organization and implementation of field campaigns in China (April -October of 2008-2013) Data collection in the field – Collection of agronomic data including biomass extraction, cutting, weighing and drying of plant samples, Yield determination Laboratory work – Nitrogen analysis, Yield analyzes Data analysis – Input of agronomic data, Statistical analysis of variance and multiple comparisons for agronomic data, Development of regression models Development of analytical methods Write the manuscript Creation of illustrations and tables Review/proofreading of the manuscript

### Chapter 4

Title	Satellite Remote Sensing-Based In-Season Diagnosis of Rice Nitrogen Status in Northeast China
Authors	<b>Huang, S.</b> , Miao, Y., Zhao, G., Yuan, F., Ma, X., Tan, C., Yu, W., Gnyp, M., Lenz-Wiedemann, V.I.S., Rascher, U. and Bareth, G. (First Author)
Status	Published
Journal	Remote Sensing
Publication time	2015
Volume and Pages	7: 10646-10667
DOI	10.3390/rs70810646
Author Contributions	Organization of field campaigns in China (April-October 2011; April-October 2012) Data collection in the field (in China) – Implementation of a

field campaign to collect data (2011-2012), including biomass extraction, Leaf area index (LAI) determination, cutting, weighing and drying of plant samples, Chlorophyll concentration determination by using chlorophyll meter, Collection of GPS data  
 Data collection – Acquisition and processing of optical satellite data (FORMOSAT-2), Georeferencing of the farmer fields, Surveys of farmers for field management  
 Laboratory work – Nitrogen analysis  
 Data analysis – Input of agronomic data, Development of a regression model, Inversion of the satellite image, Classification for the inversion product based on the diagnosis threshold  
 Development of analytical methods  
 Write the manuscript  
 Creation of illustration and tables  
 Review/Proofreading of the manuscript

**Chapter 5**

Title Potential of RapidEye and WorldView-2 Satellite Data for Improving Rice Nitrogen Status Monitoring at Different Growth Stages

Authors **Huang, S.**, Miao, Y., Yuan, F., Gnyp, M., Yao, Y., Cao, Q., Wang, H., Lenz-Wiedemann, V.I.S. and Bareth, G. (First Author)

Status Published

Journal Remote Sensing

Publication time 2017

Volume and Pages 9: 227

DOI 10.3390/rs9030227

Author Contributions Organization of field campaigns in China (April-October 2008, April-October 2009, April-October 2011)  
 Data collection in the field – Collection of agronomic data including biomass extraction, cutting, weighing and drying of plant samples, Hyperspectral measurement, Collection of the band response function data for satellite sensor from various sources (FORMOSAT-2, RapidEye, WorldView-2)  
 Laboratory work – Nitrogen analysis  
 Data analysis – Input of agronomic data, Re-sampling the hyperspectral data to the satellite wavebands (FORMOSAT-2, RapidEye, WorldView-2), Development of regression models  
 Development of analytical methods  
 Write the manuscript  
 Creation of illustration and tables

	Review/Proofreading of the manuscript
<b>Chapter 6</b>	
Title	Proximal Fluorescence Sensing for In-Season Diagnosis of Rice Nitrogen Status
Authors	<b>Huang, S.</b> , Miao, Y., Yuan, F., Cao, Q., Ye, H., Lenz-Wiedemann, V.I.S. and Bareth, G. (First Author)
Status	Unsubmitted manuscript
Journal	-
Publication time	-
Volume and Pages	-
DOI	-
Author Contributions	<p>Organization of field campaigns in China (April-October 2012, June-August 2013)</p> <p>Data collection in the field – Collection of agronomic data including sampling and measurements, the sensor Multiplex 3 measurement</p> <p>Laboratory work – Nitrogen analysis</p> <p>Data analysis – Input of agronomic data, the Multiplex data, Development of regression models, Inversion of the fluorescence data to agronomic data, Analysis the for diagnostic results</p> <p>Write the manuscript</p> <p>Creation of illustration and tables</p> <p>Review/Proofreading of the manuscript</p>

## **Appendix B: Erklärung**

Ich versichere, dass ich die von mir vorgelegte Dissertation selbständig angefertigt, die benutzten Quellen und Hilfsmittel vollständig angegeben und die Stellen der Arbeit – einschließlich Tabellen, Karten und Abbildungen –, die anderen Werken im Wortlaut oder dem Sinn nach entnommen sind, in jedem Einzelfall als Entlehnung kenntlich gemacht habe; dass diese Dissertation noch keiner anderen Fakultät oder Universität zur Prüfung vorgelegen hat; dass sie – abgesehen von unten angegebenen Teilpublikationen – noch nicht veröffentlicht worden ist, sowie, dass ich eine solche Veröffentlichung vor Abschluss des Promotionsverfahrens nicht vornehmen werde. Die Bestimmungen der Promotionsordnung sind mir bekannt. Die von mir vorgelegte Dissertation ist von Prof. Dr. Georg Bareth betreut worden.

Cologne, den 11.03.2019

## Appendix C: Publication List

\* = part of dissertation

- \***Huang, S.**, Miao, Y., Yuan, F., Gnyp, M.L., Yao, Y., Cao, Q., Lenz-Wiedemann, V.I.S., Bareth, G., 2017. Potential of RapidEye and WorldView-2 satellite data for improving rice nitrogen monitoring at different growth stages. *Remote Sens.* 9, 227. doi:10.3390/rs9030227.
- \***Huang, S.**, Miao, Y., Zhao, G., Yuan, F., Ma, X., Tan, C., Yu, W., Gnyp, M., Lenz-Wiedemann, V.I.S., Rascher, U., Bareth, G., 2015. Satellite Remote Sensing-Based In-Season Diagnosis of Rice Nitrogen Status in Northeast China. *Remote Sens.* 7, 10646-10667.
- \***Huang, S.**, Miao, Y., Cao, Q., Yao, Y., Zhao, G., Yu, W., Shen, J., Yu, K., Bareth, G., 2018. Critical Nitrogen Dilution Curve for Rice Nitrogen Status Diagnosis in Northeast China. *Pedosphere* 28, 814-822.
- Huang, S.**, Miao, Y., Yuan, F., Cao, Q., Ye, H., Lenz-Wiedemann, V.I.S., Khosla, R., Bareth, G., 2017. Proximal fluorescence sensing for in-season diagnosis of rice nitrogen status. *Adv. Anim. Biosci.* 8(2), 343-348.
- Huang, S.**, Miao, Y., Yuan, F., Gnyp, M.L., Cao, Q., Lenz-Wiedemann, V.I.S., Bareth, G., 2016. Potential Improvement in Rice Nitrogen Status Monitoring using RapidEye and WorldView-2 Satellite Remote Sensing. In: Sudduth, K. (Ed.), *Proceedings of 13th International Conference on Precision Agriculture*. ASA/CSSA/SSSA, St. Louis, Missouri, USA.
- Huang, S.**, Miao, Y., Zhao, G., Ma, X., Tan, C., Bareth, G., Rascher, U., Yuan, F., 2013. Estimating rice nitrogen status with satellite remote sensing in Northeast China. In: *Agro-Geoinformatics, 2013 Second International Conference on*, IEEE, pp. 550-557.
- Yao, Y., Miao, Y., **Huang, S.**, Gao, L., Zhao, G., Jiang, R., Chen, X., Zhang, F., Yu, K., Gnyp, M.L., Bareth, G., Liu, C., Zhao, L., Yang, W., Zhu, H., 2012. Active canopy sensor-based precision N management strategy for rice. *Agron. Sustain. Dev.* 32, 925-933.
- Cao, Q., Miao, Y., Wang, H., **Huang, S.**, Cheng, S., Khosla, R., Jiang, R., 2013. Non-destructive estimation of rice plant nitrogen status with Crop Circle multispectral active canopy sensor. *Field Crops Res.* 154, 133-144.
- Ye, H., Huang, W., **Huang, S.**, Huang, Y., Zhang, S., Dong, Y., Chen, P., 2017. Effects of different sampling densities on geographically weighted regression kriging for predicting soil organic carbon. *Spat. Stat-neth.* 20, 76-91.
- Tilly, N., Hoffmeister, D., Cao, Q., **Huang, S.**, Lenz-Wiedemann, V.I.S., Miao, Y., Bareth, G., 2014. Multitemporal crop surface models: Accurate plant height measurement and

- biomass estimation with terrestrial laser scanning in paddy rice. *J. Appl. Remote Sens.* doi.org/10.1117/1.JRS.8.083671.
- Ye, H., Huang, Y., Huang, W., Zhang, S., Chen, P., **Huang, S.**, Hou, S., 2015. Effects of Land Use Change on the Spatiotemporal Variability of Soil Organic Carbon in an Urban-rural Ecotone of Beijing. *J. Integr. Agr.* doi: 10.1016/S2095-3119(15)61065-6.
- Cao, Q., Miao, Y., Shen, J., Yu, W., Yuan, F., Cheng, S., **Huang, S.**, Wang, H., Yang, W., Liu, F., 2016. Improving in-season estimation of rice yield potential and responsiveness to topdressing nitrogen application with crop circle active crop canopy sensor. *Precis. Agric.* 17(2), 136–154.
- Gnyp, M.L., Miao, Y., Yuan, F., Ustin, S.L., Yu, K., Yao, Y., **Huang, S.**, Bareth, G., 2014. Hyperspectral canopy sensing of paddy rice aboveground biomass at different growth stages. *Field Crops Res.* 155, 42–55.
- Su, M., **Huang, S.**, Zhao, G., Zhao, Q., Yao, Y., Miao, Y., 2012. Current Rice Management Practices of Farmers in Heilongjiang Land Reclamation Area and Improvement Strategies. *North Rice* 42, 28-33.